VOLUME 3

REACTOR COOLANT SYSTEM

ASYMMETRIC LOADS

FINAL REPORT

Prepared by

COMBUSTION ENGINEERING, INC.

for

CALVERT CLIFFS 1 & 2

FORT CALHOUN

MILLSTONE 2

PALISADES

June 30, 1980

TABLE OF CONTENTS

TABLE OF CONTENTS (Continued)

TABLE OF CONTENTS (Continued)

4.5 REACTOR VESSEL, RC PIPE, AND RCS SUPPORTS

4.5.1 DESIGN BASIS

The analysis described herein was performed to evaluate the response of the reactor coolant system (RCS) major components to forces associated with design basis pipe ruptures. The design basis pipe breaks for this analysis are defined in Section 4.2. Associated forces for each of these guillotines include pipe tension release forces at the break location, subcompartment pressurization forces as described in Section 4.3, and internal asymmetric hydraulic forces acting on the vessel and internals as described in Section 4.4.

4.5.2 METHOD OF ANALYSIS

Dynamic analysis of the RCS was performed using lumped parameter models which include details of the reactor vessel (RV) and internals, steam generator (SG) and internals, reactor coolant pumps (RCP) and interconnecting reactor coolant piping.

The pipe break tension release forces, asymmetric subcompartment pressurization forces, and asymmetric reactor internal hydraulic forces were applied as simultaneous time-history forcing functions.

A non-linear time-history dynamic analysis was performed for a three-dimensional mathematical model specifically detailed for each break in order to generate mass point response of the components, support and pipe nozzle loads, and time-history motions as subsystem connection points.

Millstone was selected as the model to be used in the generic analysis, but Millstone RCP dead weight vertical hangers were not credited with pipe rupture load carrying capability. For each postulated break, assessments were made for Calvert Cliffs, Palisades and Fort Calhoun. These assessments are explained in Section 4.5.7.

4.5.3 INSTABILITY ANALYSIS OF SUPPORTS

An elastic and/or plastic analysis of each component support region was performed for two purposes. The first was to determine the non-linear load displacement relationship for inclusion in the RCS model described in Paragraph 4.5.4. The second purpose was for evaluation of the acceptability of the computed loads for each component support region. This evaluation is discussed in Paragraph 4.5.8.

4.5.3.1 Detailed Finite Element Models

The three-dimensional elastic plastic analysis of the component support regions has been performed with the MARC non-linear general purpose finite element program (Ref. 3.10). The finite element models used in the analysis must be sufficiently

4.5.3.1 Detailed Finite Element Models (Continued)

detailed to provide an accurate load displacement curve and instability load but simple enough to provide a reasonably efficient solution with the MARC program. A typical model of a reactor vessel support on an inlet nozzle is shown in two views in Figures 4.5.1 and 4.5.2. The model provides for the determination of the load displacement relationships not only at the support but at the nozzle/vessel intersection and at the nozzle/pipe intersection.

Models with an appropriate degree of detail were developed for each different RCS support region. The material properties used in the analyses were determined from laboratory tests already performed.

4.5.3.2 Load Displacement Relationships

Each support region model was loaded statically in the direction of load expected during the RCS structural analysis. The load was increased until the deformation increases without bound. The overall behavior of the region was determined for input to the RCS structural analysis as a non-linear support stiffness.

4.5.3.2.1 Load Carrying Capability of Reactor Vessel Supports

Reactor Vessel support characteristics have been determined for all plants under consideration per paragraphs 4.5.3.1 and 4.5.3.2 of the evaluation plan. These support characteristics are indicated on the Load Deflection curves for the Generic Plant on Figures 4.5.3 and 4.5.4.

a. RV Nozzle Loads

Load capability is defined as the maximum moment acting on the pipe safe end or elbow which satisfies ASME Code, Appendix F elastic limits. Finite element analysis has been used to determine a stress intensification factor for piping elbows.

4.5.3.3 Instability Analysis

The detailed stresses and strains for each loading up to instability were obtained from the analysis described in Paragraph 4.5.3.2. This information as well as the instability loads (the loads at which deformation increases without bound) were stored for later use in evaluating the effect of the loads computed by the RCS structural analysis.

4.5.3.4 Steam Generator and Pump Supports

Support regions where predicted loadings are assumed to be within the elastic loading range have been evaluated on a conservative, elastic basis. The assumption of elastic behavior is verified by comparing elastic load limits to calculated loadings. These comparisons are shown in Section 4.5.8.

4.5.3.4.1 Load Carrying Capabilities of Steam Generator and Pump Supports

4.5.3.4.1.1 Generic Analysis of Steam Generator And Pump Supports

All generic plant steam generator and RC pump supports have been evaluated on an elastic basis. Load capabilities have been determined for all supports in order to evaluate the structural adequacy of these supports when subjected to the loads calculated in the RCS dynamic analysis. Load deflection characteristic of these supports have also been conservatively calculated on an elastic basis. The calculated load capabilities are listed in Tables 4.5-4,5,6 and were determined as follows:

a. Steam Generator Lower pads, lower stop, lower keys, and upper keys

Design Loadings are less than or equal to 90% Loadings at Yield. Load Capability for these supports is defined as Design Loads/0.9, and apply to both the component support and the foundation structure.

b. Steam Generator Holddown Bolts

Load Capability is defined as loadings to cause yield based on ASME Code material properties.

c. Steam Generator Snubbers

Load Capability is reported as actual test loads.

d. Steam Generator and Reactor Coolant Pump Nozzle Loads

Load Capability is defined as the maximum moment acting on the pipe safe end or pipe elbow which satisfies ASME Code, Appendix F elastic limits. Finite element analysis has been used to determine a stress intensification factor for piping elbows.

4.5.3.4.1.2 Millstone 2

The generic support analysis is directly applicable to Millstone.

4.5.3.4.1.3 Calvert Cliffs

The generic support analysis is directly applicable to Calvert Cliffs.

4.5.3.4.1.4 Palisades

The Palisades support system is substantially different from the generic design. A plant specific analysis was performed for the Palisades supports using the same analytical methods as applied to the generic plant. In addition, the load carrying capability of the supporting foundation structure was evaluated on an elastic-plastic basis. This data was used, where applicable, as the load limiting component.

4.5.3.4.1.5 Fort Calhoun

The Fort Calhoun support system is substantially different from the generic design. A plant specific analysis was performed for the Fort Calhoun supports using the same analytical methods as applied to the Palisades plant.

4.5.4 MODELS

Condensed structural models of the major components of the RCS and component internals were developed from detailed representations of each component by incorporating response characteristics and maintaining interface response compatibility. For each analysis, a model of the RCS including reactor vessel, steam generators, reactor coolant pumps in the intact legs, and interconnecting piping was employed. Each model contained high degrees of structural detail for all components, with concentration of mass detail depending on the component to be evaluated. However, a mass representation of other RCS components is included for each model.

Load deflection characteristics of the supports and foundations of the RCS components as determined by the procedures described in 4.5.3 are included in the models.

4.5.4.1 Models for the Reactor Vessel Analysis

Design basis pipe breaks for this analysis are defined in Section 4.2 as the RV Hot Leg (Outlet) nozzle guillotine and the RV Cold Leg (Inlet) nozzle guillotine. For each of these breaks, a detailed model was developed using lumped mass parameter techniques as detailed below.

4.5.4.1.1 Generic RV Outlet Nozzle Guillotine Analysis

The three-dimensional model of the RCS constructed for this analysis contained total RCS mass and stiffness definition, with pipe break discontinuity of the pipe at the RV nozzle safe end on the #1 hot leg (Figure 4.5.5). The RV internals were modelled in detail, taking into account the three-dimensional non-linear aspects of the connections between elements such as the fuel assembly, core shroud, core support barrel (CSB), and upper guide structure (UGS), and RV as well as hydrodynamic coupling effects of the CSB-RV and CSB-shroud interfaces. The internals model used for this analysis was reduced from the more highly detailed model used in the analysis of the internals themselves (Section 4.6.2). The reduced model of the RV internals, showing its co-linear elements and non-linearities, is presented in Figure 4.5.6. In addition to parameters outlined above, lump mass parameters of the RV shell and both SG's were included in the model. The non-linearities of the RV gapped horizontal supports and vertical support pads as well as the lower stop for each SG were also modelled. The resulting model consisted of 70 mass dynamic degrees of freedom (d.d.o.f.), 8 non-linear RV internal interfaces and 5 non-linear RV support locations.

4.5.4.1.2 Generic RV Inlet Nozzle Guillotine Analysis

The details of the mathematical model analyzed (Figure 4.5.7) were identical to those for the RV Outlet Nozzle Guillotine Analysis, except that the pipe discontinuity was modelled at the 1A loop RV inlet nozzle safe end. The model contained 70 mass d.d.o.f., 8 non-linear internal interfaces, and 5 non-linear support locations.

4.5.4.1.3 Generic RV Analysis for ECCS Motion

For each RV analysis design basis pipe break the RCS models outlined above were revised to provide lump mass parameters at all RCP's and piping loops, and d.d.o.f.'s at ECCS nozzles. RV shell and SG mass and gapped support point motions resulting from the RV asymmetric load analyses were applied on a time-history basis as forcing functions to the rest of the RCS to obtain motions at the ECCS nozzle interfaces. Each of these models was linear and contained 70 mass d.d.o.f.'s.

4.5.4.2 Models for Steam Generator Support Analysis

Design basis pipe breaks for this analysis are defined in Section 4.2 as the SG outlet nozzle guillotine and the SG inlet nozzle guillotine. For each of these breaks, a detailed model was developed using lumped mass parameter techniques as detailed below.

4.5.4.2.1 Generic SG Outlet Nozzle Guillotine Analysis

The three-dimensional model of the RCS constructed for this analysis contained total RCS mass and stiffness definition, with the pipe break discontinuity of the pipe at the 1A loop SG outlet nozzle (Figure 4.5.8). Lump mass parameters of the RV, both SG's, 1B, 2A, 2B RCP's. 1B cold leg piping and #1 hot leg piping are included. Steam Generator #1 was modelled with a high degree of detail in prder to calculate its response and movement following this break. The detail includes the non-linearities of the lower stop and keys and all four vertical pads. The internals of SG #1 were also modelled, and included a gross tube bundle mass and stiffness as well as tube bundle to shell interface details. The detailed model of SG #1 for this break is presented in Figure 4.5.9, which shows the colinear elements of the SG tube bundle and shell as well as the support non-linearities. The resulting model consists of 68 mass dynamic degrees of freedom (d.d.o.f.) and 7 non-linear support locations.

4.5.4.2.2 Generic SG Inlet Nozzle Guillotine Analysis

The details of the mathematical model analyzed (Figure 4.5.10) were similar to those for the SG Outlet Nozzle Guillotine. For this analysis, discontinuity of the piping was represented at the SG #1 inlet nozzle safe end, and mass representation was also included at the 1A RCP and 1A cold leg. SG #1 contained the same detail as the model for the SG Outlet Nozzle Guillotine, except that the lower support keys were modelled as linear supports (See Figure 4.5.11). This model contained 76 mass d.d.o.f.'s and 5 non-linear support locations.

4.5.5 FORCING FUNCTIONS

4.5.5.1 Reactor Vessel Support Analysis

For each design basis pipe break in the RV cavity, a blowdown loads analysis (Section 4.4) and a cavity

4.5.5.1 Reactor Vessel Support Analysis (Continued)

pressure analysis (Section 4.3) were performed in order to generate internal asymmetric loadings and differential cavity pressure respectively. These forces and the pipe tension release force at the postulated break were used to calculate the three-dimensional time history forces applied to the exterior and internals of the RV. Forcing functions for a typical RV support analysis are shown in Figure 4.5.12.

4.5.5.2 Steam Generator Support Analysis

For each design basis pipe break in the steam generator compartment, a subcompartment pressurization analysis was performed using the procedures and models discussed in Section 4.3. Resulting pressures were used to calculate asymmetric forces on the SG. These forces and the pipe tension release force at the postulated break were used to calculate the three-dimensional time-history forces applied to the exterior of the SG. Typical simultaneous three-dimensional forcing functions for an SG support analysis are shown in Figure 4.5.13.

4.5.6 COMPUTER CODES

The physical definition of each model was supplied to the STRUDL computer code (Reference 3.2), which generated the condensed stiffness matrix as well as pipe and linear support load influence coefficients. The matrix, along with the mass definition, gapped support definition, damping, appropriate hydrodynamic coupling effects, the three-dimensional time-history forcing functions as discussed and developed in Reference 3.1, and the pressure loads calculated from the subcompartment pressurization analysis as discussed in Section 4.3, was supplied to the DAGS computer code (Reference 3.4) which calculates support loads and time history motions. The time history motions and the STRUDL-generated influence coefficients were supplied to the DAGS post-processor code FORCE (Reference 3.4), which calculates maximum pipe nozzle loads and support loads.

4.5.7 RESULTS OF ANALYSIS

The results of the analyses described above include time histories of component maximum support loads for support evaluation and time histories of motion of components and piping for subsystem analysis of vessel internals (Section 4.6), CEDM (Section 4.8), and ECCS piping (Section 4.9).

The results of the generic analysis was related to specific plants in either full or scaled form. Where necessary plant specific verifications and/or analyses were performed.

4.5.7.1 Results of the Generic Reactor Vessel Analysis

Generic reactor vessel support loads, RV nozzle loads, and RCP nozzle loads are summarized in Tables 4.5-1, 4.5-2, and 4.5-3 respectively for both pipe breaks analyzed.

Time-history motions of the RV and both SG's were also generated from these analyses and were used as forcing functions to develop motions of the ECCS nozzle at its connection with the RCP discharge pipe.

4.5.7.2 Results of the Generic Steam Generator Support Analyses

Generic steam generator support loads, SG nozzle loads and RCP nozzle loads are summarized in Tables 4.5-4, 4.5-5 and 4.5-6 respectively for both pipe breaks analyzed. These loads are shown in comparison to load capabilities as developed in Section 4.5.3.

4.5.8 EVALUATION OF COMPONENTS AND SUPPORTS

4.5.8.1 Acceptance Criteria

The reactor vessel support loads resulting from the RCS Structural Analysis, Section 4.4.8.1, have been evaluated by comparison to the instability analysis results. The initial conservative acceptance criterion was the ASME Boiler and Pressure Vessel Code Section III, Division 1, Appendix F, Article F1324. This criterion states that the violation of the pressure boundary will not occur if the applied loads do not exceed 70% of the plastic instability load.

In cases where results may not clearly satisfy this criterion, structural adequacy and pressure boundary integrity are also demonstrated by examination of the effects of the additional strain on component supports and piping. Where necessary, these effects are discussed in 4.5.8.2.1, Generic Plant RV Supports Evaluation. These acceptance criteria have also been applied to the RV shell and nozzle intersection, and to the reactor coolant pipe near the supports and component nozzles. The steam generator and pump support loads resulting from the RCS Structural Analysis have been evaluated by comparison to the elastic analysis results.

4.5.8.2 Evaluation

The maximum load experienced by the nozzle regions of the reactor vessel for each design basis pipe break in the reactor cavity was evaluated. The results of the RCS structural analysis was compared to the results of the elastic-plastic analyses of Section 4.5.3.

4.5.8.2 Evaluation (Continued)

The integrity of the reactor vessel was evaluated by comparing the computed elastic-plastic behavior to the instability load or to strain limits according to the acceptance criteria of Paragraph 4.5.8.1.

The maximum load experienced by the upport and nozzle regions of the reactor coolant piping was evaluated for each design basis pipe break. The evaluation process is similar to that discussed above. The integrity of the reactor coolant piping was evaluated by comparing the computed elastic-plastic behavior to the instability load or the strain limits according to the acceptance criteria of Paragraph 4.5.8.1.

The maximum load experienced for each RCS support was evaluated for each design basis pipe break in the steam generator compartment. The evaluation process was similar to that discussed above. The integrity of the reactor coolant system supports was evaluated by comparing the computed elastic-pastic behavior to the instability load or to strain limits according to the acceptance criteria of Paragraph 4.5.8.1.

4.5.8.2.1 Generic Plant RV Supports Evaluation

The resulting loads from generic RV support analysis are compared to the acceptance criteria for the supports in Figures 4.5.3 and 4.5.4. RV and RCP nozzle loads are compared to their acceptance criteria in Tables 4.5-2 and 4.5-3.

For the RV Outlet Nozzle Guillotine, all RV support and RV and RCP nozzle loads satisfy the initial conservative acceptance criteria of ASME Code Section III. For the RV Inlet Nozzle Guillotine, RV support loads exceed this criterion by 5%. (See Figures 4.5.3 and 4.5.4). For this case, however, it is clear from the load-deflection curves for each support that there is a considerable amount of additional strain capacity. Therefore, the supports are adequate to sustain the calculated load. For this postulated rupture, the RV nozzle loads meet the initial acceptance criteria, and the RCP discharge nozzle loads exceed the elastic analysis criterion by less than 2%. The pressure retaining integrity and geometric stability of the primary piping are not impaired.

4.5.8.2.2 Plant Specific Evaluation - RV Supports Analysis

4.5.8.2.2.1 Millstone 2

The Millstone 2 plant was used as the basis for the generic RV support analysis, with the exception that

4.5.8.2.2.1 Millstone 2 (Continued)

the generic cavity pressure loads were calculated by applying a factor of 1.1 to the Calvert Cliffs cavity pressure loads. The Millstone cavity pressures have been shown to be lower than those used for the generic RV supports analysis. Therefore, the generic results are directly applicable to Millstone.

4.5.8.2.2.2 Calvert Cliffs

The Calvert Cliffs RV, RV support system and RCP piping are identical to Millstone's, the RCP has greater potential load carrying support than Millstone, and the cavity pressure loads applied to the generic analysis are 1.1 times greater than Calvert Cliffs cavity pressure loads. Therefore, the generic results are conservative for Calvert Cliffs.

4.5.8.2.2.3 Palisades

The Palisades RV, RV and SG support system and RCP piping are similar to Millstone's, but the load-deflection characteristics of the RV supports and foundation (Figures 4.5.14 and 4.5.15), which show reduced load carrying capability, made it necessary to perform a plant specific analysis for the controlling RV Inlet Nozzle Guillotine case. In this analysis, which used models and methodology similar to those already discussed, the load carrying capability of the 1B & 2B RCP supports was utilized, but credit was taken for neither the 2A loop RCP supports, whose load carrying capability is low, nor for the ruptured 1A loop. Cavity pressure loads calculated specifically for Palisades were applied together with generic RV internal and pipe tension release loads. Results, as summarized and compared in Tables 4.5-7,8,9,10 and Figures 4.5.14 and 4.5.15, show that all support and nozzle loads generated by this plant specific analysis meet the acceptance criteria for this plant. These loads include all RV support loads, all RV and RCP nozzle loads and all applicable RCP support loads.

The results of the generic analysis for the RV Outlet Nozzle Guillotine are conservative for Palisades and still meet Palisades plant specific acceptance criteria.

Palisades specific ECCS time history motions were also generated for this break, to be used as input forcing functions to the ECCS analysis reported on in Section 4.9.

4.5.8.2.2.4 Fort Calhoun

A comparison of the Fort Calhoun plant RCS parameters to those of the generic plant, coupled with reduced load carrying capability of the Fort Calhoun RV supports and foundation (Figures 4.5.16 and 4.5.17), showed that a plant specific analysis was required for the controlling RV Inlet Nozzle Guillotine case. The modeling and methodology used for this analysis were similar to those already discussed. All applied loads were calculated specifically for the Fort Calhoun plant. Only 70% of the load carrying capacity of the supports for RCP #1A, 1B, and 2A was utilized to ensure that the RV support loads and nozzle loads generated were conservative. No credit was taken for the load carrying capability of the ruptured RCP 2B loop.

The results for RV support loads, nozzle loads and applicable RCP support loads are summarized in Tables 4.5-11,12,13,14,15. These results show that the conservative acceptance criteria of ASME Code Section III is exceeded in one instance only. The radial component of load on one RV support foot is 81% of the ultimate support capability (see Figure 4.5.17). However, it is clear from the load deflection curves for each support that there is a considerable amount of additional strain capacity. Therefore, the supports are adequate to sustain the calculated load.

Fort Calhoun specific ECCS time history motions were also generated for this break, to be used as input to the ECCS analysis (Section 4.9).

4.5.8.2.3 Generic Plant SG Supports Evaluation

The results of the generic SG support analysis (4.5.7.2) and elastic analysis of supports (4.5.3.2), summarized in Tables 4.5-4,5,6 were compared. All support and pipe nozzle loads generated by the SG support analysis are within their respective calculated load capabilities.

4.5.8.2.4 Plant Specific Evaluations - SG Support Analysis

4.5.8.2.4.1 Millstone 2

The Millstone 2 plant was used as the basis for the generic SG support analysis; therefore, the generic results of the SG supports and SG nozzle loads are directly applicable.

4.5.8.2.4.2 Calvert Cliffs

The Calvert Cliffs SG, SG support system and RCP piping is identical to Millstone's. Therefore, the generic results of the SG supports and SG nozzle loads are directly applicable.

The Calvert Cliffs RCP support system includes a horizontal snubber, a vertical snubber and a horizontal seismic support strut for each pump that the Millstone RCP's do not have. Since it has been shown that the generic RCP nozzle loads meet the acceptance criteria without the aid of any other RCP support, these generic results are conservative for Calvert Cliffs.

4.5.8.2.4.3 Palisades

System geometry, forcing functions, and those parameters which affect distribution of applied loads to each of the supports are essentially the same for Palisades and the generic plant. Consequently, generic SG support reactions and SG nozzle loads are directly applicable to Palisades. However, the Palisades SG support (and nozzle) load carrying capabilities were found to be different than the generic plant. Therefore, the generic SG support and nozzle loads were compared to plant specific load capabilities (Tables 4.5-16, 4.5-17) and were found to be acceptable. The Palisades RCP support system contains vertical supports capable of carrying significant load. Therefore, because the generic model is without pump supports, the generic RCP nozzle load results are conservative for Palisades. They are compared to Palisades specific load capability in Table 4.5-18 in order to show that they also meet the acceptance criteria.

4.5.8.2.4.4 Fort Calhoun

A comparison of Fort Calhoun plant RCS parameters to those of the generic plant showed that results of neither the generic S.G. support analysis nor the elastic analysis to determine the load carrying capability of the supports were applicable to the Fort Calhoun plant. A plant specific analysis for Fort Calhoun was, therefore, performed. Initial results showed that in order to limit the flow area development for the hot leg break and maintain the RCS piping loads within the elastic range it would be necessary to modify the existing supports. The modification made consisted of a replacement of the 3 3/8" S.G. accident ring support rods which run from the S.G. accident ring to the primary shield wall in a direction parallel to the hot leg, with rods of a higher strength material and a larger diameter. The existing rods were A36 steel, 3 3/8" diameter. The replacement

rods are C1018 steel and 4 1/4" diameter. The interface connections of the new rods remain the same and the geometry of the entire support system is unchanged by this modification. The results of the Fort Calhoun plant specific analysis using the modified S.G. supports are given in Tables 4.5-19, 4.5-20 and 4.5-21. All support loads are within the indicated capability and all RCS piping and nozzle loads are well below code limits.

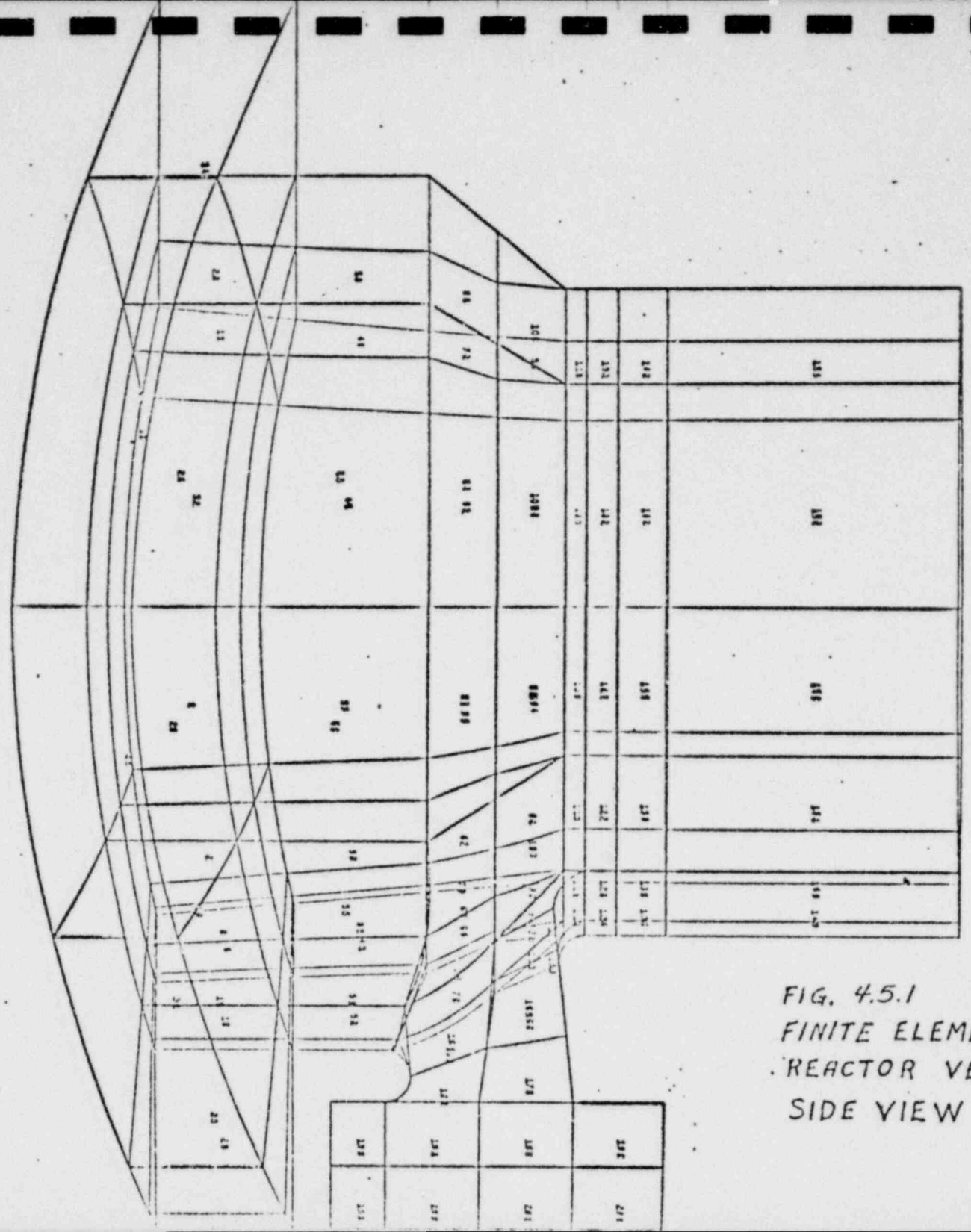

FIG. 4.5.1
FINITE ELEMENT MODEL
REACTOR VESSEL SUPPORT
SIDE VIEW

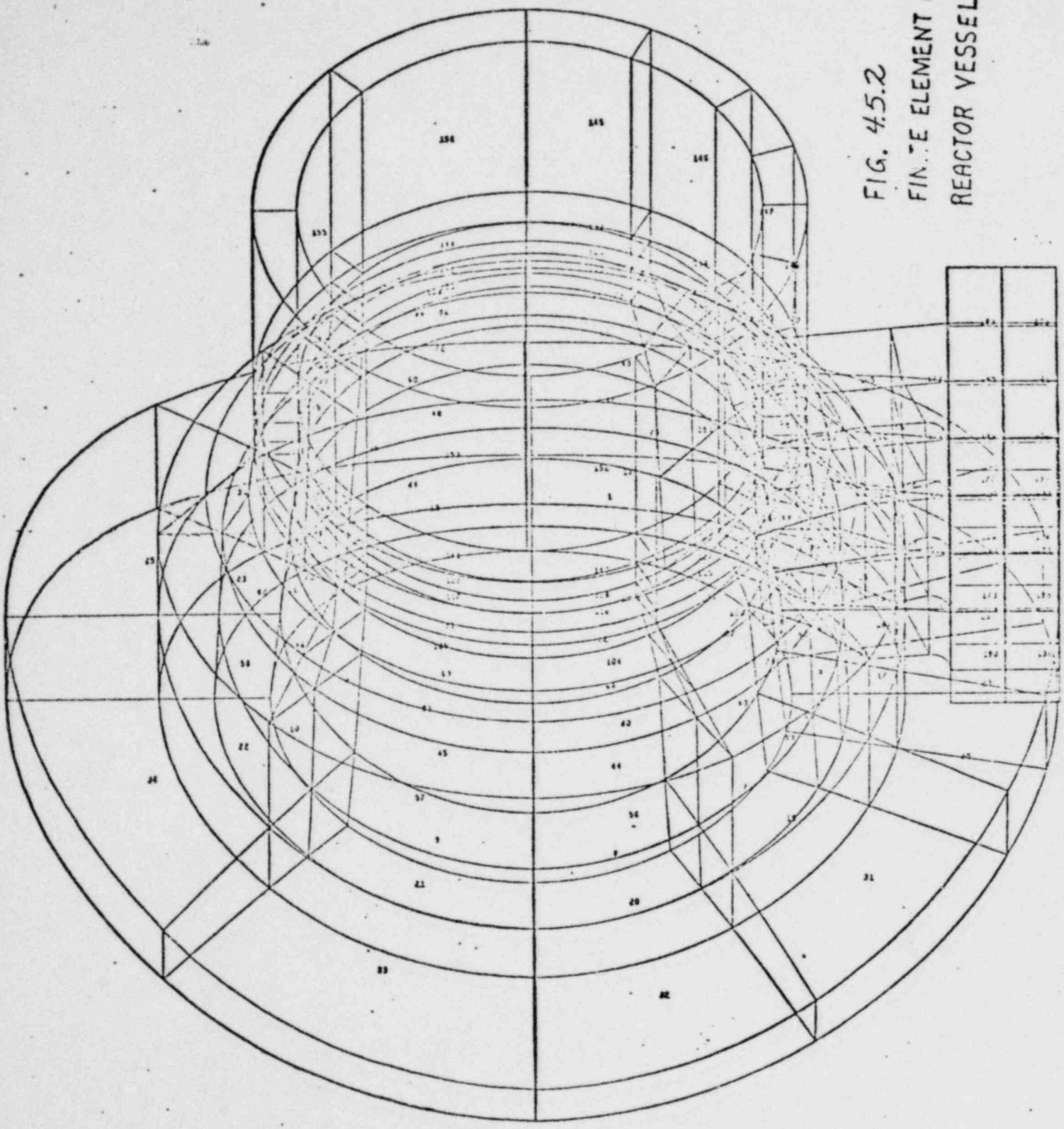

FIG. 4.5.2
FINITE ELEMENT MODEL
REACTOR VESSEL SUPPORT

FIGURE 4.5.3

GENERIC COLD LEG SUPPORT FOOT
TOTAL EFFECTIVE STIFFNESS
TOTAL STOP REACTION FORCE
VERSUS
DISP. IN STOP DIRECTION

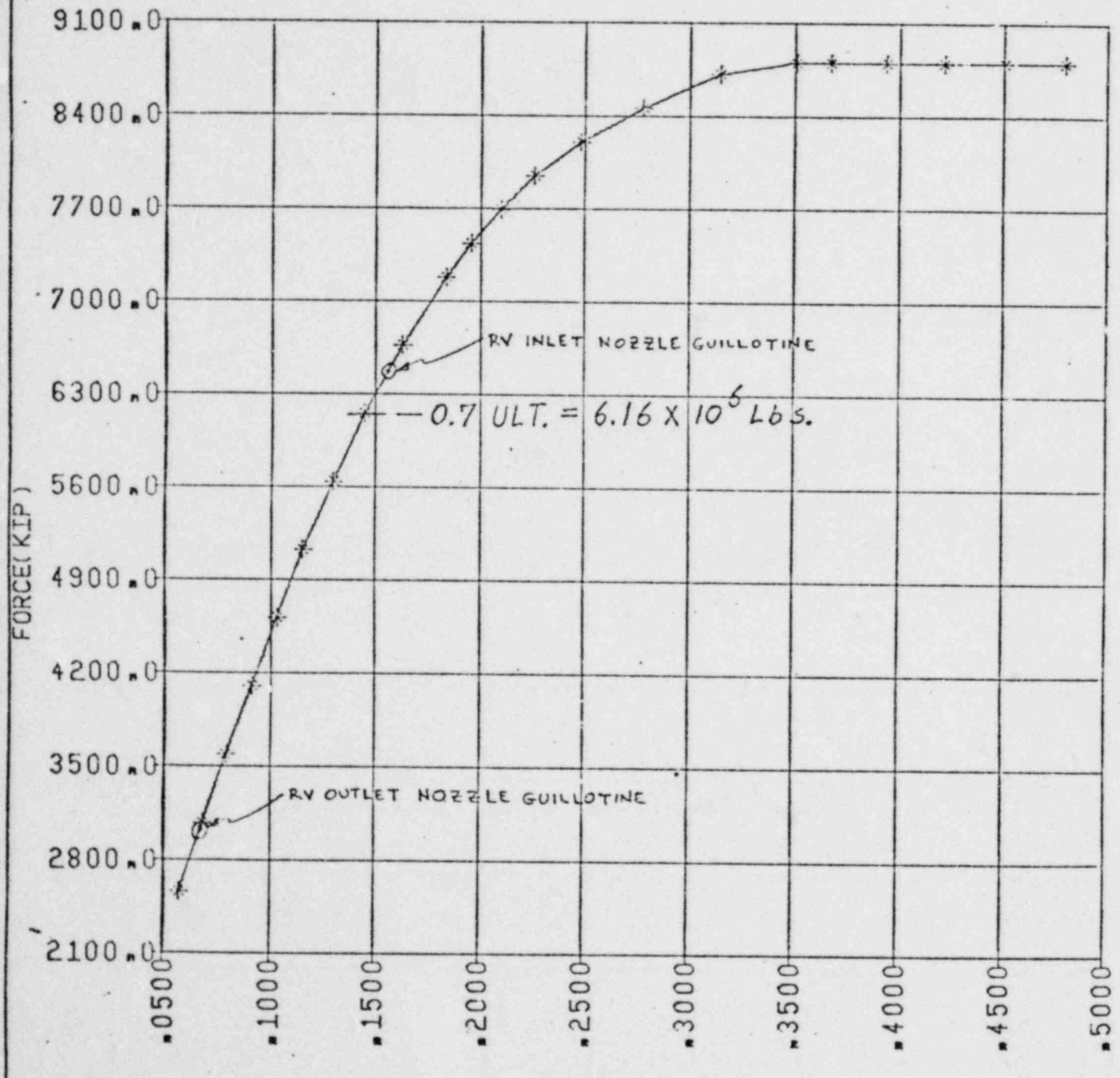

DATA CREATED BY-
PHCCWVR 01/28/79

DATA PLOTTED BY--
NULCWKM 03/20/79

GENERIC HOT LEG SUPPORT FOOT
TOTAL EFFECTIVE STIFFNESS
TOTAL STOP REACTION FORCE
VERSUS
DISP. IN STOP DIRECTION

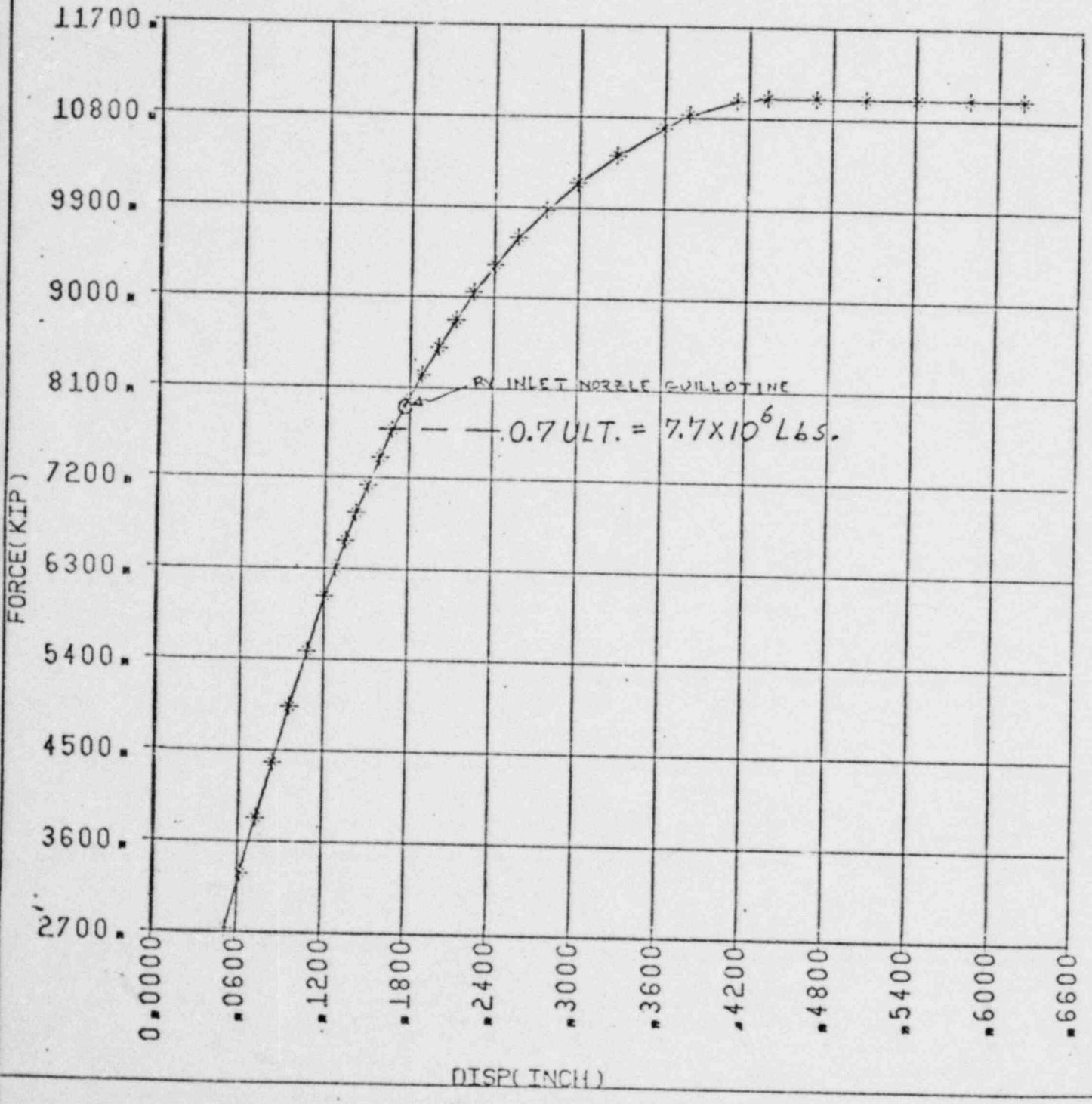

DATA CREATED BY-
PHWCCRJ 02/19/79

DATA PLOTTED BY-
NULCWJU 03/19/79

GENERIC RV ASYMMETRIC LOADS ANALYSIS

RV SUPPORT LOADS

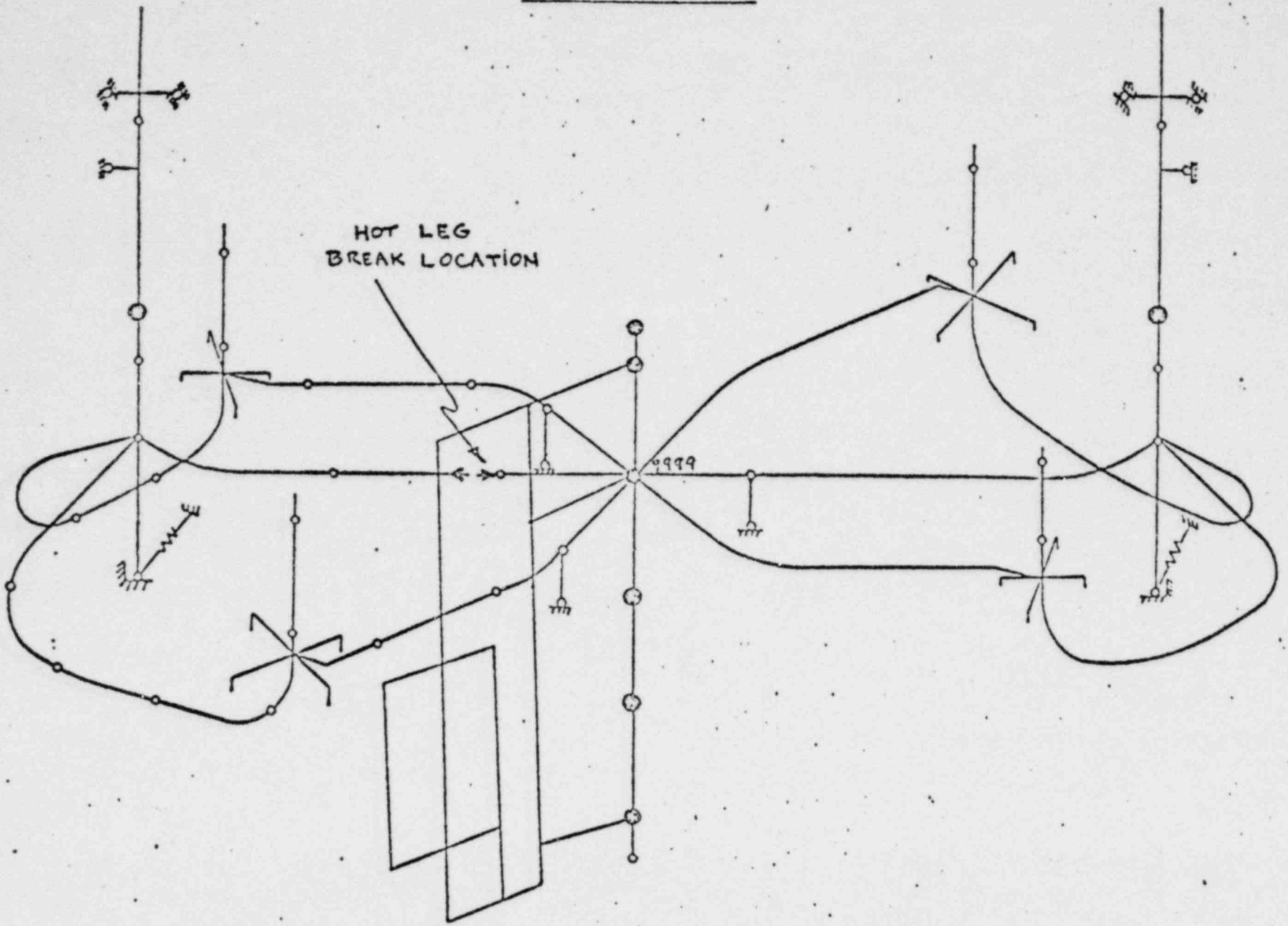

FIGURE 4.5.5

FIGURE 4.5.6

GENERIC REDUCED INTERNALS MODEL

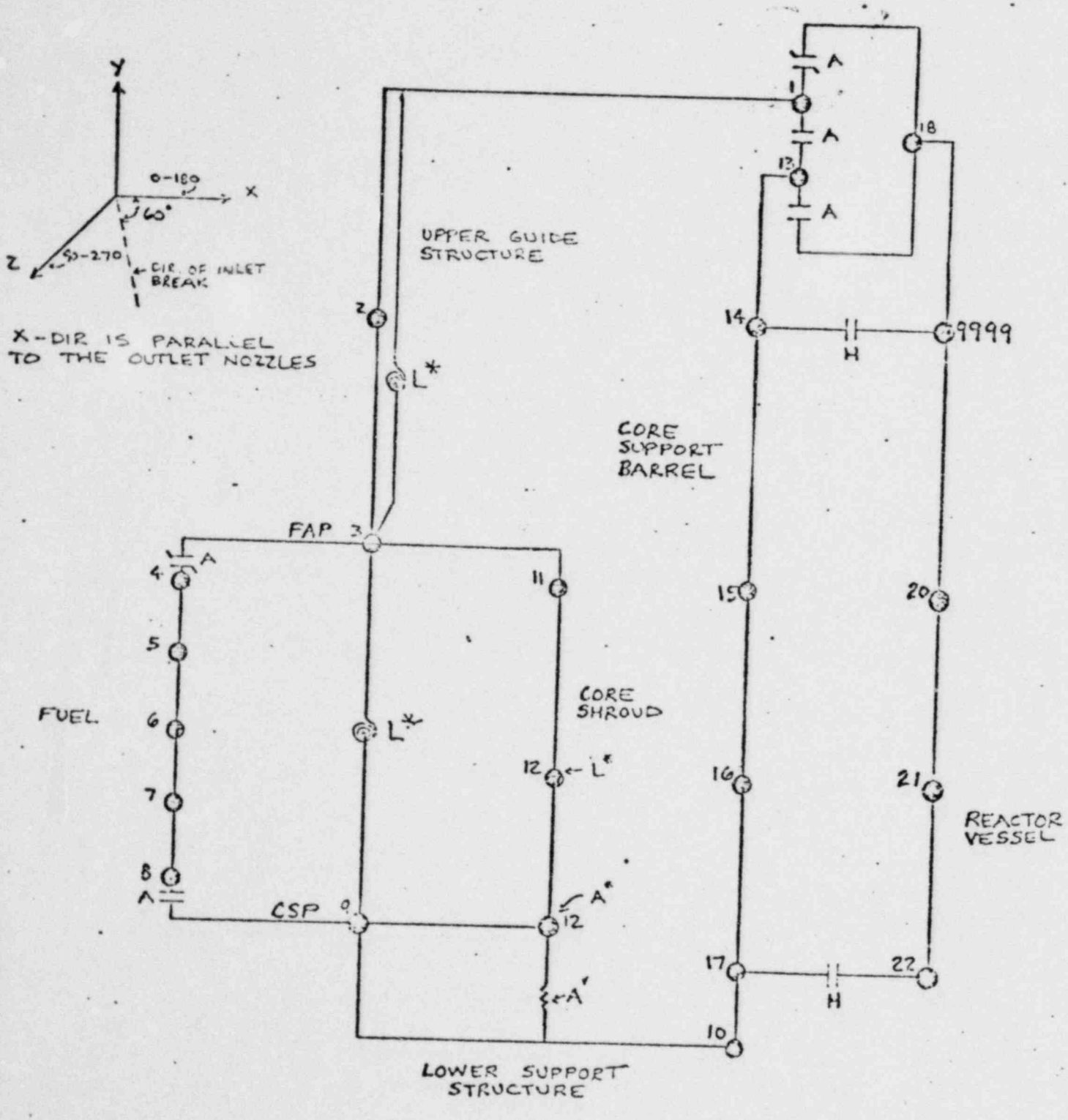

LEGEND :

A = AXIAL GAP

H = HORIZONTAL GAP

INDICATES AN AXIALLY PRELOADED COUPLING

L* = LATERAL MODELS ONLY

A* = AXIAL MODEL ONLY

GENERIC RV ASYMMETRIC LOADS ANALYSIS

RV SUPPORT LOADS

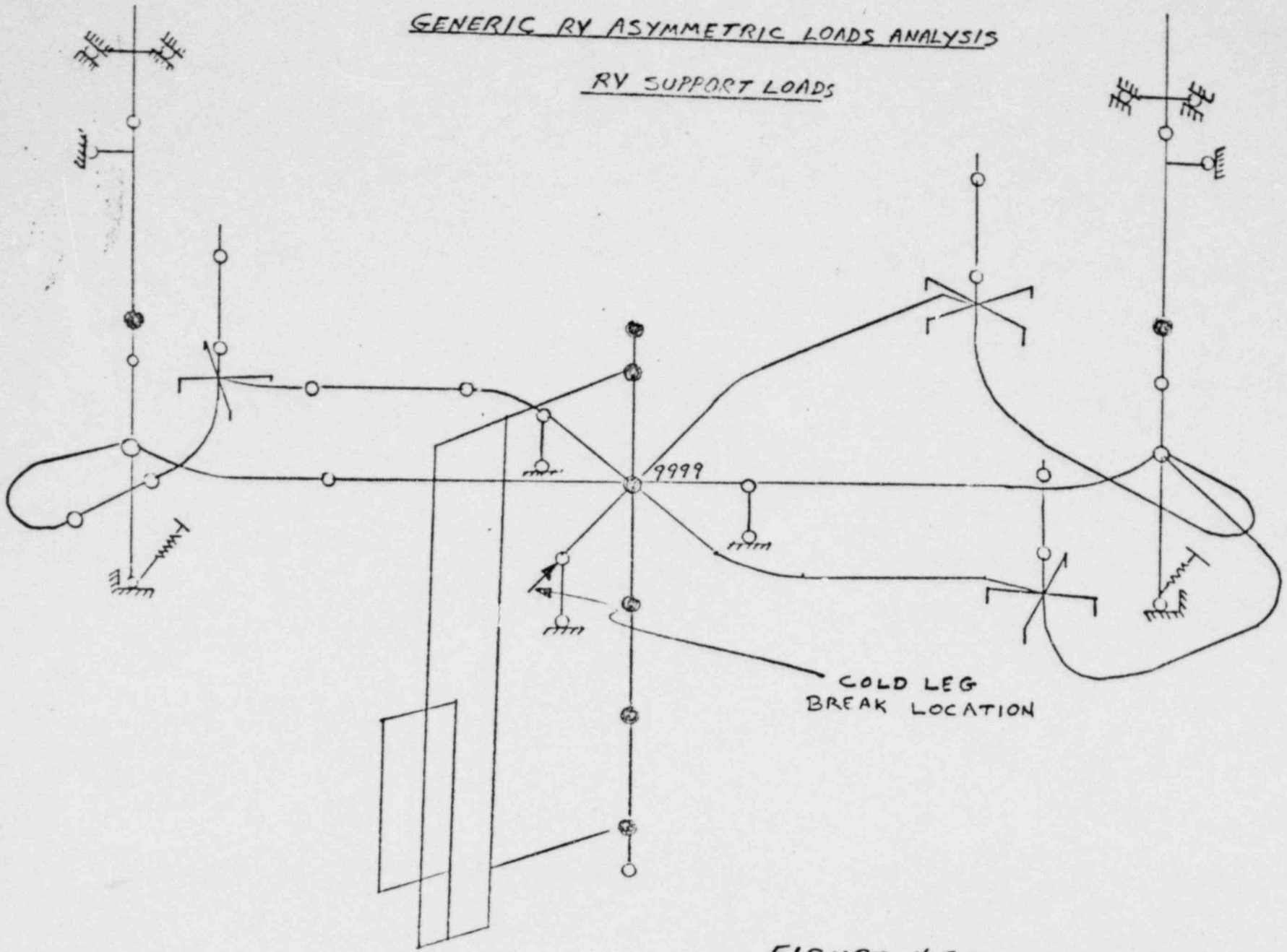

FIGURE 4.5.7

GENERIC

SG OUTLET NOZZLE GUILLOTINE BREAK

LOADS ANALYSIS

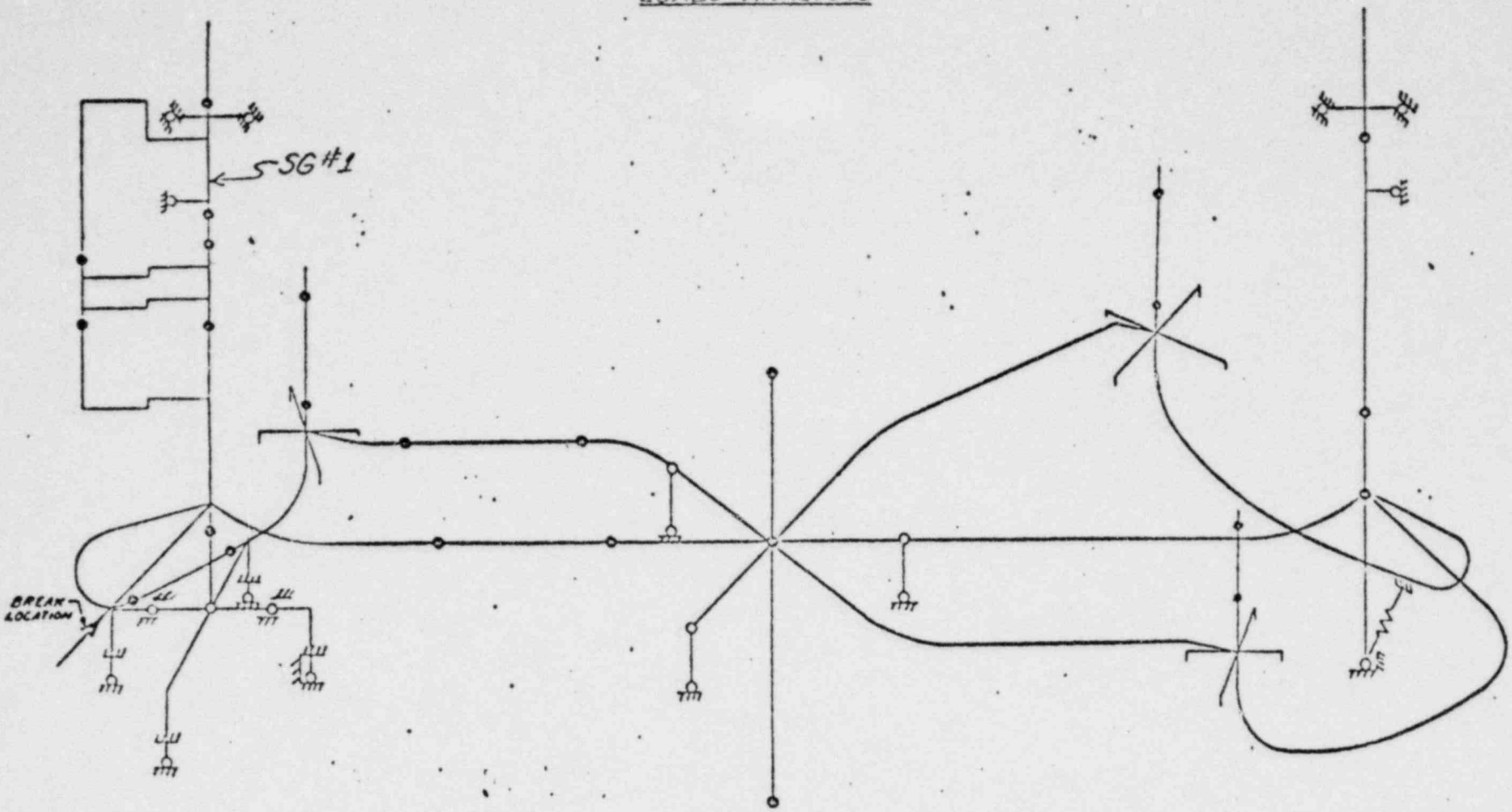

FIGURE 4.5.8

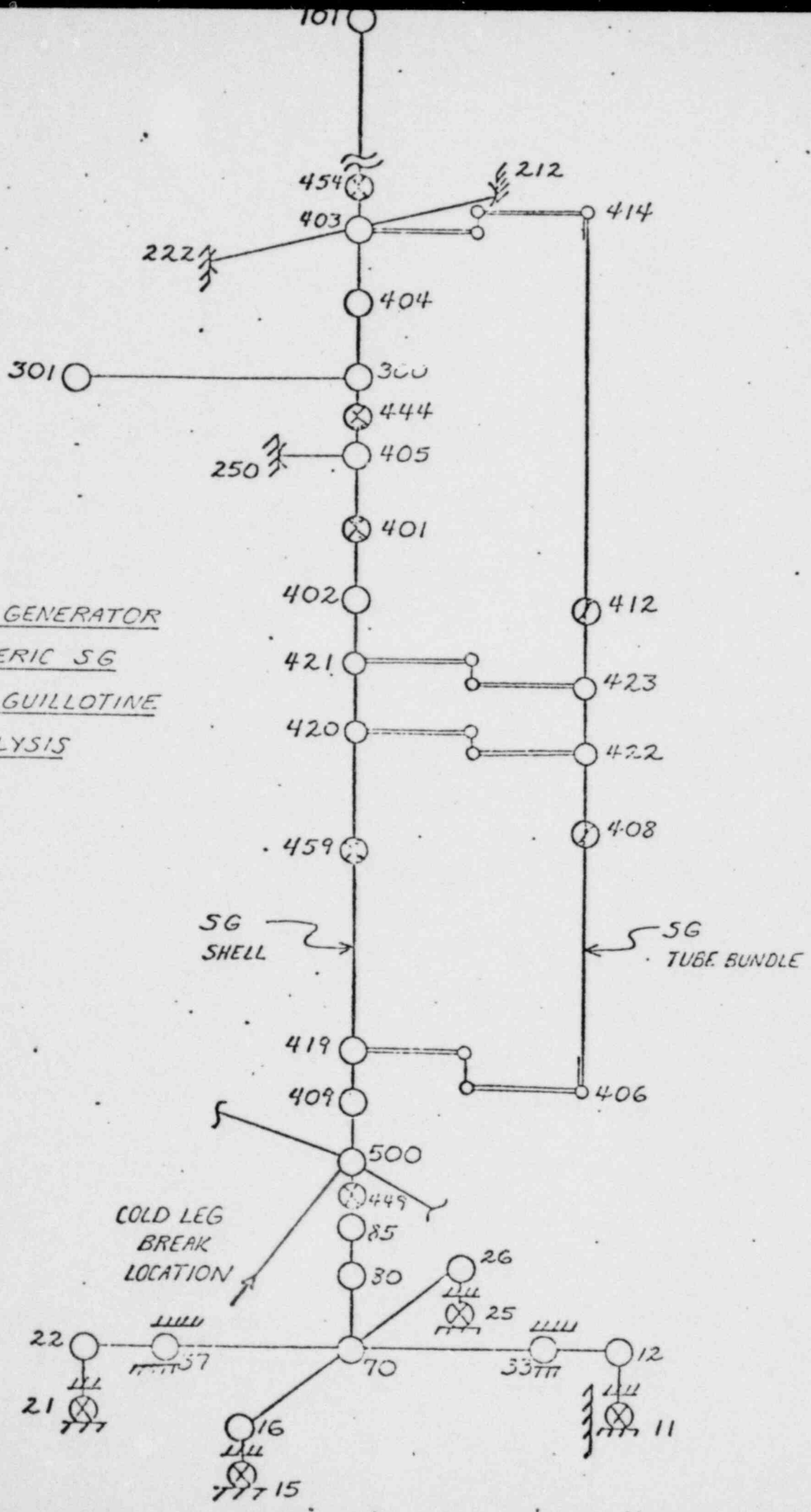

DETAILED STEAM GENERATOR MODEL FOR GENERIC SG OUTLET NOZZLE GUILLOTINE LOADS ANALYSIS

FIGURE 4.5.9

GENERIC

SG INLET NOZZLE GUILLOTINE BREAK

LOADS ANALYSIS

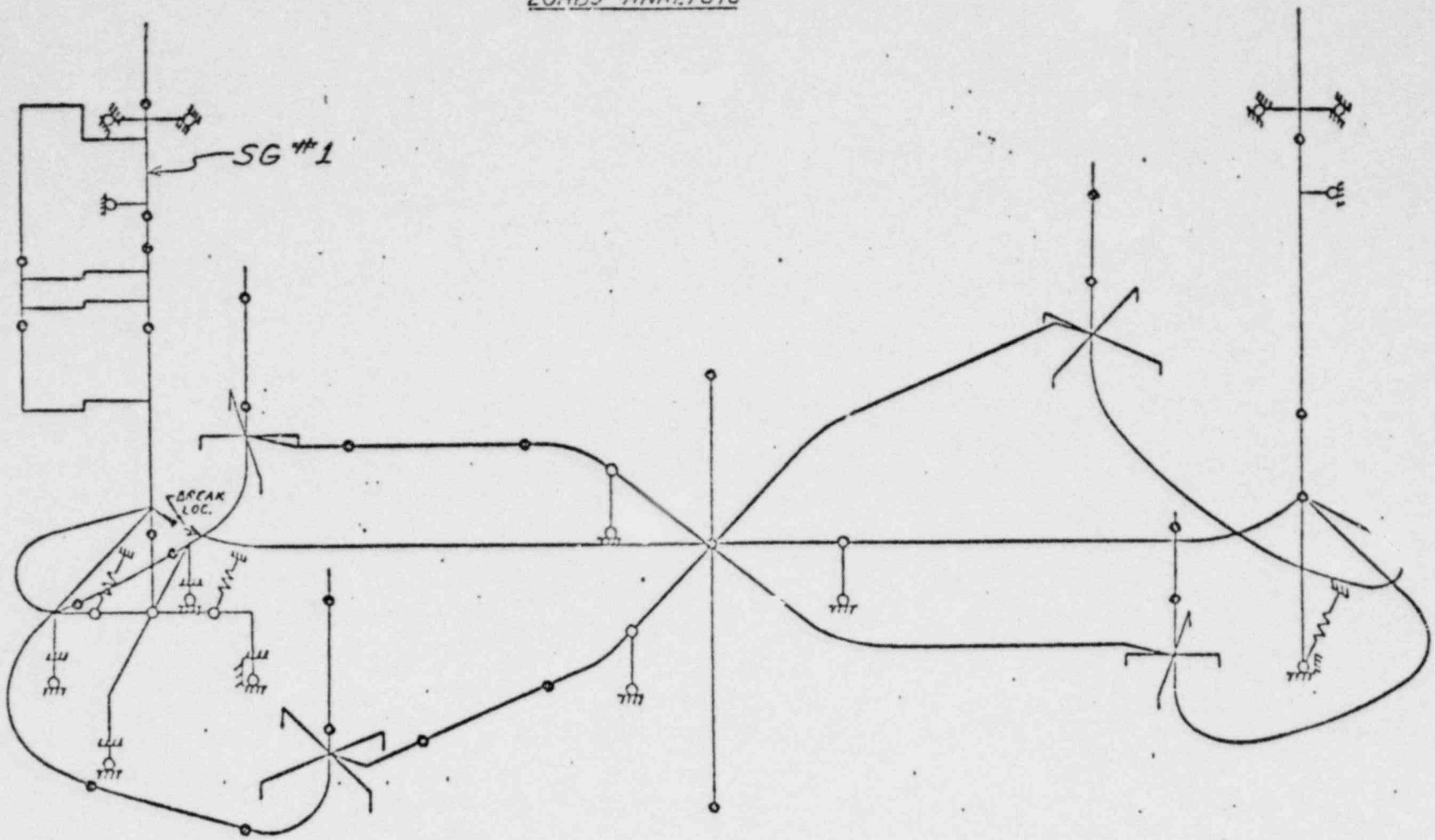

FIGURE 4.5.10

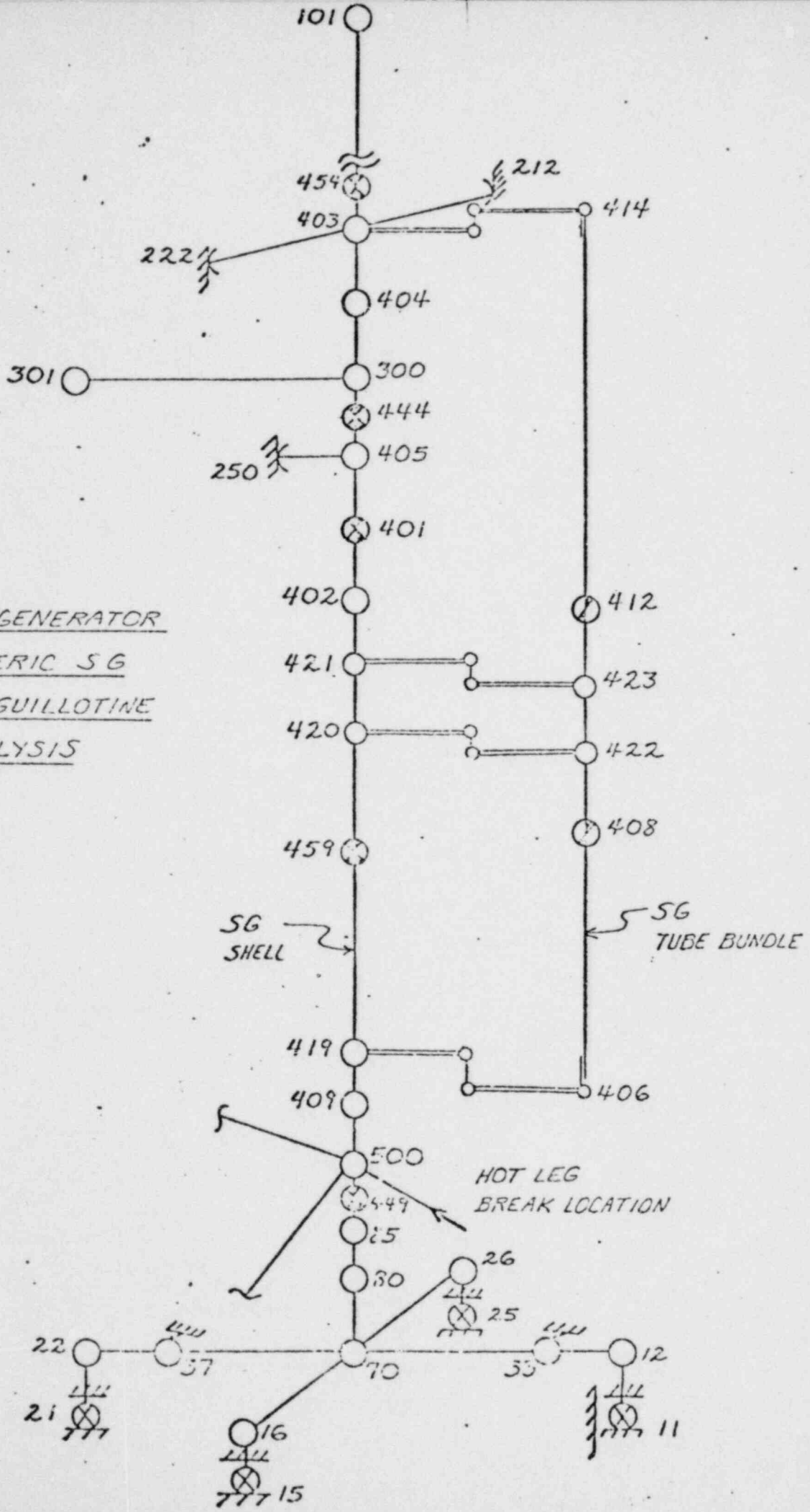

DETAILED STEAM GENERATOR MODEL FOR GENERIC SG INLET NOZZLE GUILLOTINE LOADS ANALYSIS

FIGURE 4.5.11

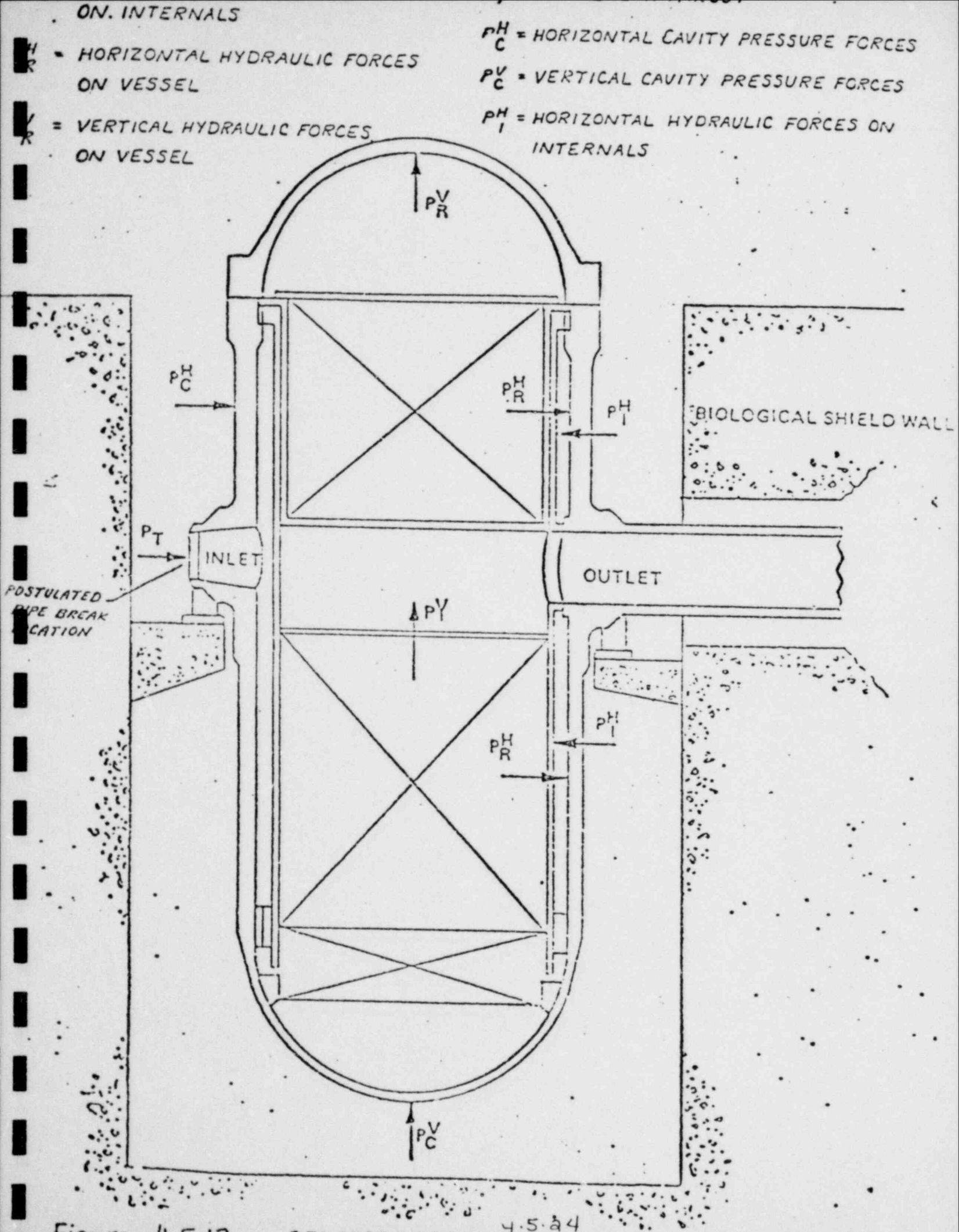

Figure 4.5.12 – REACTOR VESSEL FORCES FOLLOWING LOCA

SUBCOMPARTMENT PRESSURIZATION AND THRUST FORCES STEAM GENERATOR

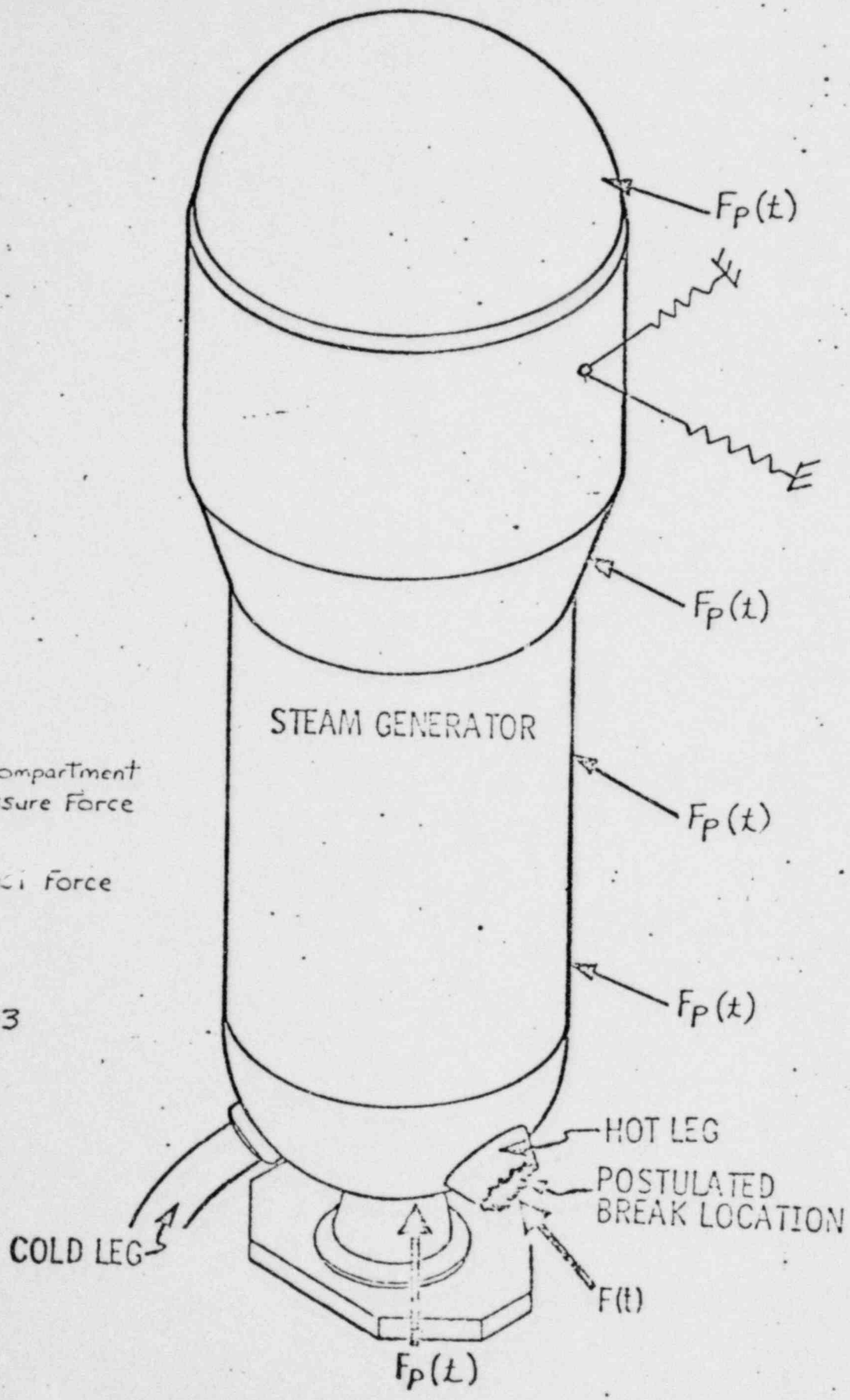

$F_p(t)$ Subcompartment Pressure Force

$F(t)$ Thrust Force

Figure 4.5.13

PALISADES C L R V SUPPT INC 38
TOTAL EFFECTIVE STIFFNESS
TOTAL STOP REACTION FORCE
VERSUS
DISP. IN STOP DIRECTION

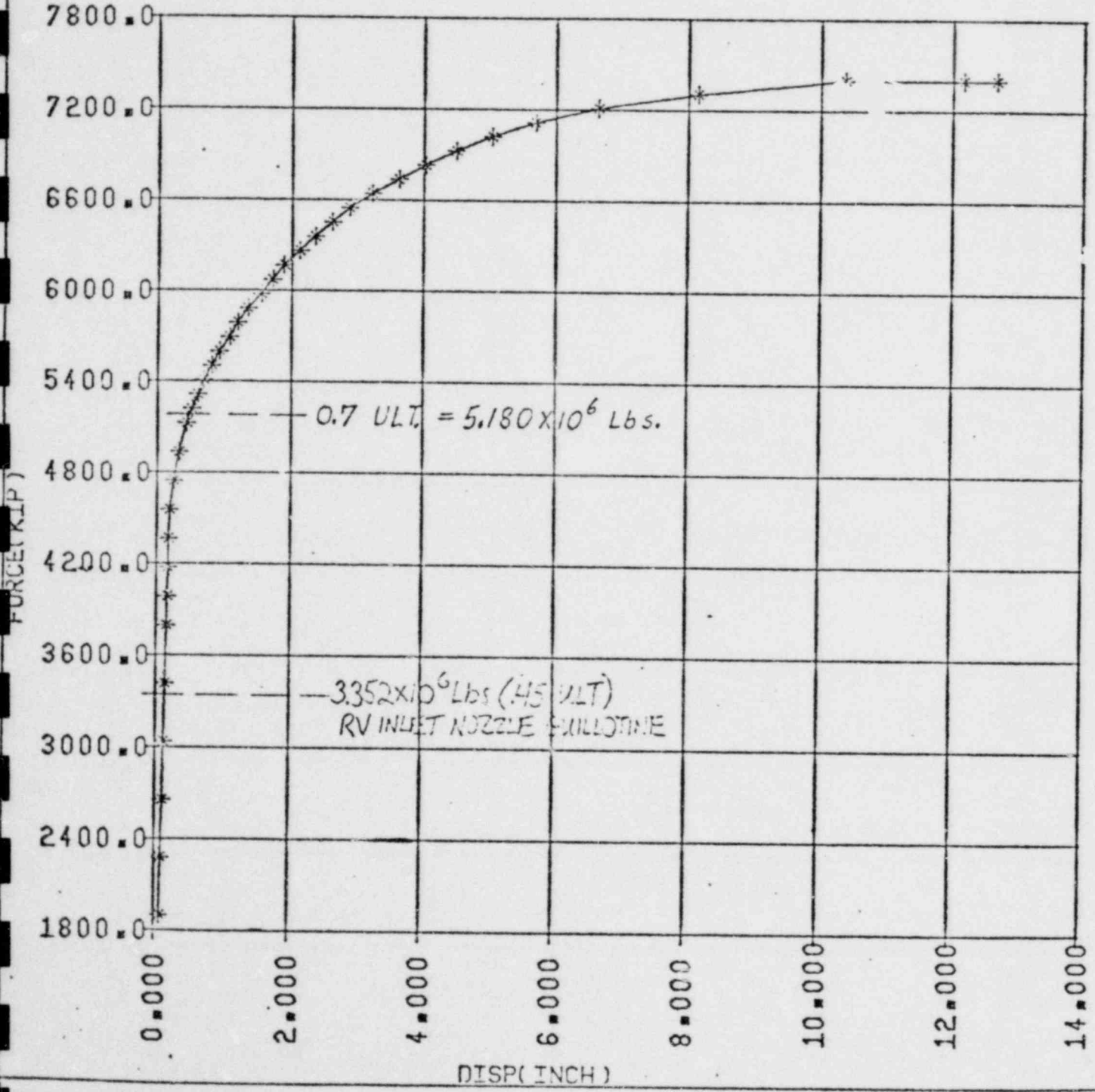

DATA CREATED BY-
PHCW1S6 07/01/79

DATA PLOTTED BY-
NULCCNH 07/17/79

PALISADES H L R V SUPPT
TOTAL EFFECTIVE STIFFNESS
TOTAL STOP REACTION FORCE
VERSUS
DISP. IN STOP DIRECTION

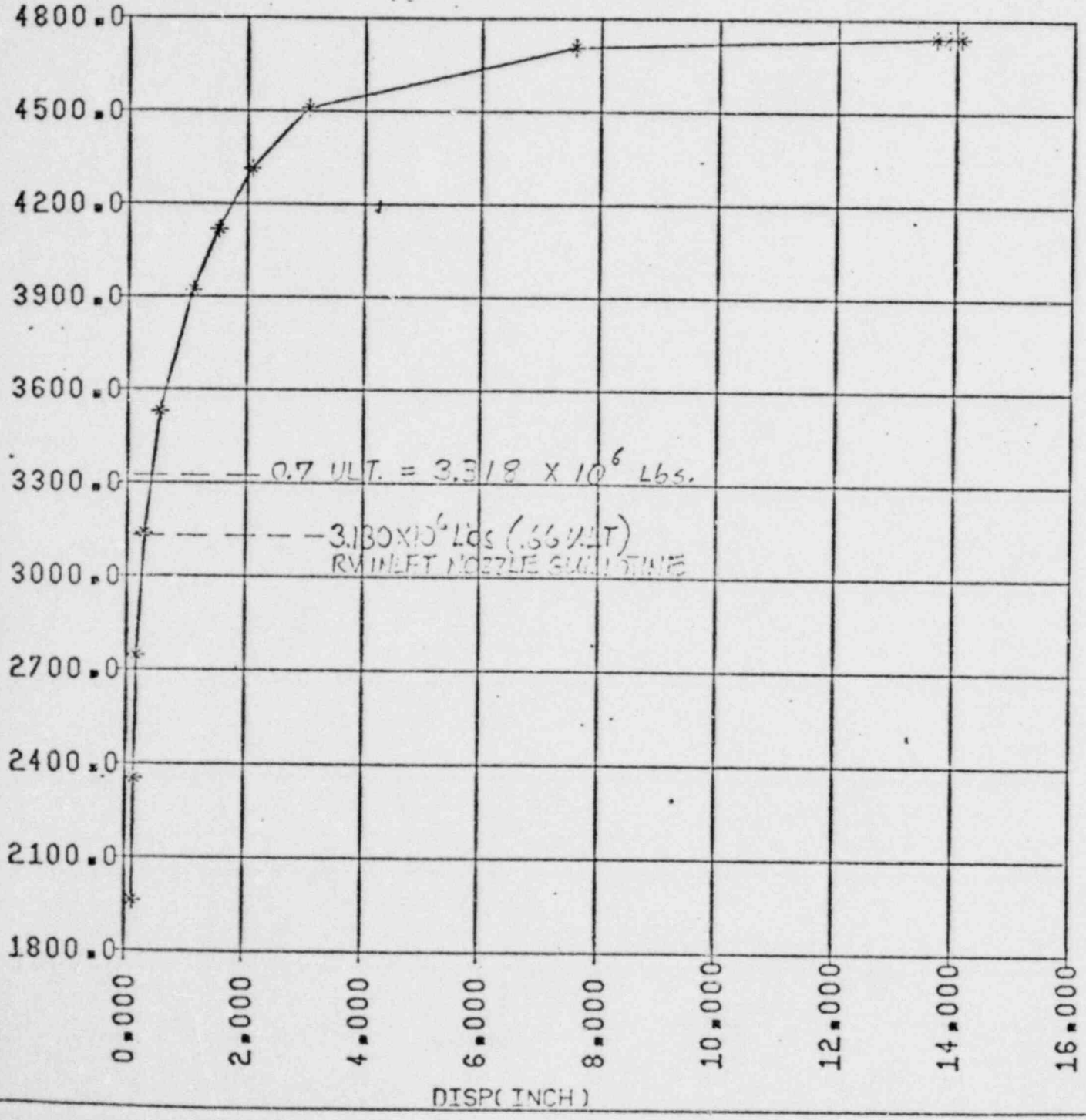

DATA CREATED BY-
PHCW2N3 06/17/79

DATA PLOTTED BY-
NULCCIY 07/20/79

Figure 4.5.16

Fort Calhoun RV Support
Total Effective Stiffness
Total Stop Reaction Force
Versus
Disp. In Tangential Direction

Tangential Load

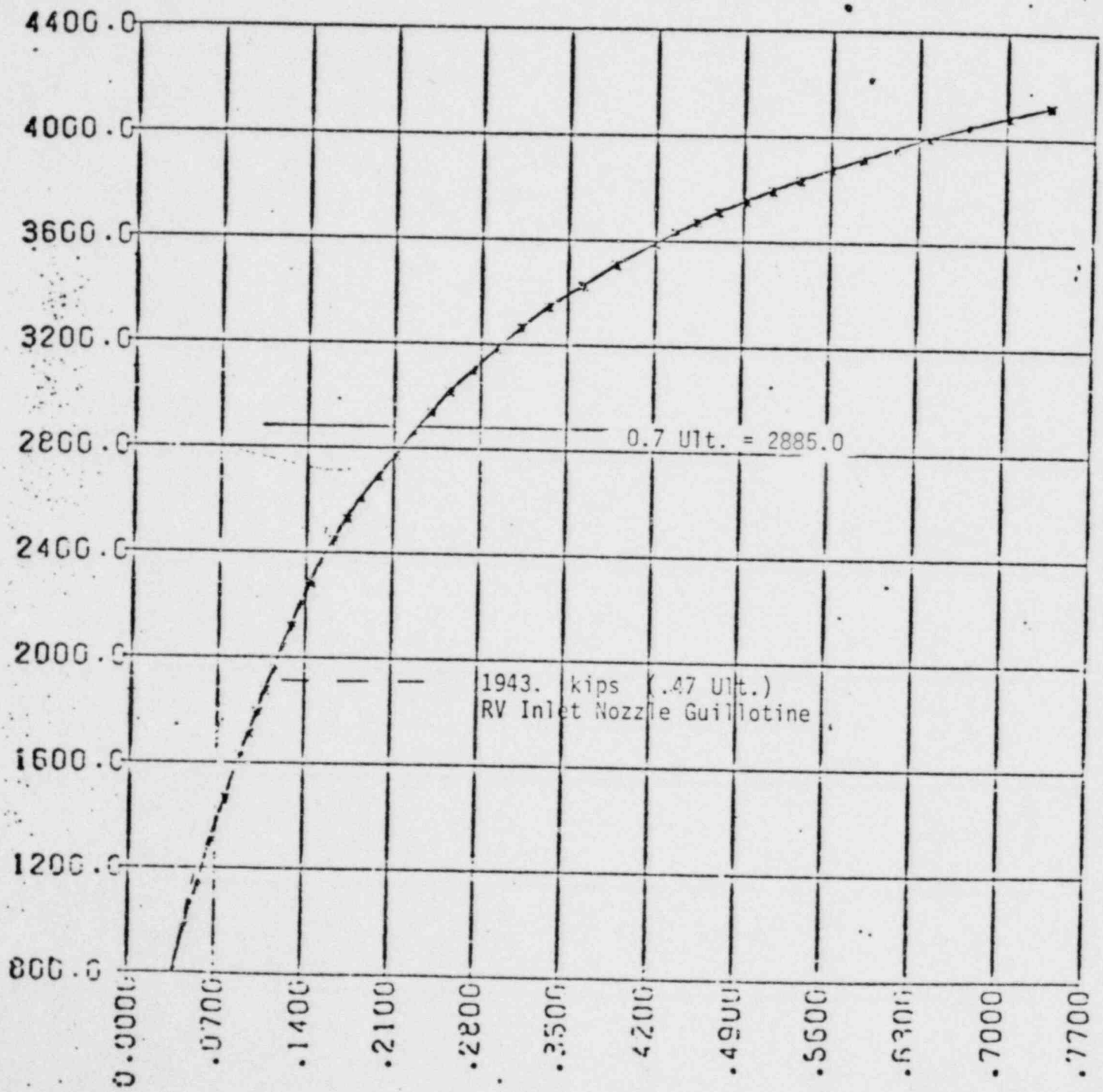

Figure 4.5.17

Fort Calhoun RV Support
Total Effective Stiffness
Total Stop Reaction Force
Versus
Disp. In Radial Direction

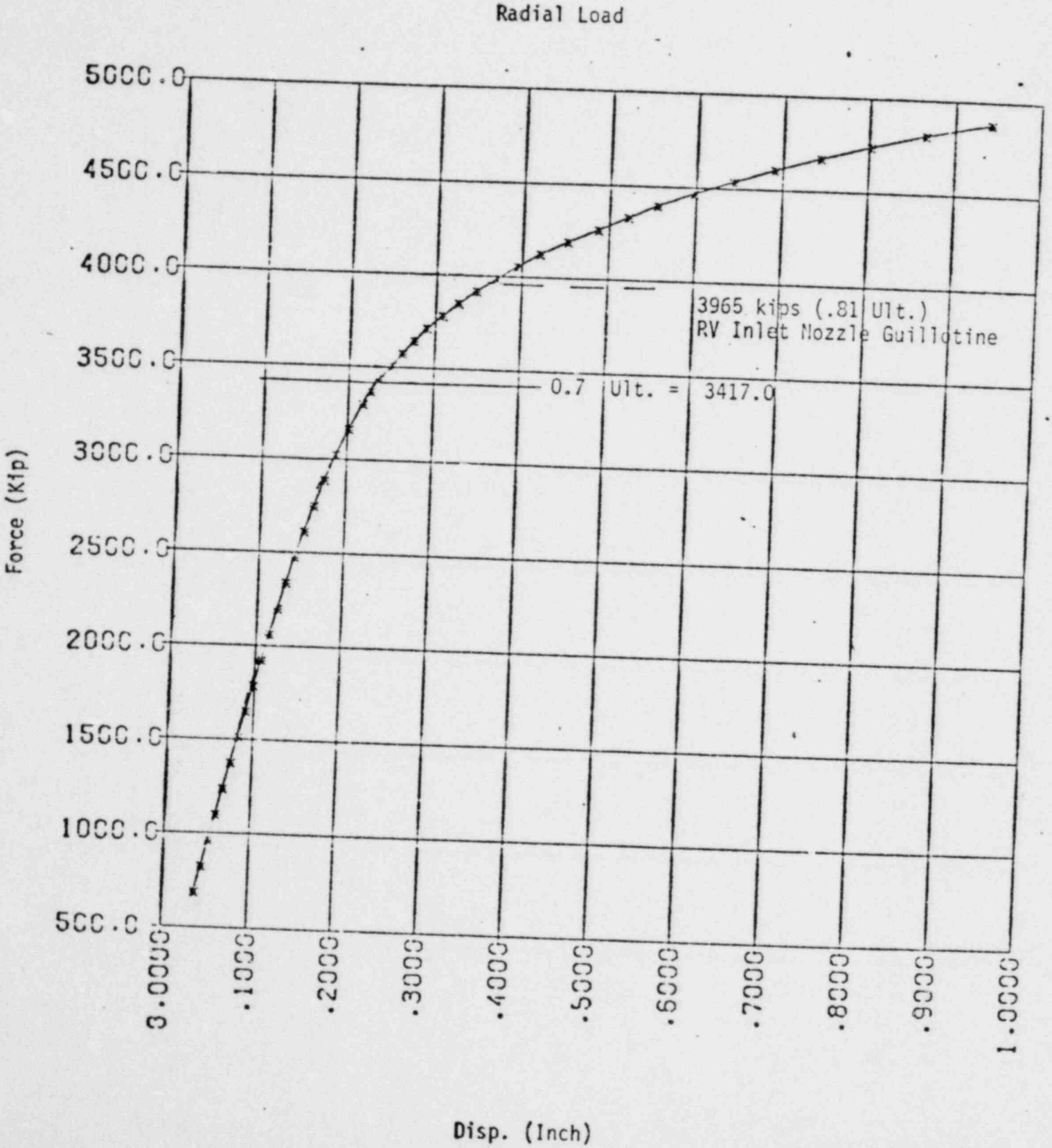

TABLE 4.5-1

GENERIC REACTOR VESSEL SUPPORT LOADS

SUPPORT LOCATION AND DIRECTION		MODEL NODE	LOADS (UNITS - KIPS)			
			RV OUTLET NOZZLE GUILLOTINE	RV INLET NOZZLE GUILLOTINE	LOAD CAPABILITY	BASIS FOR LOAD CAPABILITY
#1A COLD LEG NOZZLE	HORIZONTAL	1900	2998.	2192.	6160.	70% OF ULTIMATE LOAD
	VERTICAL		1557	4164.	6000.	LOAD TO YIELD
#1B COLD LEG NOZZLE	HORIZONTAL	2900	3005.	6452.	6160.	70% OF ULTIMATE LOAD
	VERTICAL		1584.	4642.	6000.	LOAD TO YIELD
HOT LEG NOZZLE	HORIZONTAL	3900	0.	7897.	7700.	70% OF ULTIMATE LOAD
	VERTICAL		3281.	4612.	7500.	LOAD TO YIELD

TABLE 4.5-2

GENERIC REACTOR VESSLE NOZZLE LOADS

COMPONENT	FORCE COMPONENT	LOADS (FORCES - KIPS, MOMENTS - IN.-KIPS)			
		RV OUTLET NOZZLE GUILLOTINE	RV INLET NOZZLE GUILLOTINE	LOAD CAPABILITY MOMENT	BASIS FOR LOAD CAPABILITY
INLET NOZZLE	AXIAL	734.	1140.		ASME CODE SECTION III FAULTED ELASTIC LIMIT FOR PIPE ELBOW
	SHEAR	942.	1405.		
	RSS MOM	27,340.	56,040.	78,965.	
OUTLET NOZZLE	AXIAL	3848.	2925.		ASME CODE SECTION III FAULTED ELASTIC LIMIT FOR PIPE
	SHEAR	355.	1891.		
	RSS MOM	28,670.	144,200.	279,340.	

TABLE 4.5-3

GENERIC REACTOR COOLANT PUMP NOZZLE LOADS

COMPONENT	FORCE COMPONENT	LOADS (FORCES-KIPS, MOMENTS-IN.-KIPS)			
		RV OUTLET NOZZLE GUILLOTINE	RV INLET NOZZLE GUILLOTINE	LOAD CAPABILITY MOMENT	BASIS FOR LOAD CAPABILITY
DISCHARGE NOZZLE	AXIAL	1001.	938.		ASME CODE SECTION III FAULTED ELASTIC LIMIT FOR PIPE
	SHEAR	273.	1009.		
	RSS MOM	43,730.	98,790.	96,810.	
SUCTION NOZZLE	AXIAL	203.	826.		ASME CODE SECTION III FAULTED ELASTIC LIMIT FOR PIPE ELBOW
	SHEAR	358.	801.		
	RSS MOM	23,370.	47,300.	78,965.	

TABLE 4.5-4
GENERIC STEAM GENERATOR SUPPORT LOADS

COMPONENT	MODE NODE	LOADS (UNITS - KIPS)			
		SG 1A OUTL. GUIL.	SG #1 INL. GUIL.	LOAD CAPABILITY	BASIS FOR LOAD CAPABILITY
PADS	11 15 21 25	0. 0. 198. 118.	0. 0. 197. 0.	9850. TOTAL	111% OF DESIGN LOAD
BOLTS (TOTAL PER PAD)	11 15 21 25	786. 534. 865. 438.	1893. 695. 1055. 685.	3713. 1856. 1856. 1856.	LOAD TO YIELD
LOWER STOP	11	0.	4531.	6810.	111% OF DESIGN LOAD
LOWER KEYS	33 37	792. 790.	518. 499.	5610. TOTAL	111% OF DESIGN LOAD
SNUBBERS (TOTAL)	250	613.	1909.	3500.	TEST DATA
UPPER KEYS	212 222	395. 479.	406. 421.	1910. 1910.	111% OF DESIGN LOAD

TABLE 4.5-5

GENERIC STEAM GENERATOR NOZZLE LOADS

COMPONENT	MODE NODE	FORCE COMP.	LOADS (FORCES - KIPS, MOMENTS - IN-KIPS) RUPTURE CASE SG 1A OUTL. NOZ. GUIL.	SG #1 INL. NOZ. GUIL.	LOAD CAPABILITY MOMENT	BASIS FOR LOAD CAPABILITY
INLET NOZZLE	551	AXIAL SHEAR RSS MOM.	1137. 1035. 32120.	RUPTURED NOZZLE	196,715.	ASME CODE SECTION III FAULTED ELASTIC LIMIT FOR PIPE ELBOW
1A OUTLET NOZZLE	1551	AXIAL SHEAR RSS MOM.	RUPTURED NOZZLE	344. 945. 44440.	78,965.	ASME CODE SECTION III FAULTED ELASTIC LIMIT FOR PIPE ELBOW
1B OUTLET NOZZLE	2551	AXIAL SHEAR RSS MOM.	82. 229. 13920.	355. 1003. 47590.	78,965.	ASME CODE SECTION III FAULTED ELASTIC LIMIT FOR PIPE ELBOW

TABLE 4.5-6

GENERIC R.C.P. NOZZLE LOADS

COMPONENT	MODE NODE	FORCE COMP.	LOADS (FORCES - KIPS, MOMENTS - IN-KIPS) RUPTURE CASE SG 1A OUTL. NOZ. GUIL.	SG #1 INLET NOZ. GUIL.	LOAD CAPABILITY MOMENT	BASIS FOR LOAD CAPABILITY
1A SUCTION NOZZLE	1650	AXIAL SHEAR RSS MOM.	RUPTURED LEG	268. 717. 45050"	78,965.	ASME CODE SECTION III FAULTED ELASTIC LIMIT FOR PIPE ELBOW
1A DISCHARGE NOZZLE	1750	AXIAL SHEAR RSS MOM.	RUPTURED LEG	705. 342. 35820.	96,810.	ASME CODE SECTION III FAULTED ELASTIC LIMIT FOR PIPE
1B SUCTION NOZZLE	2650	AXIAL SHEAR RSS MOM.	100. 186. 14010.	314" 783. 48860.	78,965	ASME CODE SECTION III FAULTED ELASTIC LIMIT FOR PIPE ELBOW
1B DISCHARGE NOZZLE	2750	AXIAL SHEAR RSS MOM.	276" 178. 16710.	858. 396. 45310"	96,810"	ASME CODE SECTION III FAULTED ELASTIC LIMIT FOR

TABLE 4.5-7

PALISADES REACTOR VESSEL SUPPORT LOADS

SUPPORT LOCATION AND DIRECTION		MODEL NODE	LOADS (UNITS - KIPS)		
			RV INLET NOZZLE GUILLOTINE	LOAD CAPABILITY	BASIS FOR LOAD CAPABILITY
#1A COLD LEG NOZZLE	HORIZONTAL	1900	1113.	5180.	70% OF ULTIMATE LOAD
	VERTICAL		4162.	6840.	LOAD TO YIELD
#1B COLD LEG NOZZLE	HORIZONTAL	2900	1675.	5180.	70% OF ULTIMATE LOAD
	VERTICAL		3925.	6840.	LOAD TO YIELD
HOT LEG NOZZLE	HORIZONTAL	3900	2941.	3318.	70% OF ULTIMATE LOAD
	VERTICAL		4835.	11,890.	LOAD TO YIELD

TABLE 4.5-8

PALISADES REACTOR VESSEL NOZZLE LOADS

COMPONENT	FORCE COMPONENT	LOADS (FORCES - KIPS, MOMENTS - IN-KIPS)		
		RV INLET NOZZLE GUILLOTINE	LOAD CAPABILITY MOMENT	BASIS FOR LOAD CAPABILITY
INLET NOZZLE	AXIAL	964.		ASME CODE SECTION III FAULTED ELASTIC LIMIT FOR PIPE ELBOW
	SHEAR	1580.		
	RSS MOM	43,251.	72,496.	
OUTLET NOZZLE	AXIAL	660.		ASME CODE SECTION III FAULTED ELASTIC LIMIT FOR PIPE
	SHEAR	1706.		
	RSS MOM	194,440.	270,697.	

TABLE 4.5-9

PALISADES REACTOR COOLANT PUMP NOZZLE LOADS

COMPONENT	FORCE COMPONENT	LOADS (FORCES-KIPS, MOMENTS-IN-KIPS)		
		RV INLET NOZZLE GUILLOTINE	LOAD CAPABILITY MOMENT	BASIS FOR LOAD CAPABILITY
DISCHARGE NOZZLE	AXIAL	1319.		ASME CODE SECTION III FAULTED ELASTIC LIMIT FOR PIPE
	SHEAR	1297.		
	RSS MOM	62,654.	102,545.	
SUCTION NOZZLE	AXIAL	40.		ASME CODE SECTION III FAULTED ELASTIC LIMIT FOR PIPE ELBOW
	SHEAR	294.		
	RSS MOM	15,119.	72,469.	

TABLE 4.5-10

PALISADES REACTOR COOLANT PUMP SUPPORT LOADS

SUPPORT LOCATION AND FORCE COMPONENT		MODEL NODE	LOADS (FORCES - KIPS, MOMENTS - IN-KIPS)		
			RUPTURE CASE - RV 1A INLET NOZZLE GUILL.	LOAD CAPABILITY FORCES	BASIS FOR LOAD CAPABILITY
PUMP LUG #1	AXIAL	5113	193.	1686.	DESIGN LOAD
	SHEAR		1202.	2800.	DESIGN LOAD
PUMP LUG #2	AXIAL	5117	152.	1686.	DESIGN LOAD
	SHEAR		1476.	2800.	DESIGN LOAD
PUMP LUG #3	AXIAL	5115	136.	1686.	DESIGN LOAD
	SHEAR		1413.	2616.	LOAD TO YIELD
PUMP LUG #4	AXIAL	5111	106.	1686.	DESIGN LOAD
	SHEAR		862.	2800.	DESIGN LOAD

Fort Calhoun

Load Capability Table

COMPONENT SUPPORT	LOAD CAPABILITY	BASE FOR LOAD CAPABILITY
Reactor Vessel:		
Support Feet		
Vertical Load	705 Kips	Yield Load
Radial Load	3080 Kips	.7 Ultimate Load
Tangential Load	2885 Kips	.7 Ultimate Load
Steam Generator:		
Support Lugs	1211 Kips/Lug	.7 Ultimate Load
Lower Accident Support Ring		
Toward S	2560 Kips	Yield Load
Toward N	452 Kips	Yield Load
E-W Direction	852 Kips	Yield Load
Trunnions		
N-S Direction	318.2 Kips/Trunnion	Yield Load
E-W Direction	891.6 Kips/Trunnion	.7 Ultimate Load
Vert. Direction	-312.4 Kips/Trunnion	Yield Load
Snubbers	1472.6 Kips (Total)	Test Load
Inlet Nozzle	85312 In-Kips	ASME Code, Level D Limit
Outlet Nozzle	35991 In-Kips	ASME Code, Level D Limit
Reactor Coolant Pump:		
Vert. Support Lugs		
Downward Load	204.4 Kips/Lug	.7 Ultimate Load
Upward Load	-60 Kips/Lug	.7 Ultimate Load
Snubbers		
N-S Direction	168 Kips/Pump	Test Load
E-W Direction	210 Kips/Pump	Test Load
Suction Nozzle	35991 In-Kips	ASME Code, Level D Limit
Discharge Nozzle	54471 In-Kips	ASME Code, Level D Limit

TABLE 4.5-11

TABLE 4.5-12
PALISADES STEAM GENERATOR SUPPORT LOADS

COMPONENT	GENERIC MODEL NODE	LOADS (UNITS - KIPS)			
		SG 1A OUTL. GUIL.	SG #1 INL. GUIL.	LOAD CAPABILITY	BASIS FOR LOAD CAPABILITY
PADS	11 15 21 25	0. 0. 198. 118.	0. 0. 197. 0.	3585. TOTAL	111% OF DESIGN LOAD
BOLTS (TOTAL PER PAD)	11 15 21 25	786. 534. 865. 438.	1393. 695. 1055. 685.	3713. 1856. 1856. 1856.	LOAD TO YIELD
LOWER STOP	11	0.	4531.	4913.	111% OF DESIGN LOAD
LOWER KEYS	33 37	792. 790.	518. 499.	7089. TOTAL	111% OF DESIGN LOAD
SNUBBERS (TOTAL)	250	613.	1909.	3150.	TEST DATA
UPPER KEYS	212 222	395. 479.	406. 421.	570. 570.	111% OF DESIGN LOAD

4.5-41

TABLE 4.5-13

PALISADES STEAM GENERATOR NOZZLE LOADS

COMPONENT	GENERIC MODE NODE	FORCE COMP.	LOADS (FORCES - KIPS, MOMENTS - IN-KIPS) RUPTURE CASE SG 1A OUTL. NOZ. GUIL.	RUPTURE CASE SG #1 INL. NOZ. GUIL.	LOAD CAPABILITY MOMENT	BASIS FOR LOAD CAPABILITY
INLET NOZZLE	551	AXIAL SHEAR RSS MOM.	1137. 1035. 32120.	RUPTURED NOZZLE	188,163.	ASME CODE SECTION III FAULTED ELASTIC LIMIT FOR PIPE ELBOW
1A OUTLET NOZZLE	1551	AXIAL SHEAR RSS MOM.	RUPTURED NOZZLE	344. 945. 44440.	72,469.	ASME CODE SECTION III FAULTED ELASTIC LIMIT FOR PIPE-ELBOW
1B OUTLET NOZZLE	2551	AXIAL SHEAR RSS MOM.	82. 229. 13920.	355. 1003. 47590.	72,469.	ASME CODE SECTION III FAULTED ELASTIC LIMIT FOR PIPE ELBOW.

PALISADES R.C.P. NOZZLE LOADS

COMPONENT	GENERIC MODE NODE	FORCE COMP.	LOADS (FORCES - KIPS, MOMENTS - IN-KIPS) RUPTURE CASE SG 1A OUTL. NOZZLE GUIL.	SG #1 INLET NOZ. GUIL.	LOAD CAPABILITY MOMENT	BASIS FOR LOAD CAPABILITY
1A SUCTION NOZZLE	1650	AXIAL	RUPTURED LEG	268.		ASME CODE SECTION III FAULTED ELASTIC LIMIT FOR PIPE ELBOW
		SHEAR		717.		
		RSS MOM.		45050.	72,469.	
1A DISCHARGE NOZZLE	1750	AXIAL	RUPTURED LEG	705.		ASME CODE SECTION III FAULTED ELASTIC LIMIT FOR PIPE
		SHEAR		342.		
		RSS MOM.		35820.	102,545.	
1B SUCTION NOZZLE	2650	AXIAL	100.	314.		ASME CODE SECTION III FAULTED ELASTIC LIMIT FOR PIPE ELBOW
		SHEAR	186.	783.		
		RSS MOM.	14010.	48860.	72,469.	
1B DISCHARGE NOZZLE	2750	AXIAL	276.	858.		ASME CODE SECTION III FAULTED ELASTIC LIMIT FOR PIPE
		SHEAR	178.	396.		
		RSS MOM.	16710.	45310.	102,545.	

4.5.43

FT. CALHOUN RV ASYMMETRIC LOADS ANALYSIS

RV SUPPORT LOADS

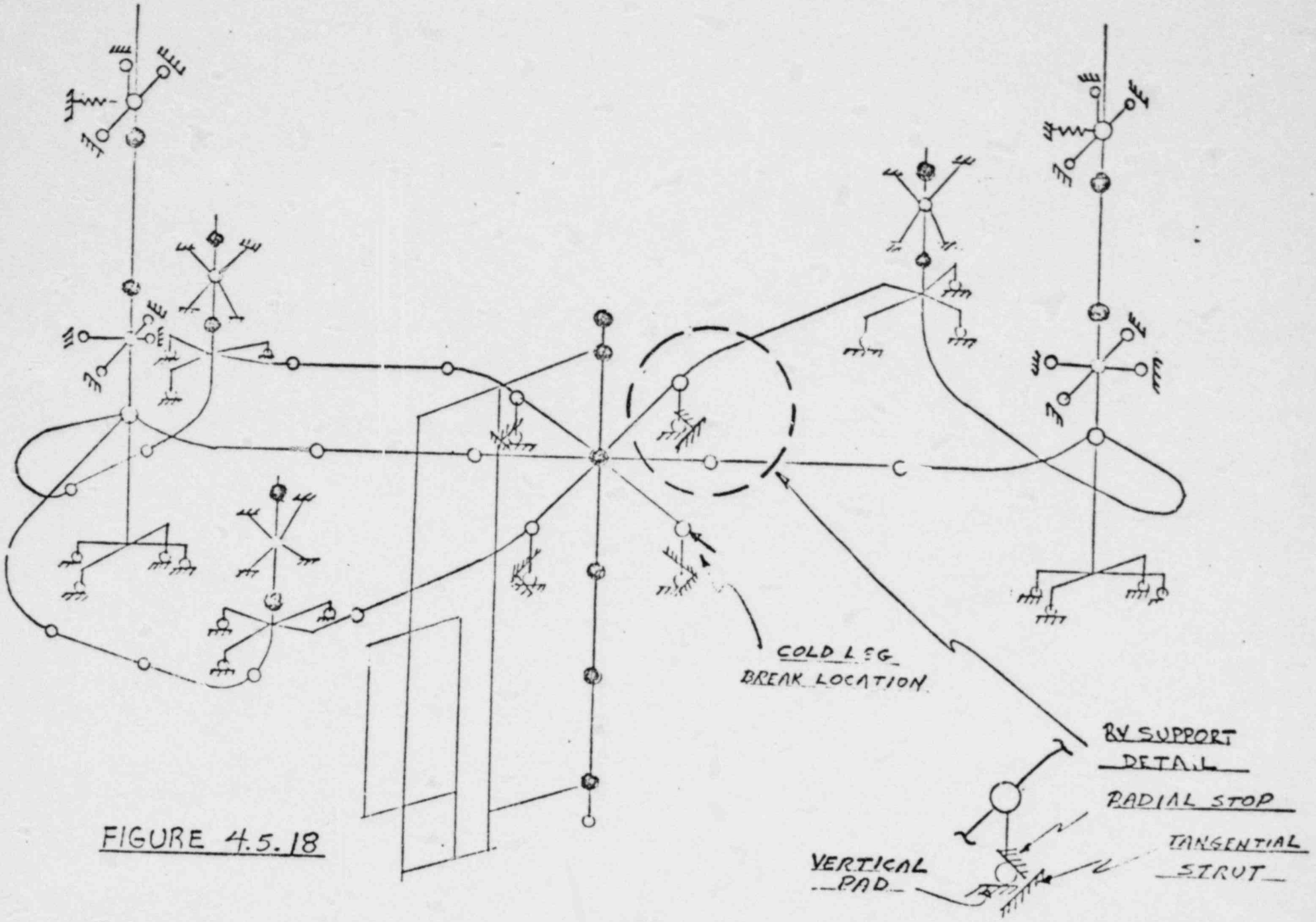

FIGURE 4.5.18

4.5.44

Table 4.5-11

Fort Calhoun Reactor Vessel Support Loads

Support Location and Direction		Model Node	Loads (Forces-Kips, Moments-In-Kips)		
			RV Inlet Nozzle Guillotine	Load Capability Forces	Basis For Load Capability
#1A Cold Leg Nozzle	Radial	1999	803.	3417.	70% of Ultimate Load
	Tangential		1943.	2885.	70% of Ultimate Load
	Vertical		1164.	6850.	Load to Yield
#1B Cold Leg Nozzle	Radial	2999	3965.	3417.	70% of Ultimate Load
	Tangential		1341.	2885.	70% of Ultimate Load
	Vertical		2260.	6850.	Load to Yield
#2B Cold Leg Nozzle	Radial	4999	0.	3417.	70% of Ultimate Load
	Tangential		684.	2885.	70% of Ultimate Load
	Vertical		772.	6850.	Load to Yield
#2A Cold Leg Nozzle	Radial	5999	3001.	3417.	70% of Ultimate Load
	Tangential		0.	2885.	70% of Ultimate Load
	Vertical		1054.	6850.	Load to Yield

Table 4.15-12

Fort Calhoun Reactor Coolant Pump Support Loads
Vertical Columns

Support Location and Force Component	Model Node	Loads (Forces-Kips, Moments-In-Kips)		
		Rupture Case - RV 2B Inlet Nozzle Guillotine*	Load Capability Forces	Basis For Load Capability
Pump 1A				Note:
Lug #1 Compressive/tensile	55	82./5.	177./60.	1/2
Lug #2 Compressive/tensile	56	67./16.	177./60.	1/2
Lug #3 Compressive/tensile	57	84./60.	177./60.	1/2
Pump 1B				
Lug #1 Compressive/tensile	45	124./60.	177./60.	1/2
Lug #2 Compressive/tensile	44	125./60.	240./60.	1/2
Lug #3 Compressive/tensile	46	124./60.	177./60.	1/2
Pump 2A				
Lug #1 Compressive/tensile	7055	116./60.	177./60.	1/2
Lug #2 Compressive/tensile	7056	124./60.	177./60.	1/2
Lug #3 Compressive/tensile	7057	124./13.	177./60.	1/2

*Credit taken for only 70% of ultimate load for conservative determination of nozzle loads, tables 4.5-14,15 .

1 Support Ultimate Load
2 Pump Lug Design Load

4.5-46

Fort Calhoun Reactor Coolant Pump Support Loads
Horizontal Supports

Support Location and Force Component	Model Node	Loads (Forces-Kips, Moments-In-Kips)		
		Rupture Case - RV 2B Inlet Nozzle Guillotine*	Load Capability Forces	Basis For Load Capability
Pump 1A				Note:
Support 1 Compressive/tensile	150	23./43.	129./85.	1/1
Support 2 Compressive/tensile		38./8.	55./33.	1/2
Support 3 Compressive/tensile		75./43.	129./85.	1/1
Support 4 Compressive/tensile		38./28.	55./33.	1/2
Pump 1B				
Support 1 Compressive/tensile	160	90./43.	129./85.	1/1
Support 2 Compressive/tensile		38./33.	55./33.	1/2
Support 3 Compressive/tensile		59./37.	129./60.	1/1
Support 4 Compressive/tensile		38./22.	55./33.	1/2
Pump 2A				
Support 1 Compressive/tensile	7150	90./37.	129./60.	1/1
Support 2 Compressive/tensile		38./33.	55./33.	1/2
Support 3 Compressive/tensile		79./43.	129./85.	1/1
Support 4 Compressive/tensile		38./29.	55./33.	1/2

*Credit taken for only 70% of ultimate load for conservative determination of nozzle loads, tables 4.5-14,15

1 Ultimate Load
2 Snubber Design Load

Table 4.5-14

Fort Calhoun Reactor Vessel Nozzle Loads

Component	Force Component	Loads (Force-kips, Moments-in.-kips)		
		RV Inlet Nozzle Guillotine	Load Capability Moment	Basis for Load Capability
Inlet Nozzle	Axial Shear RSS Moment	274. 283. 19,400.	54471.	ASME Code Section III Faulted Elastic Limit For Pipe
Outlet Nozzle	Axial Shear RSS Moment	475. 539. 69,220.	117,874.	ASME Code Section III Faulted Elastic Limit For Nozzle Safe End

Table 4.5-15

Fort Calhoun Reactor Coolant Pump Nozzle Loads

Component	Force Component	Loads (Forces-kips, Moments-in.-kips)		
		RV Inlet Nozzle Guillotine	Load Capability Moment	Basis for Load Capability
Discharge Nozzle	Axial Shear RSS Moment	245. 187. 20165.	54471.	ASME Code Section III Faulted Elastic Limit For Pipe
Suction Nozzle	Axial Shear RSS Moment	31. 79. 8285.	35991.	ASME Code Section III Faulted Elastic Limit For Pipe Elbow

TABLE 4.5-16
PALISADES STEAM GENERATOR SUPPORT LOADS

COMPONENT	GENERIC MODEL NODE	LOADS (UNITS - KIPS)			
		SG 1A OUTL. GUIL.	SG #1 INL. GUIL.	LOAD CAPABILITY	BASIS FOR LOAD CAPABILITY
PADS	11 15 21 25	0. 0. 198. 118.	0. 0. 197. 0.	3585. TOTAL	111% OF DESIGN LOAD
BOLTS (TOTAL PER PAD)	11 15 21 25	786. 534. 865. 438.	1893. 695. 1055. 685.	3713. 1856. 1856. 1856.	LOAD TO YIELD
LOWER STOP	11	0.	4531.	4913.	111% OF DESIGN LOAD
LOWER KEYS	33 37	792. 790.	518. 499.	7039. TOTAL	111% OF DESIGN LOAD
SHUBBERS (TOTAL)	250	613.	1909.	3150.	TEST DATA
UPPER KEYS	212 222	395. 479.	406. 421.	570. 570.	111% OF DESIGN LOAD

4.5-50

TABLE 4.5-17

PALISADES STEAM GENERATOR NOZZLE LOADS

COMPONENT	GENERIC MODEL NODE	FORCE COMP.	LOADS (FORCES - KIPS, MOMENTS - IN-KIPS) RUPTURE CASE		LOAD CAPABILITY MOMENT	BASIS FOR LOAD CAPABILITY
			SG 1A OUTL. NOZ. GUIL.	SG #1 INL. NOZ. GUIL.		
INLET NOZZLE	551	AXIAL SHEAR RSS MOM.	1137. 1035. 32120.	RUPTURED NOZZLE	188,163.	ASME CODE SECTION III FAULTED ELASTIC LIMIT FOR PIPE ELBOW
1A OUTLET NOZZLE	1551	AXIAL SHEAR RSS MOM.	RUPTURED NOZZLE	344. 945. 44440.	72,469.	ASME CODE SECTION III FAULTED ELASTIC LIMIT FOR PIPE-ELBOW
1B OUTLET NOZZLE	2551	AXIAL SHEAR RSS MOM.	82. 229. 13920.	355. 1003. 47590.	72,469.	ASME CODE SECTION III FAULTED ELASTIC LIMIT FOR PIPE ELBOW .

4.5-51

TABLE 4.5-18

PALISADES R.C.P. NOZZLE LOADS

COMPONENT	GENERIC MODEL NODE	FORCE COMP.	LOADS (FORCES - KIPS, MOMENTS - IN-KIPS) RUPTURE CASE SG 1A OUTL. NOZZLE GUIL.	SG #1 INLET NOZ. GUIL.	LOAD CAPABILITY MOMENT	BASIS FOR LOAD CAPABILITY
1A SUCTION NOZZLE	1650	AXIAL SHEAR RSS MOM.	RUPTURED LEG	268. 717. 45050.	72,469.	ASME CODE SECTION III FAULTED ELASTIC LIMIT FOR PIPE ELBOW
1A DISCHARGE NOZZLE	1750	AXIAL SHEAR RSS MOM.	RUPTURED LEG	705. 342. 35820.	102,545.	ASME CODE SECTION III FAULTED ELASTIC LIMIT FOR PIPE
1B SUCTION NOZZLE	2650	AXIAL SHEAR RSS MOM.	100. 186. 14010.	314. 783. 48860.	72,469.	ASME CODE SECTION III FAULTED ELASTIC LIMIT FOR PIPE ELBOW
1B DISCHARGE NOZZLE	2750	AXIAL SHEAR RSS MOM.	276. 178. 16710.	858. 396. 45310.	102,545.	ASME CODE SECTION III FAULTED ELASTIC LIMIT FOR PIPE

4.5-52

Table 4.5-19

Fort Calhoun Steam Generator Support Loads

Component	Loads (Units - Kips)			
	SG 1B Out. Guil.	SG #1 Inlet Guil.	Load Capability	Basis For Load Capability
Accident Ring // Hot Leg	0.	-3752.	-6120.	Yield Limit
Accident Ring ⊥ to Hot Leg	+852. -0.	+67.73 -0.	±852.	Yield Limit
Snubbers	+128.5 -7.615	+173.9 -0.	±638.5	Yield Limit
Trunnion Key // to Hot Leg	0.	0.	±318.	Yield Limit
Trunnion Key ⊥ to Hot Leg	+136.9 -0.	+0. -30.13	±347.5	Yield Limit
Trunnion Vertical	+312.4	+426.7	+559.2	Ultimate
Lug	-8.05	0.	-991.	.7 Ultimate

Table 4.5-20

Fort Calhoun Steam Generator Nozzle Loads

Component	Force Comp.	Loads (Forces - Kips, Moments - In-Kips)			
		Rupture Case		Load Capability Moment	Basis for Load Capability
		SG 1b Outlet Nozzle Guillotine	SG #1 Inlet Nozzle Guillotine		
Inlet Nozzle	Axial Shear RSS Mom.	657. 276. 10640.	Ruptured Nozzle	83,312.	ASME Code Section III Faulted Elastic Limit For Pipe Elbow
1A Outlet Nozzle	Axial Shear RSS Mom.	84. 203. 9491.	218. 402. 19420.	35,991.	ASME Code Section III Faulted Elastic Limit For Pipe Elbow
1B Outlet Nozzle	Axial Shear RSS Mom.	Ruptured Nozzle	218. 392. 20,510.	35,991.	ASME Code Section III Faulted Elastic Limit For Pipe Elbow

4.5.54

Table 4.5-21

Fort Calhoun RCP Nozzle Loads

Component	Force Comp.	Loads (Forces - Kips, Moments - In-Kips)			
		Rupture Case		Load Capability Moment	Basis for Load Capability
		SG 1b Outlet Nozzle Guillotine	SG #1 Inlet Nozzle Guillotine		
1A Suction Nozzle	Axial Shear RSS Mom.	106. 116. 10,910.	160. 266. 18,930.	35,991.	ASME Code Section III Faulted Elastic Limit For Pipe Elbow
1A Discharge Nozzle	Axial Shear RSS Mom.	101. 45. 7,345.	273. 82. 12,120.	54,471.	ASME Code Section III Faulted Elastic Limit For Pipe
1B Suction Nozzle	Axial Shear RSS Mom.	Ruptured Leg	166. 293. 21,490.	35,991.	ASME Code Section III Faulted Elastic Limit For Pipe Elbow
1B Discharge Nozzle	Axial Shear RSS Mom.	Ruptured Leg	285. 106. 9,738.	54,471.	ASME Code Section III Faulted Elastic Limit For Pipe

4.5.56

4.6 REACTOR VESSEL INTERNALS

4.6.1 MECHANICAL SYSTEMS AND COMPONENTS DESCRIPTION

4.6.1.1 Reactor Internals General Description

The components of the reactor internals are divided into three major parts consisting of the core support barrel, the lower core support structure (including the core shroud), and the upper guide structure (including the Control Element Assembly (CEA) shrouds and the in-core instrumentation (ICI) guide tubes). The flow skirt, although functioning as an integral part of the coolant flow path, is separate from the internals and is affixed to the bottom head of the pressure vessel. For a comparison of the Generic, Palisades, and Fort Calhoun internals design parameters, see Table 4.6.1

4.6.1.2 Reactor Internals Generic Plant

4.6.1.3 Core Support Assembly

The major support member of the reactor internals is the core support assembly. The assembled structure consists of the core support barrel, the lower support structure, and the core shroud. The major material for the assembly is Type 304 stainless steel. The reactor internals for the generic plant are shown in Figures 4.6.1 and 4.6.2.

4.6.1.3.1 Core Support Barrel

The core support barrel is a right circular cylinder with a nominal inside diameter of 148 inches and a length of 27 feet, with a heavy ring flange at the top end and an internal ring flange at the lower end. The core barrel is supported from a ledge on the reactor vessel. The core support barrel, in turn, supports the lower support structure upon which the fuel assemblies rest. The CSB (for Millstone and St. Lucie I) also has a thermal shield affixed to its outer surface and located at its mid section. Press fitted into the flange of the core support barrel are four alignment keys located 90 degrees apart. The reactor vessel, closure head, holddown ring and upper guide structure assembly flange are slotted in locations corresponding to the alignment key locations to provide alignment between these

components in the reactor vessel flange region. The upper section of the barrel contains two outlet nozzles contoured to minimize coolant by-pass leakage.

Amplitude limiting devices, or snubbers, are installed on the outside of the core support barrel near the bottom end. The snubbers consist of six equally spaced lugs around the circumference of the barrel and act as a "tongue and groove" assembly with the mating lugs on the reactor vessel, see Figure 4.6.2. During assembly, as the internals are lowered into the reactor vessel, the reactor vessel lugs engage the core support barrel lugs.

4.6.1.3.2 Thermal Shield

The thermal shield installed on the Millstone 2 and St. Lucie I reactor internals, is a cylindrical structure which reduces the neutron flux and radiation heating in the reactor vessel wall. The thermal shield is fabricated from Type 304 stainless steel. At the upper end, the shield is supported by nine equally spaced lugs on the outer periphery of the core support barrel which restrict axial and tangential motion of the shield. Directly under each support lug is a preloaded positioning pin which is threaded radially through the thermal shield and butts against the core barrel. The lower end of the thermal shield is similarly restrained radially by seventeen positioning pins.

4.6.1.3.3 Core Support Plate & Lower Support Structure

The core support plate is a Type 304 stainless steel plate into which the necessary flow distributor holes for the fuel assemblies have been machined. Fuel assembly locating pins, four for each assembly, are shrunk-fit into this plate. The fuel assemblies and core shroud are positioned on the core support plate which forms the top support member of the welded lower support structure assembly consisting of a cylinder, a bottom plate, support columns, and support beams.

4.6.1.3.4 Core Shroud

The core shroud provides an envelope for the core and limits the amount of coolant by-pass flow. The shroud consists of two Type 304 stainless steel ring sections secured to each other and to the core support plate by pre-tensioned tie rods. The core shroud is shown in Figure 4.6.3.

4.6.1.4 Upper Guide Structure Assembly

This assembly, shown in Figure 4.6.4, consists of the upper support structure, 65 (69 for Millstone 2 and St. Lucie 1) control element assembly shrouds, fuel assembly alignment plate and a holddown ring. The upper guide structure assembly aligns and laterally supports the upper end of the fuel assemblies, maintains the Control Element Assembly (CEA) spacing, holds down the fuel assemblies during operation, prevents fuel assemblies from being lifted out of position during a severe accident condition, protects CEA's from the effect of coolant cross flow in the upper plenum, and supports the ICI plate assembly.

The upper end of the assembly is a structure consisting of a support plate welded to a grid array of 24 inch deep beams and a 24 inch deep cylinder, which encloses and is welded to the ends of the beams. The periphery of the plate contains four accurately machined equally spaced alignment keyways, which engage the core barrel alignment keys. This system of keys and slots provides an accurate means of aligning the core with the closure head and with the Control Element Drive Mechanism (CEDM).

The CEA shrouds extend from the fuel assembly alignment plate to above the upper guide structure support plate. The single CEA shrouds consist of cylindrical upper sections welded to integral bottom sections, which are shaped to provide flow passages for the coolant through the alignment plate while shrouding the CEA's from cross flow. Dual CEA shrouds accommodate two adjacent and interconnected CEA's. These shrouds have an oval shaped upper

section welded to a flow diverting base section. The shrouds are bolted and lockwelded to the fuel assembly alignment plate. At the upper guide structure support plate, the single shrouds are connected to the plate by spanner nuts. The dual shrouds are attached to the upper plate by welding.

4.6.1.4.1 Fuel Assembly Alignment Plate

The fuel assembly alignment plate is designed to align the upper ends of the fuel assemblies and to support and align the lower ends of the CEA shrouds. Precisely machined holes in the fuel assembly alignment plate align the fuel assemblies. The fuel assembly alignment plate also has four equally spaced slots on its outer edge which engage with Stellite hardfaced guide lugs protruding from the core shroud to limit lateral motion of the upper guide structure assembly during operation. The fuel alignment plate bears the upward force of the fuel assembly holddown springs. This force is transmitted from the alignment plate through the CEA shrouds to the upper guide structure support plate flange and thence to the holddown ring.

4.6.1.4.2 Holddown Ring

The holddown ring is positioned on the upper guide structure and engages with the reactor vessel head. The holddown ring functions to resist axial upward movement of the upper guide structure and core support barrel assemblies and to accommodate axial differential thermal expansion between the core barrel flange, upper guide structure flange, the reactor vessel support ledge, and reactor vessel head.

4.6.1.4.3 In-Core Instrumentation

The upper guide structure assembly also supports the in-core instrumentation guide tubes. The tubes are conduits which protect the in-core instrumentation and guide them during removal and insertion operations.

4.6.1.5 Flow Skirt

The Ni-Cr-Fe flow skirt is a right circular cylinder, perforated with flow holes, and reinforced at the top and bottom with stiffening rings. The flow skirt function is to improve core inlet flow distribution and to prevent formation of large vortices in the lower plenum. The skirt is supported by nine equally spaced sections which are welded to the bottom head of the reactor vessel.

4.6.1.6 Plant Specific (Fort Calhoun)

4.6.1.7 Core Support Assembly

The reactor internals for the Fort Calhoun plant are shown in Figure 4.6.5. These internals accommodate a smaller number of fuel assemblies and are shorter in length than those of the generic plant and differ from them in the following respects:

The core support barrel is 120 5/8 inches inside diameter and 25 feet long. The core support plate is attached at its periphery to the core support barrel. The plate is supported by columns which transmit the loads to support beams welded to the core support barrel.

A thermal shield is supported at the upper end by eight lugs on the outer periphery of the core support barrel. The lower end is positioned radially by 16 pins which pass through the shield and butt against the core support barrel.

The core shroud consists of an assembly of vertical rectangular plates attached to the core support barrel by horizontal stiffening plates, and at the bottom, to the core support plate by means of anchor blocks.

4.6.1.8 Upper Guide Structure Assembly

The upper guide structure assembly, shown in Figure 4.6.6, consists of a grid support plate assembly, 41 control element assembly

shrouds, a fuel assembly alignment plate and a holddown ring. The upper end of the assembly is a flanged grid structure consisting of an array of 24 inch deep beams. The grid is encircled by a 24 inch deep cylinder with a 3 inch thick plate welded to the cylinder. The periphery of the plate contains four accurately machined and located alignment keyways, spaced at 90 degree intervals, which engage the core barrel alignment keys.

The Control Element Assembly (CEA) shrouds extend from the fuel alignment plate to an elevation about 8 inches above the support plate. There are 29 single-type shrouds. These consist of centrifugally cast cylindrical upper sections welded to cast bottom sections, which are shaped to provide flow passages for the coolant passing through the fuel alignment plate while shrouding the CEA's from cross flow. There are also 12 dual-type shrouds which consist of two single-type shrouds connected by a rectangular section, shaped to accommodate the dual control element assemblies.

The shrouds are bolted to the fuel assembly alignment plate. At the upper guide structure support plate, the single shrouds are connected to the plate by the spanner nuts. The dual shrouds are attached to the UGS support plate by welding.

A holddown ring is located between the reactor vessel head flange and the upper guide structure to resist upward movement of the UGS and core support assembly. This arrangement permits differential axial thermal expansion of the reactor vessel flange and the core support barrel and UGS flanges.

4.6.1.9 Plant Specific (Palisades)

4.6.1.10 Core Support Assembly

The reactor internals for the Palisades plant are shown in Figure 4.6.7. These internals differ from the generic design as follows:

The core support barrel has a nominal diameter of 149-3/4", a length of 27 feet, and a minimum wall thickness, in local reduced barrel sections, of 1 inch. The core support plate, 1½ inches thick, is a perforated plate with flow distribution and locating holes for each fuel bundle. The plate is supported by a ledge and by columns. The ledge on the CSB supports the periphery of the plate and the plate is pinned, bolted, and lockwelded to this ledge thus maintaining accurate location of the plate. A series of columns are placed between the plate and the beams located across the bottom of the core support barrel. The core shroud consists of a series of rectangular plates 145 inches long and of varying widths. The bottom edges of these plates are fastened to the core support plate by use of anchor blocks. The gap between the outside of the peripheral fuel assemblies and the shroud plates is maintained by seven tiers of centering plates positioned during initial assembly by adjusting bushings located in the core support barrel. Also within the core support barrel just below the nozzles are four guide pins which align the lower end of the upper guide structure relative to the core support barrel.

The Inconel flow skirt is a perforated right circular cylinder, reinforced at the top and bottom with stiffening rings. The skirt is hung by welded attachments from the core stop lugs near the bottom of the pressure vessel and is not attached to the core support barrel.

4.6.1.11 Upper Guide Structure Assembly

The upper guide structure assembly, shown in Figure 4.6.8, consists

of a flanged grid structure, 45 control rod shrouds and a fuel alignment plate.

The upper end of the assembly is a flanged grid structure consisting of a grid array of 18 inches deep long beams in one direction with 9 inch deep short beams at 90 degrees to the deeper beams. The grid is encircled by an 18 inch deep cylinder with a 3 inch deep flange welded to the cylinder. The grid aligns and supports the upper end of the control rod shrouds.

The control rod shrouds are of cruciform configuration and extend from about 1 inch above the fuel bundles to about 2 inches above the top of the pressure vessel flange. They are 136 inches long and enclose the control rods in their fully withdrawn position above the core, thereby protecting them from adverse effects of flow forces. The shrouds consist of four formed plates, which are welded to four end bars to form a cruciform shaped structure. The shrouds are fitted with support pads at the upper end machined for a bolted and lockwelded attachment to the flanged grid structure. The lower ends of the shrouds are also fitted with support pads machined for a bolted and lockwelded attachment to the fuel bundle alignment plate.

The fuel bundle alignment plate is designed to align the upper end of the fuel bundles and to support and align the lower ends of the control rod shrouds. The fuel bundle alignment plate also has four equally spaced slots on its outer edge which engage with Stellite hardfaced pins protruding from the core support barrel to prevent lateral motion of the upper guide structure assembly during operation.

An arrangement of Bellville Type springs is mounted on the top of the internals flanges to resist movement of the UGS and CSB, and to accommodate differential thermal expansion between the two flanges and the reactor vessel seating area.

The upper guide structure assembly also supports the in-core instrument guide tubes.

4.6.2 INTERNALS ANALYSIS MODELS

The postulated pipe breaks in the reactor cavity result in horizontal and vertical forcing functions which cause the internals to respond in both beam and shell modes. This section describes the structural models used for determining these responses.

4.6.2.1 DETAILED NON-LINEAR INTERNALS MODELS

Detailed structural models were developed for the various plants and accounted for the various differences in geometry. These mathematical models consisted of lumped masses connected by bar or beam elements which represented the elastic properties of the actual structures. The method used to develop these models followed the procedures described in CENPD-42 (Reference 3.12) and, in addition, included a more detailed representation of the interfaces between the core support barrel, upper guide structure, and reactor vessel. Hydrodynamic coupling effects caused by the water on either side of the core support barrel were also included. These coupling terms were calculated as a function of the structural geometry and boundary conditions.

Detailed lateral structural models were developed for the Calvert Cliffs, Palisades, and Ft. Calhoun reactor internals. The Calvert Cliffs or generic model is being used to represent the Millstone 2 and St. Lucie 1 internals because of geometrical similarities (other than the thermal shield). This approach results in conservative loads for Millstone 2 since the results presented in CENPD-42 show that the presence of a thermal shield reduces the lateral LOCA loadings. The detailed lateral generic model is shown in Figure 4.6.9 and the nodal locations are presented in Table 4.6.2. Similarly,

the detailed plant specific lateral models are shown in Figures 4.6.11 and 4.6.4 and the node locations are presented in Tables 4.6.4 and 4.6.5.

In the axial direction, a detailed model was developed only for the Calvert Cliffs reactor internals. This generic axial model is assumed to be conservatively representative of the other plant internals. Figure 4.6.10 shows the generic detailed axial model and Table 4.6.3 presents the nodal locations.

The computer program CESHOCK (Reference 3.13) was used to determine the dynamic responses of the models when subjected to LOCA excitation. The program solves the differential equations of motion for lumped parameter systems using a direct step-by-step numerical integration procedure. The displacement, velocity and acceleration of each mass are determined as a function of time. In addition, the member developed loads in all of the couplings are calculated at each time step and the maximum displacements and forces are summarized for each problem.

4.6.2.1.1 HORIZONTAL MODELS AND LOADS

For the generic plant, the model for the horizontal direction was developed using beam elements to represent the lateral stiffness between mass points. Flexible components such as the fuel assemblies and the CEA shrouds were modeled in greater spatial detail than those representing more rigid structures such as the pressure vessel to assure accurate structural responses. The lumped mass model represents the continuous distribution of mass and stiffness exhibited by the actual structure. Rotary inertias are included to properly account for angular accelerations.

Finite element models were used to compute the stiffnesses of complex components such as the core support barrel upper and lower flanges. Non-linear springs were used to represent the possible impacting between various components. A non-linear rotational spring between the upper guide structure support plate and the fuel alignment plate represents the rotational restraint exerted by the control element assembly shrouds.

The core support barrel upper region was modeled in detail to represent the possible interactions between the core support barrel upper flange, upper guide structure support plate and the pressure vessel ledge. Linear, non-linear, hysteresis and friction couplings represent this complex interface region. Rotational springs exhibiting bi-linear moment-rotation characteristics are used to calculate the relative rotation between the upper flanges which are held together by the holddown ring.

The non-linear gap springs used in the above interface region represent possible impacting between the pressure vessel ledge, the core support barrel upper flange and upper guide support structure plate, and between the core support barrel cylinder and upper guide structure cylinder. The hysteresis couplings account for the shear resistance of the alignment keys to relative translational motion between the upper region components and the friction elements represent the resistant forces developed by the normal forces at this elevation. The four types of couplings described above model the complex interactions that may occur in the flange interface region during a LOCA.

The reactor core is represented in enough detail in the lateral internals model to account for feedback effects on core plate motion. Nodes are located at

each spacer grid elevation in each of the five columns of fuel which represent the entire core. Non-linear couplings are used on the peripheral bundles to represent the effects of spacer grid impacting.

Hydrodynamic mass effects are included for all of the components in the reactor system. The effect of water in the core barrel/reactor vessel annulus is accounted for by computing hydrodynamic coupling terms based on the structural geometry and boundary conditions. Hydrodynamic masses are computed for all other components in the system and directly combined with structural masses.

The control element assembly shrouds are combined into four groupings which are selected on the bases of similarity in lateral crossflow load distribution.

During a cold leg break LOCA, a rarefaction wave initially propagates downward in the annulus between the core support barrel and reactor vessel. This sudden depressurization causes the pressures in the circumferential direction to vary asymmetrically with time. For this reason, a set of horizontal axes both parallel and perpendicular to the hot leg nozzles centerline were chosen to represent the two dimensional state of lateral LOCA loadings.

For the calculation of lateral direction cold leg break LOCA loads, a Fourier decomposition of the asymmetric pressure distribution is first performed. Of these coefficients, only the sine and cosine components result in a beam type loading. These coefficients are then integrated over the surface area of the core support barrel to obtain the dynamic LOCA forcing function. Figures 4.6.18 and 4.6.19 show the total core support barrel loads acting in two

perpendicular directions for the generic plant.

A hot leg break produces lateral crossflow loads which act on the control element assemblies. These loads act in a direction parallel to the axis of the hot legs and depend on the transverse pressure differentials and drag effects. The total crossflow loads for the generic plant are shown in Figure 4.6.20.

The development of the Palisades and Ft. Calhoun internals models followed the same procedures used in developing the generic plant model except that in complex regions stiffnesses were calculated using approximate strength of materials formulations instead of detailed finite elements models. The CEA shroud groupings were determined on the basis of similar crossflow load distributions. The modeling of the interactions between the reactor vessel, core support barrel and upper guide structure followed the same procedures as for the generic plant. In addition, the Ft. Calhoun and Palisades models have linear springs representing the core shroud former plates which connect the core shroud to the core support barrel.

The lateral cold leg break LOCA loads were computed in directions both parallel and perpendicular to the hot leg nozzle for Palisades and Ft. Calhoun following the same procedures used in calculating the generic plant loads. The generic plant lateral LOCA loads can be conservatively applied to Millstone 2 and St. Lucie 1. Plots of the total core support barrel loads for Palisades and Ft. Calhoun are shown in Figures 4.6.21 through 4.6.24.

For the hot leg break, lateral LOCA crossflow loads on the CEA shrouds were

computed separately for the generic plant, Palisades, and Ft. Calhoun. The crossflow loads on the Millstone 2 and St. Lucie 1 plants are assumed to be the same as those for the generic plant. The generic plant shroud loadings are larger due to the arrangement and greater number of the larger dual CEA shrouds. Figures 4.6.25 and 4.6.26 show the crossflow loads for Palisades and Ft. Calhoun, respectively.

During the development of the generic plant horizontal model, several different friction coefficients were used with constant normal forces in the core support barrel upper flange interface region in order to determine the effects on the internals responses. The chosen bounding case coefficients were selected for stainless steel sliding on stainless steel. The lower bound represented the generic plant baseline case using nominal values and the upper bound included larger but justifiable values. Normal forces resulting from the steady state loads on the internals were used in these studies and the results indicated that many of the maximum loads were reduced in the upper bound case.

Since the bending moments or, in effect, the normal forces vary with the amount of relative rotation between the various surfaces, average preloads were determined from the bounding cases. In order to calculate these values, average resultant moments were first determined for each bounding case from a vector summation of the moments from the horizontal response analyses which were performed in directions parallel and perpendicular to the hot legs. The average values of normal forces were then determined from the sinusoidal force distributions produced by the bending moments.

The above procedure was only used to calculate normal forces between the core support barrel flange and reactor vessel ledge, the core support barrel flange and upper guide structure flange, and between the upper guide structure flange and the reactor vessel for the generic plant. Average values of normal forces were computed from the hot and cold leg break baseline cases. The results indicated that only the average normal force between the core support barrel and the reactor vessel increased from the values used in the baseline case.

Additional horizontal response analyses were performed using the above revised values of normal forces with nominal values of static and dynamic friction coefficients. These increased friction cases were used to determine factors which were defined as the ratios of loads calculated in the nominal friction case and the baseline case. The results for the generic plant are presented in Section 4.6.5 for the internals and in Section 4.7.7 for the fuel. It is assumed that the use of nominal friction values in the plant specific analyses would result in similar benefits.

4.6.2.1.2 VERTICAL MODELS AND LOADS

The generic plant vertical model stiffnesses were calculated using bar elements for most of the model members. Finite element analyses were employed for computing the stiffnesses of the core support barrel and

upper guide structure flanges, the upper guide structure, and the lower support structure. Non-linear couplings were included to account for such effects as friction between the fuel rods and guide tubes, and impacting between the various structural components.

The core support barrel upper region was modeled in detail to represent the interaction between the core support barrel and upper guide structure flanges with the pressure vessel ledge. The preloaded hold down ring was modeled as a non-linear member which allows the flanges to move until the ring is flattened. The axial members connecting the upper guide support flange, and pressure vessel ledge were modeled with compression only springs. Finite element analyses were used to compute the multi-linear stiffnesses of the core support barrel and upper guide structure flanges. Several analyses were required since the fixed support boundary conditions imposed on the models changed with the direction of loading.

Additional spatial detail was added in the fuel to accurately compute the dynamic responses. The fuel rods and guide tubes were separately modelled

using the properties of Zircaloy 4. Friction elements, which accounted for the static and dynamic resistive forces, were used to represent the sliding interactions between the fuel rods and spacer grids. A non-linear member was used to represent the lower end fitting which can only develop compressive loads against the core support plate. The upper end fitting was also modelled as a non-linear member and accounts for the steady state preload forces exerted on the fuel and also the changes in preload as the fuel moves relative to the fuel alignment plate.

The applied LOCA loads were calculated using a control volume formulation. In this method, the internals structure and contained water are sectioned into solid plus fluid control volumes. Across each volume, the fluid momentum equation is solved as a function of time to compute the LOCA loads. This method accounts for fluid pressure and momentum effects which act on all of the structures within each control volume.

Steady state initial preloads and static deflections were also calculated for the generic plant models. These preloads are the result of structural weights, holddowns, and normal operating flow forces. Without these values, the model would not be initially at rest.

4.6.2.2 REDUCED INTERNALS MODELS

Reduced three-dimensional models of the generic plant and Ft. Calhoun reactor internals were developed from the detailed internals models for incorporation into the reactor coolant system models. The Ft. Calhoun reduced internals model was specifically developed because of the major

differences in the internals, reactor vessel supports, and applied LOCA loadings. The purpose of these condensed internals models is to account for the effects of the interaction between the internals and the vessel. They are not intended to be used in the calculation of internals responses. The reduced internals models are compatible with the reactor coolant system model and the computer programs utilized in the analysis of the coolant system. The generic plant condensed internals model is shown in Figure 4.6.13 and nodal locations are described in Table 4.6.6. Similarly, the Ft. Calhoun condensed internals model is shown in Figure 4.6.16 and the nodal locations are presented in Table 4.6.7.

The reduced internals models were developed to produce reactor vessel support loadings equivalent to those obtained from the detailed internals models in both the axial and horizontal directions. Figure 4.6.14 shows a comparison of the generic detailed and reduced model reactor vessel support lateral responses following a cold leg break LOCA. In this case, the core support barrel is subjected to LOCA loadings caused by the asymmetric pressure differentials acting on it. Figure 4.6.15 shows a similar generic model comparison of the reactor vessel axial support loads following a cold leg break. Also, Figure 4.6.17 shows a similar comparison of the lateral support loads between the Ft. Calhoun detailed and reduced internals models following the cold leg break.

4.6.2.3 CORE SUPPORT BARREL SHELL MODELS

Separate finite element models of the core support barrel were developed for response analyses following both the hot and cold leg breaks. For the cold leg break a dynamic response analysis was performed because of the asymmetric nature of the resultant applied loading on the barrel. Conversely,

the hot leg break results in uniform, axially varying compressive loads on the barrel and its response to these loads was determined through a stability analysis.

4.6.2.3.1 SHELL VIBRATION MODEL (COLD LEG)

The core support barrel was modeled in detail using a finite element representation. Thin cylindrical shells of revolution joined at their nodal point circles were used as elements. The length of each element was a fraction of the shell attenuation length and, at areas of structural discontinuity, where rapid changes in the stress function occur, the nodal points were more closely spaced. Separate shell models were developed for Calvert Cliffs, Palisades, and Ft. Calhoun. The results of the generic Calvert Cliffs analysis were used to conservatively assess the structural integrity of the Millstone 2 and St. Lucie 1 core support barrels since it has been shown in Reference 3.12 that the presence of the thermal shield reduces the intensity of the LOCA loads acting on the barrel. The shell vibration models for the generic model, Palisades and Ft. Calhoun, are presented in Figures 4.6.27 through 4.6.29 respectively.

Several boundary conditions were imposed on the finite element models to simulate the proper restraints. At the upper flange, motion was restricted in the axial, radial, and tangential directions. The core support barrel lower flange was restricted from moving in the radial direction by the lower support structure and the snubbers prevented the adjacent elements from displacing the tangential direction. In addition, the effect of the weight of the internals components resting on the lower flange was considered by increasing the mass density of the flange.

4.6.2.3.2 SHELL DYNAMIC STABILITY MODEL

A single generic plant (Calvert Cliffs) finite element model of the core support barrel shown in Figure 4.6.30 was formulated for use in the shell stability analysis. The model and the results of the analyses were assumed to conservatively apply to the other plants even though the Palisades and Ft. Calhoun barrels contain reduced thickness sections. This model is applicable to the latter elements because the barrels are joined to the core shroud with former plates that act as radial stiffners.

The core support barrel model consisted of a series of cylindrical shell elements joined at their nodal point circles and included detailed representations of the upper and lower flanges. The length of each element was a fraction of the shell attenuation length and the nodal points were more closely spaced at areas of structural discontinuities. Due to the symmetric nature of the hot leg break applied loadings, the core support barrel shell model was subjected to uniform pressure differentials which were assumed to vary linearly in the axial direction. Since the barrel upper flange is constrained against vertical motion by the reactor vessel ledge, upper guide structure flange, and the hold down ring, an axial restraint was imposed to prevent motion in this direction.

4.6.3 INTERNALS RESPONSE ANALYSES

The dynamic responses of the reactor internals to the postulated pipe breaks were determined using the various models described in the previous sections. Horizontal and vertical analyses were performed for both the hot and cold leg breaks to determine the lateral and axial beam mode responses of the reactor internals to the simultaneous LOCA forces and reactor vessel motion excitation. Shell response analyses of the core support barrel were also performed for both breaks to obtain the shell mode contributions to the barrel stresses. Each of the above analyses were performed for the Calvert Cliffs or generic plant. In addition, several of the analyses were also specifically performed for Palisades and Ft. Calhoun. A detailed summary of the various analyses is presented in Table 4.6.8.

4.6.3.1 INLET (COLD LEG) BREAK ANALYSIS

The postulated cold leg break results in simultaneous vertical and horizontal beam and shell mode excitation. The horizontal responses to these excitations were calculated for the generic plant, Palisades, and Ft. Calhoun using the methods described below. The results of the generic plant internals horizontal responses can be conservatively applied to Millstone 2 and St. Lucie 1 since the presence of a thermal shield has been shown to reduce the responses (Reference 3.12). An axial response analysis was performed only for the generic plant. Shell response analyses of the core support barrels were performed for the generic plant, Palisades, and Ft. Calhoun to obtain the shell mode contributions of the components.

4.6.3.1.1 HORIZONTAL RESPONSE

The dynamic time history responses of the reactor internals to the horizontal loads resulting from the cold leg break were determined with the CESHOCK

code. The input to these analyses were the core support barrel force time history and the reactor vessel motion time history which was determined using the reduced internals models in the reactor coolant system analyses. These motions were calculated at the reactor vessel ledge and snubber elevations only for the generic plant and Ft. Calhoun. The generic plant motions were also conservatively used in the Palisades response analyses. The motions calculated for Ft. Calhoun account for its reduced size and the smaller pipe break area.

The horizontal response analyses were performed in directions both parallel and perpendicular to the hot legs because of the asymmetric nature of the applied loadings. The results of these analyses were time dependent member loads and nodal displacements, velocities and accelerations in both directions. Time phased combined loadings were computed for all of the linear members. For the non-linear members such as the snubbers and core shroud guide lugs, the maximum tangential loadings were used. In addition, the core support plate, core shroud, and fuel alignment plate displacement time histories were saved as input to the detailed core model.

These loads were later compared to those presented in CENPD-42 for the generic plant, Millstone 2, and St. Lucie 1. Similar comparisons were also made against previously obtained results of pipe break analyses for Palisades and Ft. Calhoun. The loads were compared in the vertical direction and with the resultant of the horizontal directions. Conservatively calculated component stresses using the combined maximum lateral and axial loads were computed if the loads in a given direction exceeded any of the previously calculated values.

Time phased combined axial and horizontal loads were used to reduce conservatism whenever any of the conservatively calculated component stresses from the set of maximum loads exceeded the ASME code allowables. Since the maximum horizontal and axial loads occurred at different times and resulted in different component stresses, several calculations were made and the "worst cases" were compared to the allowables. A further description of this procedure and the results are presented in Section 4.6.5.

In order to determine the total core support barrel stresses, the beam mode loadings (CESHOCK results) were combined with the shell mode loadings (ASHSD results) at the times of peak loadings. The ASHSD results consisted of shell forces, moments, and stresses as a function of time for each element in the model. These combinations included the maximum generic plant axial internals response loads from the CESHOCK analysis. Several time points were investigated in order to determine the most conservative stresses and stress intensities. Time phased load combinations were also used to reduce the conservatism. Stress analyses using these methods were performed for the generic plant, Palisades, and Ft. Calhoun core support barrels. The results of the generic plant assessment are conservatively applied to the Millstone 2 and St. Lucie 1 plants which have a thermal shield. This method of combining loads more accurately represents the dynamic effects of the internals and fuel on the beam response of the core support barrel.

4.6.3.1.2 VERTICAL RESPONSE

A detailed vertical response analysis was performed only for the generic plant following the cold leg break. This approach resulted in internals and fuel loads which are conservative for Millstone 2, Ft. Calhoun, and St. Lucie 1 because of the presence of the thermal shield. The results of this analysis are also directly applicable to Palisades.

In this analysis, the internals model (Figure 4.6.10) was subjected to LOCA forces and reactor vessel motions obtained from the reactor coolant system analysis using the generic plant reduced internals model. The CESHOCK code was used to perform the axial response analysis and the results consisted of maximum member loads and nodal displacements, velocities, and accelerations. These loads were compared to the values previously calculated in CENPD-42 for the generic plant, Millstone 2, and St. Lucie 1 and to the results of similar analyses for Palisades and Ft. Calhoun. Whenever any of the new axial loads exceeded the previous values, component stresses were calculated using the maximum axial and combined horizontal loadings. Time phased load combinations were used to reduce the stresses whenever the conservatively calculated stresses based on the maximum load combination resulted in values which exceeded the ASME code allowables. A further description of the procedures used and the final results is presented in section 4.6.5.

The generic plant detailed axial response analysis also provided detailed fuel assembly loads and deflections. The maximum developed fuel bundle end fitting loads were later used in the detailed stress analyses of the fuel rods and guide tubes for the generic plant and Ft. Calhoun. The generic plant axial fuel bundle responses were conservatively assumed to be applicable to all of the other plants.

4.6.3.1.3 SHELL VIBRATION RESPONSE (COLD LEG)

A cold leg break will cause the pressure transients to vary both circumferentially and axially. During the calculation of the blowdown loads, these pressures are computed at several equally spaced circumferential locations and at several axial elevations. In order to compute the core support barrel asymmetric LOCA loads a Fourier decomposition of the pressures is performed at each axial station. A linear distribution is assumed between axial stations. The resulting pressure coefficients are then integrated over the surface area of the barrel to obtain the dynamic LOCA loads.

The dynamic responses of the generic plant, Palisades, and Ft. Calhoun core support barrel shell models following the cold leg break with the beam loadings (sin θ, cos θ) removed were determined by the ASHSD computer code, (Reference 3.17). The code is applicable to axisymmetric structures of arbitrary shape subjected to asymmetric static or dynamic loads. The ASHSD code considers each load harmonic (Fourier term) separately and superimposes the response of each barrel harmonic to obtain the total response. The output of the ASHSD code consists of nodal displacements, resultant shell forces and shell stresses as a function of time.

The maximum displacements, forces, and stresses were later computed for the various barrels using the results from ASHSD. The results of the generic analysis were conservatively assumed to be applicable to the Millstone 2 and St. Lucie 1 barrels because of geometric similarities and the fact that the presence of the thermal shield reduces the intensity of the LOCA loads (Reference 3.12). The maximum loads obtained from these analyses were combined with the horizontal and vertical CESHOCK core support barrel response loads in order to obtain the resulting conservatively calculated stresses and stress intensities. Time phased load combinations were also used wherever any of the ASME code allowables were exceeded.

4.6.3.2 CUTLET (HOT LEG) BREAK ANALYSIS

Horizontal and vertical nonlinear internals and core support barrel shell response analyses were performed for the hot leg break. Separate horizontal analyses were performed for the generic plant, Palisades, and Ft. Calhoun. The generic plant results were conservatively applied to the Millstone 2 and St. Lucie 1 internals. In the axial direction, a response analysis was only performed

for the generic plant. In addition, a single core support barrel shell dynamic stability response analysis was performed for the generic plant core support barrel and the results were conservatively applied to the plant specific core support barrels.

4.6.3.2.1 HORIZONTAL RESPONSE

The dynamic time history responses of the generic plant, Palisades and Ft. Calhoun reactor internals to the horizontal loads resulting from the hot leg break were determined with the CESHOCK code. Input to these analyses were the control element assembly shroud crossflow forces and the reactor vessel motion time history determined from the generic plant reactor coolant system analysis. The forces consider pressure differentials and drag contributions which depend on the different locations and geometries. Due to the symmetric nature of the pressure differentials around the core support barrel, the transverse forces on the barrel and other internals were negligible.

The response analyses were performed only in the direction parallel to the hot legs. The results consisted of the maximum time dependent member loads and nodal displacements, velocities, and accelerations. These loads were compared to those presented in CENPD42 for the generic plant, Millstone 2, and St. Lucie 1. The Palisades and Ft. Calhoun responses were compared to the previously calculated results of pipe break analyses. Whenever any of the new loads exceeded the previously calculated values, detailed combined load stress analyses were performed using the maximum axial loads from the generic plant vertical response analysis. Time phased combinations were also used to reduce

the conservatism whenever the above procedure resulted in calculated stresses which exceeded the ASME code allowables. The results of the analyses and a further description of the procedures used are presented in Section 4.6.5.

4.6.3.2.2 VERTICAL RESPONSE

A single vertical response analysis was performed for the generic plant and the results were conservatively used to evaluate the other plant specific internals. The methods used in Section 4.6.3.1.2 are applicable to both the hot and cold leg breaks.

4.6.3.2.3 SHELL DYNAMIC STABILITY RESPONSE

The SAMMSOR/DYNASOR code (Reference 3.14) was used to determine the buckling potential of the generic plant core support barrel following a hot leg break. The SAMMSOR portion of the code was used to generate the mass and stiffness matrices for the shell and the DYNASOR portion of the code calculated the dynamic response using the Houbolt numerical procedure.

The analyses were performed for the second, third, and fourth cosine harmonics using the maximum values of as built initial imperfections for the generic plant. In these analyses, the applied transient loadings were circumferentially uniform but varied linearly in the axial direction. Overload analyses using factors of 1.33, 2.0, and 4.0 were also performed to determine the buckling potential of the barrel. The resulting maximum radial displacements were linear and were therefore well within the ASME code requirements for dynamic stability. The results of this analysis can be conservatively applied to the

other plants because the presence of a thermal shield reduces the Millstone 2 and St. Lucie 1 core support barrel loads (Reference 3.12) and the presence of the core shroud former plates in the Palisades and Ft. Calhoun internals reduce the deflections of the core support barrel in the region of the core shroud. In addition, the low level of load input magnitude and the results of the analysis indicate that all of the responses are far removed from stability considerations.

4.6.4 ACCEPTANCE CRITERIA

The acceptance criteria for the reactor internals following a loss of coolant accident (LOCA) is based upon maintaining the core in place and assuring that adequate core cooling is preserved. This can be accomplished if the following criteria are met. For the core support components, the stress intensities must be less than those listed in the ASME Boiler and Pressure Vessel Code, Section III, Division I, Appendix F. Meeting the stress criteria for core support components assures that the core will be held in place during a LOCA. The difference between the ASME Code allowables and the calculated stress intensities is reported as margin. For the internal structures, the component deflections are limited so that the core is held in place, adequate core cooling is preserved, and resulting loads do not adversely effect the core support components.

4.6.4.1 Definition of Margin

The difference between the calculated stress intensity and the allowable stress intensity per the ASME Boiler and Pressure Vessel Code, Appendix F, is reported as margin. The margin was calculated as a percentage using the following equation:

$$\text{Margin} = \frac{(S_{allow} - S_{calc})}{S_{allow}} \times (100\%)$$

where the term S_{calc} is the calculated component stress intensity being evaluated and the term S_{allow} represents the ASME Code allowable stress intensity of $2.4S_m$ for a membrane condition or $3.6S_m$ for a membrane plus bending condition. The reported margin is therefore a measure of the percent of the stress intensity remaining beyond the calculated stress before the ASME Code allowable stress intensity is reached.

4.6.5 EVALUATION OF REACTOR INTERNALS

The reactor vessel internals have been analyzed for the asymmetric LOCA loads. All structures analyzed were shown to have met the acceptance criteria established in Section 4.6.4 of this report.

4.6.5.1 Load Comparison

The initial phase of the evaluation consisted of a comparison of the design verification LOCA loads used in the original analysis as reported in CENPD-42 (Reference 3.12), and the present asymmetric LOCA loads considering vessel motion. The three components of the load, including the vertical and horizontal shear forces and the horizontal moment, were compared to the original loads to determine if any portion of the load increased. Any area of the reactor internals with a load component higher than the design verification LOCA loads was evaluated by performing a new analysis using the new asymmetric loads.

The results of the load comparison indicated that the only areas of the reactor internals which did not show an increase in loads with the asymmetric load analysis were the Core Support Barrel (CSB) upper and lower flanges for the Generic Plant. No further analysis was performed for these components since the original, Ref. 3.12, analysis had shown these areas to meet the requirements of Section 4.6.4 and the margin shown in Table 4.6.9 is conservatively based on the previous design loads. All other areas of the reactor internals for the Generic plants and all areas of the reactor internals for the Fort Calhoun and Palisades plants were re-analyzed using the asymmetric loads to compute stress intensities.

4.6.5.2 Stress Analysis of Reactor Internals

The core support structure components are analyzed for the loads resulting from a LOCA, both inlet or outlet break, in combination with the mechanical loads associated with normal operating conditions. The calculated stresses are combined to determine the

maximum stress intensity which is compared with the membrane allowable of $2.4S_m$ or the membrane plus bending allowable of 3.65_m (as applicable) as defined in the ASME Boiler and Pressure Vessel Code, Section III, Appendix F. The elastic material properties and stress allowables are conservatively taken at the reactor internals design temperature of 650°F.

The vertical loads, from the C-E SHOCK code, derived for the Generic plant were conservatively used for the plant specific stress analysis. The reactor internal component sizes are smaller in cross section for Fort Calhoun since there are fewer fuel assemblies, 133 for Fort Calhoun and 217 for the Generic plant, see Table 4.6.1. In addition, the Fort Calhoun pipe break sizes are less than the Generic plant. The only exception to using generic vertical loads was the Fort Calhoun CSB center section which was scaled by the ratio of the cross sectional areas:

$$\text{Vertical Force}_{\substack{\text{Fort}\\\text{Calhoun}}} = \frac{\text{Area}_{\substack{\text{CSB Fort}\\\text{Calhoun}}}}{\text{Area}_{\text{CSB Gereric}}} \times \text{Vertical Force}_{\text{Generic}}$$

This ratio reduces the loads in the vertical direction, that were calculated by applying a pressure time history to the component areas for the Generic plant and then applying them to the smaller area of the Fort Calhoun reactor internals. The vertical force scaled in this manner for Fort Calhoun, is still conservative since the break size for Fort Calhoun is less than the break size used to generate the Generic plant vertical loads.

The stresses from the vertical loads were combined with the stresses from the horizontal shears and moments to obtain the stress intensity for the reactor internals. The horizontal shears and moments were calculated for the specific plants by performing the dynamic structural analysis using the C-E SHOCK code, once each for the Generic, Palisades, and Fort Calhoun plants.

For the Generic plants, additional dynamic analyses were performed to compute the horizontal core support structure member loads using different values of friction resulting in different values of

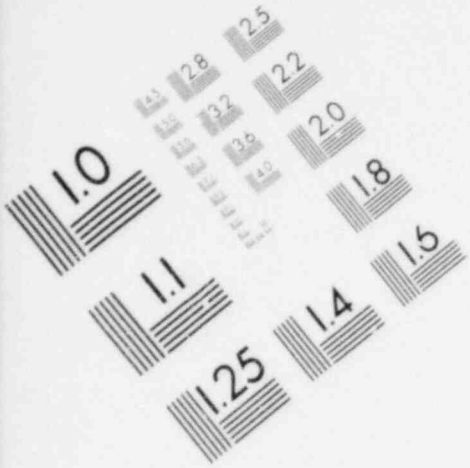

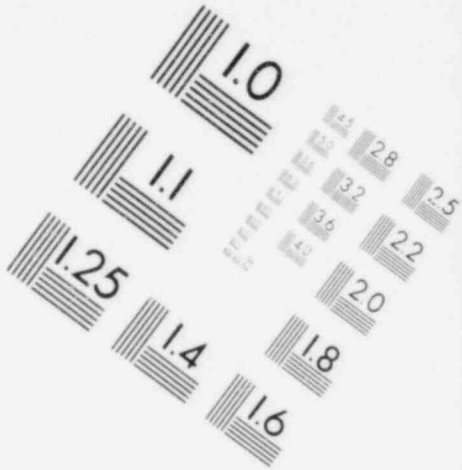

IMAGE EVALUATION
TEST TARGET (MT-3)

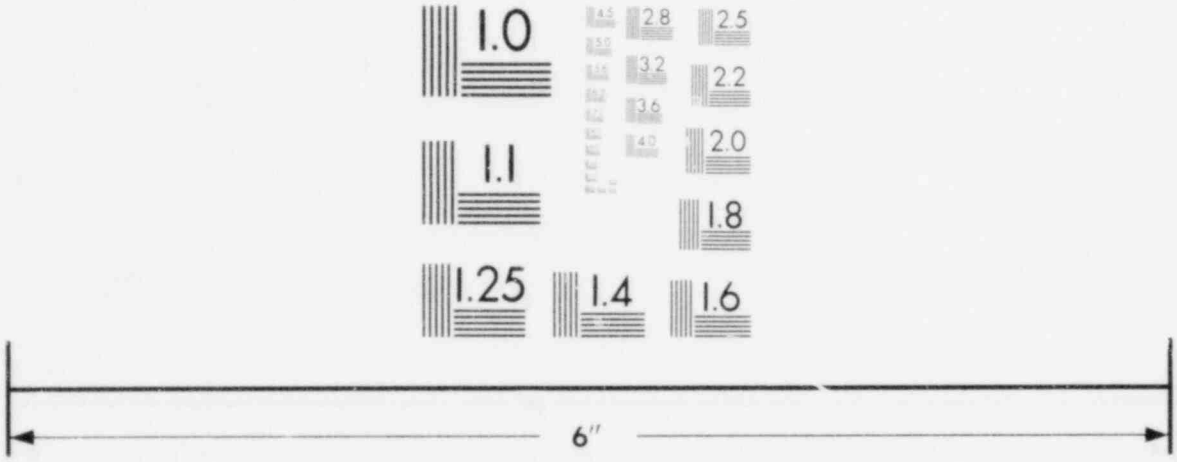

MICROCOPY RESOLUTION TEST CHART

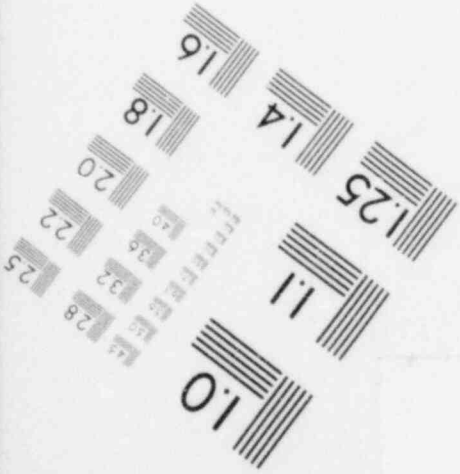

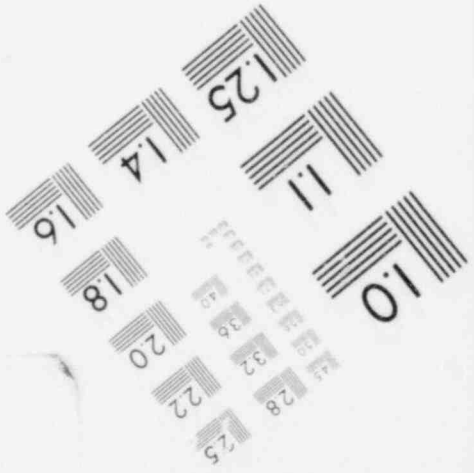

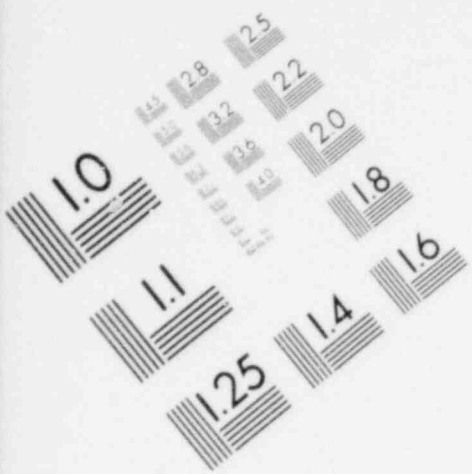

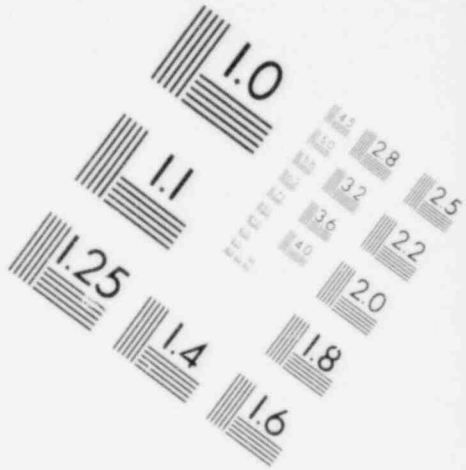

IMAGE EVALUATION
TEST TARGET (MT-3)

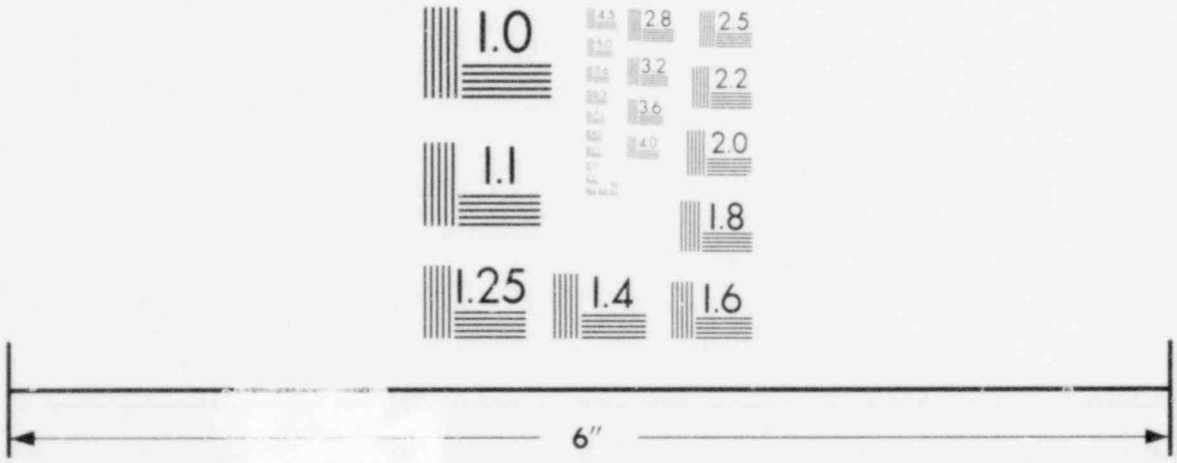

MICROCOPY RESOLUTION TEST CHART

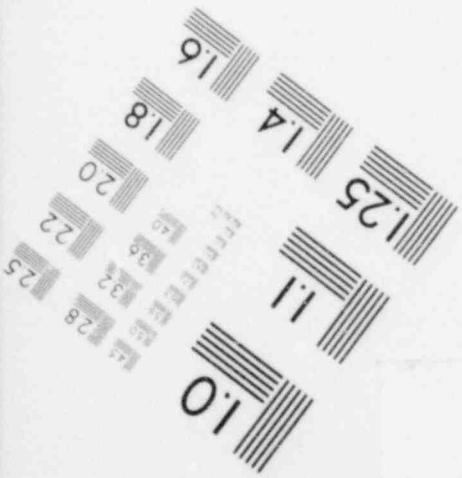

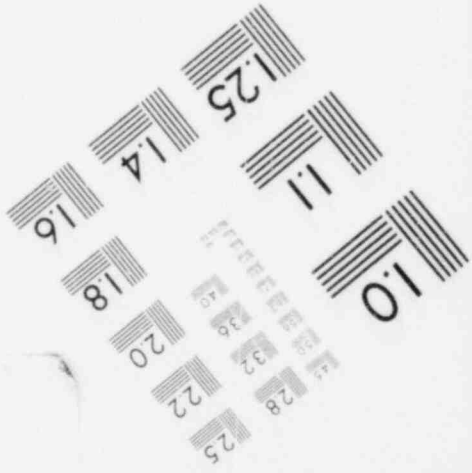

constraint at the CSB flange to reactor vessel ledge interface. The horizontal loads used in the analysis were conservatively based on the lower friction values, since the lower friction resulted in higher loads on all components except the lower support beams and cylinder and the Control Element Assembly (CEA) shrouds. These components showed negligible increase in load with the lower friction value.

For an inlet break, the analysis of the CSB cylinder was based on the vertical and horizontal C-E SHOCK loads plus the stresses calculated for the shell effects from the ASHSD. For an outlet break, the stresses from the vertical and horizontal loads were combined with the buckling stresses from the SAMMSOR/DYNASOR results. The stresses on the reactor internals were largest for the inlet break.

4.6.5.3 Results of Component Analysis

Tables 4.6.9, 4.6.10, and 4.6.11 indicate that, for the asymmetric LOCA loads, all the core support structures meet the acceptance criteria as stated in Section 4.6.4. Although the reported margins are small, less than 5% for some components, the analysis was conservatively based on the C-E SHOCK loads using the lower friction value at the CSB flange to reactor vessel ledge interface. Use of the nominal friction case would increase the margin for all components listed except the lower support columns and cylinder which, because of a slight increase in load, shows negligible change in margin with increased friction. The lower friction case was the only one examined for Fort Calhoun and Palisades. It is expected that the nominal friction case, if run for Fort Calhoun and Palisades, would provide similar load reductions for these plants. This, in conjunction with the conservative use of the Generic plant vertical loads on the smaller set of Fort Calhoun internals, indicates that the stress margins reported are conservative.

The internal structures, which do not provide direct restraint to the core, were evaluated and it has been shown that their deflection will not adversely effect the function of the core support structures, satisfying the acceptance criteria of Section 4.6.4.

4.6.5.3.1 Generic Plant (Calvert Cliffs 1 & 2 and Millstone II)

The calculated margins for the reactor internals components are shown on Table 4.6.9.

4.6.5.3.2 Palisades

The calculated margins for the reactor internals components are shown on Table 4.6.10.

4.6.5.3.3 Fort Calhoun

The calculated margins for the reactor internals components are shown on Table 4.6.11.

TABLE 4.6.1

MECHANICAL SYSTEMS AND COMPONENTS

COMPARISON OF STRUCTURAL

DESIGN PARAMETERS

Parameters	Generic Plant +	Fort Calhoun	Palisades
Structural			
Upper CSB R_{mean}, in.	75-1/4	61-5/16	75-7/8
Upper CSB t, in.	2- 1/2	2	2
Upper CSB L, in.	135-5/8	101-3/8	109-1/4
Middle CSB R_{mean}, in.	74-7/8	61-1/16	75-5/8
Middle CSB t, in.	1-3/4	1-1/2	1-1/2
Middle CSB L, in.	144-3/4	166-1/8	166-3/4
Lower CSB R_{mean}, in.	74-5/8	60-11/16	75-3/8
Lower CSB t, in.	2-1/4	2-1/4	2
Lower CSB L, in.	38	35-5/8	38-1/2
Lower cylinder ID, in.	141	Integral	Integral
Core cylinder OD, in.	145	Integral	Integral
Support cylinder L, in.	42	Integral	Integral
Structure supported	CSB Lower Flange	Integral	Integral
CSB OAL, in.	328½	311¼	318½
Core shroud support	Core support plate	Bolted to CSB	Bolted to CSB
UGS			
Cylinder R_{mean}, in.	72-5/8	59-1/16	73-1/2
Cylinder t, in.	2	1-1/2	2
Cylinder L, in.	24	24	18
Beams, in.	24x1-1/2	24x1-1/2	18 x 1-1/2
Plate t, in.	4	3-1/4	None
Thermal shield	No *	Yes	No
No. of loops	2	2	2
Inlet ID, in.	35-3/16	28-3/4	35-1/8
Outlet ID, in.	48 1/8	37	48

CSB = Core support barrel

UGS = Upper guide structure

* Millstone & St. Lucie I have a thermal shield.

+ Calvert Cliffs 1 & 2, Millstone 2, St. Lucie I

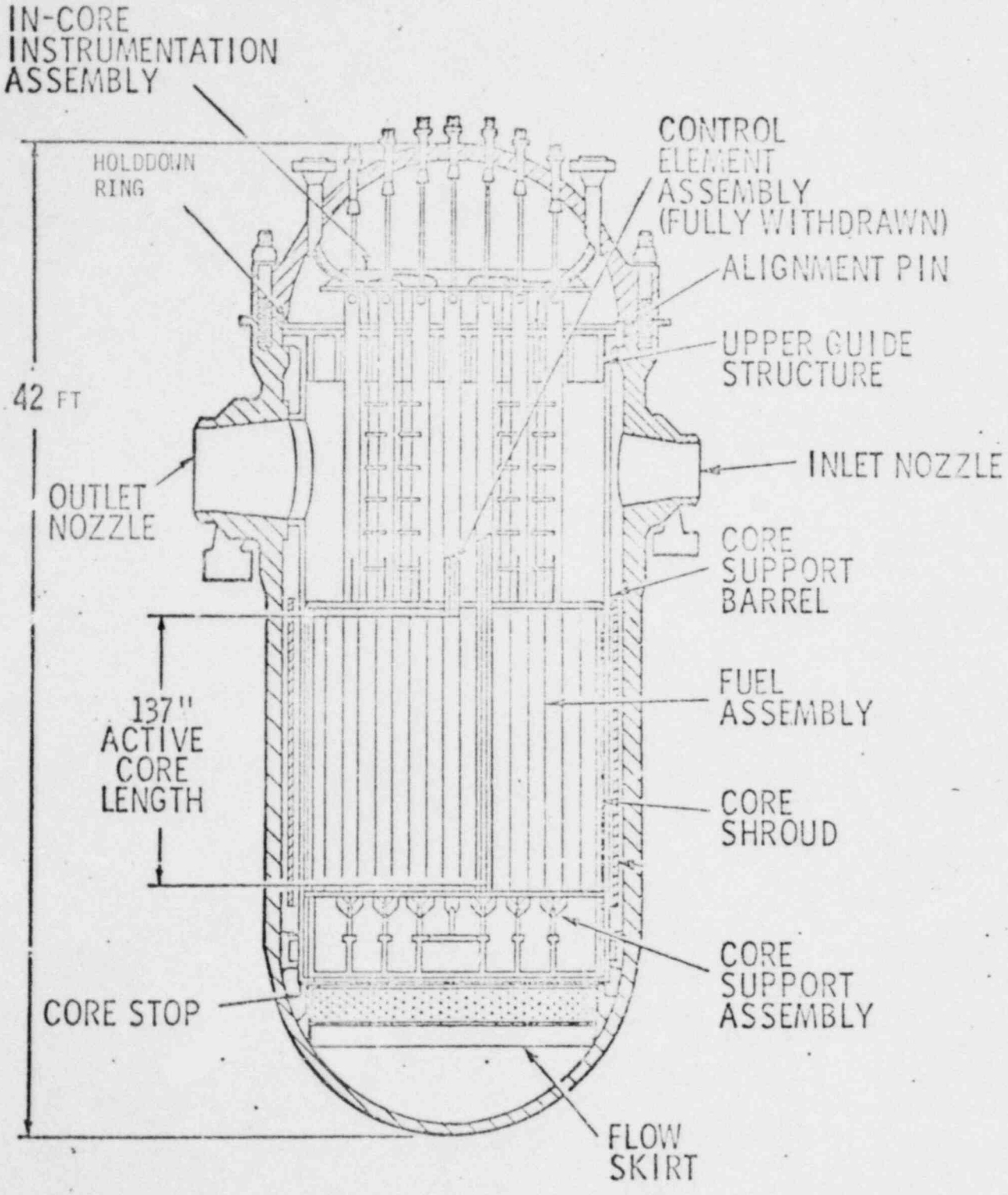

Reactor Vertical Arrangement
(GENERIC)

Figure
4.6.1

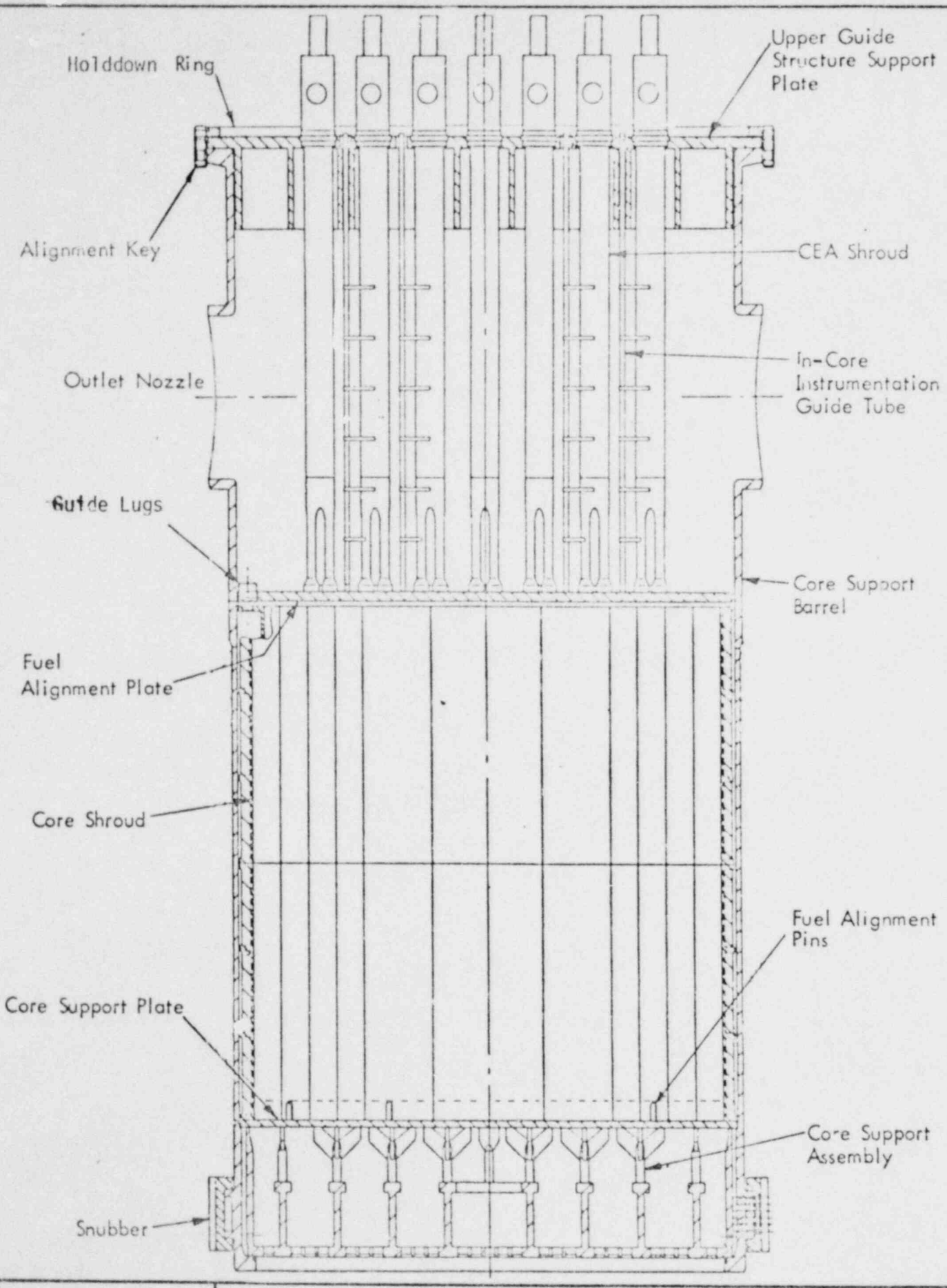

Reactor Internals Assembly
(GENERIC)

Figure 4.6.2

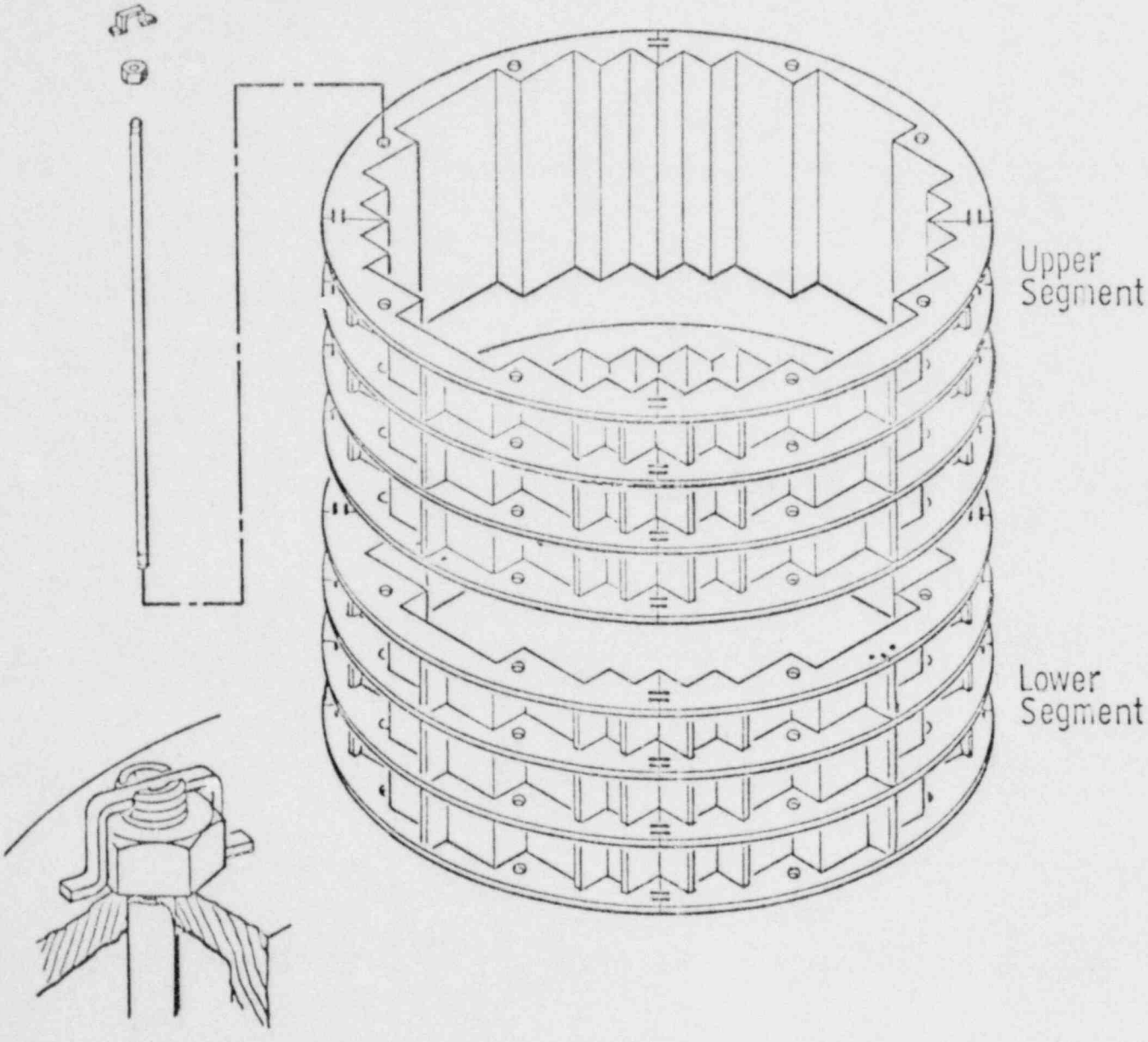

Core Shroud Assembly
(GENERIC)

Figure
4.6.3

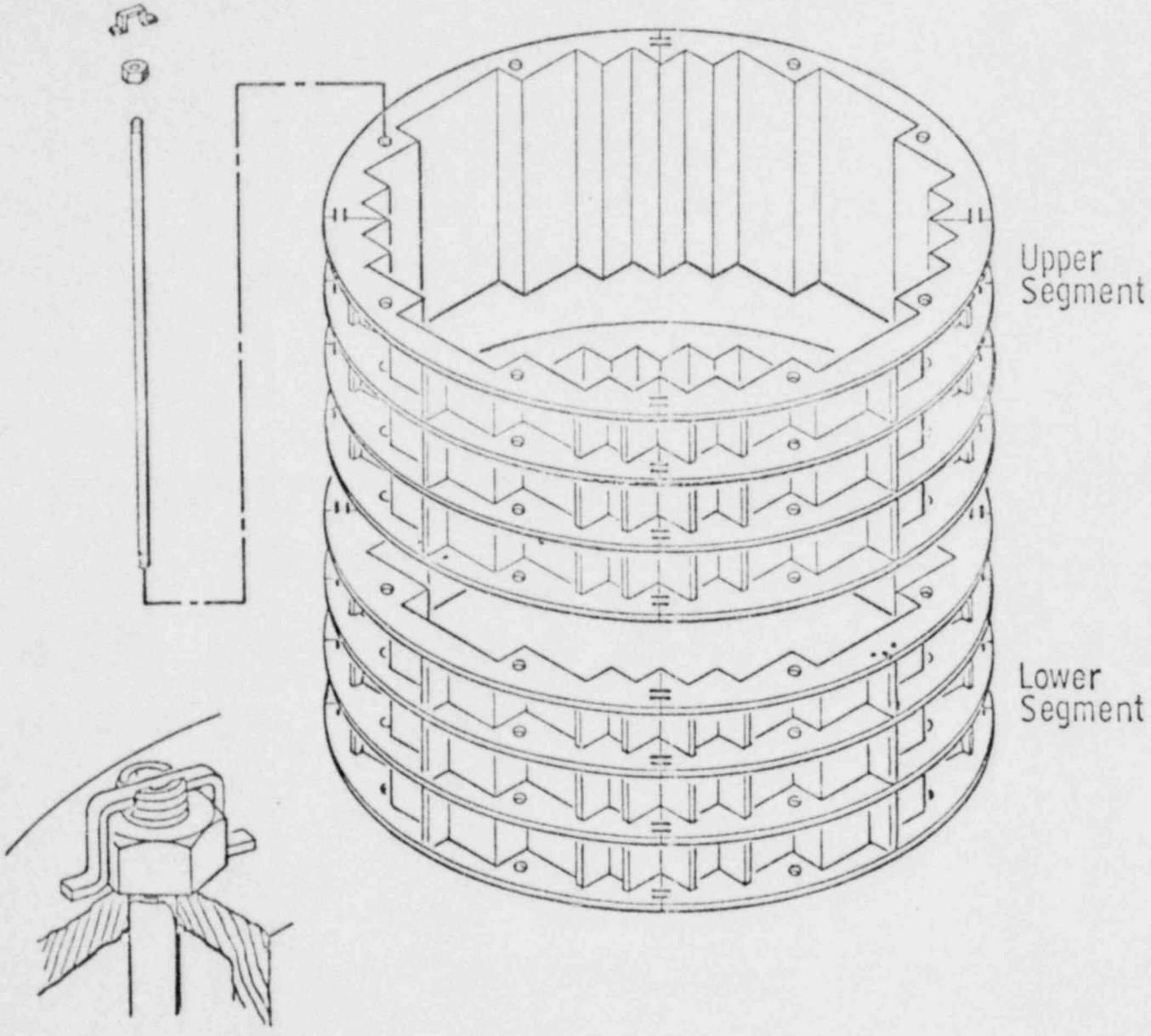

Core Shroud Assembly
(GENERIC)

Figure
4.6.3

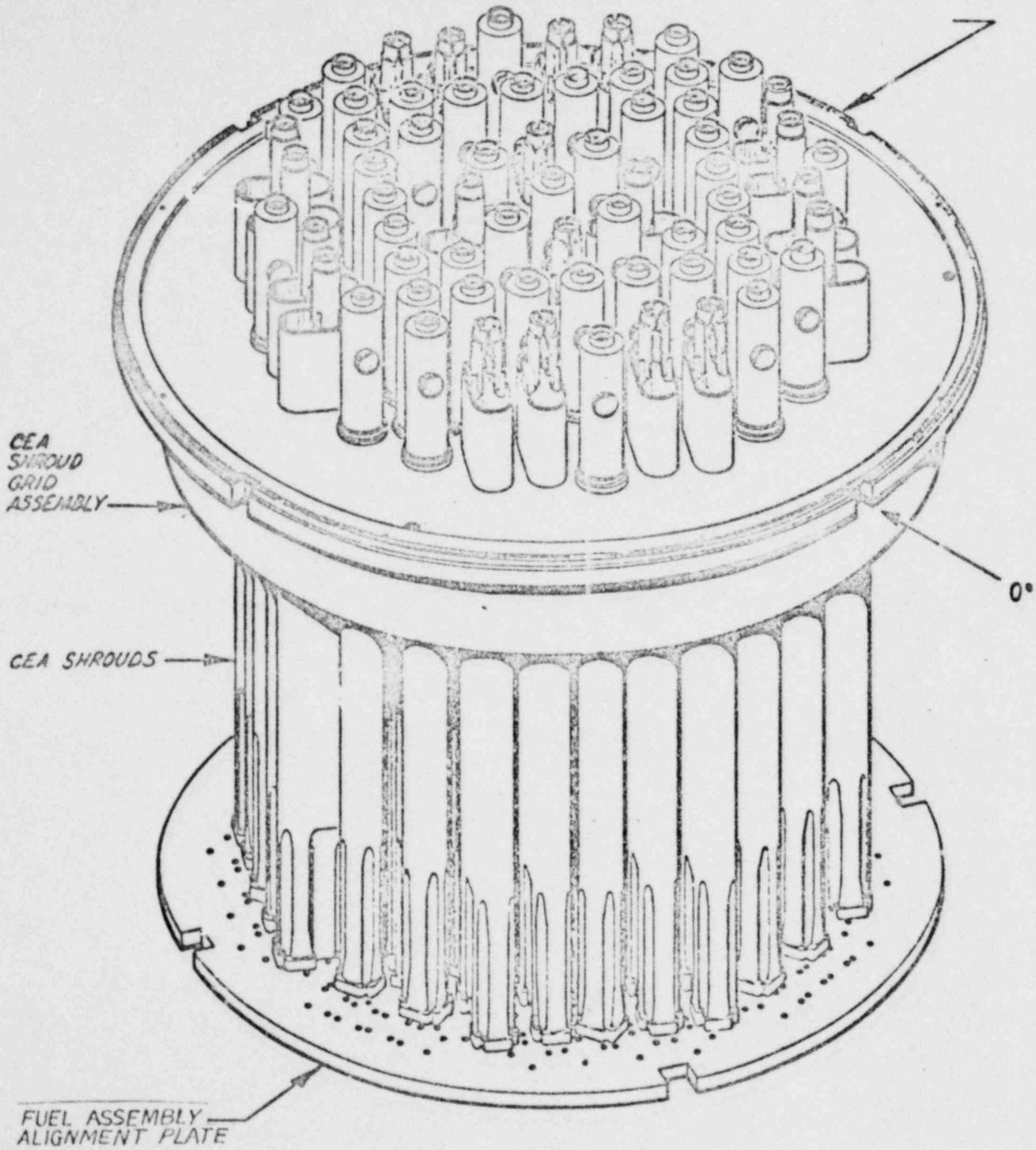

UPPER GUIDE STRUCTURE ASSEMBLY
(GENERIC)

Figure
4.6.4

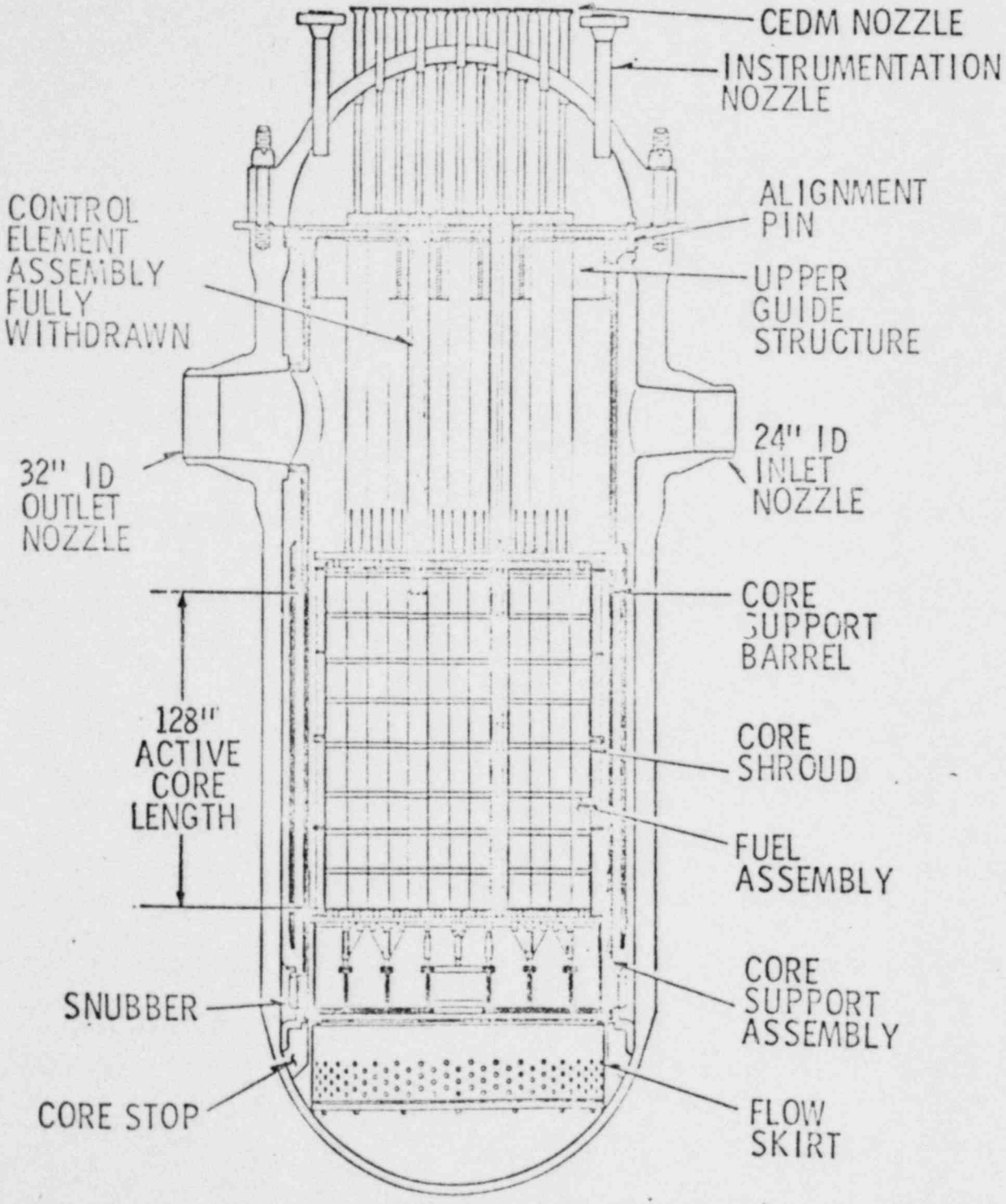

Reactor Internal Arrangement
(FORT CALHOUN)

4.6.40

Figure 4.6.5

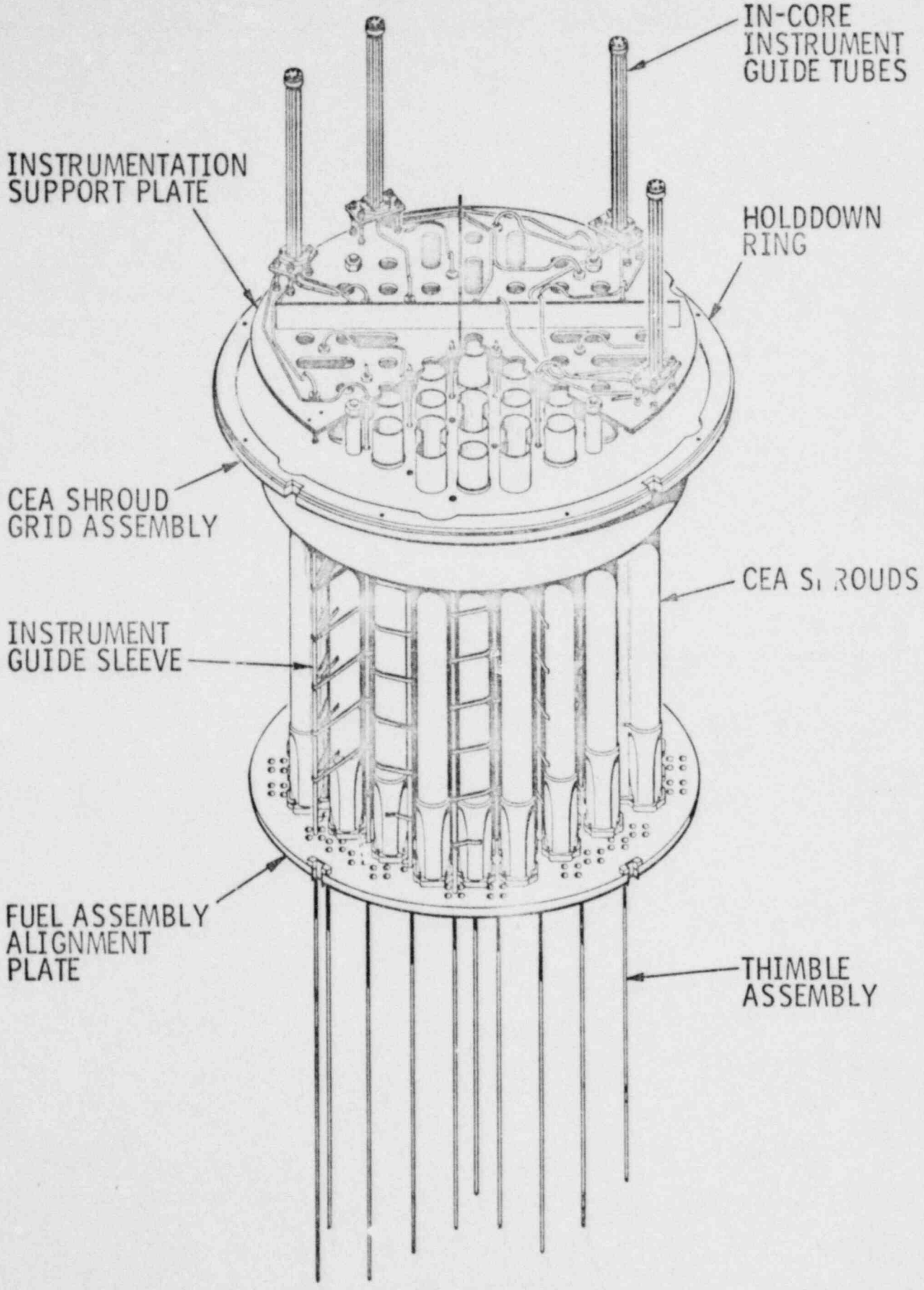

(FORT CALHOUN)

UPPER GUIDE STRUCTURE ASSEMBLY

FIGURE 4.6.6

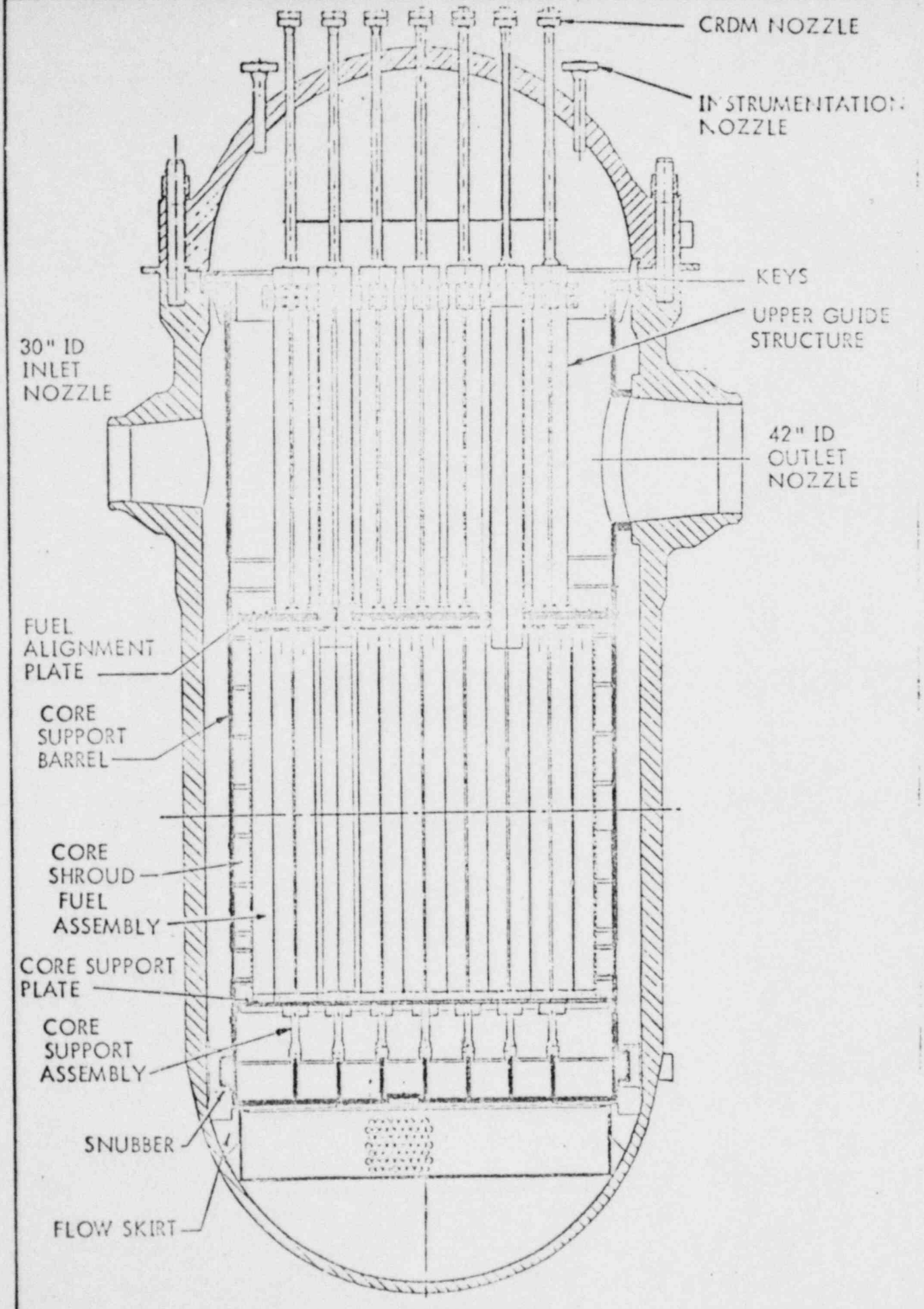

Reactor Arrangement
(PALISADES)

COMBUSTION ENGINEERING, INC.
WINDSOR, CONNECTICUT

Figure 4.6.7

PALISADES

UPPER GUIDE STRUCTURE ASSEMBLY

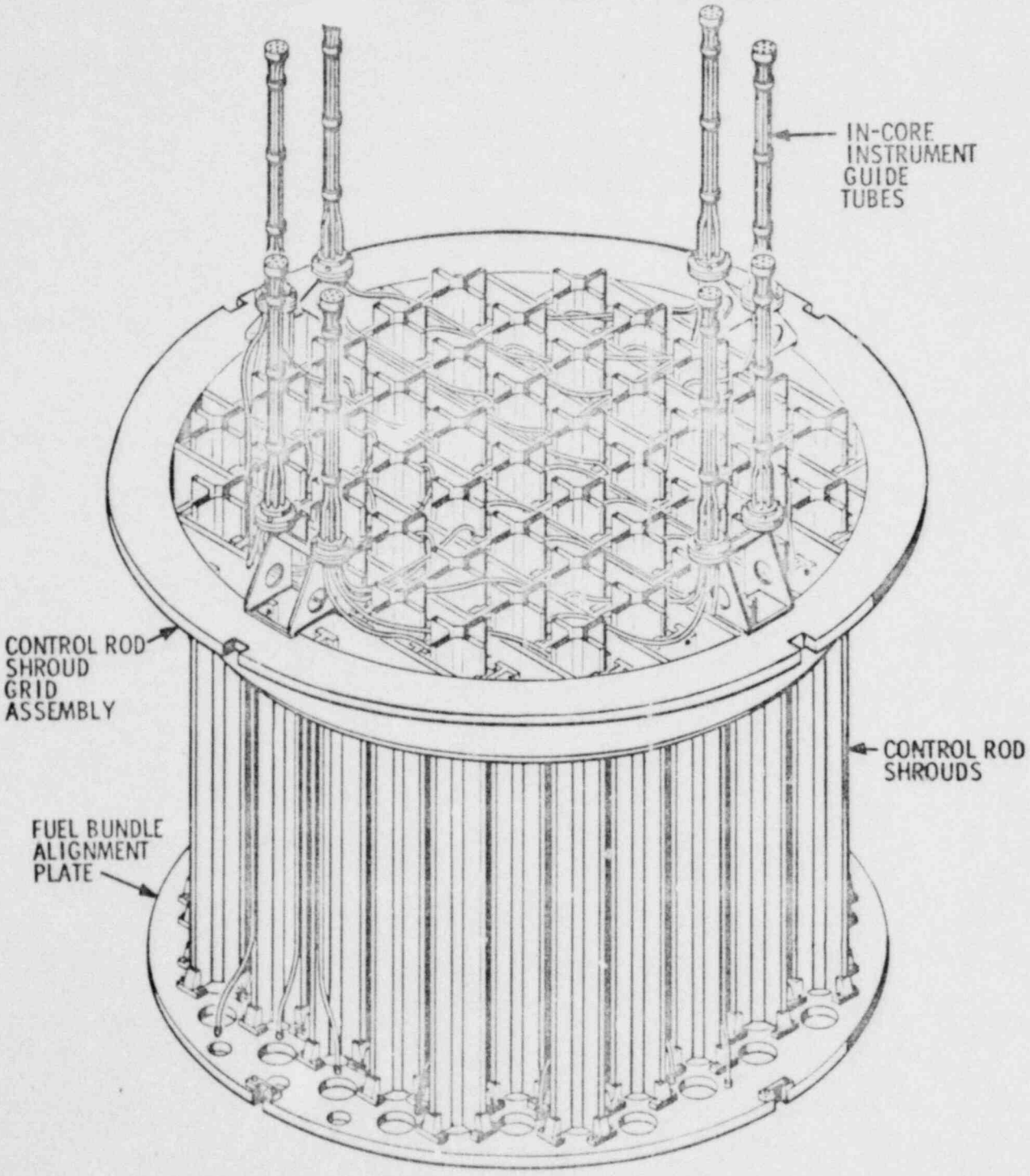

FIGURE 4.6.8

FIGURE 4.6.9

GENERIC PLANT

DETAILED LATERAL INTERNALS MODEL

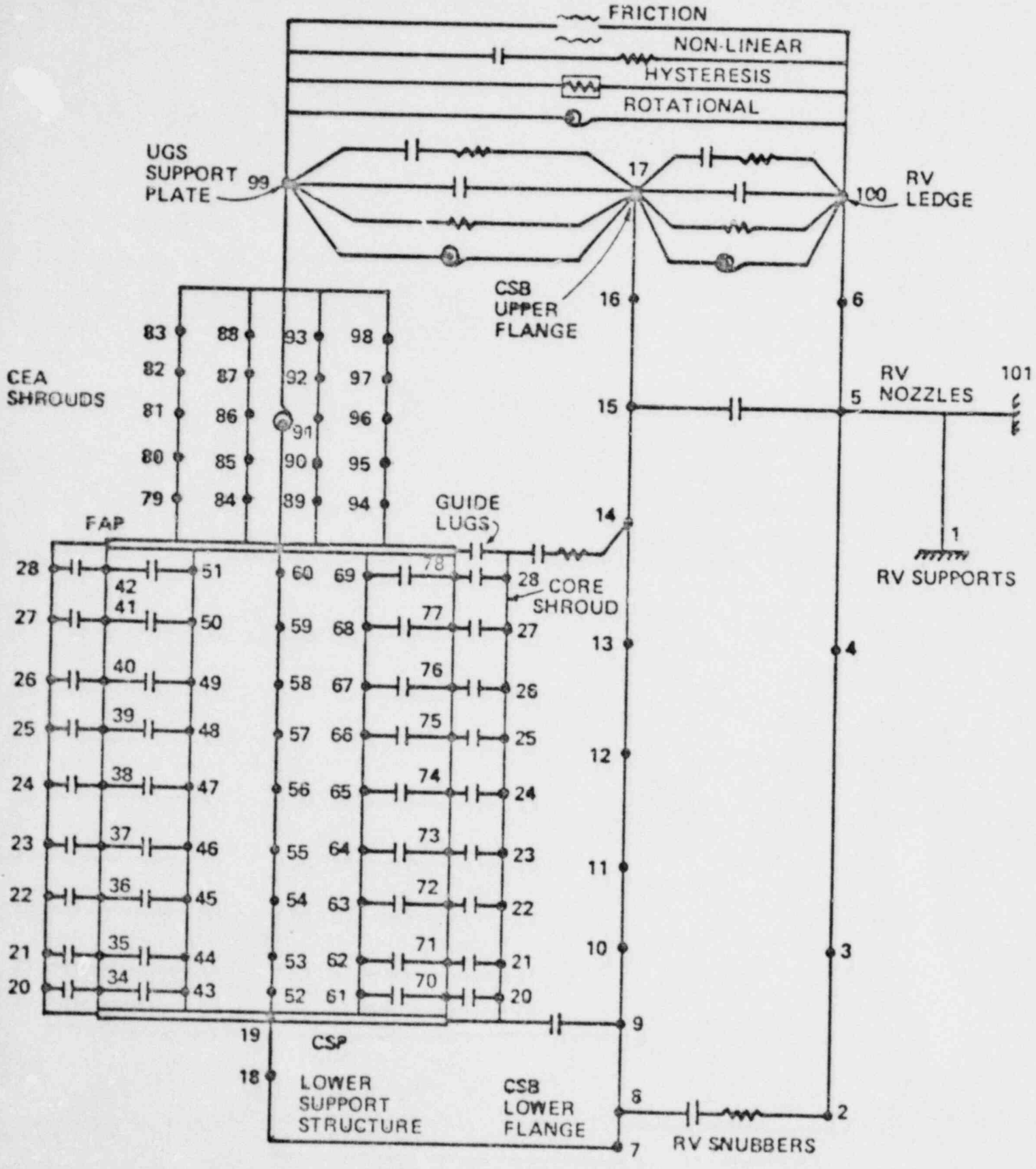

GENERIC PLANT

DETAILED VERTICAL INTERNALS MODEL

FIGURE 4.6.10

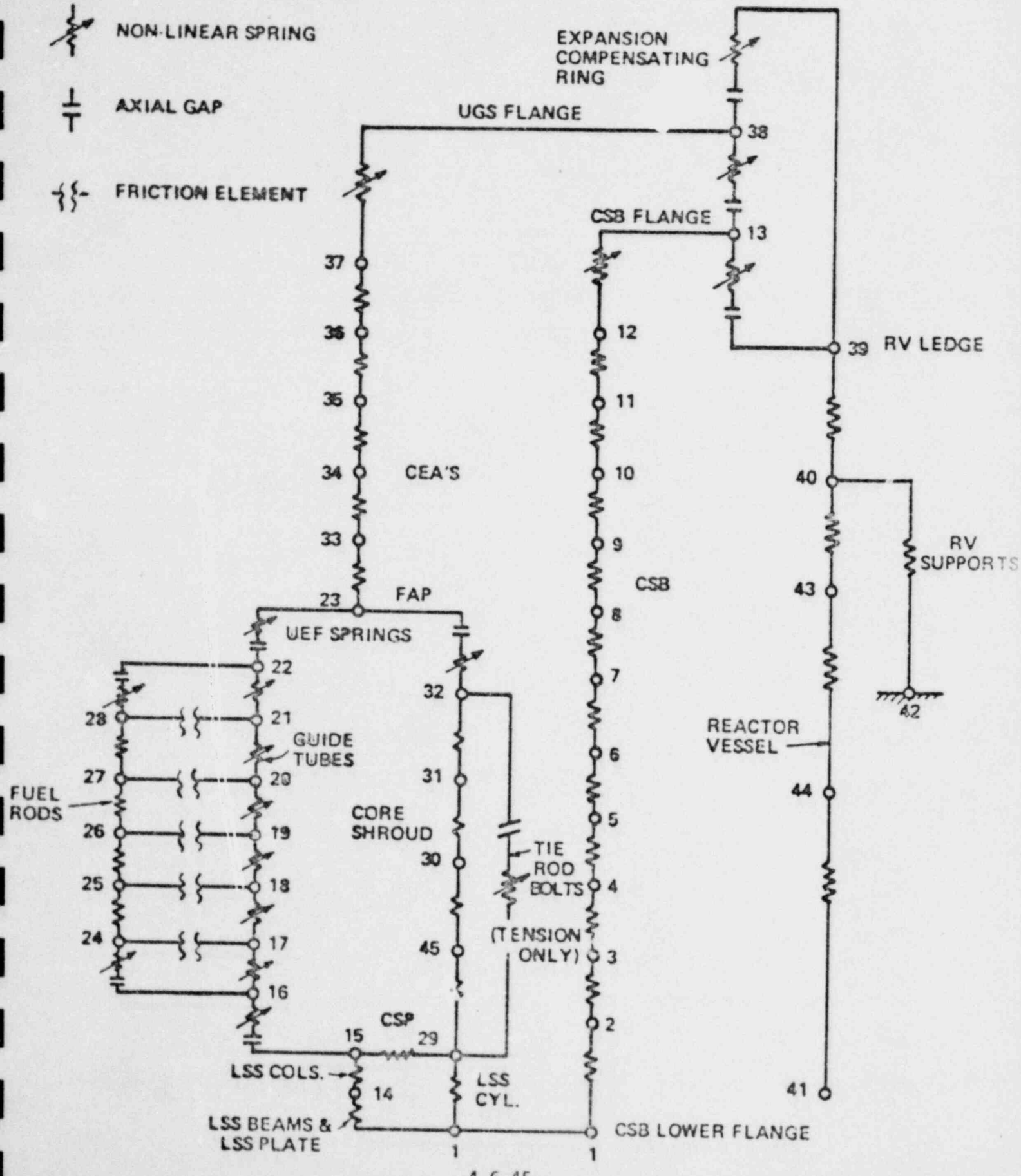

FIGURE 4.6.11

FT. CALHOUN

DETAILED LATERAL INTERNALS MODEL

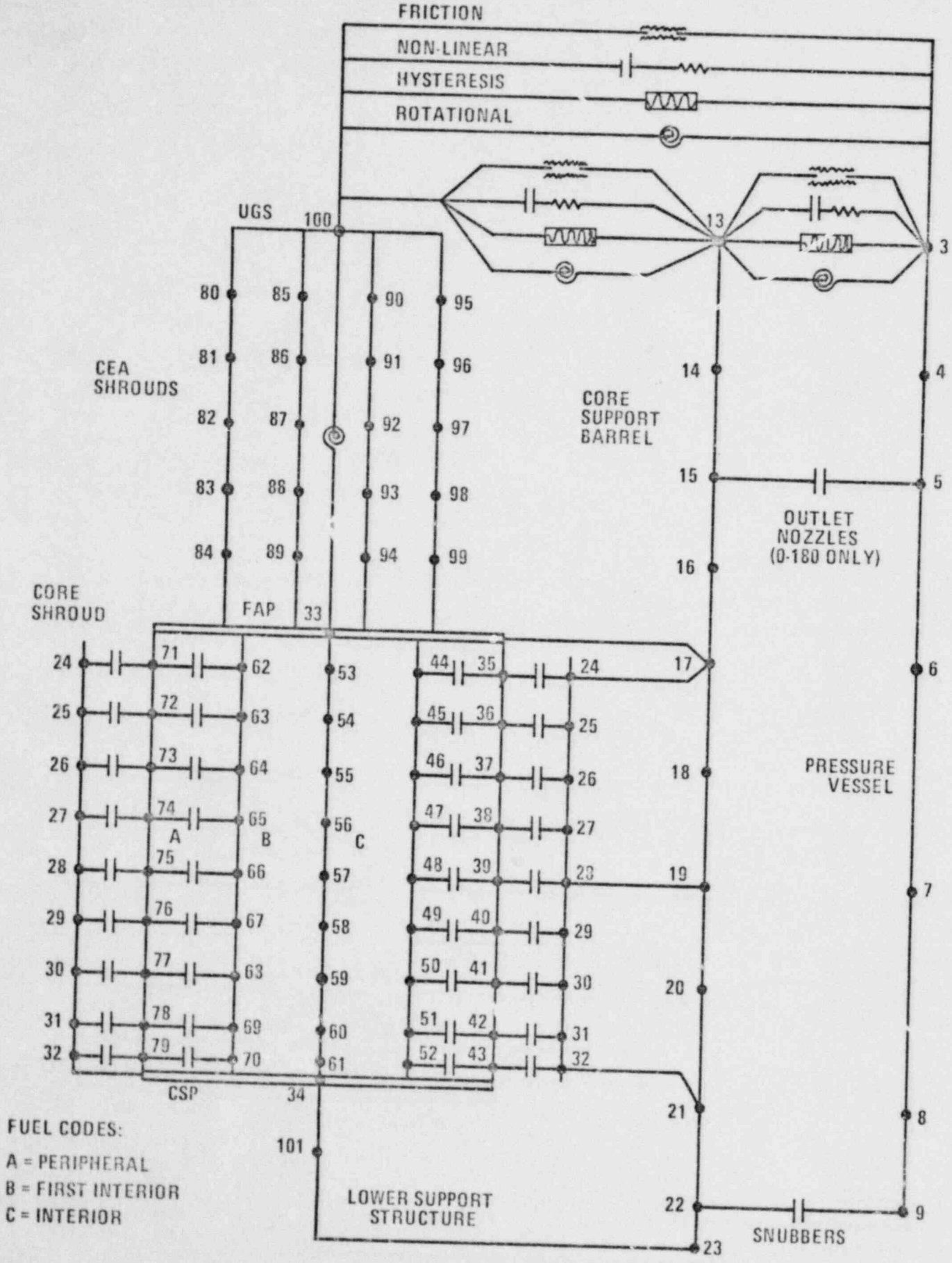

FIGURE 4.6.12

PALISADES

DETAILED LATERAL INTERNALS MODEL

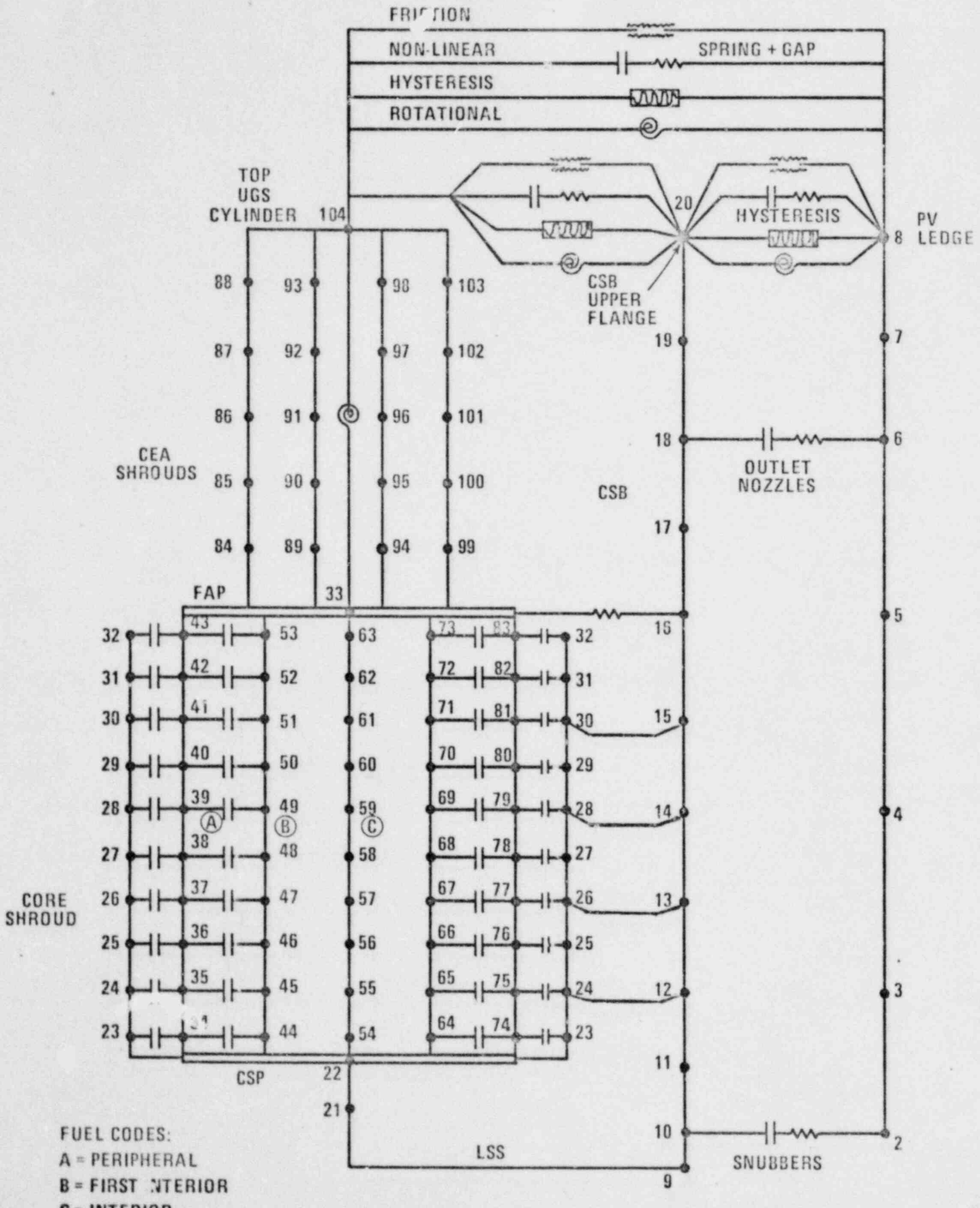

FIGURE 4.6.13

GENERIC PLANT REDUCED INTERNALS MODEL

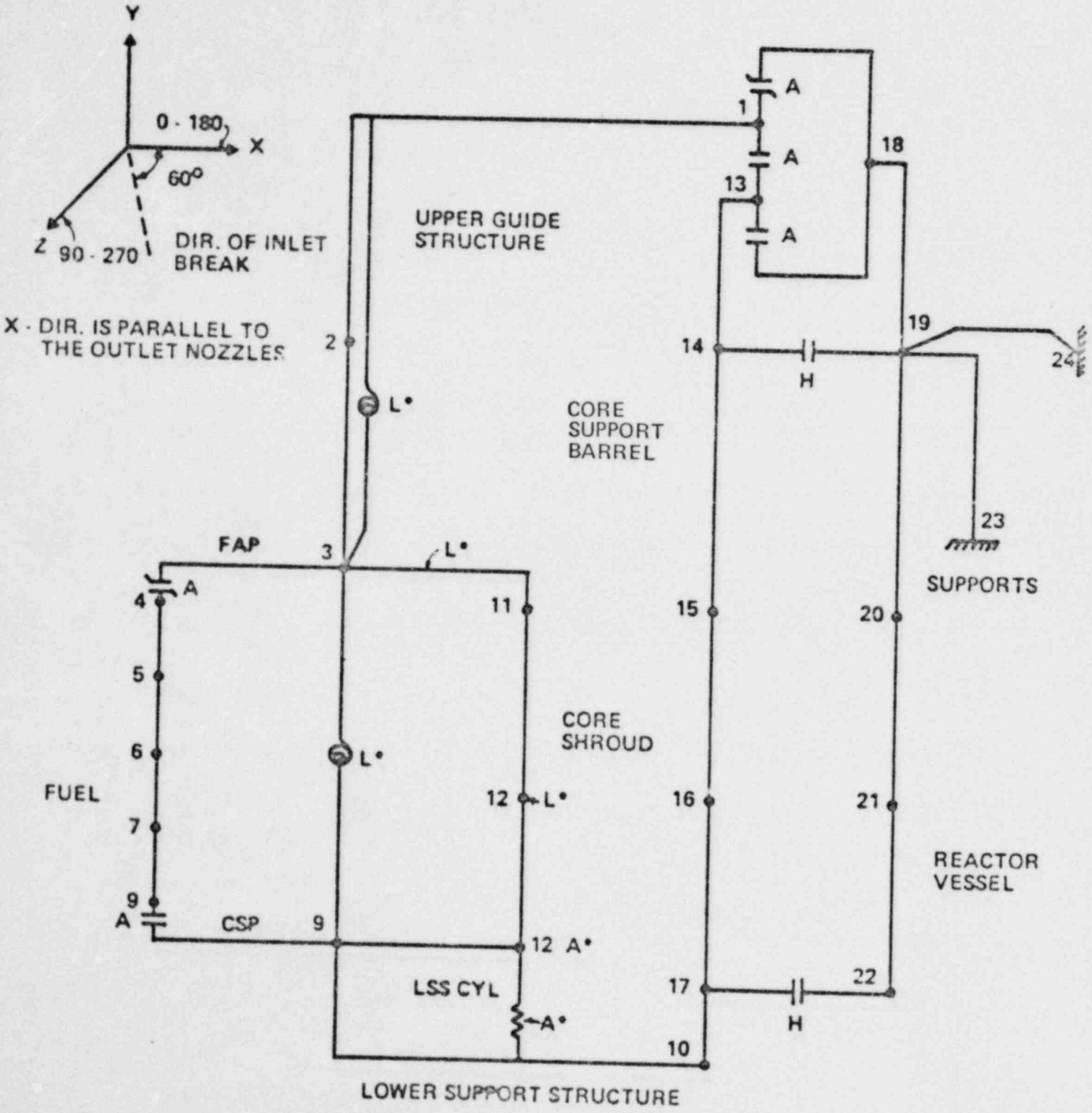

LEGEND:

A = AXIAL GAP

H = HORIZONTAL CAP

INDICATES AN AXIALLY PRELOADED COUPLING

L* = LATERAL MODEL ONLY

A* = AXIAL MODEL ONLY

FIGURE 4.6.1

GENERIC PLANT LAT MOD RV SUPP SHEAR - X DIR
COLD LEG BREAK

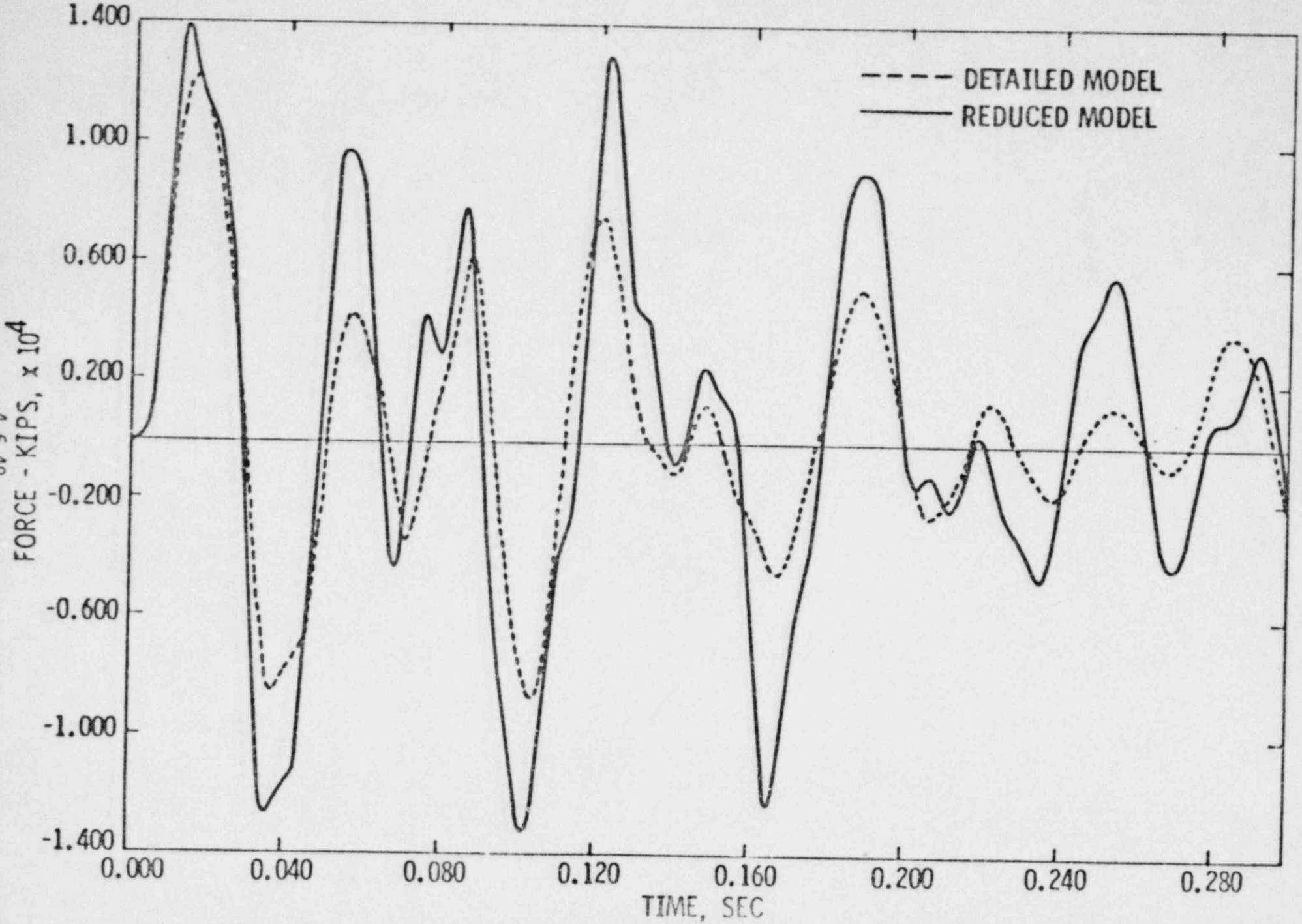

4.6.49

FIGURE 4.6.15

GENERIC PLANT AXIAL MOD RV SUPP LOADS

COLD LEG BREAK

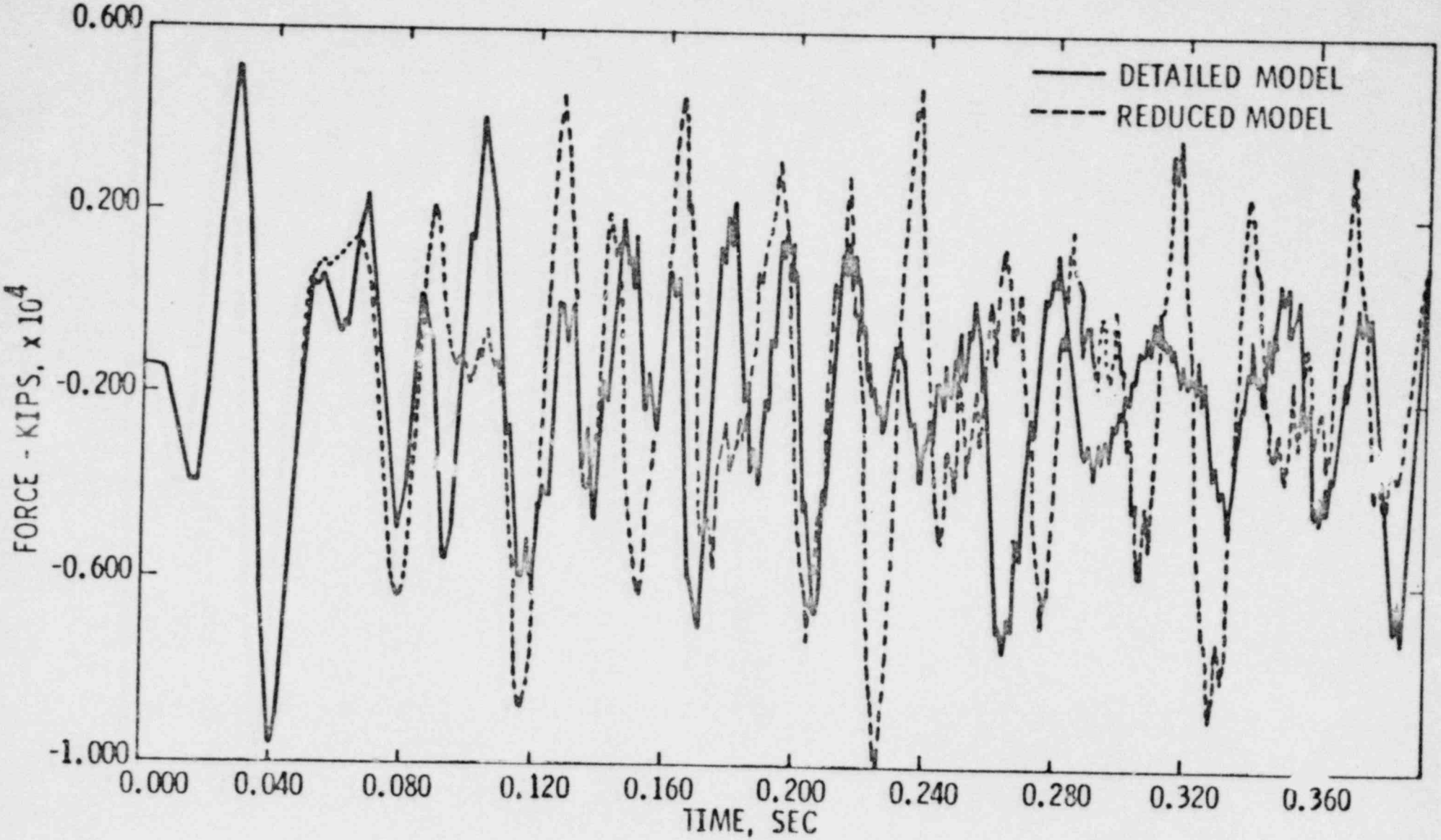

FIGURE 4.6.16

FT. CALHOUN

REDUCED LATERAL INTERNALS MODEL

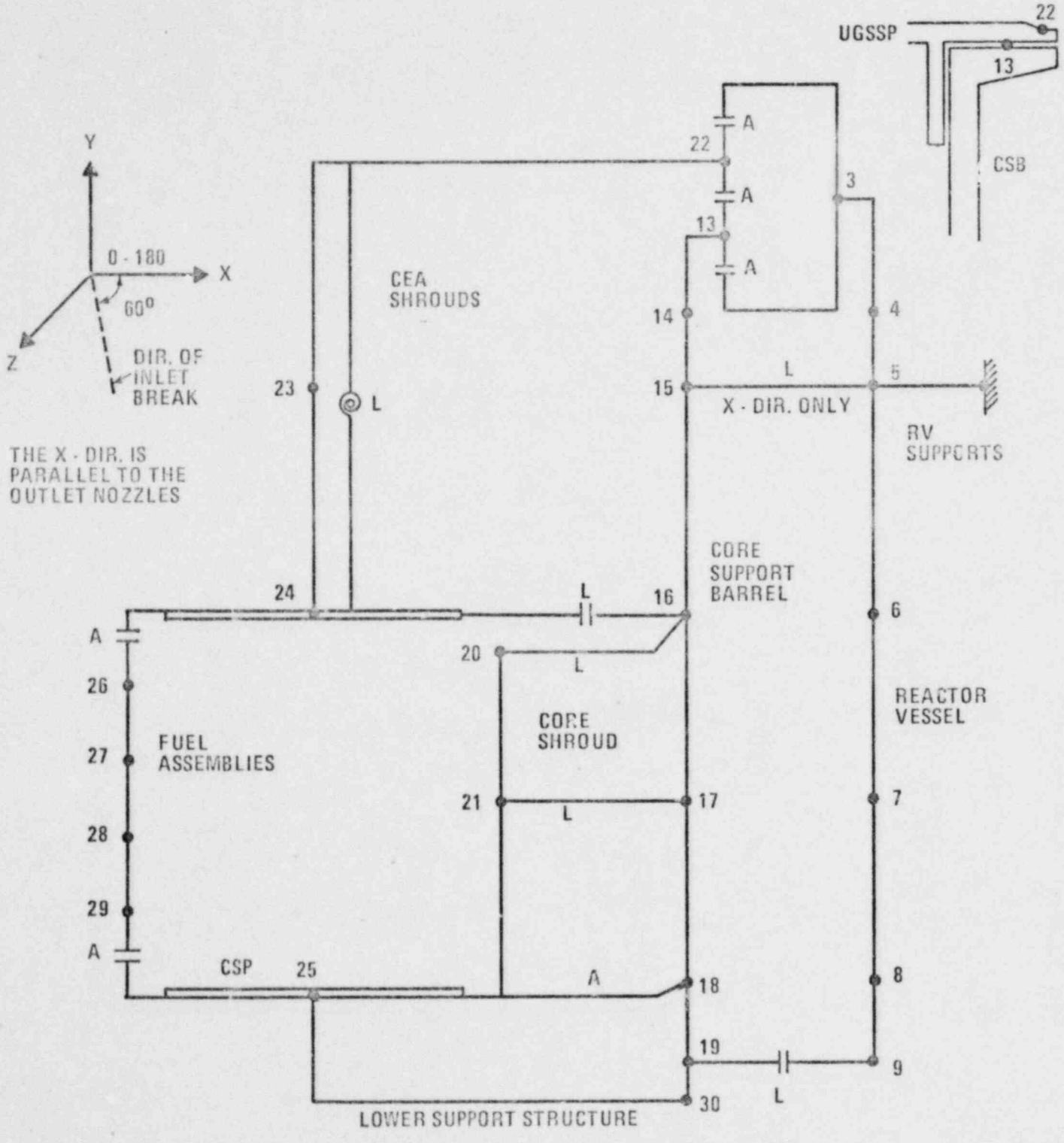

LEGEND: A = AXIAL
L = LATERAL

FIGURE 4.6.17

FT. CALHOUN LAT MOD RV SUPP SHEAR - Z DIR

COLD LEG BREAK

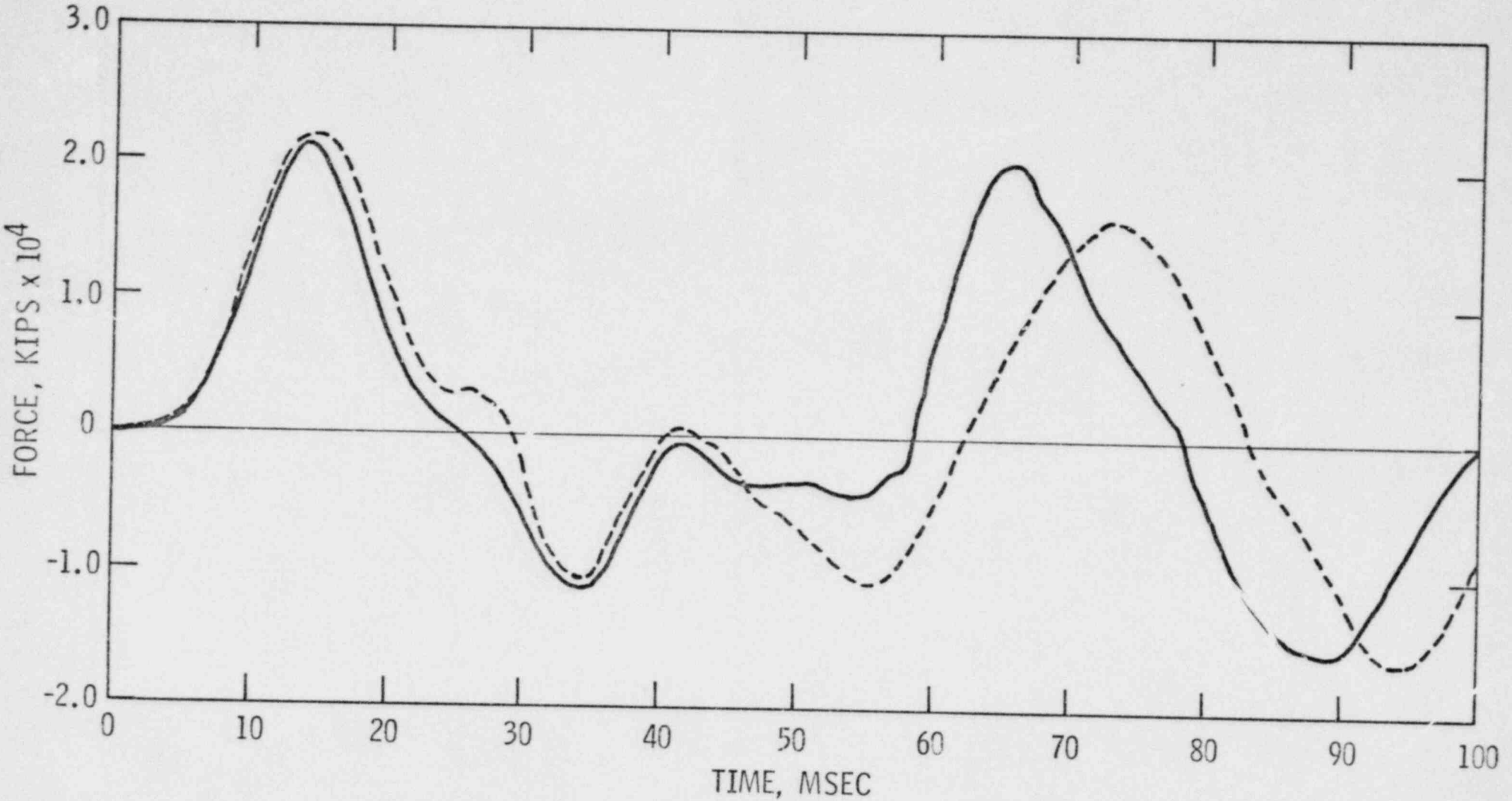

FIGURE 4.6.18

GENERIC PLANT COLD LEG BREAK CORE SUPPORT

BARREL TOTAL LOADS PARALLEL TO HOT LEGS

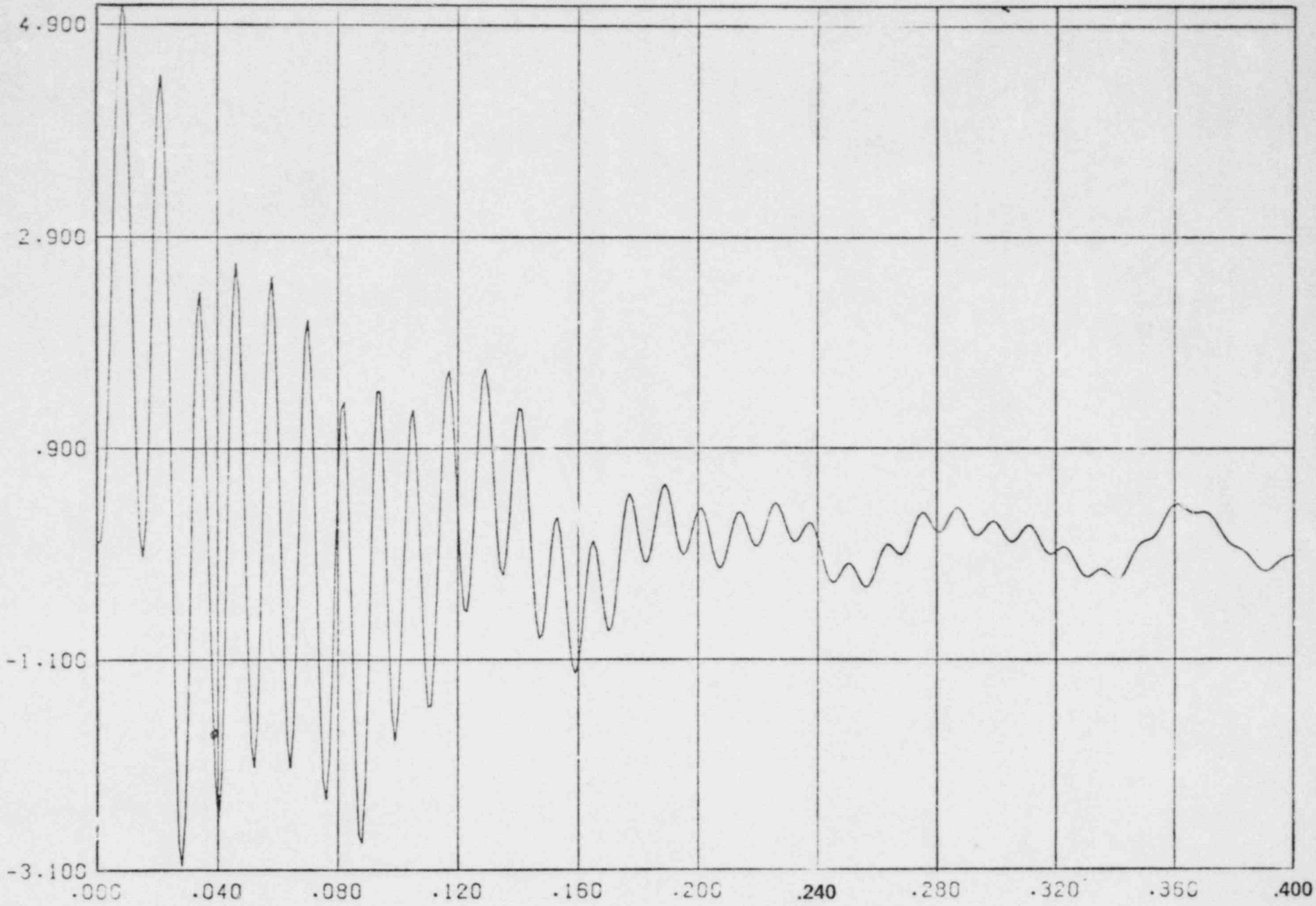

FIGURE 4.6.19

GENERIC PLANT COLD LEG BREAK CORE SUPPORT
BARREL TOTAL LOADS PERPENDICULAR TO HOT LEGS

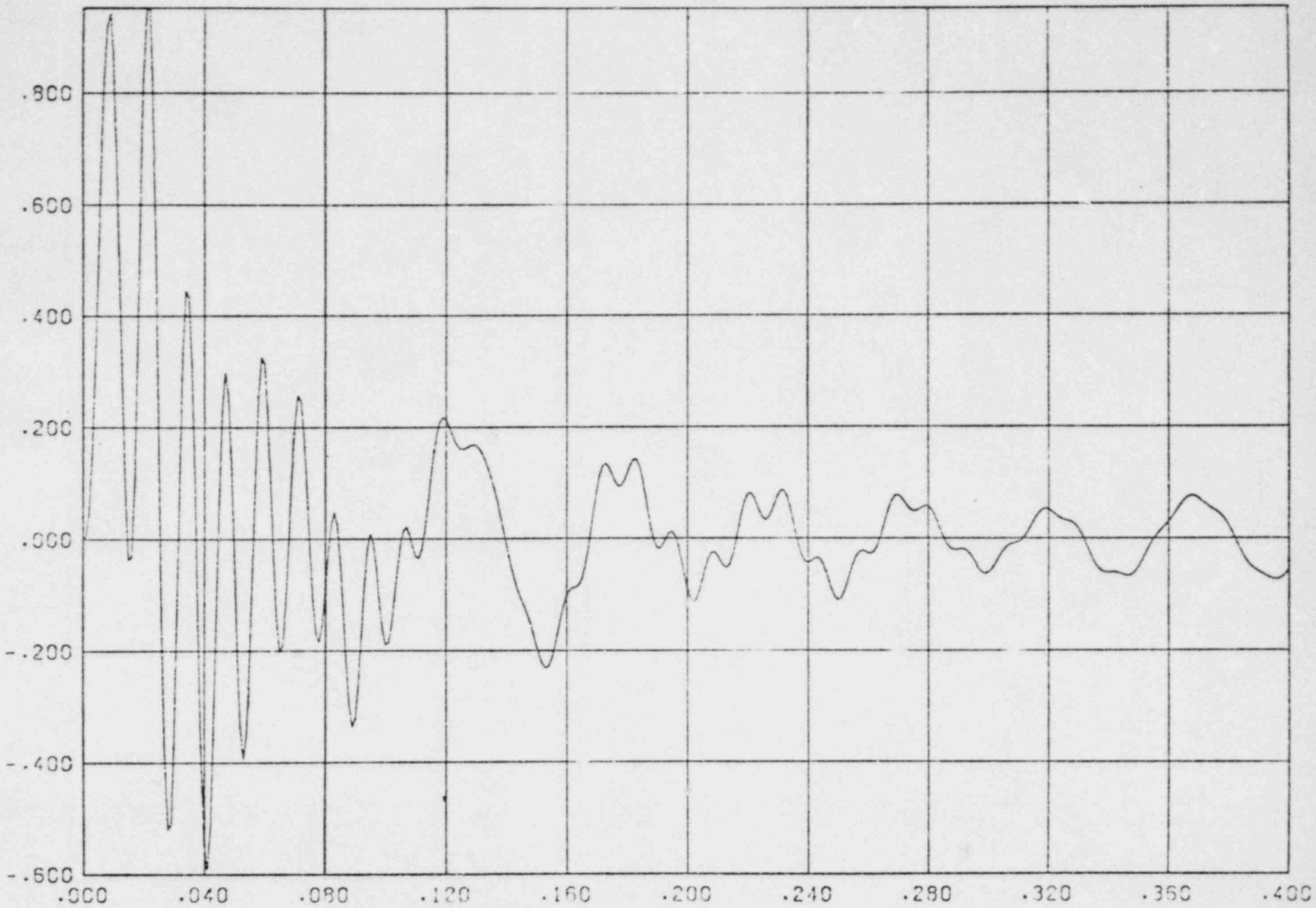

FORCE-LBS
(X10)

4.6.54

FIGURE 4.6.20

GENERIC PLANT HOT LEG BREAK LATERAL CROSSFLOW
LOADS ON CEA SHROUDS

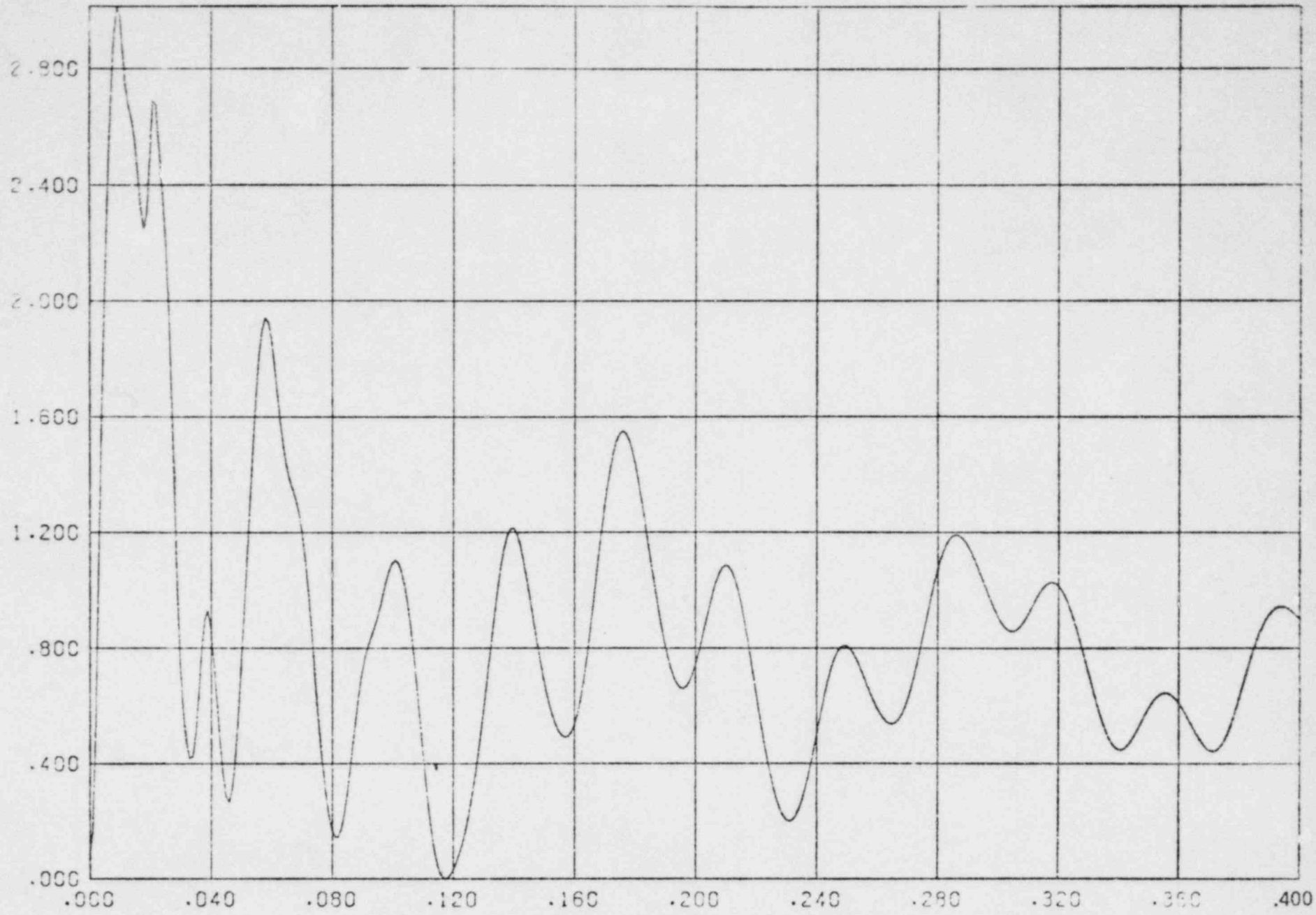

4.6.55

FIGURE 4.6.21

PALISADES COLD LEG BREAK CORE SUPPORT BARREL

TOTAL LOADS

PERPENDICULAR TO HOT LEGS

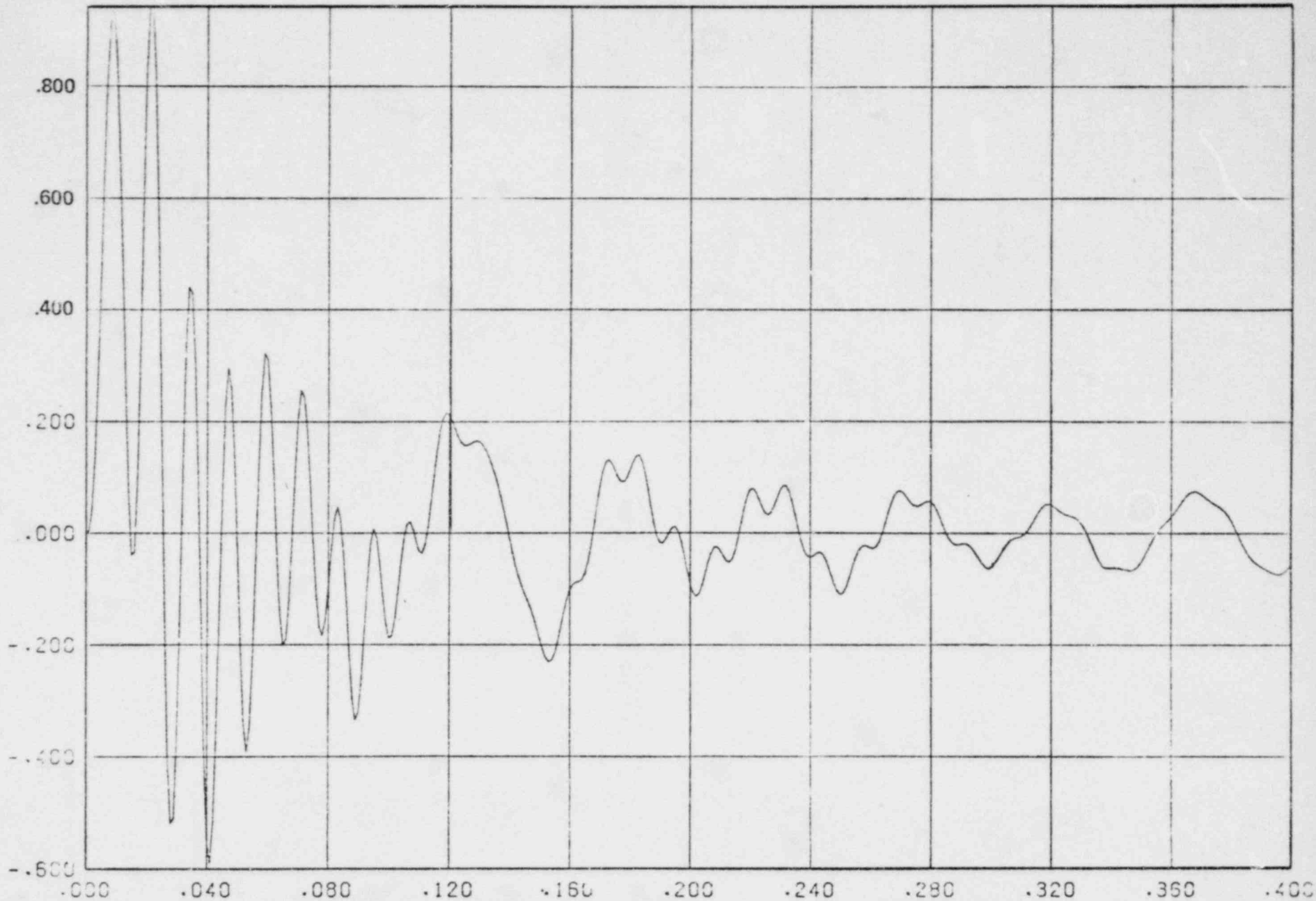

4.6.56
FORCE-LBS
(X10⁷)

TIME-SEC
(X10⁰)

FIGURE 4.6.22

PALISADES COLD LEG BREAK CORE SUPPORT BARREL
TOTAL LOADS
PARALLEL TO HOT LEGS

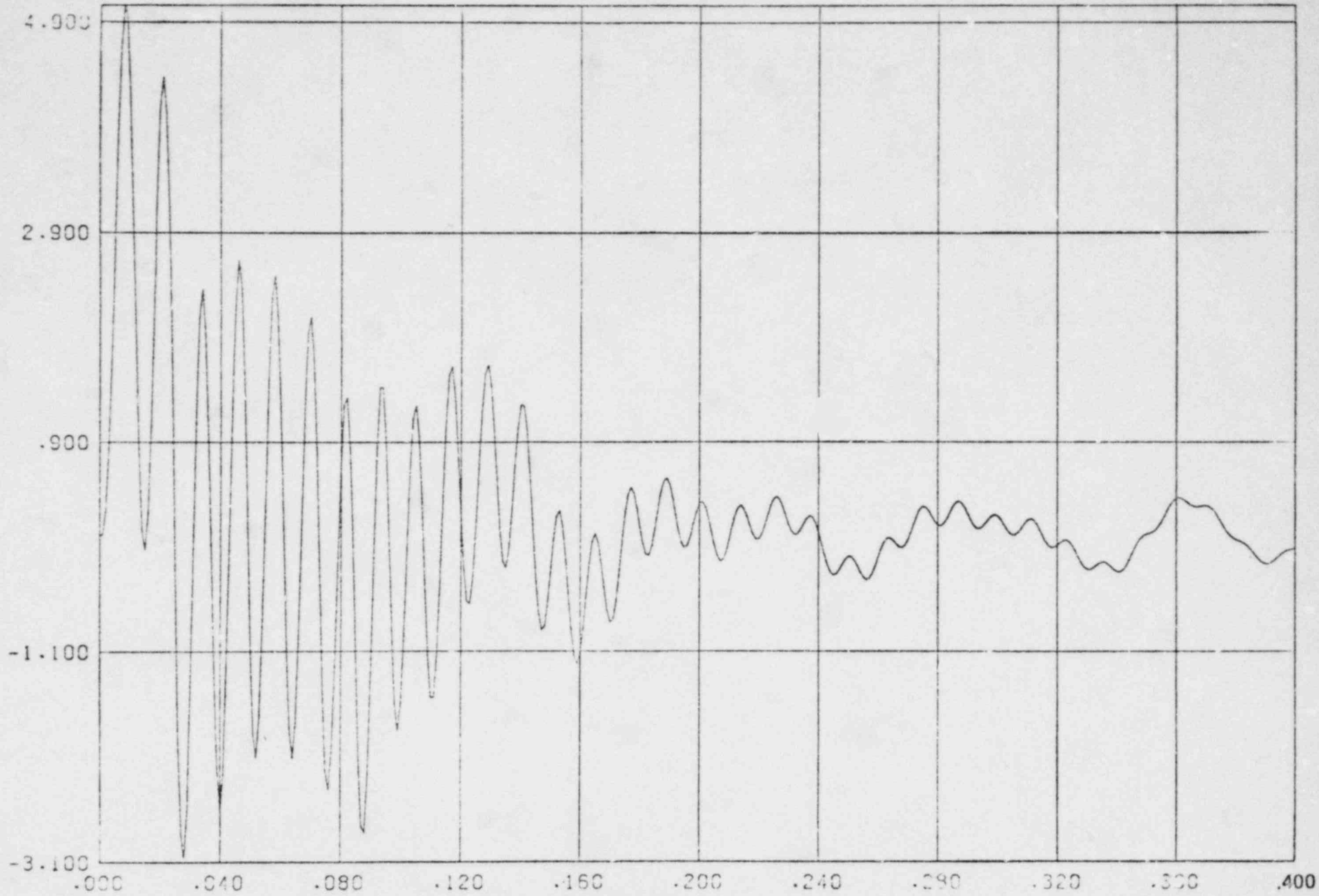

4.6.57

FIGURE 6.2

FT. CALHOUN COLD LEG BREAK CORE SUPPORT BARREL
TOTAL LOADS
PERPENDICULAR TO HOT LEGS

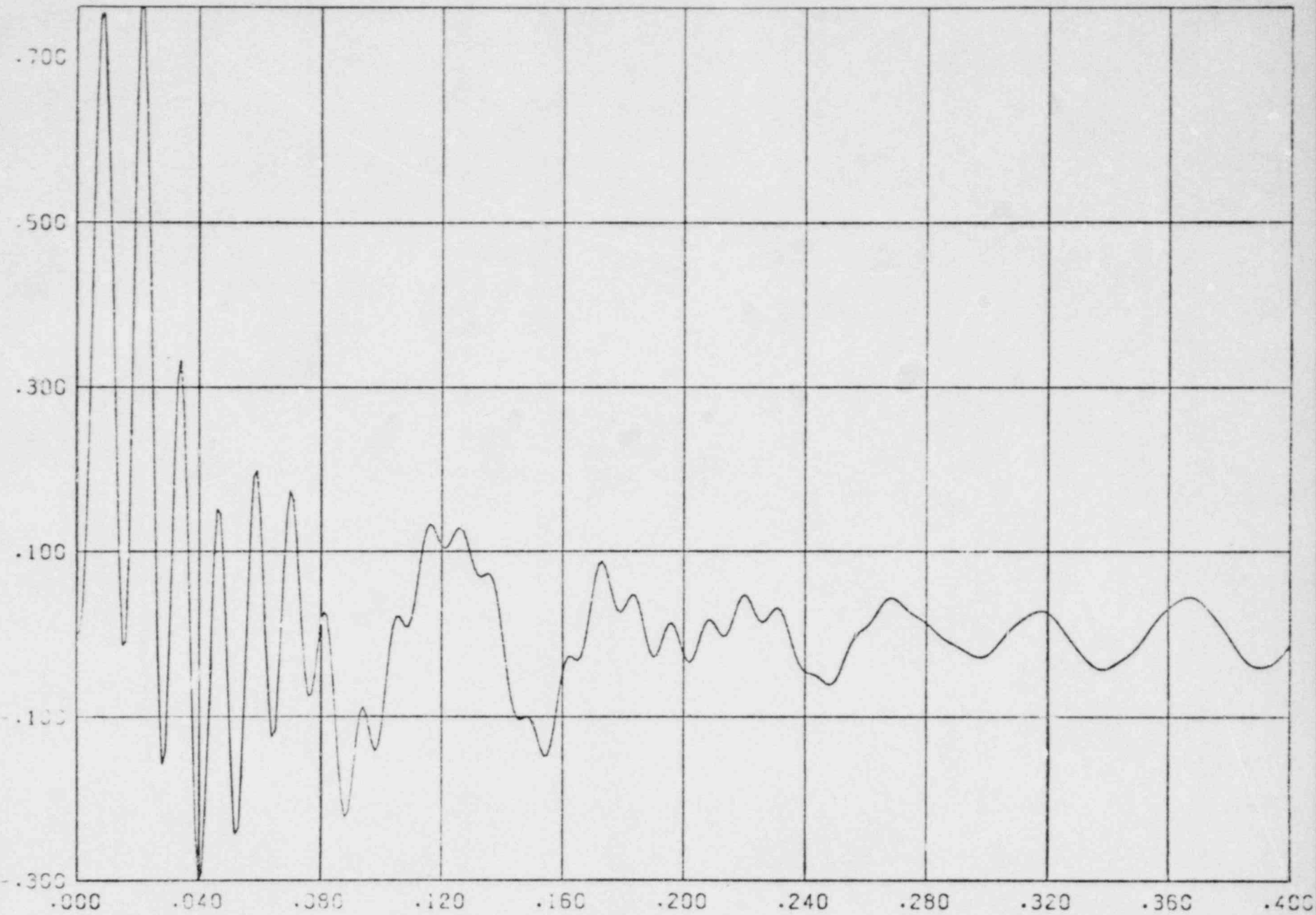

4.6.58

FIGURE 4.6.24

FT. CALHOUN COLD LEG BREAK CORE SUPPORT BARREL

TOTAL LOADS

PARALLEL TO HOT LEGS

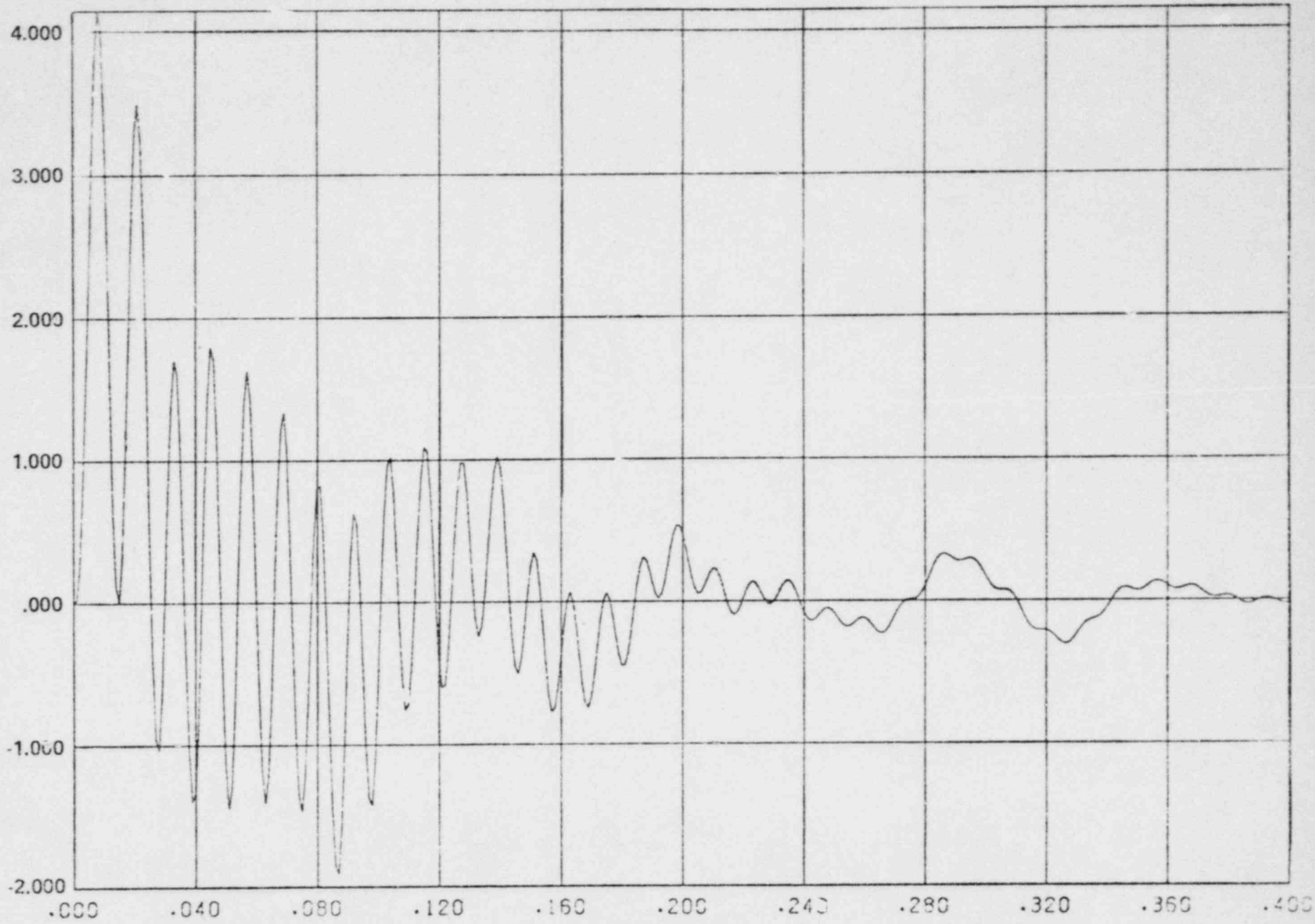

4.6.59

FIGURE 4.6.25

PALISADES HOT LEG BREAK

TOTAL LATERAL CROSSFLOW LOADS

ON CEA SHROUDS

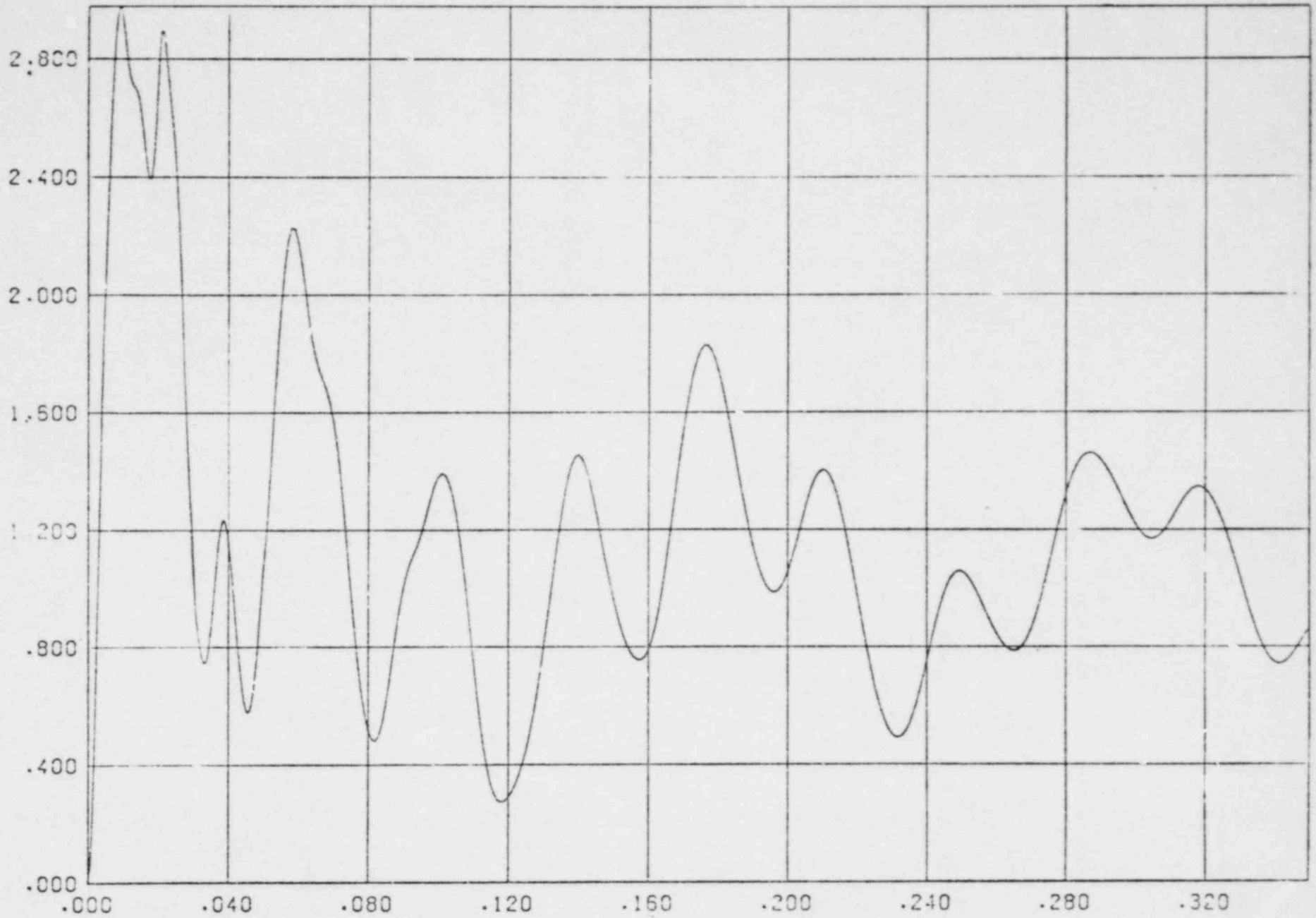

4.6.60

FIGURE 4.6.26

FT. CALHOUN HOT LEG BREAK
TOTAL LATERAL CROSSFLOW LOADS
ON CEA SHROUDS

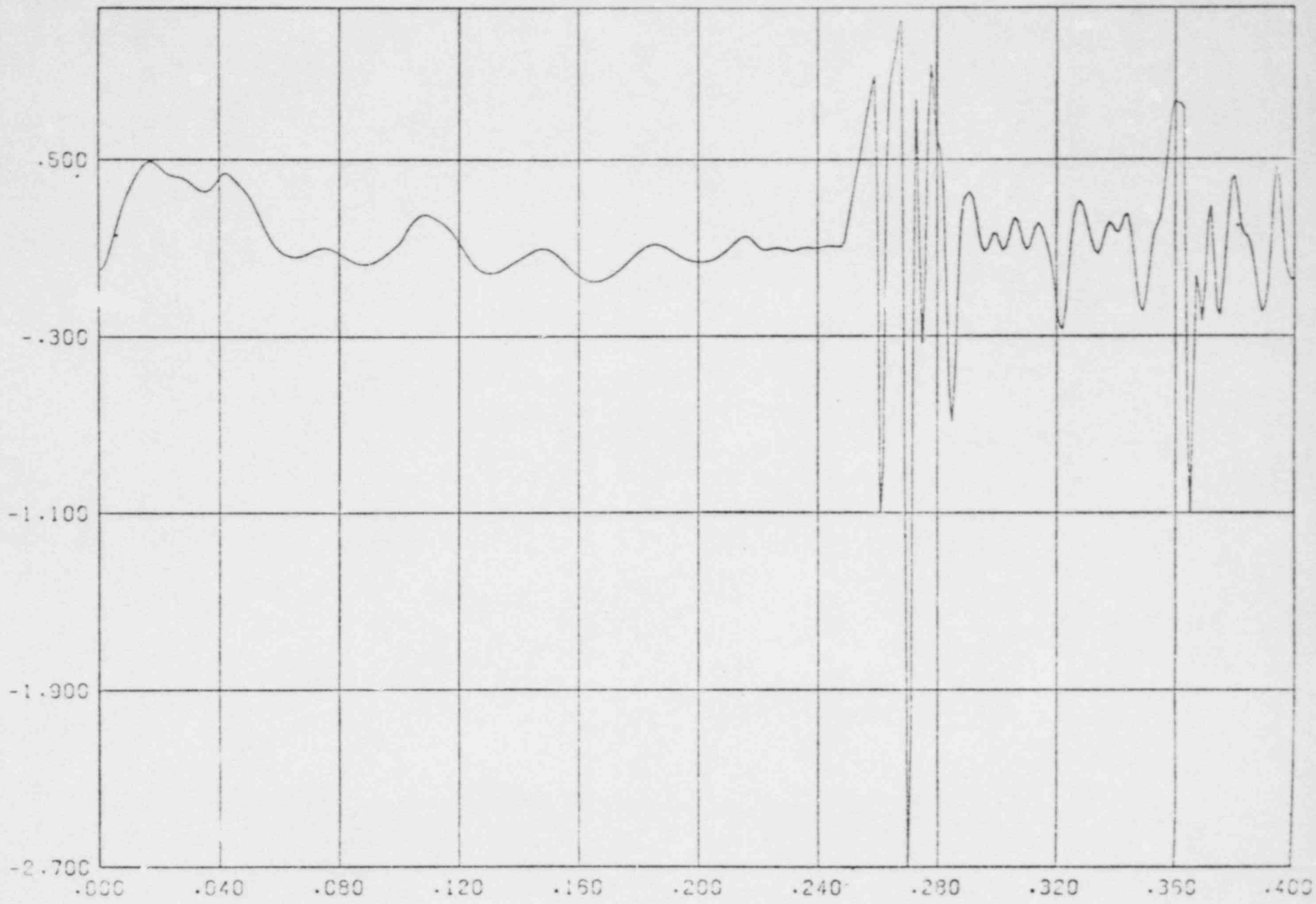

4.6-1

FIGURE 4.6.27

GENERIC PLANT CSB

FINITE ELEMENT MODEL FOR

COLD LEG BREAK RESPONSE ANALYSIS

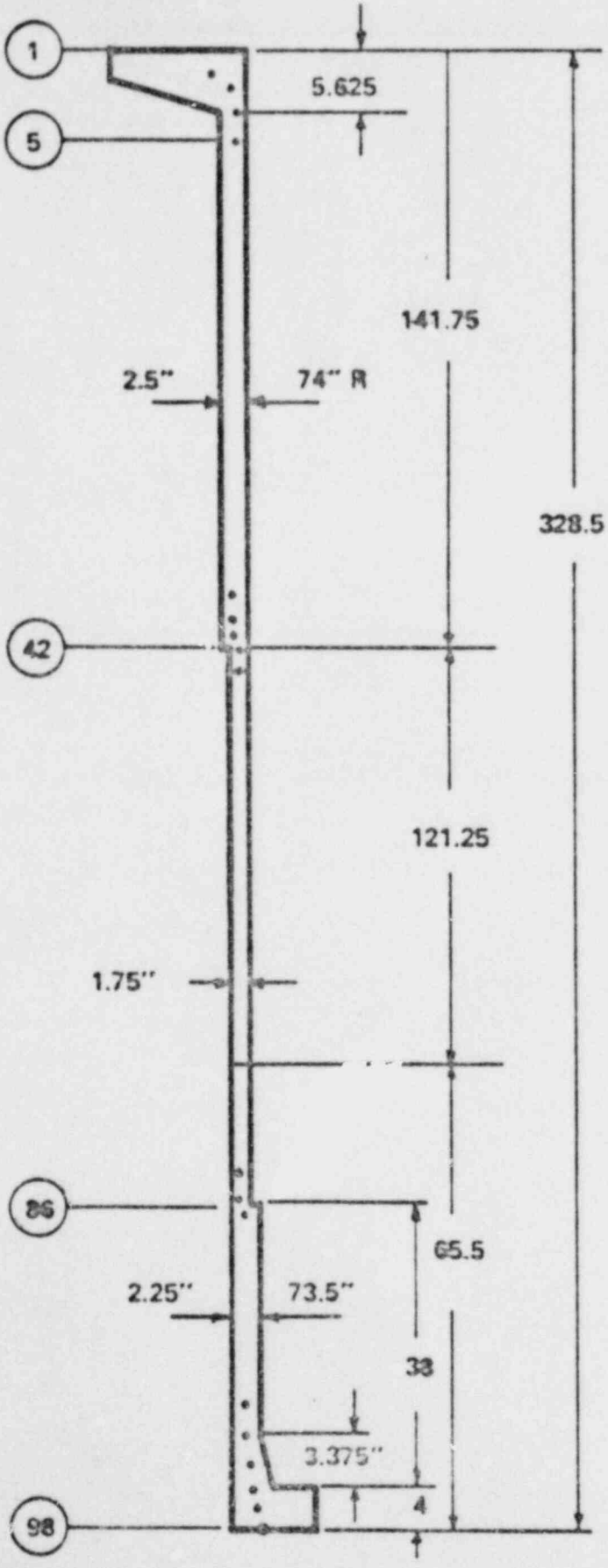

FIGURE 4.6.28

PALISADES CSB MODEL
FOR COLD LEG BREAK RESPONSE ANALYSIS

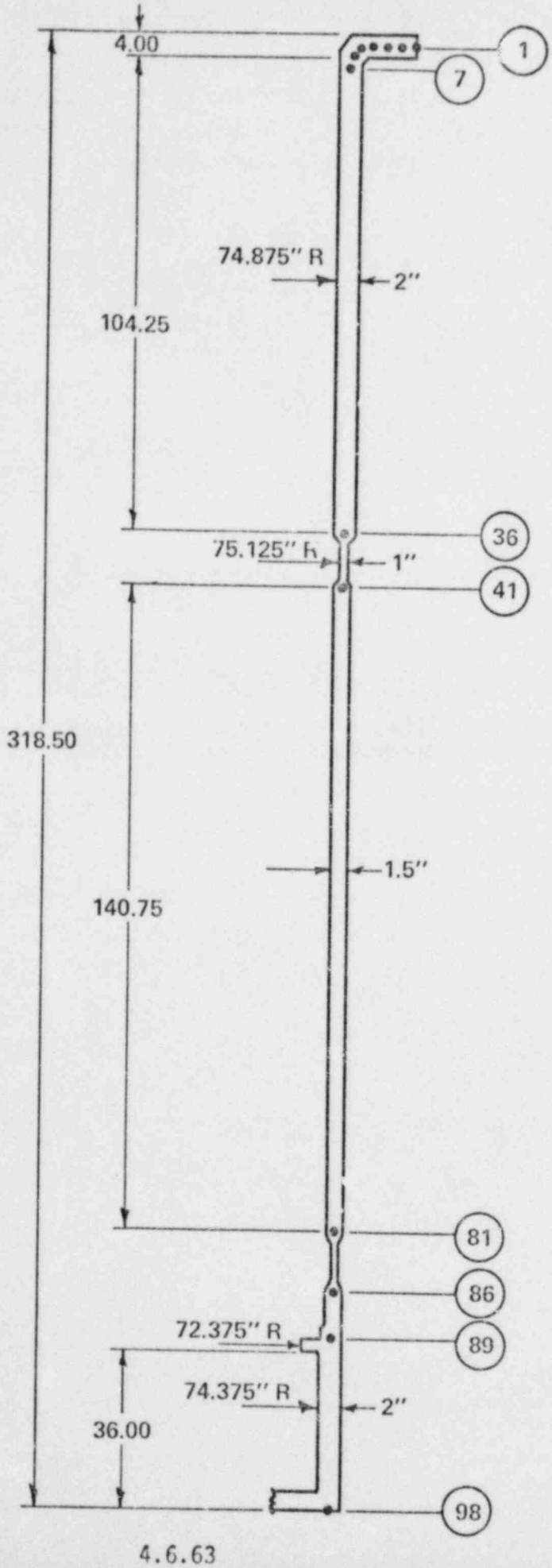

FIGURE 4.6.29
FT. CALHOUN CSB MODEL
FOR COLD LEG BREAK RESPONSE ANALYSIS

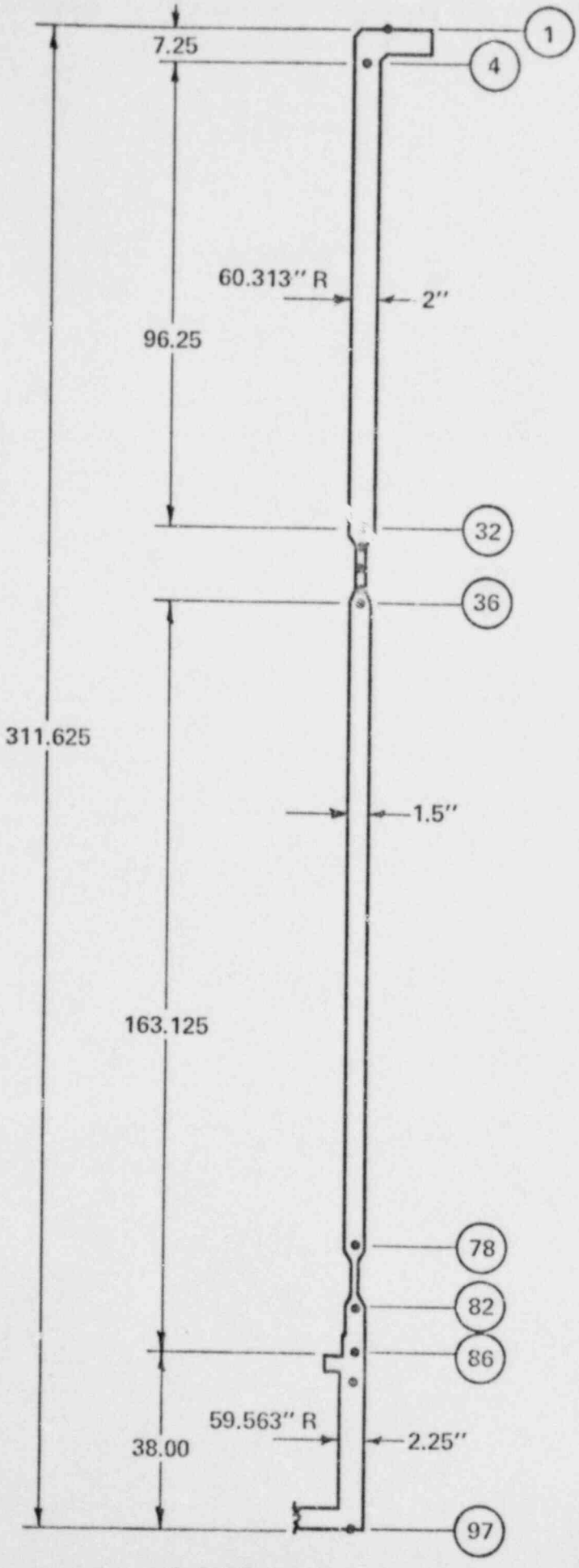

FIGURE 4.6.30

GENERIC PLANT CSB
FINITE - ELEMENT MODEL
FOR STABILITY ANALYSIS

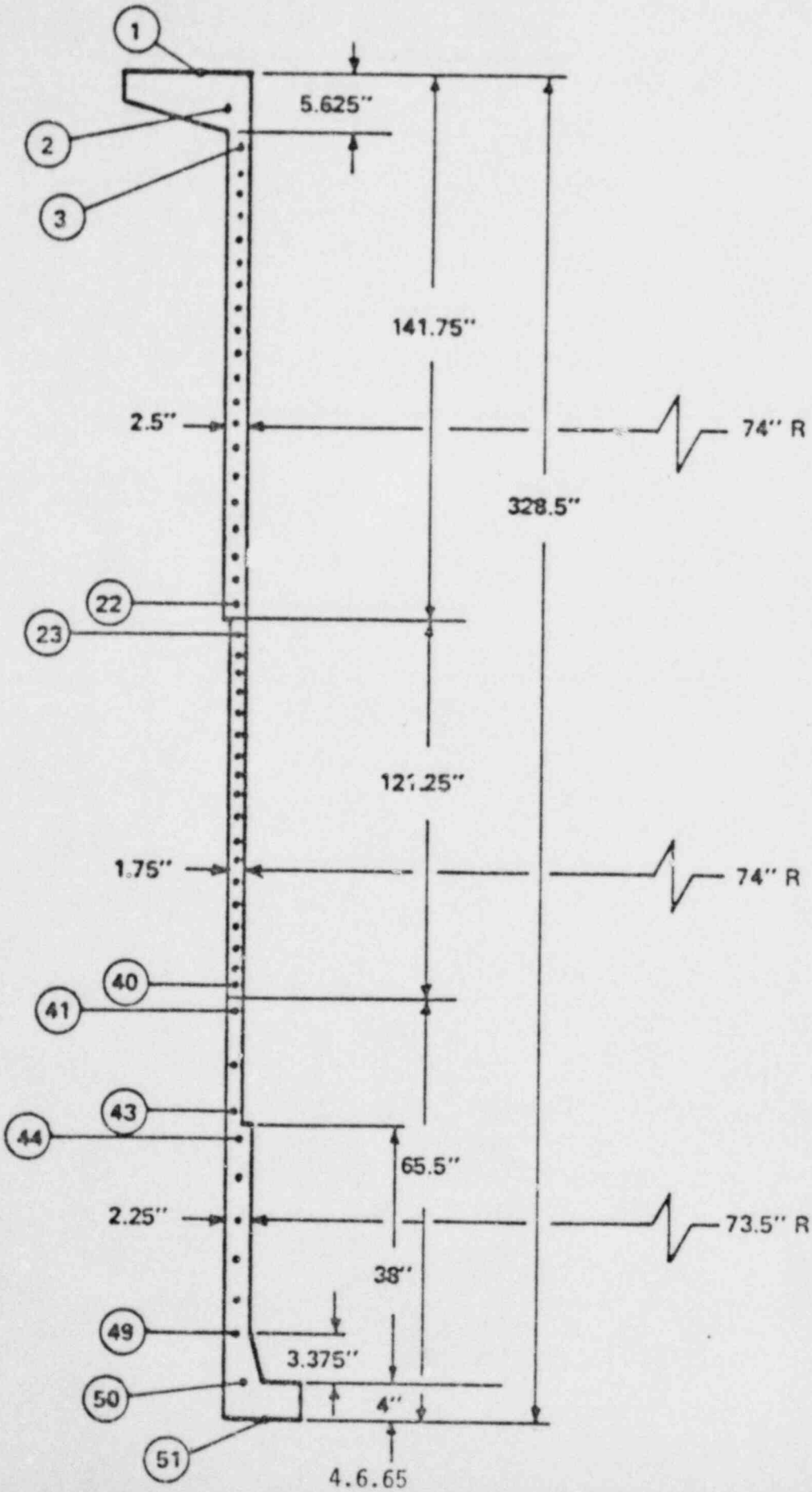

Table 4.6.2

Generic Plant

Lateral Model Node Locations

NODE	DESCRIPTION
1	Ground
2	RV @ snubber location
3	RV
4	RV
5	RV @ nozzle
6	RV
7	CSB lower flange
8	CSB @ snubber location
9	CSB
10	CSB
11	CSB
12	CSB
13	CSB
14	CSB
15	CSB @ nozzle
16	CSB
17	CSB upper flange (top surface)
18	LSS
19	Core support plate (center)
20	Core shroud
21	Core shroud
22	Core shroud
23	Core shroud
24	Core shroud
25	Core shroud
26	Core shroud
27	Core shroud
28	Core shroud
29	Fuel alighment plate (center)
34 + 9i	Fuel
35	Fuel
36	Fuel
37	Fuel
38	Fuel
39	Fuel
40	Fuel
41	Fuel
42 + 9i	Fuel
79 + 4i	CEA shrouds
80	CEA shrouds
81	CEA shrouds
82	CEA shrouds
83 + 4i	CEA shrouds
99	UGS support plate

Table 4.6.3

Generic Plant

Vertical Model Node Locations

NODE	NODE LOCATION DESCRIPTION
1	CSB @ upper surface of lower flange
2	CSB @ snubbers
3	CSB @ lower section thickness change
4	CSB
5	CSB
6	CSB
7	CSB
8	CSB
9	CSB
10	CSB
11	CSB
12	CSB
13	CSB @ top of upper flange
14	LSS @ top of grid beams
15	Core support plate center
16	Fuel assembly @ CEF plate
17	Guide tubes
18	Guide tubes
19	Guide tubes
20	Guide tubes
21	Guide tubes
22	Fuel assembly @ UEF plate
23	Center of fuel alignment plate
24	Fuel rods
25	Fuel rods
26	Fuel rods
27	Fuel rods
28	Fuel rods
29	Base of core shroud
30	Core shroud
31	Core shroud
32	Top of core shroud
33	CEA's
34	CEA's
35	CEA's
36	CEA's
37	CEA's
38	Top of UGS support plate
39	Reactor vessel ledge
40	Reactor vessel @ outlet nozzle
41	Reactor vessel
42	Reactor vessel supports
43	Reactor vessel @ top of core shroud
44	Reactor vessel
45	Core shroud node

Table 4.6.4

Omaha Lateral Model

Node Locations

NODE	DESCRIPTION
3	R.V. Ledge
4	R.V.
5	R.V. @ outlet nozzle centerline
6	R.V. @ TS lug
7	R.V.
8	R.V. @ TS pin
9	R.V. @ snubbers
10	TS
11	TS
12	TS
13	CSB upper flange (top surface)
14	CSB
15	CSB @ outlet nozzle centerline
16	CSB
17	CSB @ TS lug
18	CSB
19	CSB
20	CSB
21	CSB @ TS pin
22	CSB @ snubbers
23	CSB Bot. surface of lower plate
24	Core shroud
25	Core shroud
26	Core shroud
27	Core shroud
28	Core shroud
29	Core shroud
30	Core shroud
31	Core shroud
32	Core shroud
35+9i	Fuel
36	Fuel
37	Fuel
38	Fuel
39	Fuel
40	Fuel
41	Fuel
42	Fuel
43	Fuel
33	Center FAP
34	Center CSP
80+5i	CEA shrouds
81	CEA shrouds
82	CEA shrouds
83	CEA shrouds
84	CEA shrouds
100	UGS flange (top surface)
101	Top surface LSS beam flanges

Table 4.6.5

Palisades Lateral Model

Node Locations

NODE	DESCRIPTION
2	Pressure vessel @ snubber location
3	Pressure vessel
4	Pressure vessel
5	Pressure vessel @ FAP location
6	Pressure vessel @ outlet nozzle centerline
7	Pressure vessel
8	Pressure vessel @ ledge
9	CSB Bot. surface of lower plate
10	CSB @ snubber location
11	CSB @ CSP location
12	CSB
13	CSB
14	CSB
15	CSB
16	CSB @ FAP location
17	CSB
18	CSB @ outlet nozzle centerline
19	CSB
20	CSB @ top of upper flange
21	LSS-top of support beam flanges
22	Core support plate (CSP)
23	Core shroud (CS)
24	CS
25	CS
26	CS — Note: Each CS node is located
27	CS — adjacent to a spacer grid.
28	CS
29	CS
30	CS
31	CS
32	CS
33	Fuel alignment plate (FAP)
34+10i	Fuel
35+10i	Fuel
36+10i	Fuel
37+10i	Fuel — Note: Each fuel node is located
38+10i	Fuel — at a spacer grid.
39+10i	Fuel
40+10i	Fuel
41+10i	Fuel
42+10i	Fuel
43+10i	Fuel
84+5i	Control element assy. shroud (CEA)
85+5i	CEA
86+5i	CEA
87+5i	CEA
88+5i	CEA @ bottom of UGS cylinder
104	Top surface of UGS cylinder

Table 4.6.6

Generic Plant

Reduced Internals Model Node Locations

Node	Description
1	Top surface UGS flange
2	Center CEA shrouds
3	Center fuel alignment plate
4	Upper end fitting fuel
5	Fuel
6	Fuel
7	Fuel
8	Lower end fitting fuel
9	Center core support plate
10	Top surface CSB lower flange
11	Core shroud
12	CS
13	Top surface CSB upper flange
14	CSB at outlet nozzle centerline
15	CSB
16	CSB
17	CSB at snubbers
18	PV ledge
19	PV at outlet nozzles
20	PV
21	PV
22	PV at snubbers
23	PV support
24	PV support

Table 4.6.7

Omaha

Reduced Internals Model Node Locations

Node	Description
1	PV Support
2	PV Support
3	Pressure Vessel @ Ledge
4	Pressure Vessel
5	P.V. @ Outlet Nozzle Centerline
6	P.V. @ TS Support Lug
7	P.V.
8	P.V. @ TS Support Pin
9	P.V. @ Snubbers
10	TS @ Support Lug
11	TS
12	TS @ Support Pin
13	CSB Upper Flange (Top Surface)
14	CSB
15	CSB @ Outelt Nozzle Centerline
16	CSB
17	CSB
18	CSB
19	CSB @ Snubbers
20	TS (Top Surface)
21	TS
22	UGS Flange (Top Surface)
23	CEA Shrouds
24	FAP (Center)
25	CSP (Center)
26	Fuel
27	Fuel
28	Fuel
29	Fuel
30	Bot. Surface of Lower Plate

SUMMARY OF INPUT AND ANALYSES PERFORMED

Operating Plant Asymmetric Loads Evaluation

	Calvert Cliffs (Generic Plant)	Palisades	Ft. Calhoun
Generic Plant Lateral Vessel Motions	X	X	(1,2)
Plant Specific Lateral LOCA Loads	X	X	X
Internals Axial Response Analysis	X	-	-
CSB Vibration Analysis	X	X	X
CSB Stability Analysis	X	-	-
Lateral Fuel Analysis	X	(3)	(4)
Axial Fuel Analysis	X	-	-
Beam Column Analysis	X	-	-

NOTES:
1. Generic plant lateral vessel motions were used only for the hot leg break.
2. Ft. Calhoun reactor vessel motions were used in the cold leg break analyses.
3. Generic plant model with Palisades input displacement time histories.
4. Plant specific analyses

TABLE 4.6.8

CALCULATED REACTOR INTERNALS STRESS MARGIN
GENERIC PLANT
(CALVERT CLIFFS 1 & 2, MILLSTONE 2)

TABLE 4.6.9

CORE SUPPORT COMPONENT	STRESS MARGIN* (PERCENT)
CORE SUPPORT BARREL	
UPPER FLANGE	39%
UPPER CLYINDER	52%
CENTER CYLINDER	32%
LOWER CYLINDER	36%
LOWER FLANGE	2%
LOWER SUPPORT STRUCTURE	
SUPPORT COLUMNS	48%
BEAMS & CYLINDER	22%
CORE SUPPORT PLATE	6%
UPPER GUIDE STRUCTURE	
UGS FLANGE	19%
GRID BEAMS	2%
CEA SHROUDS	1%

* STRESS MARGIN AS DEFINED IN SECTION 4.6.4.1

CALCULATED REACTOR INTERNALS STRESS MARGINS
PALISADES

TABLE 4.6.10

CORE SUPPORT COMPONENT	STRESS MARGIN (PERCENT)
CORE SUPPORT BARREL	
UPPER FLANGE	6%
UPPER CYLINDER	7%
CENTER CYLINDER	11%
LOWER CYLINDER	16%
LOWER SUPPORT STRUCTURE	
CORE SUPPORT PLATE	13%
SUPPORT COLUMNS	2%
BEAMS	3%
UPPER GUIDE STRUCTURE	
FLANGE & CYLINDER	23%
GRID BEAMS	1%
CONTROL ROD SHROUDS	38%

CALCULATED REACTOR INTERNALS STRESS MARGINS
FORT CALHOUN

TABLE 4.6.11

CORE SUPPORT COMPONENT	STRESS MARGIN (PERCENT)
CORE SUPPORT BARREL	
UPPER FLANGE	17%
UPPER CYLINDER	3%
CENTER CYLINDER	2%
LOWER CYLINDER	19%
LOWER SUPPORT STRUCTURE	
CORE SUPPORT PLATE	1%
SUPPORT COLUMNS	38%
BEAMS	13%
UPPER GUIDE STRUCTURE	
FLANGE AND CYLINDER	12%
GRID BEAMS	20%
CEA SHROUDS	9%

4.7 FUEL

4.7.1 COMBUSTION ENGINEERING FUEL ASSEMBLY DESCRIPTION

The Combustion Engineering 14x14 fuel assembly (Figure 4.7.1) consists of 176 fuel rods, five control element guide tubes, one Inconel and eight Zircaloy fuel rod spacer grids, a lower end fitting, and an upper end fitting which incorporates a holddown device. The guide tubes, spacer grids and end fittings form the structural frame of the fuel assembly.

The lower end fitting consists of four posts and a flow plate, fabricated as a single strainless steel casting. The posts are designed to receive the alignment pins of the core support plate and thereby provide positive lateral locating of the lower end of the fuel assembly. The flow plate consists of an open lattice-work of interconnecting ribs which permit the coolant flow to enter the fuel assembly and at the same time provide bottom support for the fuel and poison rods. Portions of the lower end fitting are machined to accept the guide tube lower ends and the flow skirt of the Inconel grid.

The upper end fitting assembly consists of two cast CF-8 stainless steel plates, five 304 stainless steel machined posts, and five helical Inconel X-750 springs. The upper end fitting assembly attaches to the guide tubes and has features which provide for grappling of the fuel assembly, locating the top end of the fuel assembly laterally, and a holddown capability (except in the Ft. Calhoun plant, where the springs serve only to locate one of the stainless plates for fuel handling).

The lower cast plate is similar to the plate of the lower end fitting in that it also has an open lattice-work of interconnecting ribs which permits coolant flow to leave the fuel assembly with little restriction. The plate has four machined holes which receive the outer posts and a threaded center hole to receive the center post.

The upper cast plate consists of four arms connected by a central ring and has features which permit positive grappling during fuel handling. Both the arms and the central ring are machined to permit free passage of the plate over the interfacing post surfaces.

The four outer posts of the upper end fitting mate with holes in the fuel alignment plate to locate the upper end of the fuel assembly. The center post is threaded into the lower cast plate of the upper end fitting and locked in place by welding.

The upper end fitting is assembled to the fuel assembly by the four outer posts which are threaded into the mating portion of the outer guide tubes. When assembled, the upper cast plate of the upper end fitting is preloaded by the springs which surround each post. In the Calvert Cliffs and Millstone 2 plants, the upper cast plate reacts with the fuel alignment plate to further compress the springs in order to develop the force necessary to keep the fuel assembly seated upon the core support plate during reactor operation.

The outer guide tubes are Zircaloy-4 and are fabricated by welding a fitting to each end. The lower threaded portion mates with the lower end fitting. The upper threaded portion provides a means by which the upper end fitting may be assembled to the guide tubes. The center guide tube, also of Zircaloy-4, is of one piece construction.

The guide tubes provide a path for the control element assembly fingers, house in-core instrumentation and neutron sources, provide a deceleration zone for scramming control element assemblies, and provide a basic frame to which the grids are assembled and welded in place. The subassembly of grids and the lower end fitting form what is called a grid cage and when coupled with the upper end fitting form the basic structural frame of the fuel assembly.

The fuel rod spacer grids (Figure 4.7.2) are fabricated from preformed Zircaloy or Inconel strips (the lower spacer grid material is Inconel), interlocked in an egg crate fashion, and welded together. The spacer grids maintain the fuel rod pitch over the full length of the fuel rods by providing positive lateral restraint. The fuel rods are restrained from axial motion by the frictional forces developed by the spacer grid leaf springs. Each cell of the spacer grid contains two leaf springs and four arches. Each leaf spring presses the fuel rod against two arches, thereby restricting relative motion between the grids and the fuel rods. The spring and arch positions are reversed from grid to grid to provide additional restriction to relative motion. The perimeter strips which surround the egg crate construction also contains springs and arches in addition to features which prevent hangup of grids during fuel handling.

The eight Zircaloy-4 spacer grids are fastened to the Zircaloy-4 guide tubes by welding. Each grid is welded to each guide tube at eight locations, four on the upper face of the grid and four on the lower face of the grid, where the spacer strips contact the guide tube surface. The lowest spacer grid (Inconel) is not welded to the guide tubes because of material differences. The perimeter strip of the Inconel grid is welded to the perimeter of the lower end fitting.

The fuel rods consist of UO_2 pellets, a compression spring, and spacer discs, all encapsulated within a Zircaloy-4 tube which is welded into a hermetic enclosure. The fuel cladding is slightly cold worked Zircaloy-4 tubing.

The Calvert Cliffs 1 and 2, Millstone 2, and Ft. Calhoun fuel assemblies are identical except for the slightly reduced lengths in Ft. Calhoun as indicated on Figure 4.7.1. The shorter guide tubes, fuel rods, and end fitting posts in Ft. Calhoun do have identical diameters as those in the same components in the other plants.

4.7.2 FUEL TESTING

All fuel assembly structural testing has been completed in accordance with the test scope originally outlined. These tests were conducted on 14 x 14 fuel assembly components representative of the plants covered by this report. The discussion below outlines each test and presents some of the actual test data.

4.7.2.1 Static Load-Deflection Tests

For the lateral load-deflection tests, the full size fuel assembly was mounted in the seismic test stand and withdrawn laterally in specified increments. Measurements include: lateral load, lateral deflection at several spacer grids, and guide tube strain at several locations. Additional measurements were made which allowed calculation of the stiffness of the spacer grid/guide tube joint. A schematic of the test set-up is shown in Figure 4.7.3.

A typical load-deflection curve is shown in Figure A-1 of Appendix A. Fuel assembly lateral stiffness and hysteretic response were established by this data. At each increment of lateral load, strain and guide tube-spacer grid rotation measurements were made.

4.7.2.2 Fuel Bundle Dynamic Tests

For the lateral fuel assembly impact test, the bundle was mounted in the same test stand as was used for the load-deflection test. The bundle was withdrawn a specified distance, released, and allowed to strike a plate which simulated the core shroud. The dynamic response of the bundle was monitored by measurement of displacement vs. time at three (3) spacer grid locations and velocity vs. time at the central spacer grid. A load cell recorded impact load at the central spacer grid. This test was performed in air and water environments in order that water effects might be evaluated. A schematic of the test set-up is shown in Figure 4.7.4.

Figure A-2 in Appendix A shows typical impact load data.

Figures A-3 and A-4 of Appendix A show typical data on fundamental frequency and damping ratio for the free vibration decay. (These data were taken on the above test fixture with the impact plate removed so that no impacting occurred.)

4.7.2.3 Spacer Grid Impact Test

For the spacer grid impact tests, a fuel assembly section consisting of a spacer grid with guide tubes and fuel rods corresponding to one spacer grid span was mounted in a test fixture. With this fixture, the entire fuel assembly section could be dropped from a specified height and allowed to strike an impact surface, or a weight could be dropped and allowed to impact on the spacer grid. From these tests, spacer grid dynamic characteristics and structural strength were determined. In addition, the fuel assembly section drop tests were performed in water to establish fluid cushioning behavior during impact. A schematic of the test setup is shown in Figure 4.7. 5.

The air "weight drop" test was used to determine grid strength when a through grid load is applied. This loading is representative of a bundle being simultaneously loaded from both sides. The fuel section drop test was used to determine grid strength when a one-sided load is applied. This loading is representative of a free bundle impacting against another bundle or the core shroud. For both of these tests, drop height was incrementally increased until the grid strength was established. The cold grid strengths determined for through-grid and one-sided loads are shown in Table A-1 of Appendix A.

The drop tests in water were conducted with flow restriction plates that simulated fluid effects for the in-reactor geometry. Figure A-5 shows typical data from this test.

4.7.3 FUEL ANALYSIS MODELS

Detailed structural lumped mass-spring models of the fuel assemblies were developed based on a correlation with static and dynamic test results. These models were analyzed for both hot and cold leg breaks with the CESHOCK code (Reference 3.13). The resulting component loads and displacements were used to determine fuel assembly stresses and spacer grid impact loads. A beam column model of a full assembly was also developed for use in an analysis of simultaneous axial and lateral loading.

4.7.3.1 HORIZONTAL MODEL

A generic horizontal fuel assembly model was developed for Calvert Cliffs, St. Lucie 1, and Millstone 2 from correlation studies with test data. The model was used to represent the core in the detailed internals model and a row of fuel assemblies in the fuel analysis model (Figure 4.7.6). The detailed core model was excited by applying the fuel alignment plate, core shroud and core support plate motions obtained from the detailed internals models with pipe rupture loads and vessel motions considered.

The lateral fuel assembly model was developed to exhibit a dynamic response similar to that of the test bundle. The fuel assembly was modeled with a

constant flexural rigidity and a rotational spring at each end. The magnitude of the bending stiffness and torsional spring constants were obtained from a correlation of static deflection test data in conjunction with observed fundamental frequencies derived from the pluck vibration tests of the bundle in air. The added mass coefficients for the fuel assembly were determined from the pluck vibration tests in water.

The detailed fuel model includes non-linear elements which represent the possible impact between adjacent fuel assemblies and peripheral assemblies and the core shroud. The magnitude of the impact stiffness was derived from correlation with pluck impact test results. Also, the grid strengths and coefficient of restitution were determined from spacer grid tests.

A separate core model was developed for Ft. Calhoun. The model deviates from the generic model with respect to the number and size of the fuel assemblies, and the number of columns of fuel modeled across the core. The fuel structural properties for the Ft. Calhoun core were determined using factors applied to the generic fuel model which accounted for changes in length and the differences in end fittings.

The generic plant model was also used for a preliminary assessment of the Palisades fuel; however, additional evaluations are needed to account for the differences between the Palisades fuel which is supplied by EXXON Nuclear Co. and the generic plant fuel. These evaluations are discussed in Appendix B.

4.7.3.2 VERTICAL MODEL

A vertical fuel assembly model was developed for use only in the generic plant detailed axial internals model (Fig. 4.6.10). The model included nonlinear

couplings to represent the end fittings and separate parallel branches representing the grid cages and the fuel rods. Friction elements were used to represent the stick-slip motion between the rods and spacer grids. The model was subjected to both LOCA and drag loads which were computed with the control volume method utilizing an integrated fluid momentum equation. The drag loads were composed of both frictional and spacer grid form drag. Frictional drag was apportioned to both the fuel rods and guide tubes and was calculated using friction factor which was dependent on the flow channel equivalent diameter, cross sectional area, fluid flow rates and densities. The form drag was calculated using an experimentally determined loss factor correlation as a function of Reynolds Number. In addition, crud effects were accounted for by multiplying the drag loads by an emperically determined factor. The results of the LOCA response analyses with reactor vessel motion applied were conservatively applied to the plant specific analyses.

4.7.3.3 DYNAMIC BEAM - COLUMN MODEL

A detailed mathematical model of the generic plant fuel assembly shown in Figure 4.7.2 was developed based on correlation with static and dynamic test results. The test results included lateral static stiffness, pluck vibration and spacer grid impact data. The guide tubes and upper and lower end fittings were modeled with two dimensional beam elements. The fuel rods were modeled with a series of spar elements such that vertical sliding forces between the fuel rods and spacer grids and impact forces between the fuel rods and flow plates are accounted for in the model. The flexural rigidity of the fuel assembly is included in the structural properties of the guide tube and end fitting members. These members form the grid cage space frame which supports the fuel rod arrays.

At locations where gaps may occur (e.g., fuel rod/lower end fitting flow plate interface) spring/gap elements acting in the direction normal to the impact surface are used to represent its dynamic characteristics. Nodal locations and coordinates of the beam-column are presented in Figure 4.7.3. The beam-column fuel assembly model was used in a dynamic response/stability analysis of simultaneous axial and lateral LOCA loading.

Hydrodynamic mass effects are modeled via dynamic fluid coupling elements between the guide tube nodes and a fixed point of reference. The fluid coupling element modifies the structural mass matrix. The properties of the fluid coupling element were selected to yield a beam-column model fundamental natural frequency in the lateral direction equivalent to that obtained from free vibration test data in water.

The dynamic characteristics of the beam column model in the vertical direction are verified by comparing its calculated natural frequencies to those obtained via theoretical eigenvalue analysis of the fuel assembly components.

Effects of adjacent structures in both the lateral and vertical directions were included in the beam-column model. See Figure 4.7.4. Structural members between the subject peripheral fuel assembly (results of Section 4.7.4.1 demonstrate the peak lateral response to occur in the peripheral

assembly) and the adjacent fuel assembly or core shroud represent the appropriate impact stiffness and initial nominal gap. Interface between the fuel assembly and core support plate (CSP) or fuel alignment plate (FAP) is represented by rotational spring and spring/gap elements. However, vertical analyses described in Section 4.7.4.1 indicate the linear hold down springs located between the FAP and fuel assembly to be active throughout the dynamic response history. Therefore, only a linear member is required at this location to model the interface between the fuel assembly and FAP.

4.7.4 FUEL RESPONSE ANALYSES

The detailed horizontal core models consisting of the longest row of fuel assemblies across the core were analyzed for both hot and cold leg breaks. The CESHOCK code was used to perform these analyses which were done in directions both parallel and perpendicular to the hot legs following the cold leg break and parallel to the hot leg for the hot leg break. The results of these analyses included spacer grid impact loads and component loads and displacements which were later used in the fuel assembly stress evaluation. Detailed axial core response analyses were not performed since the fuel loads obtained from the axial generic plant internals analysis were conservatively assumed to apply to all of the other plants. The procedures used and the results of the fuel evaluation are presented in Section 4.7.6 and Appendix A.

4.7.4.1 INLET BREAK ANALYSIS

Detailed lateral response analyses for a cold leg break were performed using CESHOCK for the generic plant, Palisades, and Ft. Calhoun. The input excitation was the core support plate, fuel alignment plate, and core shroud displacement time histories which were calculated from the detailed internals response analyses. The results of the analyses were the maximum fuel bundle moments, shears, and displacements and the maximum one sided spacer grid loads. The maximum through grid or the steady state components of loading acting simultaneously on both sides of the grids were also calculated. These results were later used to perform a stress evaluation of the fuel.

The results of the generic plant fuel are directly applicable to Millstone 2, St. Lucie 1, and Calvert Cliffs 1 and 2. The Ft. Calhoun analyses were performed

using motions obtained from the plant specific internals analyses and the Palisades analyses were performed using the generic plant model with plant specific motions used as the input excitation.

4.7.4.2 OUTLET BREAK ANALYSIS

Lateral response analyses for a hot leg were performed in the direction parallel to the hot legs using the detailed fuel models. The methods described in Section 4.7.4.1 are directly applicable to the hot leg breaks.

4.7.4.3 DYNAMIC BEAM-COLUMN ANALYSIS

The dynamic beam-column analysis determined any additional bending stress and stability of the fuel assembly due to concurrent lateral and axial loading. The response included interaction with other structural components in the lateral and vertical directions. The detailed beam-column model was developed to be consistent with the general purpose finite element code ANSYS (Reference 3.22). A planar non-linear transient dynamic response analysis of the beam-column model was performed via ANSYS similar to that described in Reference 3.11, Section 5. By employing the large deformation option, deflection under load was used to continuously redifine the structural geometry, thus producing a revised stiffness matrix.

The starting time of the dynamic beam-column analysis was selected to include regions of the LOCA response history during which peak lateral loads coexcited with significant axial loads. Results of the analyses presented in Sections 4.7.4.1 and 4.7.4.2 indicated that the peak fuel assembly responses in separate lateral and axial directions occurred during a full power inlet break

in the Z-direction (Figure 4.6.9). The peak axial responses occurred at approximately 100 msec. Preliminary beam-column analyses have shown that beam-column effects are more sensitive to lateral bending moments than to axial forces. Therefore, the critical time range with respect to beam-column effects is 180 to 200 msec. A 170 msec start time was selected and the detailed beam-column analysis was performed to 210 msec.

Initial conditions obtained from the separate axial and lateral analyses at 170 msec were applied to the beam-column model. Axial displacements and velocities at 170 msec were applied to the model at guide tube, fuel rods, core support plate and fuel alignment plate node locations. In addition, axial LOCA and drag loads were applied to the guide tubes and fuel rods. In the lateral direction displacements, rotations, velocities, and angular velocities were applied at guide tube, core support plate, and fuel alignment plate node locations. In addition, the lateral displacements and velocities of the nodes representing the adjacent fuel assembly and core shroud were defined at 170 msec.

Loading time histories were specified from 170 msec to 210 msec. These consisted of axial LOCA and drag loads on the guide tubes and fuel rods; displacements (in both axial and horizontal direction) at the core support plate and fuel alignment plate; rotations at the core support plate and fuel alignment plate and lateral displacements of the nodes representing the adjacent fuel assembly and core shroud. Therefore, the beam-column analysis accounted for all interactions between the subject fuel assembly and the

remainder of the reactor internal components in the lateral and axial direction.

The results of the analysis included transverse shears, moments, axial loads, and nodal displacements as a function of time. These results were later used to perform a stress analysis of the fuel assembly. The results of this analysis indicate that the beam column effect does not significantly increase the maximum fuel bundle stresses.

4.7.5 LOCA CONDITION CRITERIA FOR FUEL ASSEMBLY EVALUATION

The basic functional requirement which must be satisfied by the fuel assembly during the event is that the structural components of the assembly (end fittings, guide tubes and grids) must be capable of maintaining the fuel rods in a coolable array when subjected to the mechanical loads predicted to result from the occurrence of the event.

In order to permit analytical determination of the capability of the fuel assembly to satisfy the above functional requirement, specific quantitative criteria are established for each structural component in the fuel assembly. These specific criteria (listed by component) are discussed in the following sections.

4.7.5.1 Upper and Lower End Fitting Castings

The end fitting castings are made from 304 stainless steel, Grade CF-8. The adequacy of these components to withstand the mechanical loads is determined by calculating the stress intensities resulting from loads and comparing the calculated stress intensities with limits defined by:

a. The primary membrane stress intensity, P_m, must not exceed 2.4 S_m, where S_m is the design stress intensity value for nominal conditions and is equal to 10,500 psi. Therefore, the maximum allowable primary membrane stress intensity is equal to 2.4 x 10,500 or 25,200 psi.

b. The sum of the primary membrane stress intensity, P_m, and the primary bending stress intensity, P_b, must not exceed the product of 2.4 S_m and a shape factor, P_s, which depends on the cross section over which the bending moment acts.

4.7.5.2 Upper End Fitting Posts

The five upper end fitting posts are made from wrought 304 stainless steel. The performance of these components is evaluated in exactly the same way as that of the end fitting castings discussed above, except that the difference between properties of wrought and cast 304 stainless steel results in a slightly higher design stress intensity (S_m = 12,000 psi) for the posts than for the castings.

4.7.5.3 Upper End Fitting Holddown Springs

The upper end fitting springs are fabricated from Inconel X-750 wire. The performance of these components is evaluated by calculating the shear stress resulting from the spring being compressed to its solid height. This calculated shear stress must not exceed the yield strength in shear for this material. This maximum allowable shear stress is equal to 99,000 psi.

4.7.5.4 Guide Tubes

There are no specific stress criteria applied to the evaluation of fuel assembly guide tubes for the large-break LOCA analysis, for the following reasons:

a. Control rod scram is not a requirement.

b. The existance of the fuel rod coolable array is dependent upon the spacer grid performance during the event. Minor distortions of the guide tubes will not affect the assembly inlet or outlet flow conditions (controlled by the end fittings), nor the individual flow channel conditions (controlled by the spacer grids).

4.7.5.5 Spacer Grids

The spacer grids are the primary factor in assuring that fuel rods remain in a coolable array. The capability of the grids to perform this function is determined by comparing the predicted lateral impact loads associated with the postulated event to the lateral crush strength of the spacer grid, which was determined by test. Resulting values are listed in Table A-1 (room temperature) and Table A-3 (operating temperature).

4.7.5.6 Fuel Rods

It is a requirement that the fuel rod cladding be capable of withstanding the loads resulting from the mechanical excitations occurring during the postulated event.

The adequacy of the fuel rods to withstand the calculated loads is determined by comparing the calculated stress intensities which result from the axial and lateral loads to allowable stresses defined by the following formulae:

a. The primary membrane stress intensity, P_m, shall not exceed 0.7 times the ultimate tensile strength, S_u.

b. The sum of the primary membrane stress intensity, P_m, and the primary bending stress intensity, P_b, shall not exceed the product of the allowable primary stress intensity (see Part a, above) and the 1.46 section factor appropriate to the fuel rods.

The stress intensity limits are listed in Appendix A.

4.7.6 STRESS ANALYSIS OF FUEL

As discussed in Section 4.7.3, the pipe rupture response analysis model produces results in the form of the spacer grid impact load, axial and lateral loads on the fuel end fittings, and lateral deflected shapes for the fuel assembly. These results are then applied to the analysis of the fuel assembly in the following manner.

Calculated spacer grid impact loads are compared directly to the experimentally determined load/deformation capability of the spacer grids.

Axial and lateral end fitting loads are applied (analytically) to the appropriate portions of the upper and lower end fittings, and the resultant stresses are calculated using relatively basic strength of materials methods.

Lateral deflected shapes are inputed directly into a computer model which then makes use of these shapes to calculate the resultant stress intensities in the axial structural members of the fuel assembly and in the fuel rods. Since the fuel assembly response to the LOCA is a dynamic phenomenon, with an essentially infinite number of axial shapes which could be analyzed, it is necessary to be selective in establishing which shapes are likely to correspond to maximum stress conditions. This is accomplished by evaluating all shapes which correspond to either maximum deflection, shear or moment at each of the axial nodes in the pipe rupture response model.

4.7.7 EVALUATION OF COMBUSTION ENGINEERING FUEL

This section compares the calculated fuel assembly component loads and stresses to the corresponding criteria discussed in Section 4.7.5.

The loads and stresses resulting from the postulated inlet and outlet breaks have been compared. The inlet break results are governing in each case, and in fact no component is overstressed or overloaded by the outlet break. Therefore, the discussion is limited to the effects of the inlet break.

The inlet break produces fuel assembly movement in two directions. Maximum stress intensities for each component have been calculated by combining the maximum stress intensities from each of the two directions by the square root of the sum of the squares (SRSS)

method. Maximum spacer grid loads are reported separately for the two directions since channel closure across one grid width is not affected by loading across the other width.

4.7.7.1 Generic Plant Results (Calvert Cliffs I and II, Millstone 2)

As described in Sections 4.6.2, 4.6.3, and 4.7.4, two fuel assembly analyses were performed. The first analysis (Base Case) related friction at the core barrel flange and reactor vessel ledge to nominal operating loads. The results of this approach were overly conservative. In order to remove some of the conservatism, a second (Revised Model) analysis was performed, which accounted for an increased value of friction at the flange. The stresses and loads calculated from both analyses are presented in Appendix A, and discusses below.

The ratios between the maximum stresses and maximum loads for the two cases are also presented. Each ratio is equal to the revised model result divided by the base case result.

4.7.7.1.1 End Fitting Castings and Posts

Table A-2 in Appendix A lists the maximum end fitting stress values along with the allowable values.

The maximum predicted stress values are less than the stress criteria.

4.7.7.1.2 Upper End Fitting Holddown Springs

The standard Combustion Engineering reload design includes holddown springs which are designed to have shear stresses below the criterion value (99,000 psi) at solid height. Therefore, no specific calculation was performed as part of the asymmetric loads evaluation.

4.7.7.1.3 Guide Tubes

Table A-2 in Appendix A lists maximum stress intensities for the guide tubes. As discussed in Section 4.7.5.4, there is no criterion on guide tube stress for the large break LOCA event. Yield strength of the guide tube material is referenced for information, and guide tube stress values are discussed further in Section 4.7.7.3.

4.7.7.1.4 Fuel Rods

Maximum fuel rod stress values are listed in Table A-2 of Appendix A. The stress criterion is also provided.

The maximum predicted stresses are less than the criterion.

4.7.7.1.5 Spacer Grid Impact Loads

Spacer grid impact loads are determined directly in the CESHOCK detailed core model described in Section 4.7.4. The impact loads for the generic plant fuel are listed in Table A-3 of Appendix A. Also shown are the spacer grid impact strengths from Table A-1 corrected for operating temperature.

Two categories of grid impact loads are listed in Table A-3. The one-sided load type corresponds to the case where a freely-moving bundle impacts an adjacent assembly or the core shroud, or where a free-standing bundle is impacted by another assembly. Thru-grid loads correspond to cases in which an assembly already rests against the shroud or another assembly, and is then impacted on its opposite face. These two load categories have been distinguished in both the analysis and test methods.

Except for loads on peripheral fuel assemblies, the grid strength is greater than the loads imposed on the grids during the postulated LOCA event.

In the row of fuel assemblies chosen for dynamic analysis, a total of four spacer grids are predicted to exceed the allowable load (two in each of the two peripheral assemblies). The maximum thru-grid loading is predicted for one of the same grids subject to a high one-sided loading.

Figures A-6 and A-7 show the core-wide distribution of one-sided and thru-grid loadings for all fuel assemblies in the row, for the case where the maximum loads were predicted.

The beneficial effect of irradiation on spacer grid strength is discussed in Section 4.7.7.3. Irradiation will increase grid strength by a factor of at least 1.5 by the time of fuel discharge, which is sufficient to provide the required load capability.

An evaluation of the effects of reduced channel flow area in peripheral spacer grids is presented in Appendix E. Fuel temperature calculations are presented to demonstrate core coolability following the grid loadings induced by the postulated pipe break at the vessel inlet nozzle.

4.7.7.2 Ft. Calhoun Results

A single (Base Case) fuel assembly analysis was performed. The results of this analysis were modified by the ratios obtained from the two generic fuel assembly analyses (revised model/base case) to obtain estimated revised model results. The stresses and loads from both cases are presented in Appendix A, and discussed below.

4.7.7.2.1 End Fitting Castings and Posts

Table A-4 in Appendix A lists the maximum end fitting stress values along with the allowable values.

The maximum predicted stress values are less than the stress criteria.

4.7.7.2.2 Upper End Fitting Holddown Springs

The standard Combustion Engineering Ft. Calhoun reload design includes holddown springs which are designed to have shear stresses below the criterion value (99,000 psi) at solid height. Therefore, no specific calculation was performed as part of the asymmetric loads evaluation.

4.7.7.2.3 Guide Tubes

Table A-4 in Appendix A lists maximum stress intensities for the guide tubes. As discussed in Section 4.7.5.4, there is no criterion on guide tube stress for the large break LOCA event. Yield strength of the guide tube material is referenced for information, and guide tube stress values are discussed further in Section 4.7.7.3.

4.7.7.2.4 Fuel Rods

Maximum fuel rod stress values are listed in Table A-4 of Appendix A. The stress criterion is also provided.

The maximum predicted stresses are less than the criterion.

4.7.7.2.5 Spacer Grid Impact Loads

Spacer grid impact loads are determined directly in the CESHOCK detailed core model described in Section 4.7.4. The impact loads for the Ft. Calhoun fuel are listed in Table A-5 of Appendix A. Also shown are the spacer grid impact strengths from Table A-1 corrected for operating temperature.

Two categories of grid impact loads are listed in Table A-3. The one-sided load type corresponds to the case where a freely-moving bundle impacts an adjacent assembly or the core shroud, or where a free-standing bundle is impacted by another assembly. Thru-grid loads correspond to cases in which an assembly already rests against the shroud or another assembly, and is then impacted on its opposite face. These two load categories have been distinguished in both the analysis and test methods.

Except for loads on peripheral fuel assemblies, the grid strength is greater than the loads imposed on the grids during the postulated LOCA event.

For Ft. Calhoun, only one spacer grid in a peripheral assembly is predicted to exceed its allowable load following the application of the appropriate ratio. Figure A-8 shows the core-wide distribution of one-sided loadings for all fuel assemblies in the row analyzed, for the base case situation where the maximum loads were predicted.

The effect of irradiation on spacer grid strength is discussed in Section 4.7.7.3. Irradiation is expected to increase grid strength to the point where it exceeds the predicted maximum loading value after only a short period of reactor operation (approximately 3 months).

An evaluation of the effects of reduced channel flow area in peripheral spacer grids is presented in Appendix E. Fuel temperature calculations are presented to demonstrate core coolability following the grid loadings induced by the postulated pipe break at the vessel inlet nozzle.

4.7.7.3 Effects of Operating Conditions on Zircaloy Components

As discussed in the preceeding sections, maximum calculated guide tube stresses exceed the BOL unirradiated yield strength of the material, but do not violate any structural criteria. In addition, the maximum calculated spacer grid impact loads exceed the BOL unirradiated grid strengths, but are to be addressed by a coolability analysis (Appendix E).

For information, this section presents a discussion of the effects of irradiation and high strain rates on zircaloy mechanical properties. Both conditions will make zircaloy components less prone to permanent deformation than indicated by out-of-pile testing.

4.7.7.3.1 Guide Tubes

Figure A-9 of Appendix A shows the effect of irradiation on the guide tube yield strength at operating temperatures. These data were obtained at the standard ASTM tensile test strain rate (0.00008 in/in/sec). Figure A-10 depicts the estimated yield strength function at a strain rate which is representative of that occurring during the LOCA transient (0.1 in/in/sec).

The axial distribution of maximum guide tube stresses from the generic plant analysis is shown in Figure A-11. By comparing these stresses to Figure A-10, it can be seen that the effects of strain rate and irradiation will begin to limit the region of permanent distortion after only a short period of reactor operation*. It should also be pointed out that the maximum stresses shown in Figure A-11 do not occur over all five guide tubes, nor over the full length of the span between grids. They are in fact confined to one side of two guide tubes, at a location near the spacer grids. The other stresses in the section of the fuel assembly would be considerably lower.

The axial distribution of maximum guide tube stresses from the scaled Ft. Calhoun analysis is shown in Figure A-12. In this case, Figure A-10 would indicate that the effects of strain rate alone would be sufficient to prevent permanent distortion of the guide tubes at essentially a BOL condition.

The ability of the guide tube material to withstand a given strain without fracture (at exposures lower than those estimated to be necessary to achieve a certain yield strength) is provided in Figures A-13 and A-14. Figure A-13 shows the total elongation (plastic) capability of the material as a function of irradiation, and Figure A-14 shows the total strain (elastic plus plastic) capability.

* The relationship between fluence and irradiation is approximately 3 weeks at full power per 10^{20} nvt.

The guide tube stress calculation was performed under the assumption of elastic behavior, so only elastic strains can be obtained from the analysis. These are shown on Figure A-15 as a function of axial position. It can be seen by comparison with Figure A-14 that the maximum calculated elastic strain is lower than the material total strain capability. (The actual guide tube strains would be somewhat different in an elastic-plastic analysis; however, these differences should be small since each fuel assembly is still deflection-limited by the close proximity of surrounding assemblies and the reactor internals). Therefore, the calculated elastic guide tube stresses should not produce permanent distortions of Ft. Calhoun guide tubes, and should not produce fracture of the generic plant guide tubes.

4.7.7.3.2 Spacer Grids

The effect of strain rate on spacer grid strength has already been accounted for in the dynamic test simulation method discussed in Section 4.7.2.

The Combustion Engineering spacer grid design has been shown by testing to exhibit a yielding characteristic rather than buckling behavior, so that the grid strength at a given fluence equals the ratio of the yield strength at that fluence divided by the unirradiated yield strength (both at high strain rates).

The effect of irradiation at an extremely high strain rate (4.0 in/in/sec) is shown in Figure A-16. The local strain rates in the spacer grid are unknown but are believed to be at least this large.

This graph demonstrates that the spacer grids are expected to become at least 50% stronger by the time of discharge (about 6×10^{21} nvt). Applying a factor of 1.5 to the spacer grid impact strengths would result in strength values higher than the maximum predicted impact loads in Table A-3 for the generic plant.

For the Ft. Calhoun results in Table A-5, it is obvious that a much shorter period of irradiation would be required to increase grid strength above the maximum predicted impact load. A fluence of approximately 4×10^{20} nvt (3 months operation) provides a minimum of 6% increase in yield strength, which is sufficient to eliminate the difference between calculated load and grid impact strength in Table A-5.

4.7.7.4 Summary of Fuel Evaluation

Calculations have demonstrated acceptable performance for all end fittings, holddown springs, and fuel rods in both the generic plant and Ft. Calhoun analyses. A limited number of spacer grids in both plants have calculated impact loads in excess of the BOL grid strength in a few peripheral core locations for the inlet break condition. The number of locations at which this condition exists is reduced as a function of time if credit is taken for spacer grid irradiated mechanical properties. An evaluation of core coolability for damaged peripheral grids is described in Appendix E.

For the outlet break condition, all fuel assembly components demonstrate acceptable stress and load values.

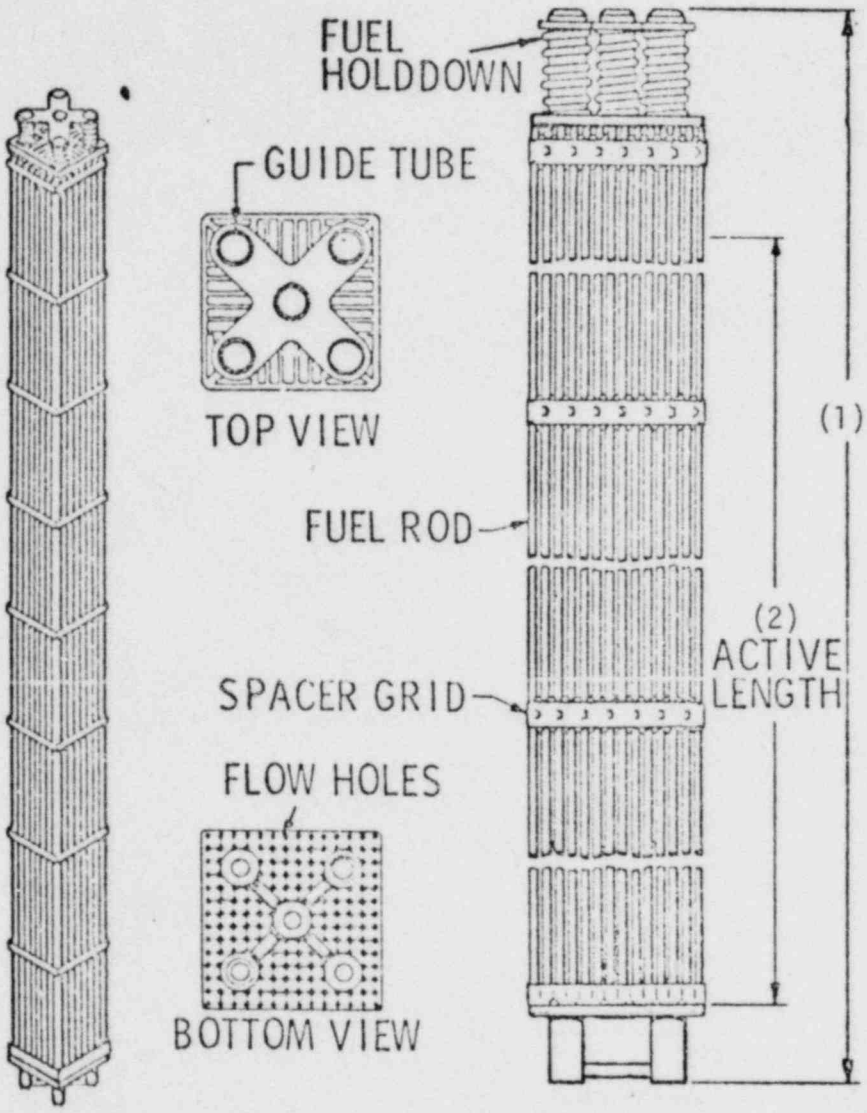

Assembly Dimensions	Baltimore 1 and 2, Millstone 2	Ft. Calhoun
(1) Overall Length	157.2 in	146.3 in
(2) Active Length	136.7 in	128.0 in

	Fuel Assembly	Figure 4.7.1

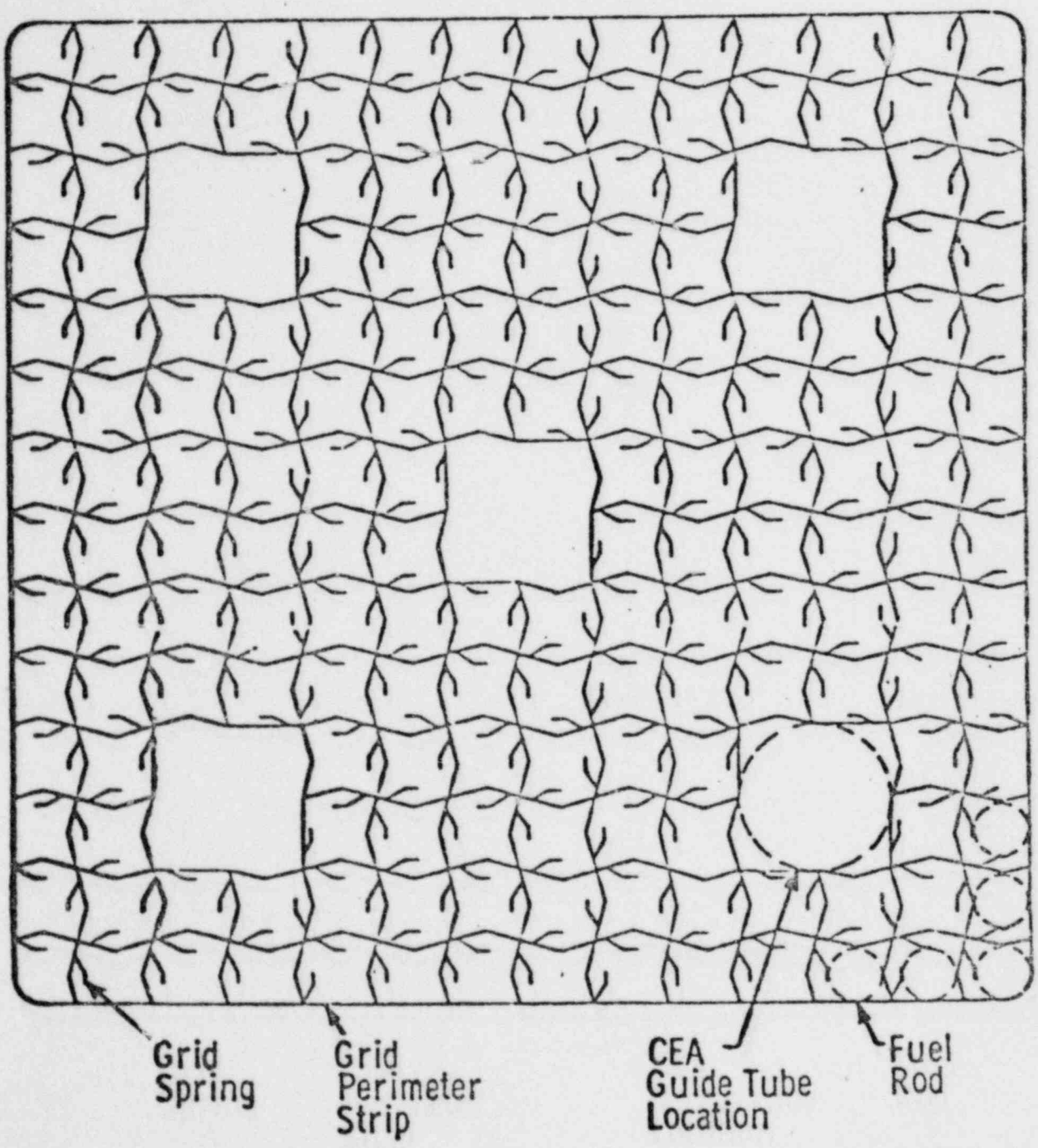

	Fuel Spacer Grid	Figure 4.7.2

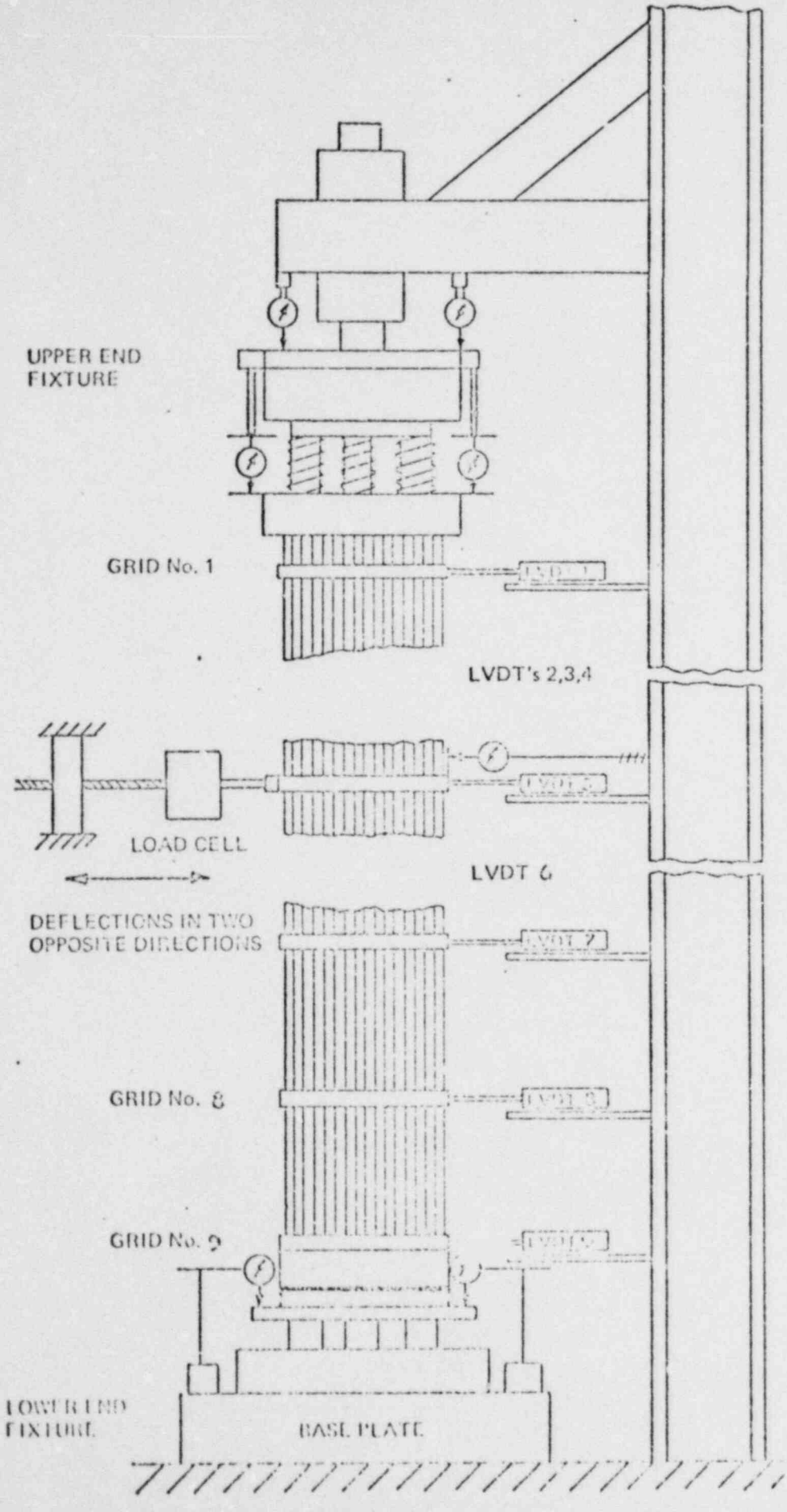

FIGURE 4.7.3

TEST SET-UP FOR LATERAL LOAD DEFLECTION TEST

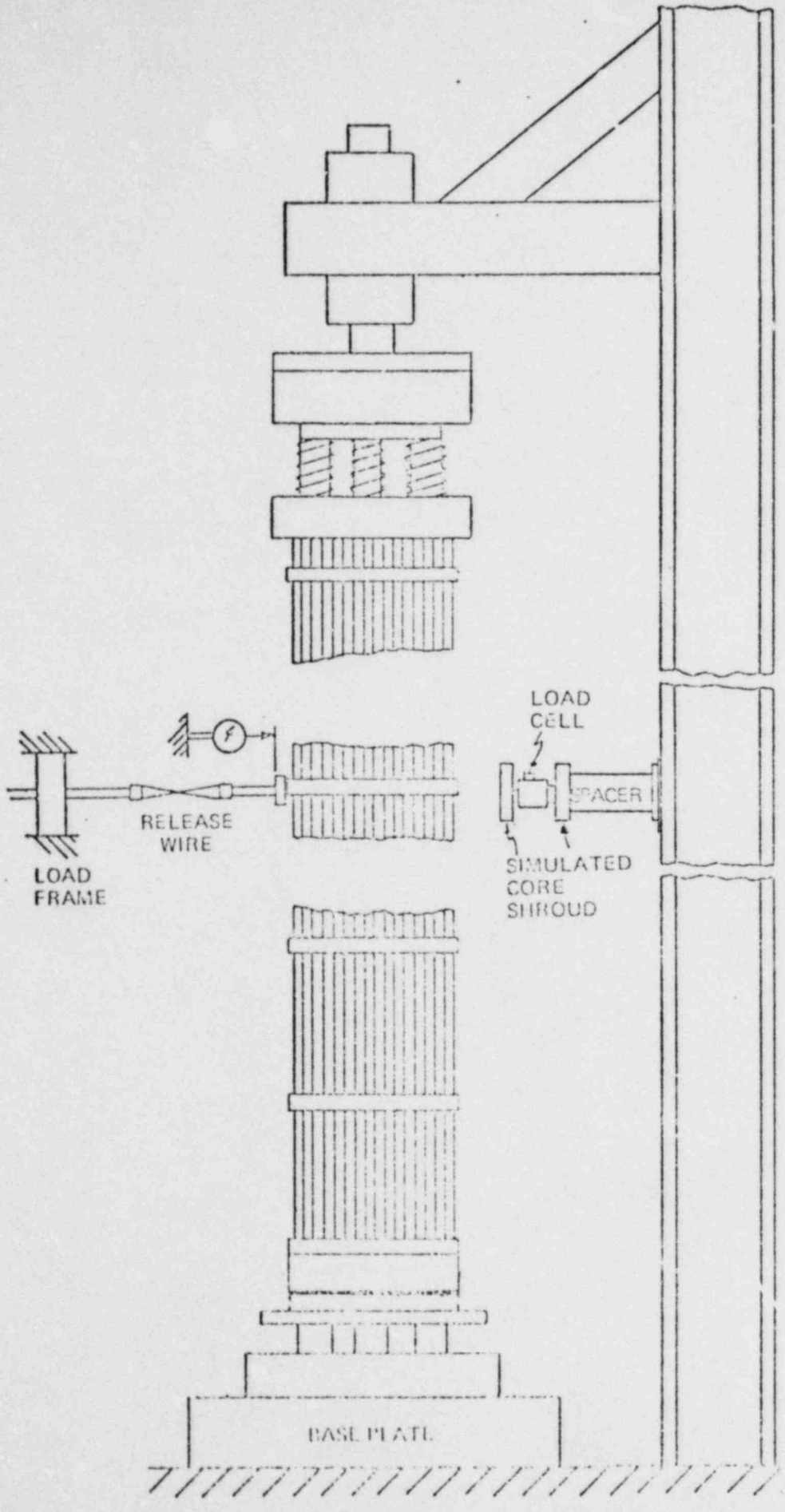

TANK FOR TESTING IN WATER ENVIRONMENT NOT SHOWN

FIGURE 4.7.4

TEST SET-UP FOR PLUCK VIBRATION AND PLUCK IMPACT TESTS

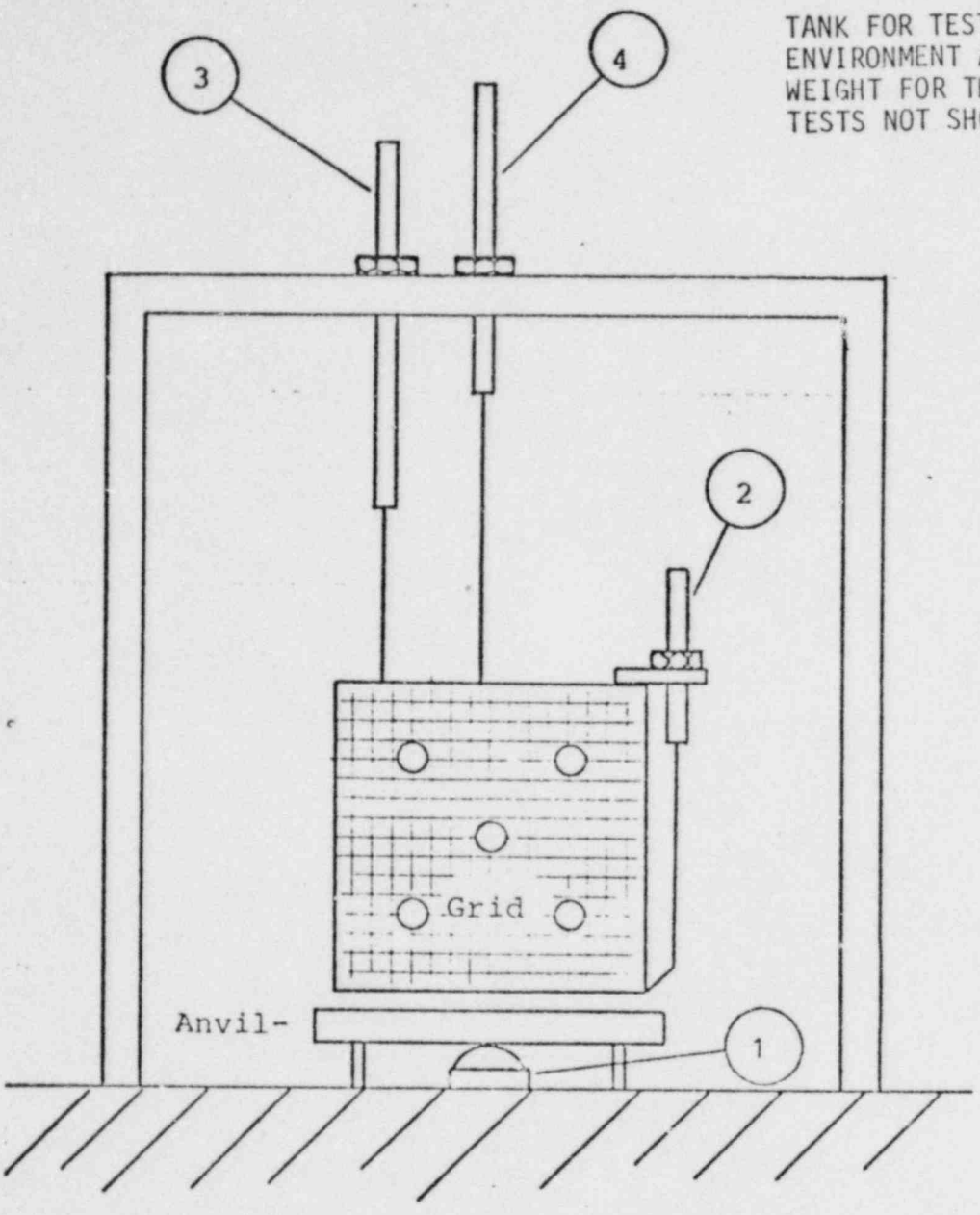

1. Load Cell
2. Grid Compression LVDT
3. Velocity Transducer
4. Grid Position LVDT

FIGURE 4.7.5
TEST SET-UP FOR SPACER GRID IMPACT TESTS

Figure 4.7.6

GENERIC PLANT DETAILED LATERAL CORE MODEL

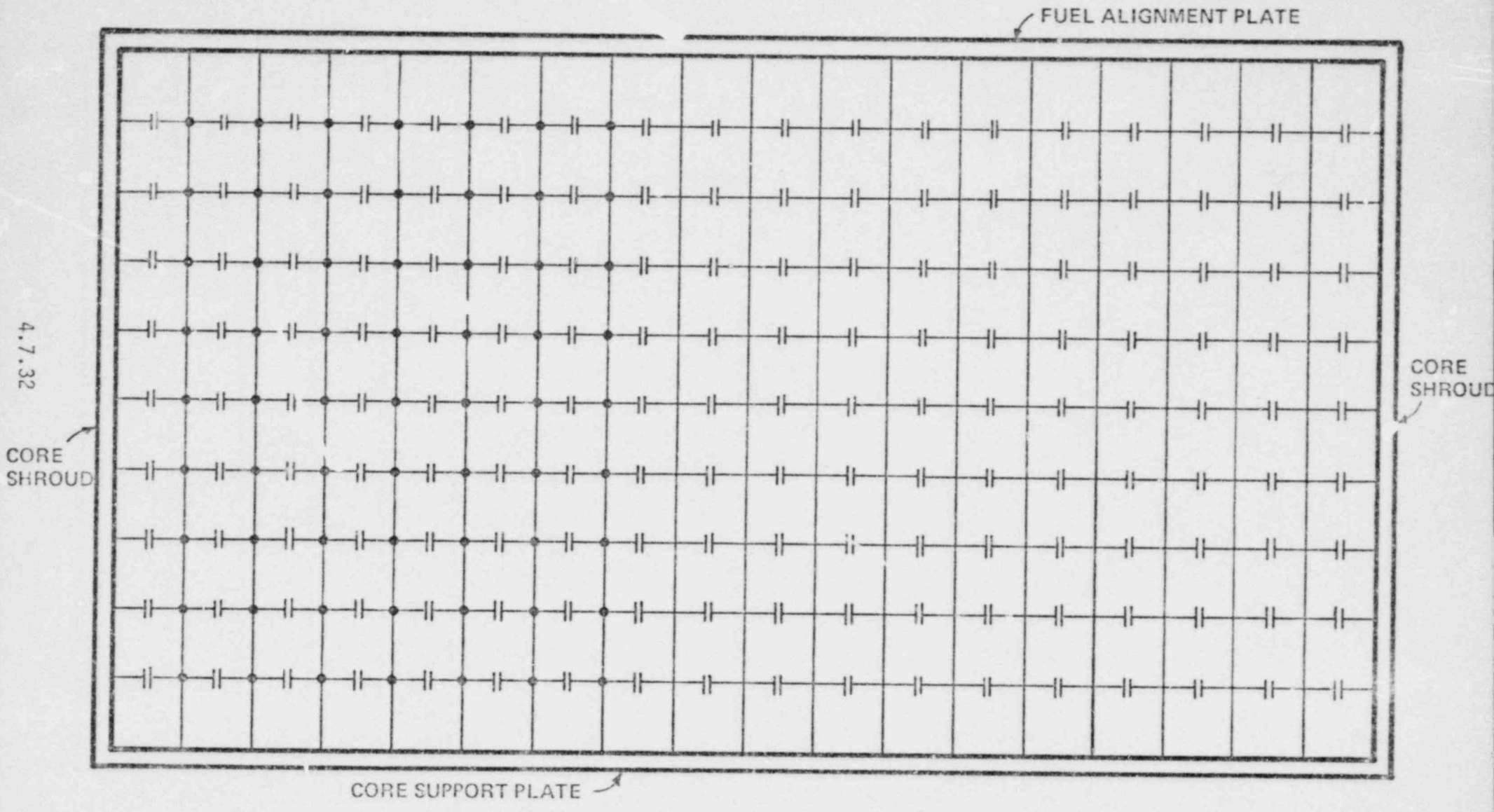

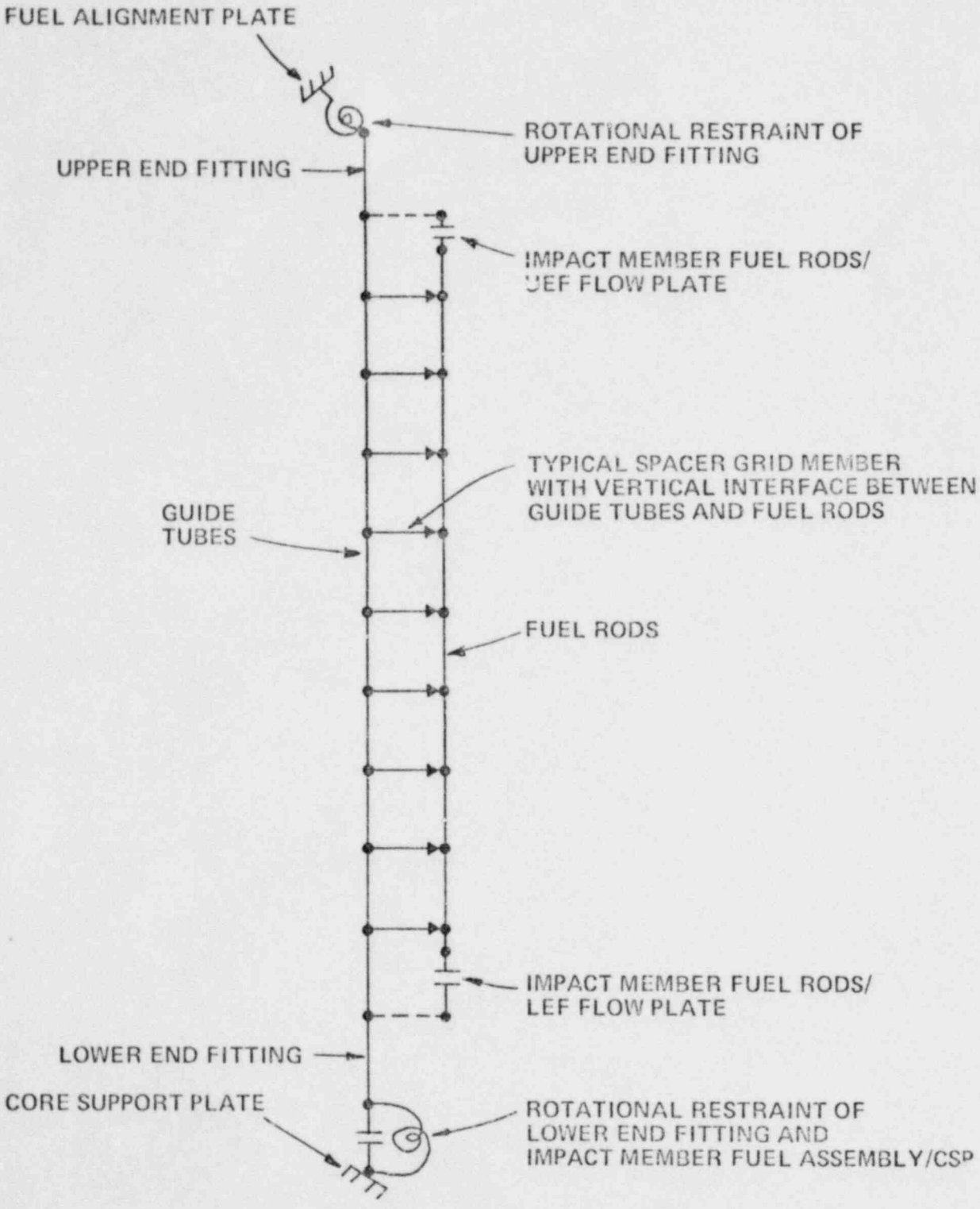

Figure 4.7.7
GENERIC PLANT FUEL ASSEMBLY BEAM COLUMN MODEL

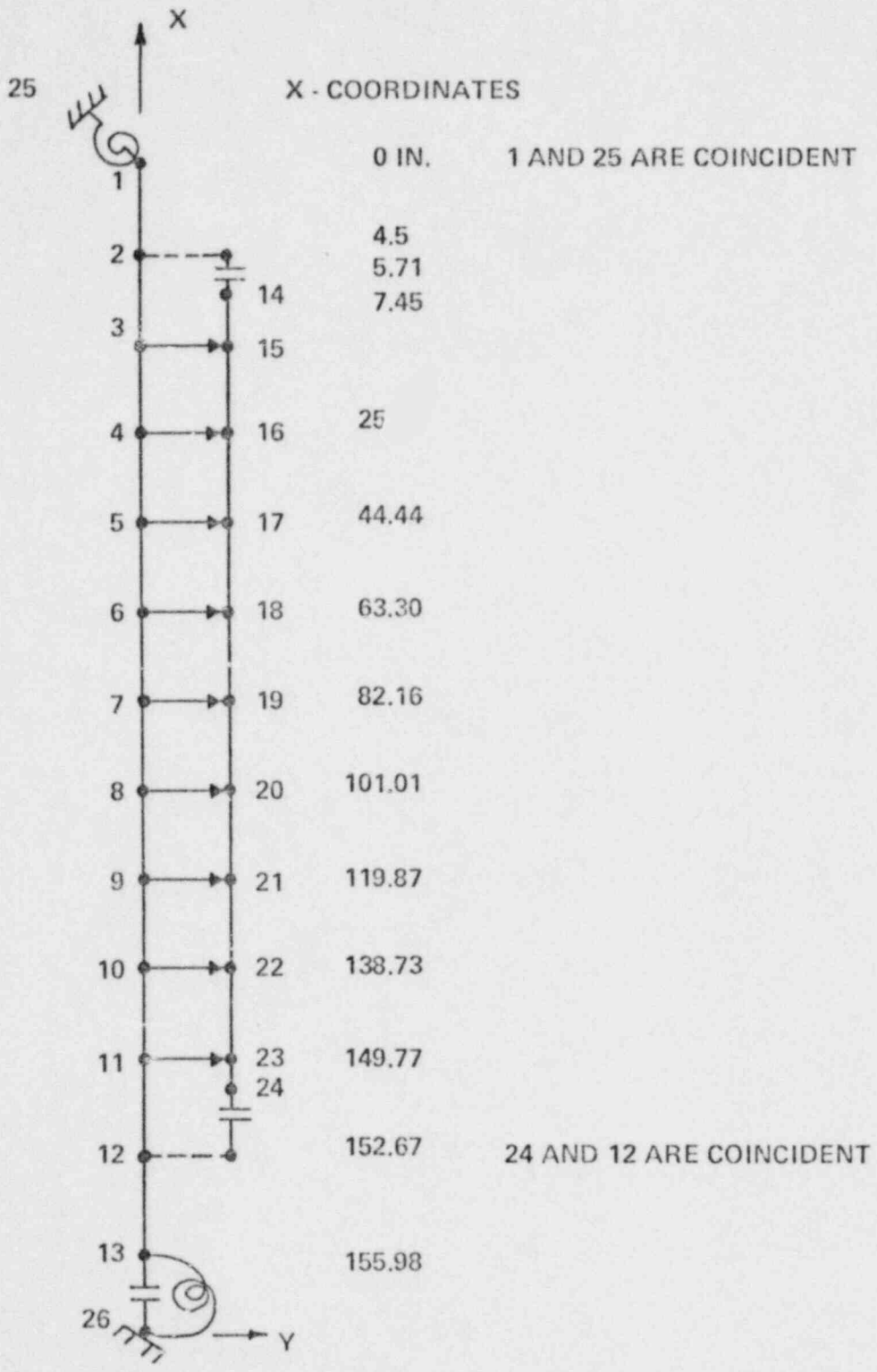

Figure 4.7.8
BEAM COLUMN MODEL: NODE NUMBERS AND COORDINATES

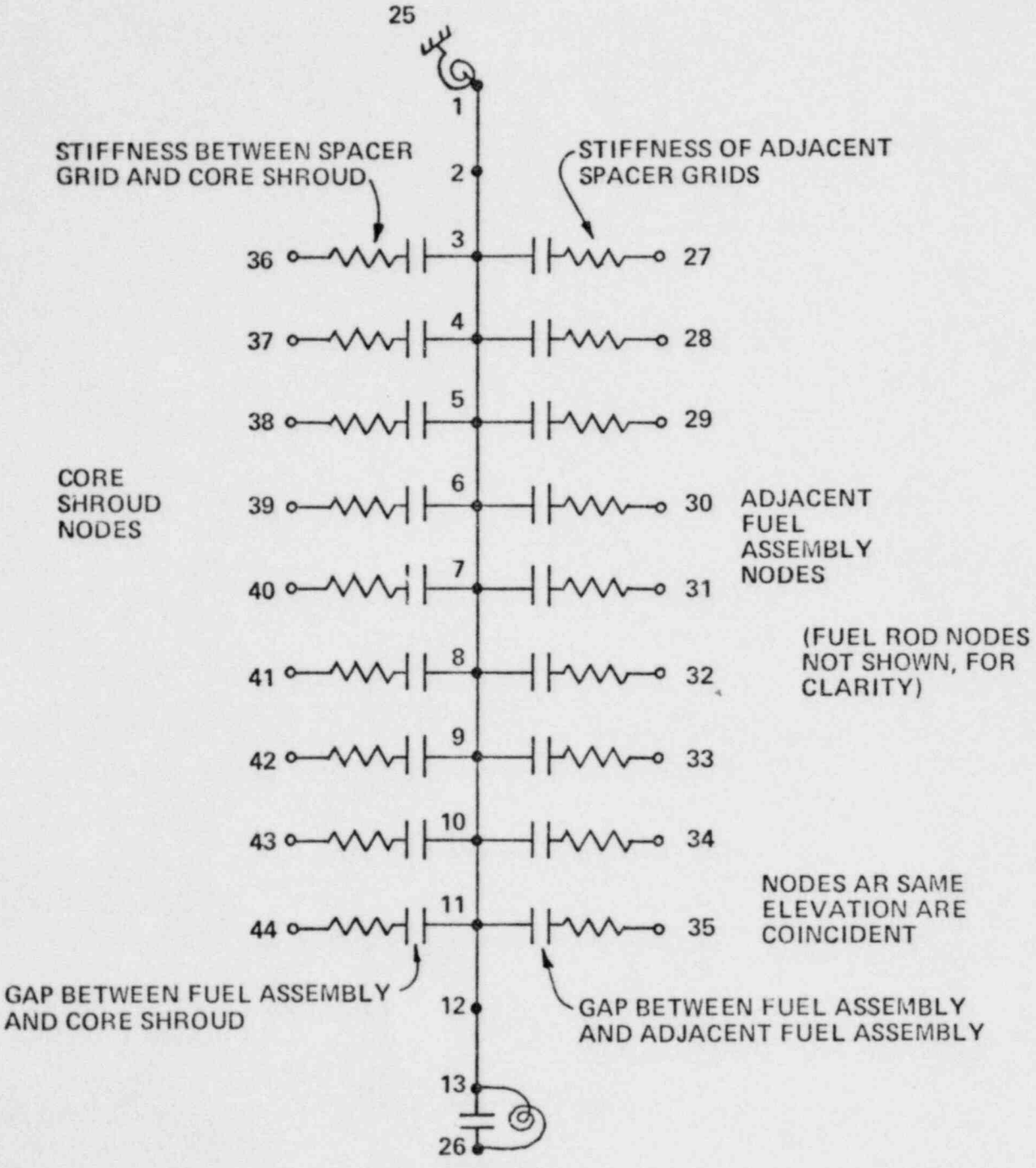

Figure 4.7.9

BEAM COLUMN MODEL'S INTERFACE WITH ADJACENT STRUCTURES

4.8 CONTROL ELEMENT DRIVE MECHANISMS (CEDMs)

4.8.1 DESIGN BASIS

The capability of the control element drive mechanisms (CEDMs) to withstand the effects of design basis pipe breaks has been evaluated by analysis. The effect of each break is experienced by the CEDM through the motion of the reactor vessel head computed by the system structural analysis described in Section 4.5.

4.8.2 METHOD OF ANALYSIS

The CEDMs were analyzed by traditional dynamic elastic analysis and evaluated according to appropriate elastic stress limits for ASME Level D conditions. The elastic Level D stress limits were exceeded for each plant and each pipe break motion input. Therefore, a detailed elastic plastic analysis was performed for each plant.

4.8.2.1 Detailed Analysis

An elastic plastic dynamic analysis of the CEDM for each plant which was anticipated to be most severely loaded was analyzed. This analysis was performed by the MARC (Ref. 3.10) computer program. The displacements of the reactor vessel head computed by the system structural analysis were applied to the base of the CEDMs.

The stresses, strains and moments throughout the CEDM were calculated for the duration of the loading event.

4.8.2.2 Material Properties

The material properties available for the CEDM materials were found to be inadequate for a realistic elastic plastic analysis. In order to obtain material properties for the analysis, samples of all the materials used in the CEDM's were tested in the CE Metallurgy Laboratory. The resulting stress strain curves were conservatively scaled to the ASME Code minimum yield stress according to ASME Level D analysis procedures. The material property test curves and the scaled curves used in the analysis are shown in Figures 4.8.1 to 4.8.4.

4.8.3 RESULTS OF ANALYSIS

The results of each detailed elastic plastic analysis are stress, strain, moment and deformation history of the most

4.8.3 RESULTS OF ANALYSIS (Continued)

severely loaded CEDM for each design basis pipe break. The total moment, the square root of the sum of the squares of the x and z moments, is compared to acceptance criteria.

4.8.3.1 Calvert Cliffs and Millstone II

The bending moment,at the contact point with the head, about the two horizontal directions resulting from the most severe loading are shown in Figures 4.8.5 and 4.8.6. The severity of the loading event, in terms of stress or increase in strain, is greatest at about 200 milliseconds into the transient. After 400 milliseconds the CEDM response damps away.

4.8.3.2 Palisades

The bending moment, at the contact point with the head, about the two horizontal directions resulting from the most severe loading are shown in Figures 4.8.7 and 4.8.8. By 200 milliseconds, the moment has reached a steady oscillation which damps out because:

1) the actual LOCA loading in the system structural analysis itself damps out compared to the constant LOCA loading used and

2) the event disappears after 400 milliseconds

A substantial bending moment is computed at the rotation restraints between CEDMs which were installed to reduce seismic loads. An analysis was performed presuming that the rotation restraints were to fail. The moments produced from this calculation are shown in Figures 4.8.9 and 4.8.10. The maximum total moments are only slightly higher if the rotation restraints fail.

4.8.3.3 Ft. Calhoun

The reactor vessel head motions are input to the Ft. Calhoun CEDM model at the base of the CEDM and at the connection with the head lift rig. This results in a conservative application of the head motion history. The bending moments at the contact point with the head about the two horizontal directions resulting from the most severe loading are shown in Figures 4.8.11 and 4.8.12. The total moment has reached a steady oscillation which subsequently damps out after 400 milliseconds.

4.8.4 EVALUATION OF CEDMs

4.8.4.1 Acceptance Criteria

The CEDMs are not required to operate for safe shutdown after a loss of coolant event resulting from the design basis pipe breaks. In order to comply with existing ECCS analysis methods, however, the integrity of the CEDMs must be maintained and leakage must be prevented. The ASME Boiler and Pressure Vessel Code Section III Division 1 Appendix F lists a number of criteria which assure that the pressure boundary will not be violated. These criteria include stress limits for comparisons to the elastic analysis results and an instability limit for comparison to elastic plastic analysis results. The integrity of the pressure boundary is assured if the applied loads do not exceed 70% of the plastic instability load. An alternate criterion based on strain limits in which a suitably conservative strain limit must be justified may also be employed.

4.8.4.2 Calvert Cliffs and Millstone II

An elastic plastic instability analysis was performed to determine the maximum moment that the CEDM can withstand at the most severely loaded section, the contact point with the head. The maximum axial, shear and pressure loads were applied to the model and then an increasing moment was applied until the deformations increased with no increase in load. The material properties used in this analysis are the conservatively scaled ones of Section 4.8.2.2. Actual properties would result in much higher moment capabilities. The results of this instability limit analysis are shown in Figure 4.8.13. Also shown is the maximum total moment computed in the CEDM analysis of Section 4.8.3.1. The maximum moment is clearly below 70% of the plastic instability load indicating that ASME Level D criteria are met and integrity is assured.

4.8.4.3 Palisades

An elastic plastic instability analysis similar to that performed in Section 4.8.4.2 was performed for the Palisades plant. The result of this instability limit analysis is shown in Figure 4.8.14. Also shown are the maximum total moment for the cases where the rotation restraints remain intact and for when they are assumed to fail.

4.8.4.3 Palisades (Continued)

The maximum total moments are 66% and 70% respectively of the plastic instability load. Since the instability load was computed using material properties scaled to code minimum yield stress and the test results are significantly higher, the moments, equal to the ASME Level D criteria are considered acceptable.

4.8.4.4 Ft. Calhoun

The Ft. Calhoun CEDM has the same load carrying capability as the Palisades CEDM. This capability curve is shown in Figure 4.8.15 and includes the maximum total moment computed in Section 4.8.3.3. The maximum total moment is 77% of the load carrying capability of the CEDM. Because of the conservatism inherent in all steps of the analysis, especially the plastic instability analysis, the applied moment is considered acceptable, and integrity will be maintained.

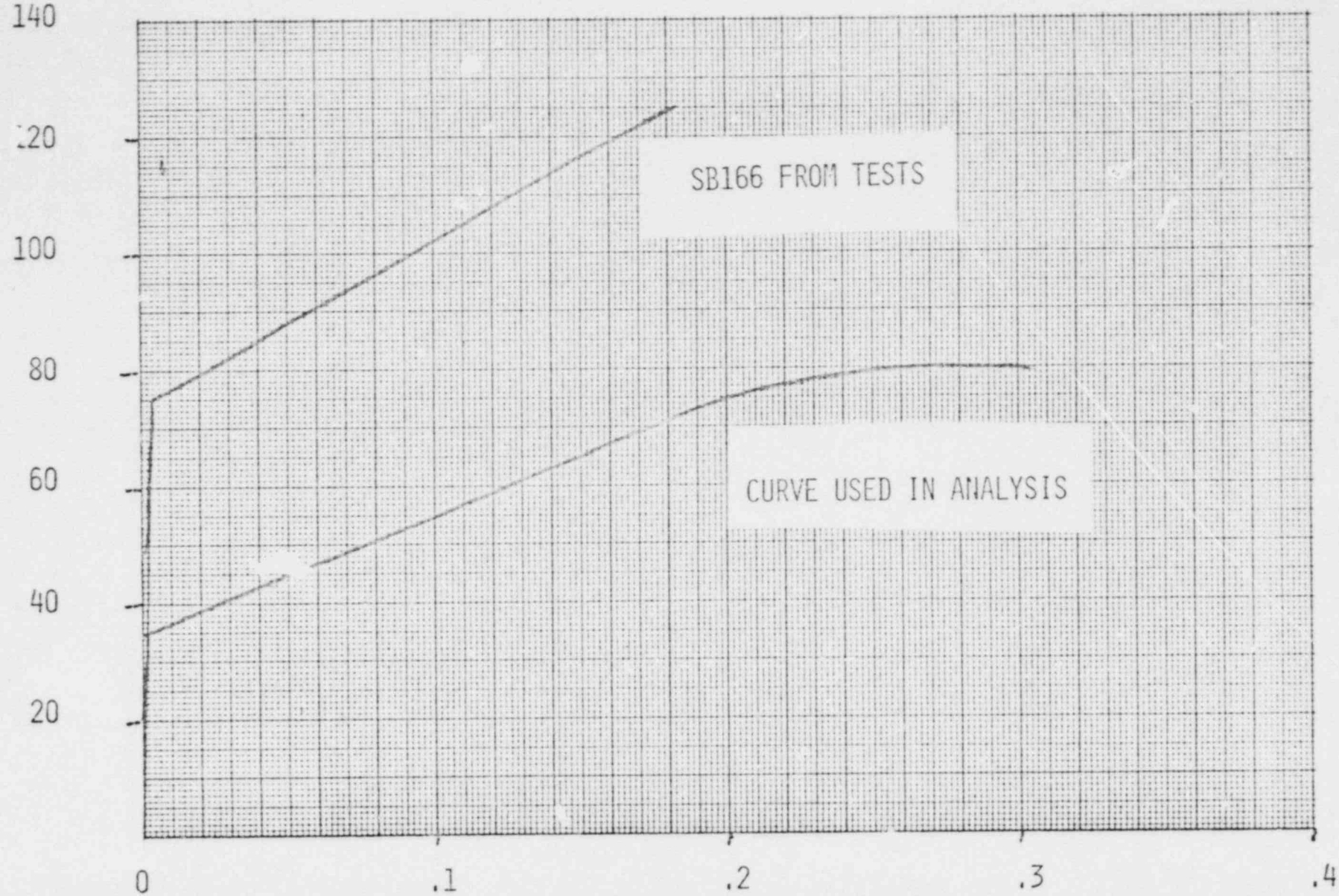

FIGURE 4.8.1 MATERIAL STRESS-STRAIN CURVE FOR SB166, 167

(NOZZLE MATERIAL FOR CALVERT CLIFFS, MILLSTONE II, PALISADES AND FT. CALHOUN PLANTS)

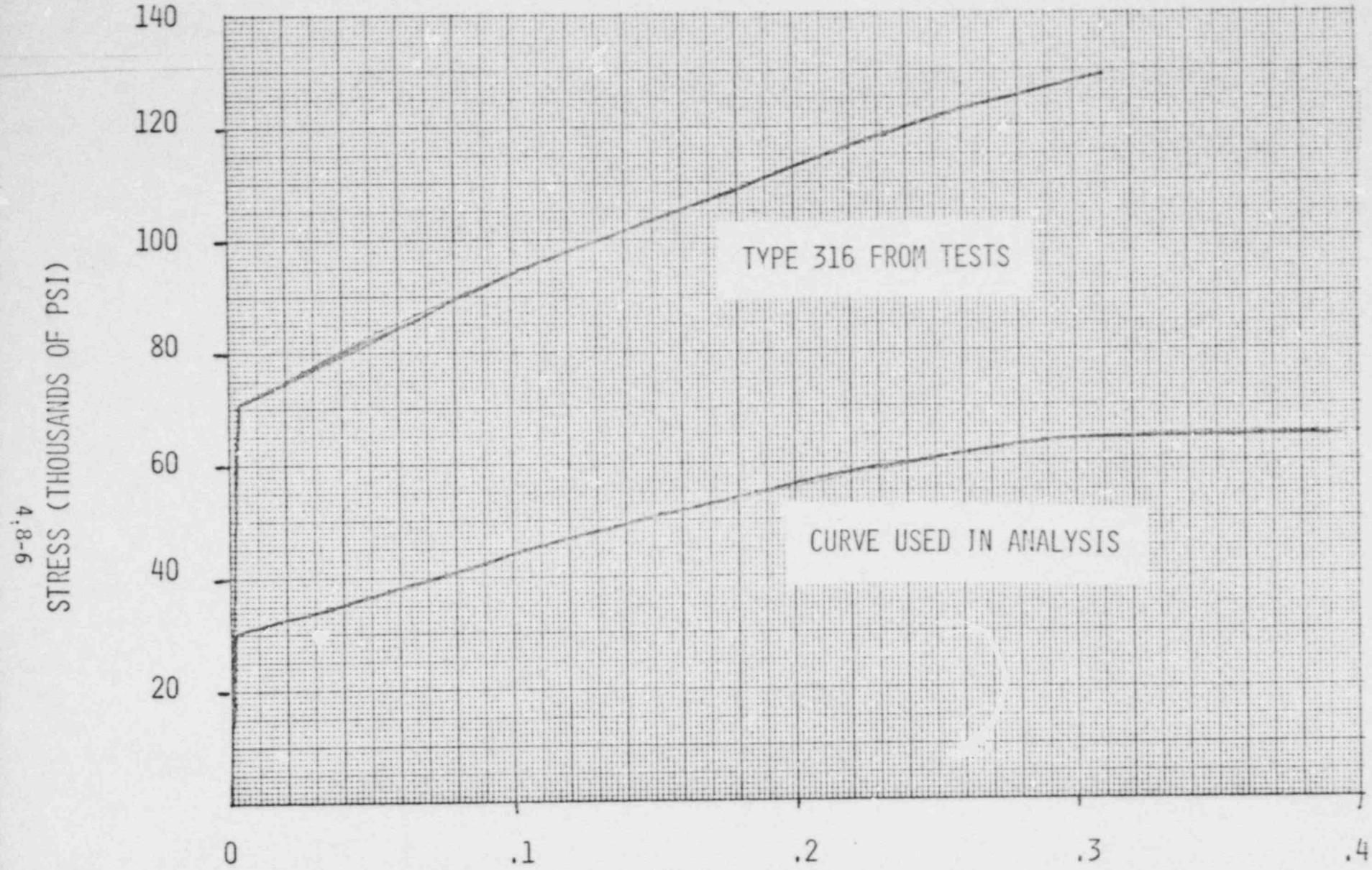

FIGURE 4.8.2 MATERIAL STRESS-STRAIN CURVE FOR SA182-F316
(NOZZLE MATERIAL FOR CALVERT CLIFFS & MILLSTONE II PLANTS)

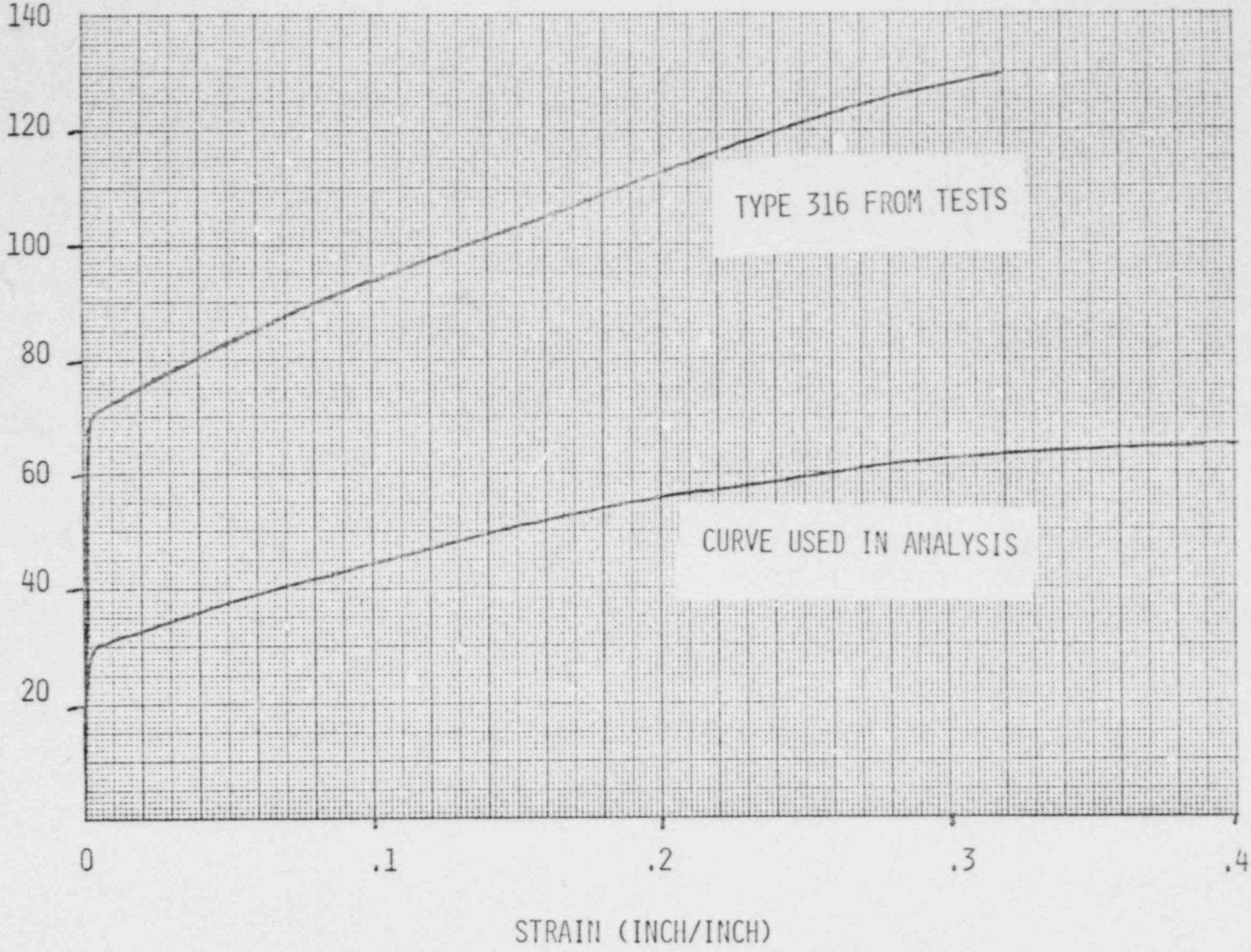

FIGURE 4.8.3 MATERIAL STRESS-STRAIN CURVE FOR SA213-TP316
(UPPER PRESSURE HOUSING TUBE MATERIAL FOR CALVERT CLIFFS & MILLSTONE II PLANTS)

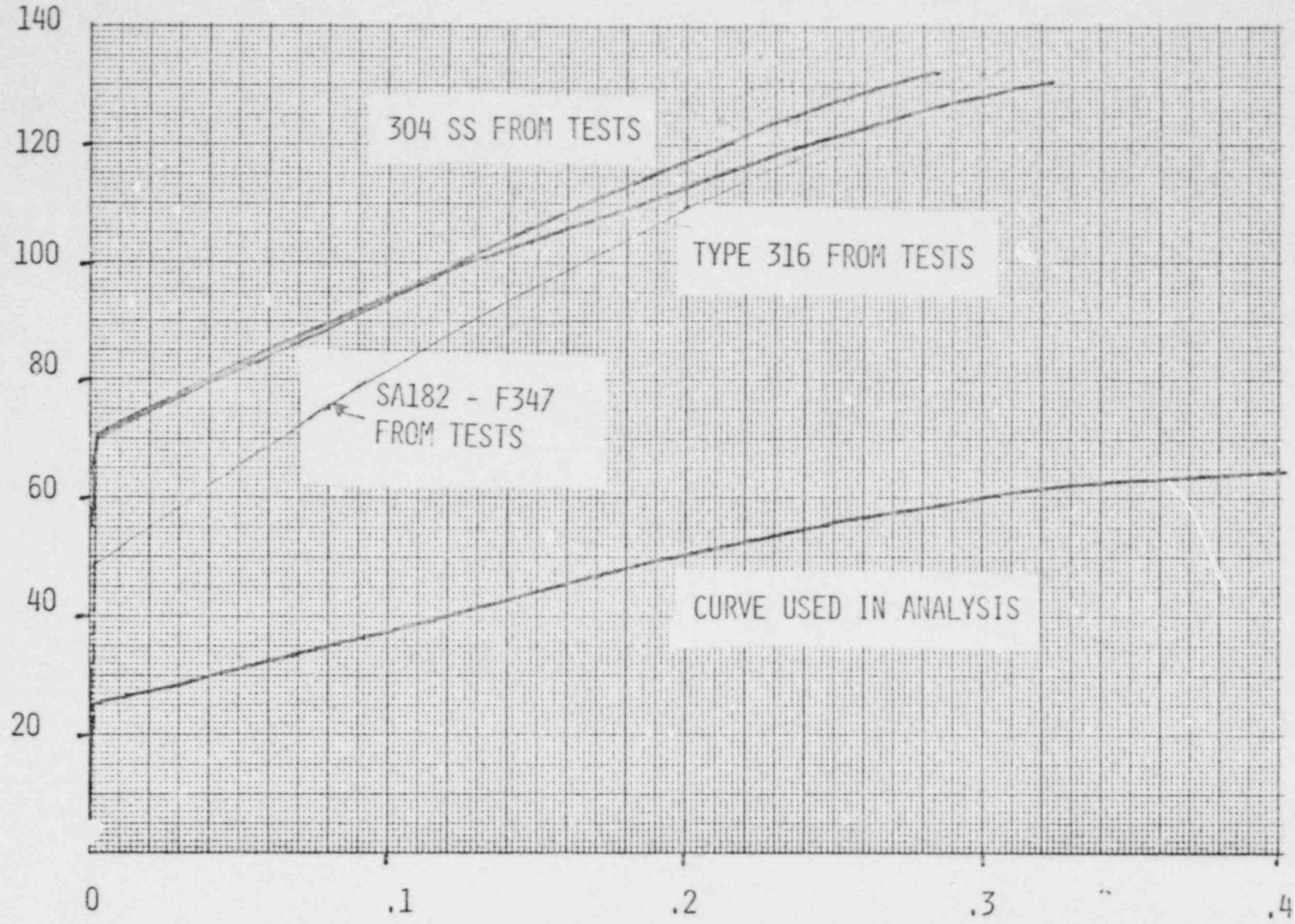

FIGURE 4.8.4 MATERIAL STRESS-STRAIN CURVE FOR SA479-TP316 AND 304 SS, SA 182-F347,348
(LOWER END FITTING OF UPPER PRESSURE HOUSING AND SHROUD MATERIALS FOR CALVERT CLIFFS & MILLSTONE II PLANTS)
(MATERIAL FOR ALL COMPONENTS EXCEPT NOZZLE - PALISADES AND FT. CALHOUN PLANTS)

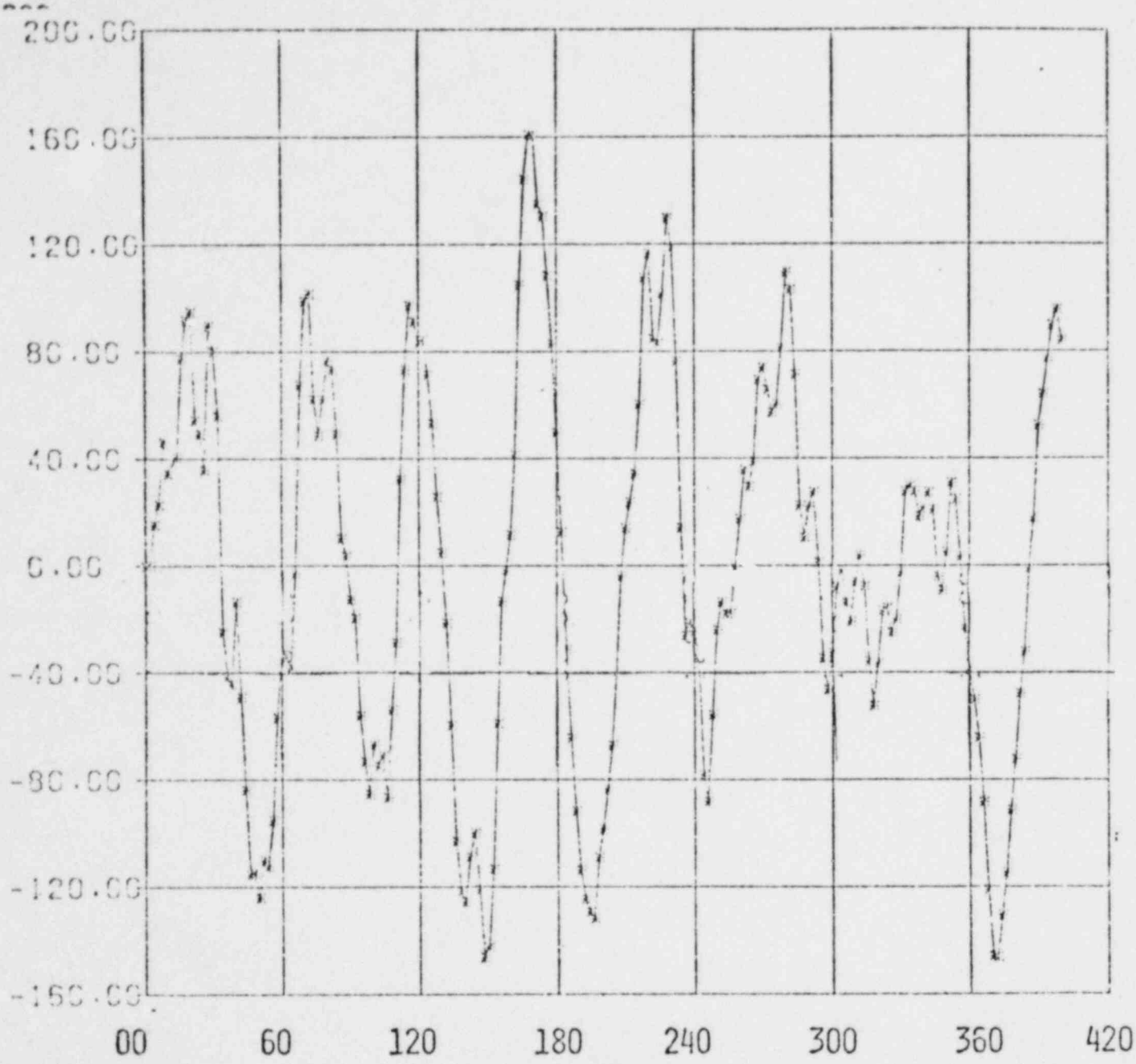

FIGURE 4.8.5 CALVERT CLIFFS AND MILLSTONE II CEDM NOZZLE
X-(HORIZONTAL) BENDING MOMENT
(COLD LEG BREAK)

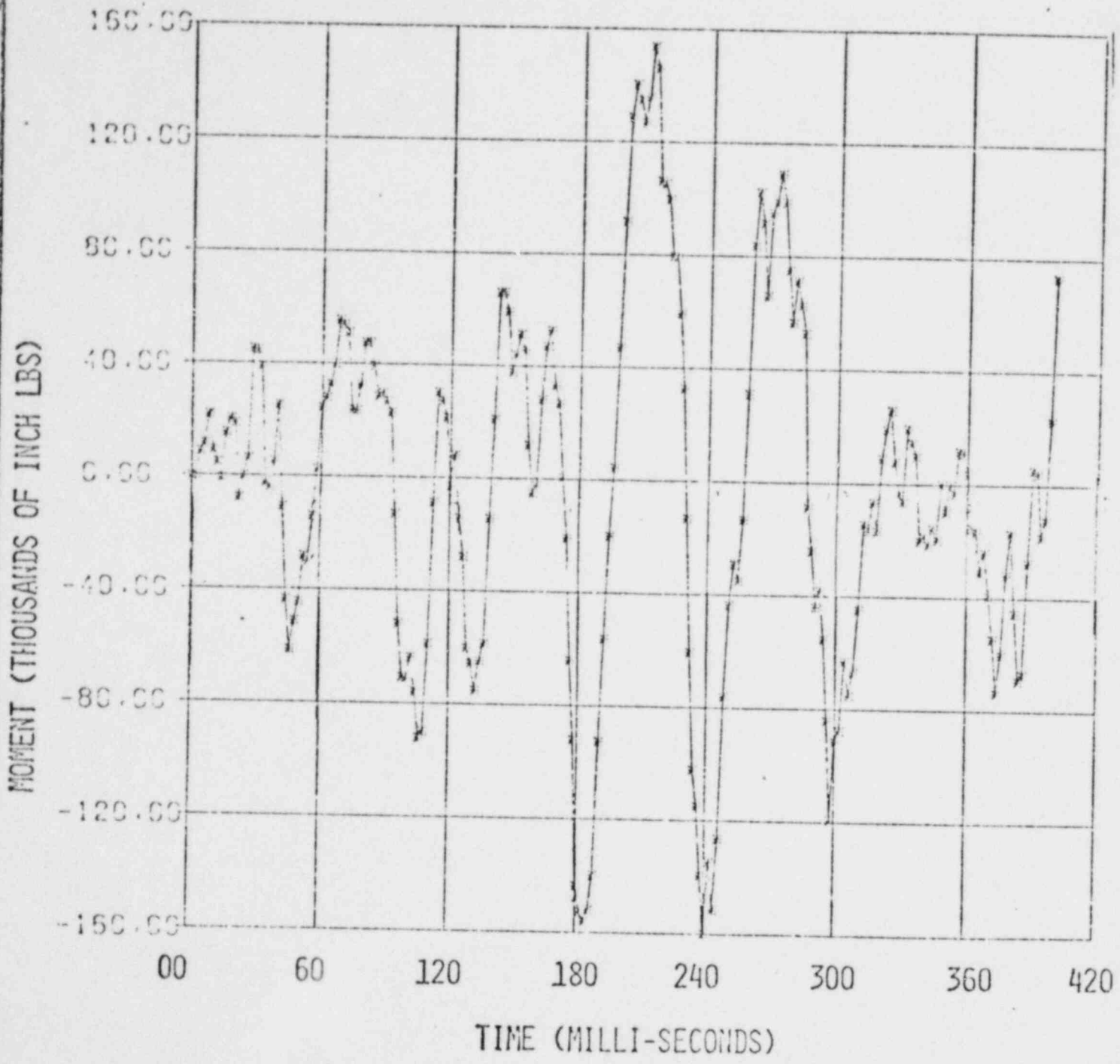

FIGURE 4.3.6 CALVERT CLIFFS AND MILLSTONE II CEDM NOZZLE
Z-(HORIZONTAL) BENDING MOMENT
(COLD LEG BREAK)

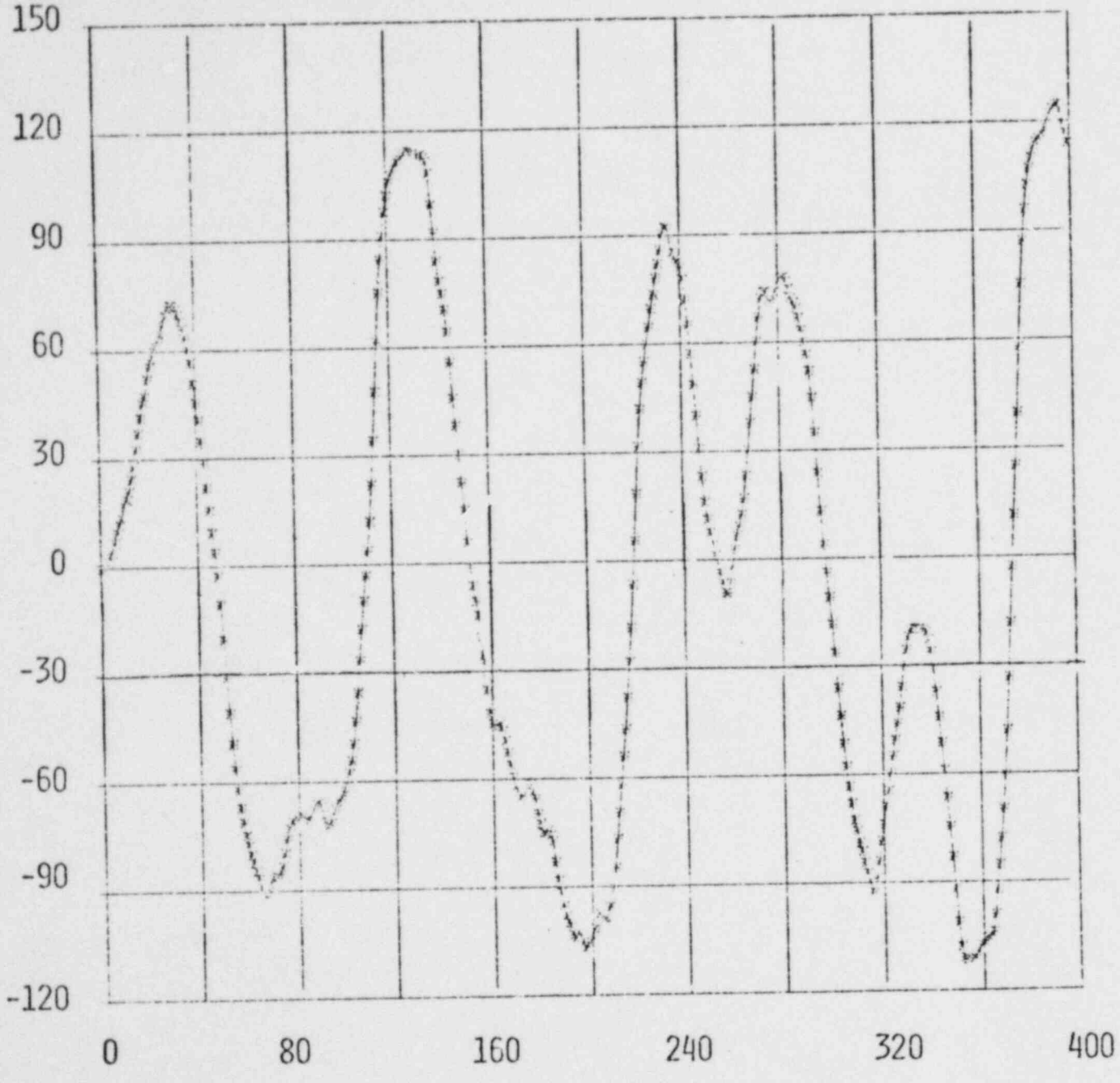

FIGURE 4.8.7 PALISADES CEDM NOZZLE
X-(HORIZONTAL) BENDING MOMENT
(WITH RESTRAINTS FROM SEISMIC SUPPORTS)

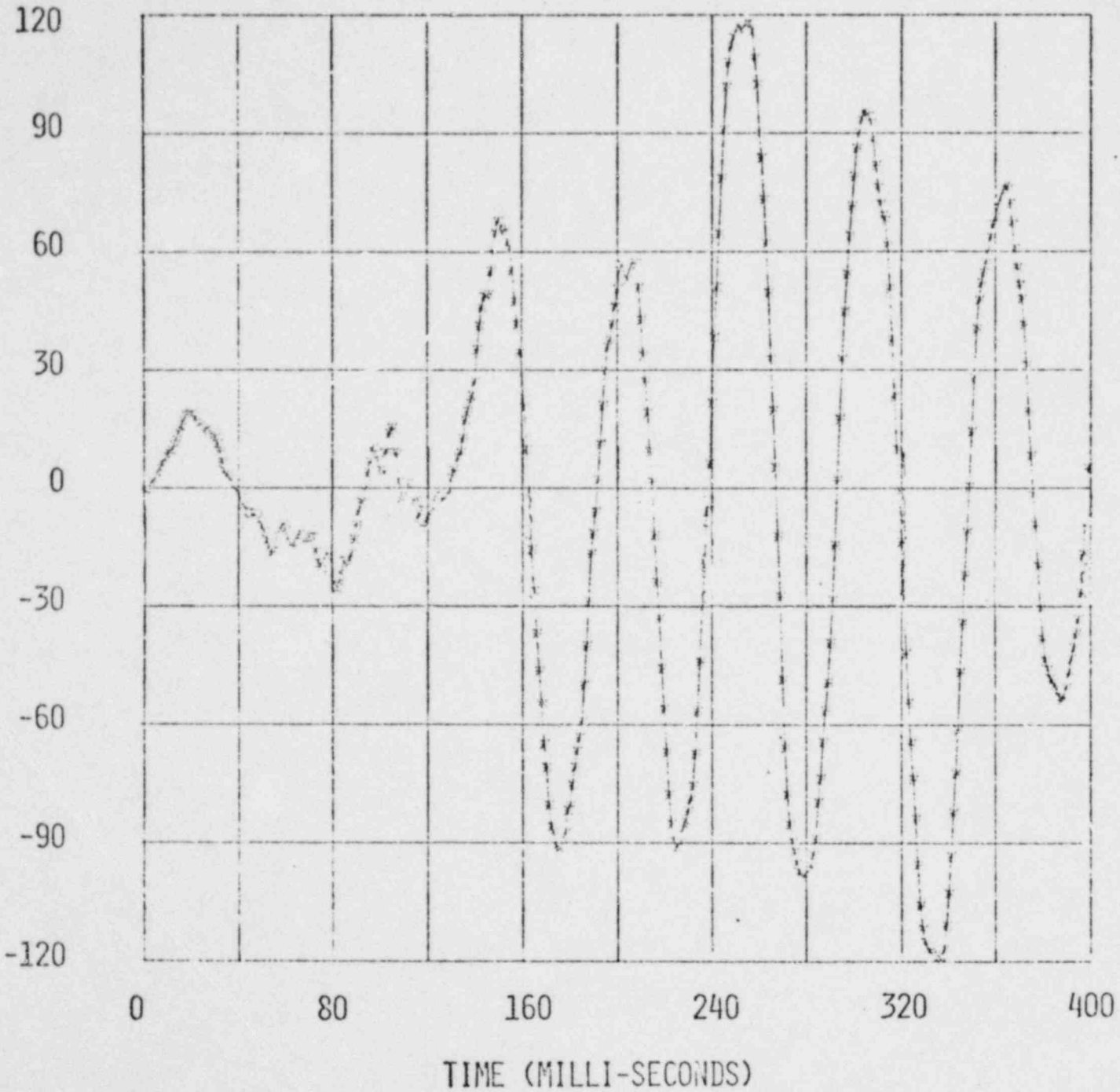

FIGURE 4.8.8 PALISADES CEDM NOZZLE
Z-(HORIZONTAL) BENDING MOMENT
(WITH RESTRAINTS FROM SEISMIC SUPPORTS)

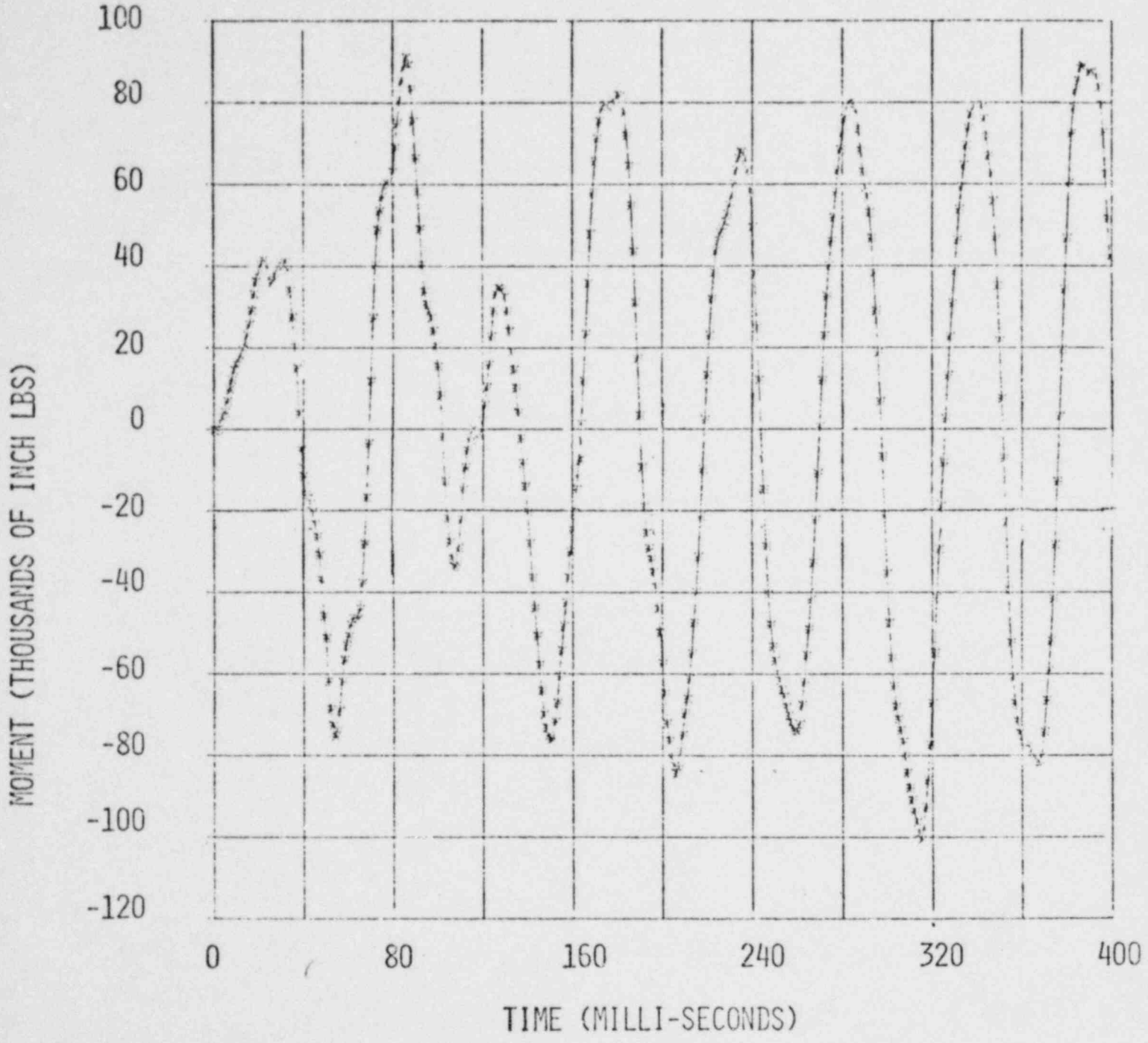

FIGURE 4.8.9 PALISADES CEDM NOZZLE X-(HORIZONTAL) BENDING MOMENT (WITHOUT RESTRAINTS)

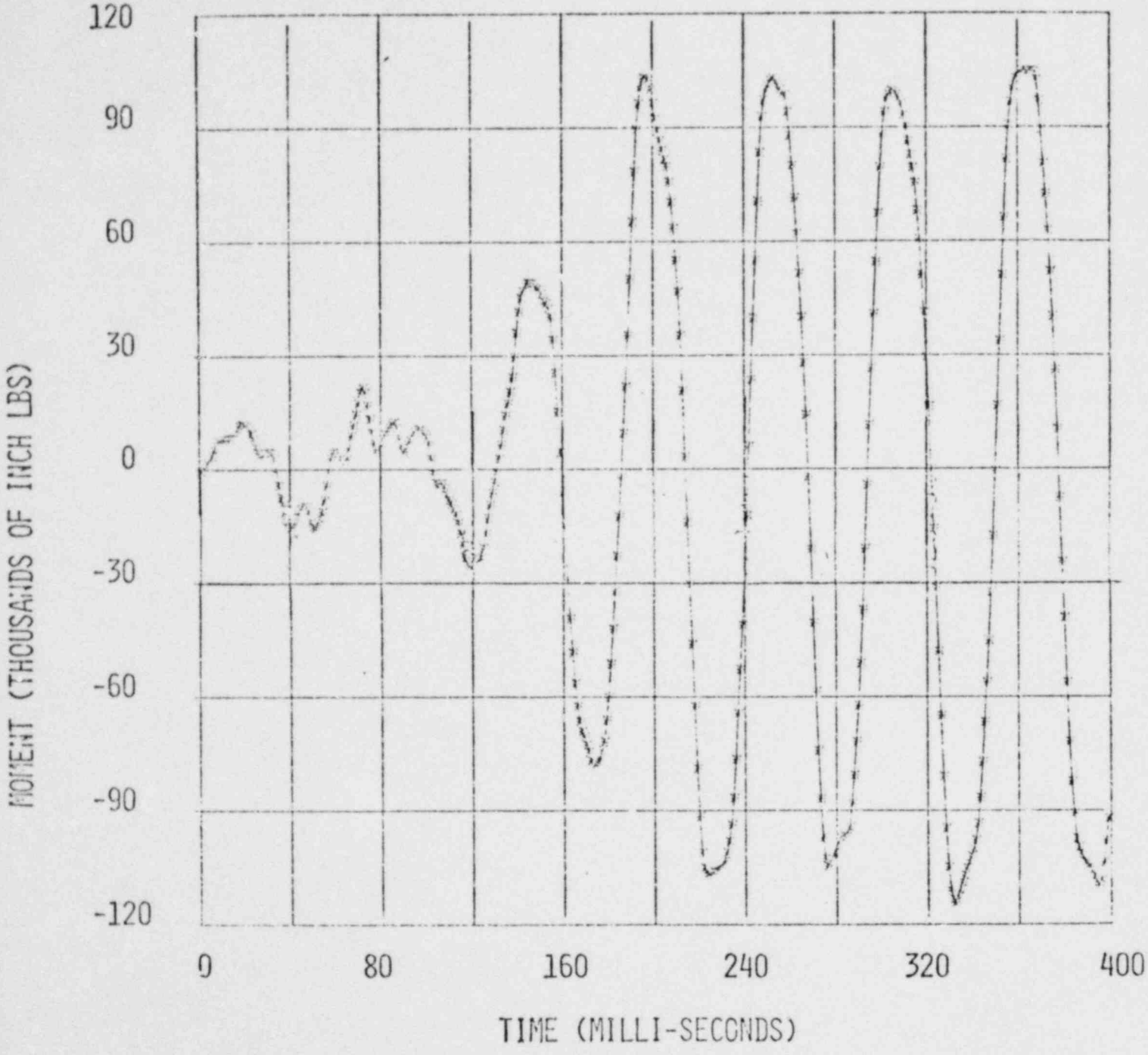

FIGURE 4.8.10 PALISADES CEDM NOZZLE
Z-(HORIZONTAL) BENDING MOMENT
(WITHOUT RESTRAINTS)

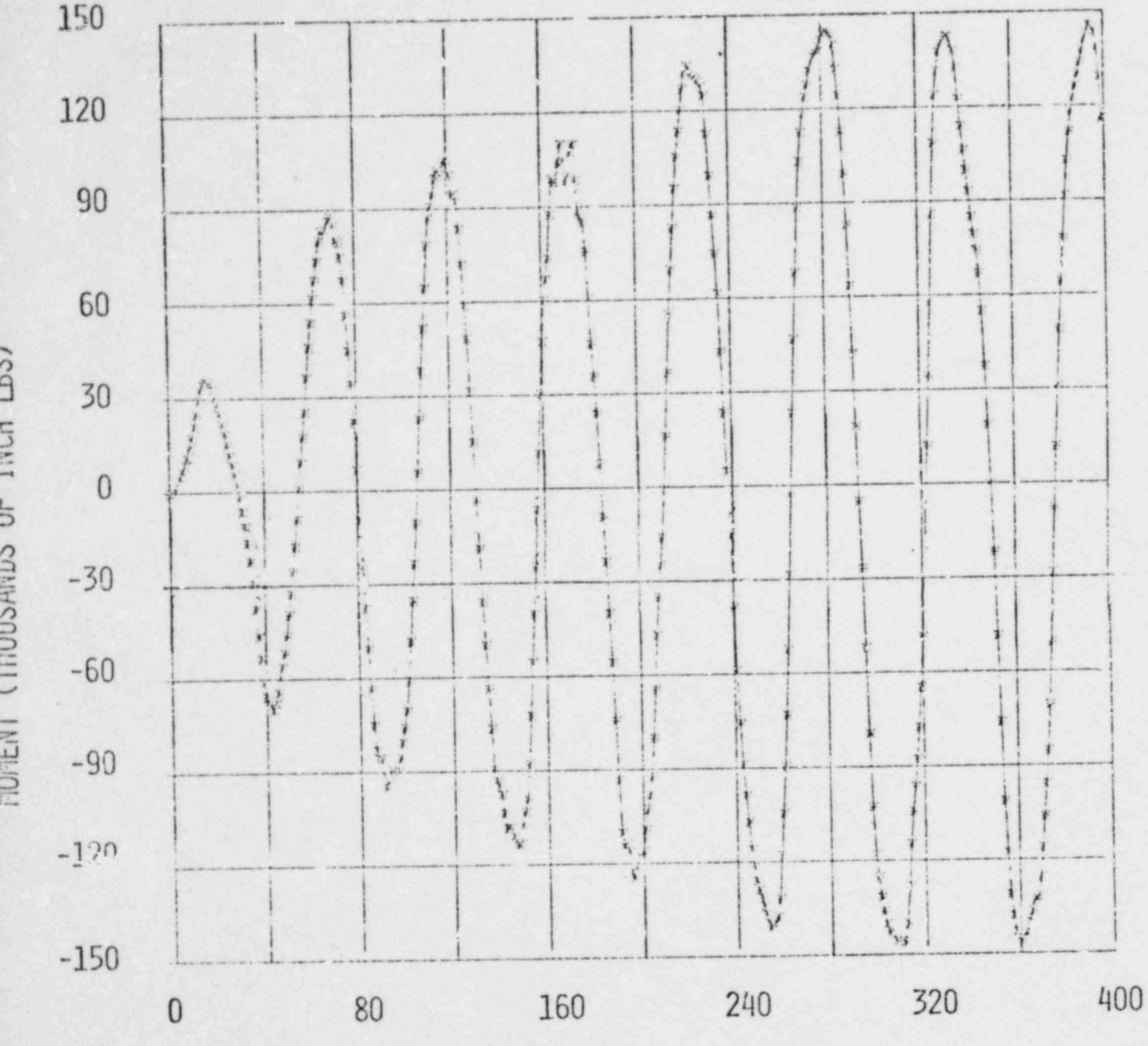

FIGURE 4.8.11 FORT CALHOUN CEDM NOZZLE
X-(HORIZONTAL) BENDING MOMENT

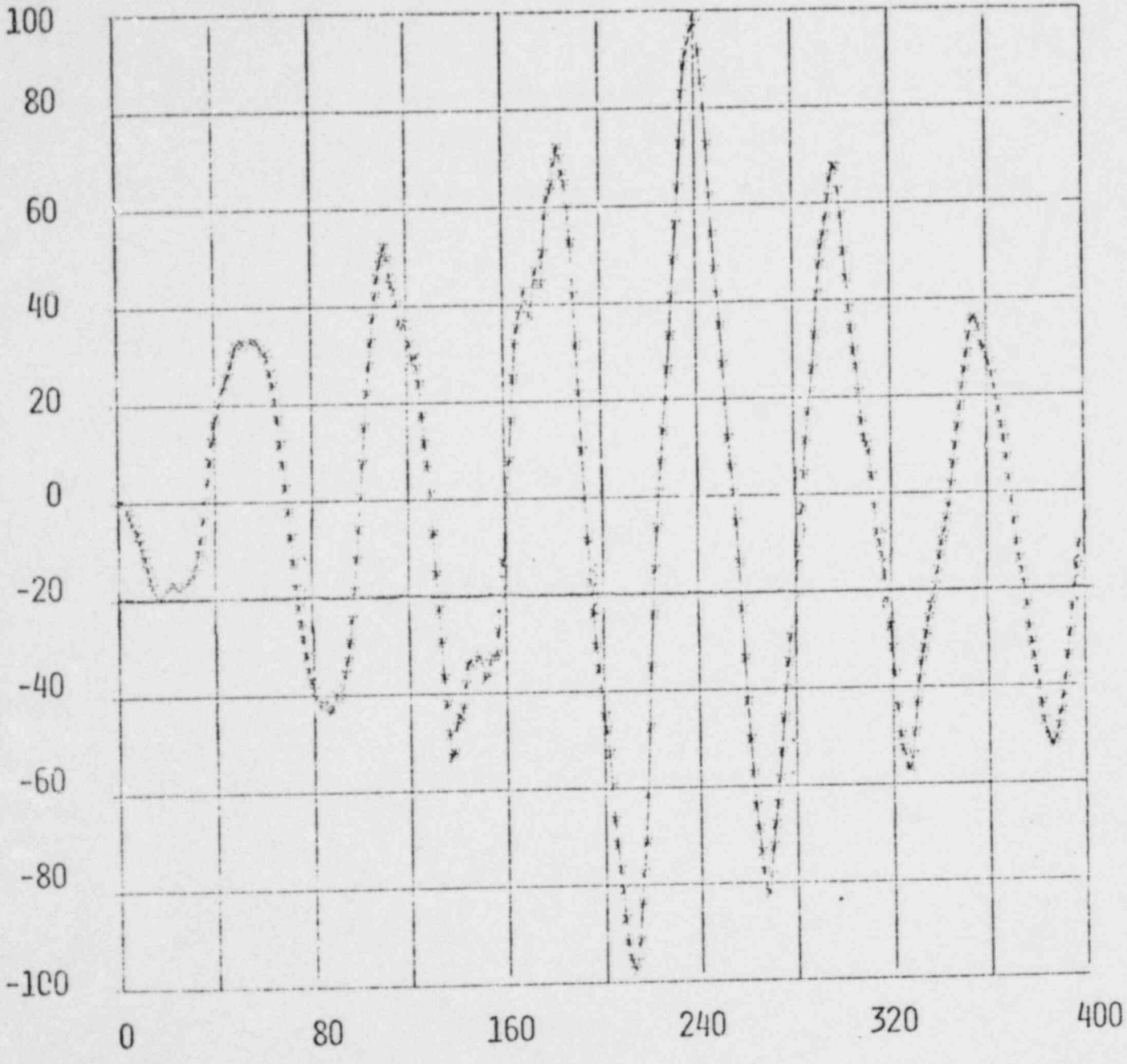

FIGURE 4.8.12 FORT CALHOUN CEDM NOZZLE
Z-(HORIZONTAL) BENDING MOMENT

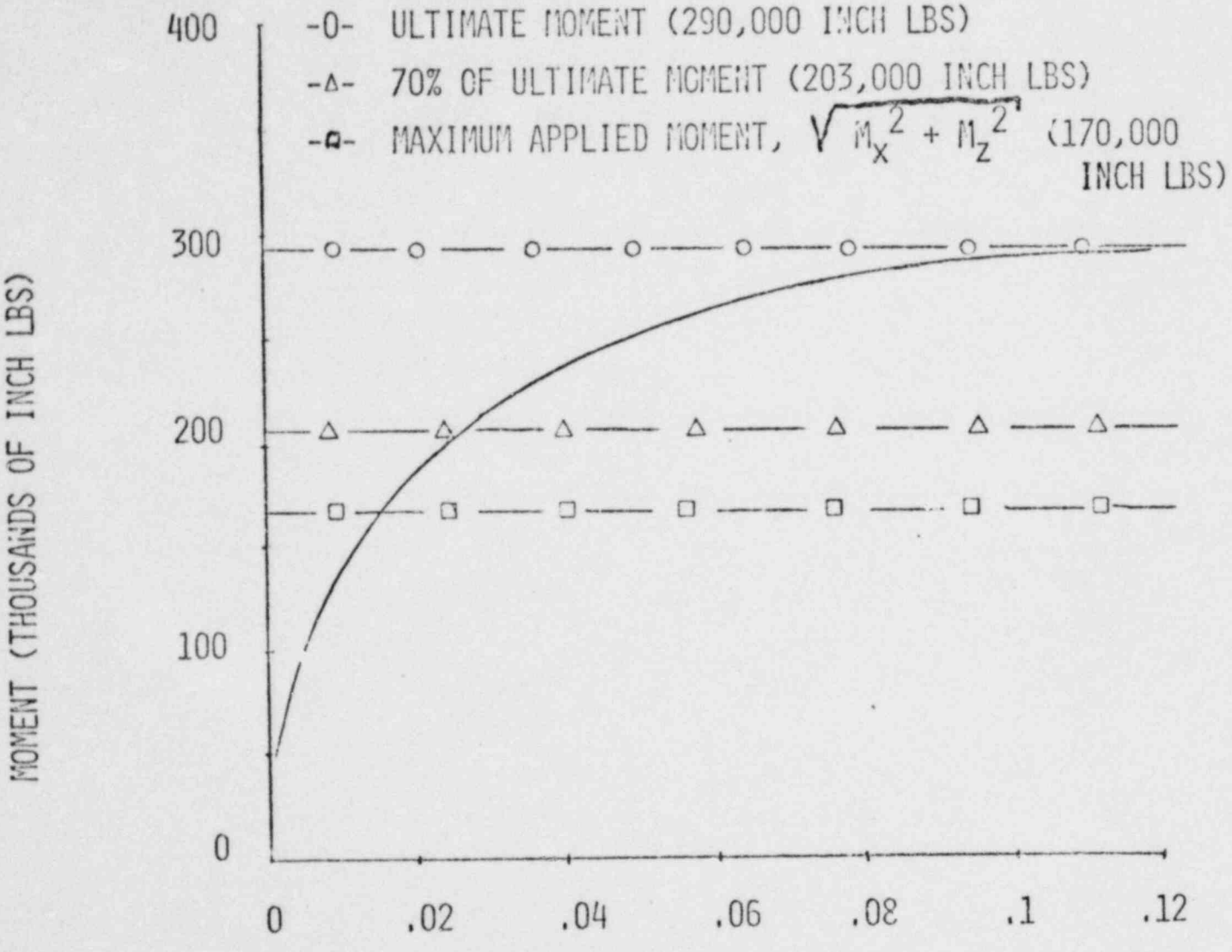

FIGURE 4.8.13 COMPARISON OF BENDING MOMENTS
IN CALVERT CLIFFS AND MILLSTONE II
CEDM NOZZLE

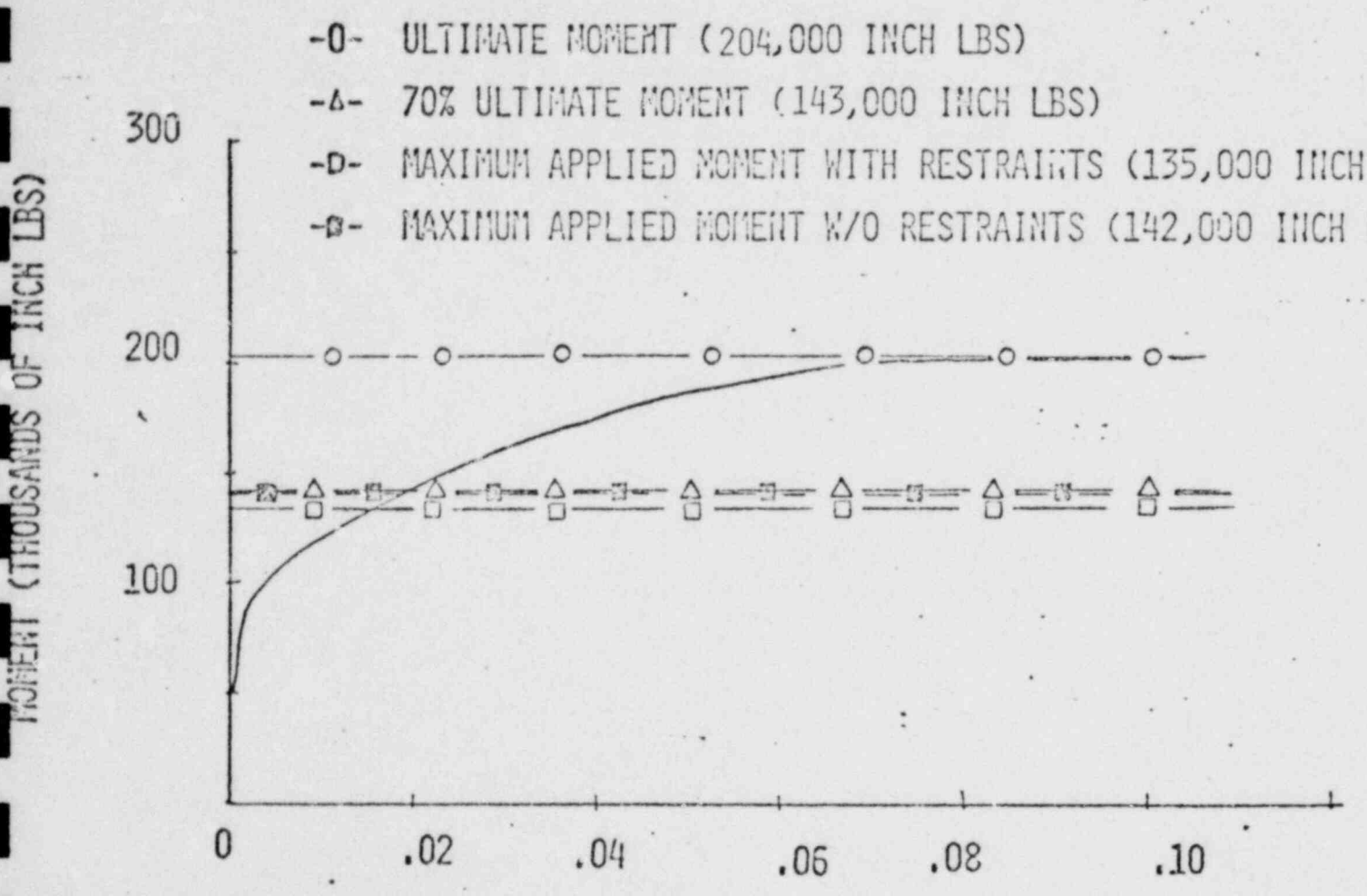

FIGURE 4.8.14 COMPARISON OF BENDING MOMENTS IN PALISADES CEDM NOZZLE

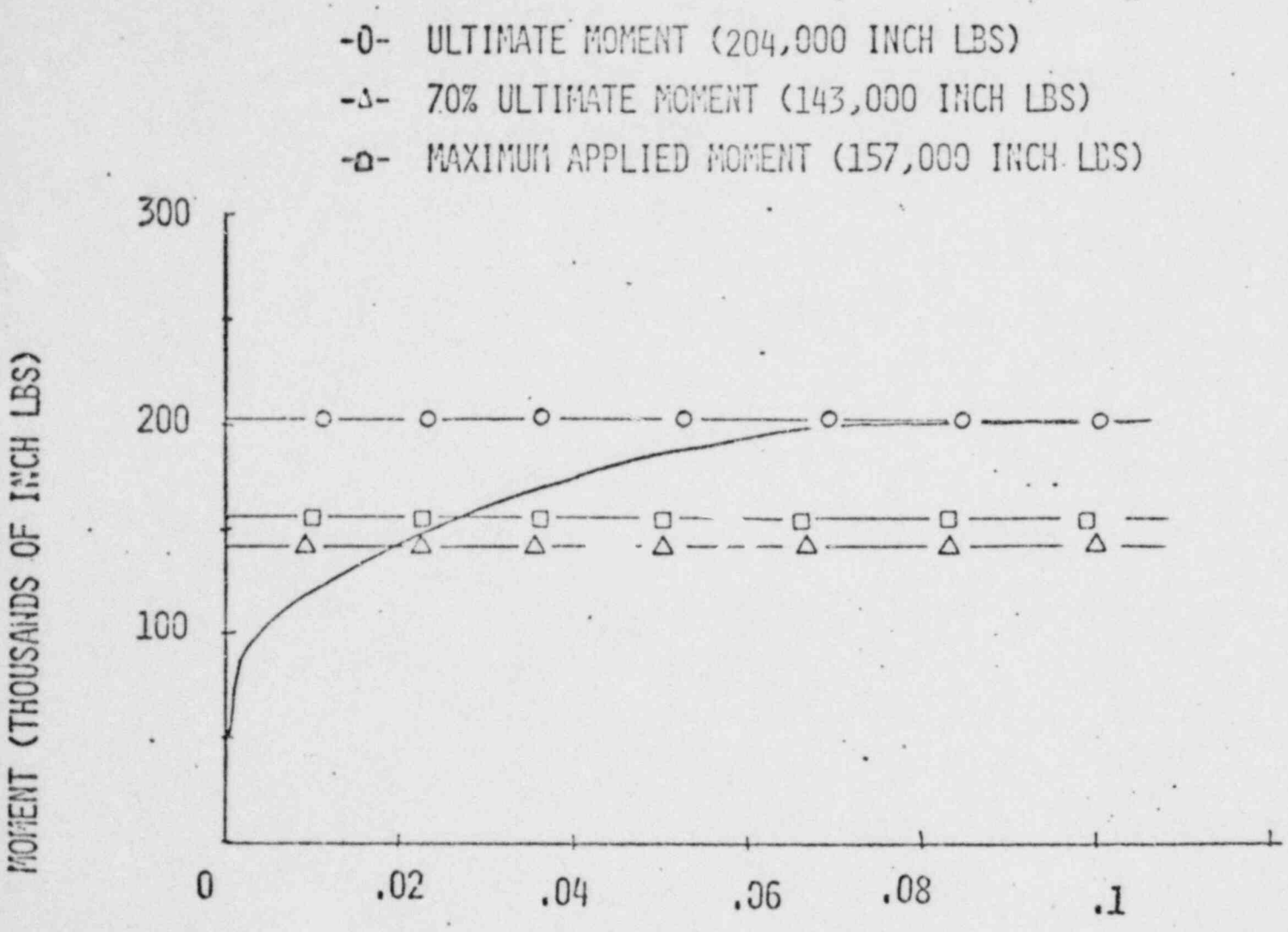

FIGURE 4.8.15 COMPARISON OF BENDING MOMENTS IN FT. CALHOUN CEDM NOZZLE

4.9 EMERGENCY CORE COOLING SYSTEM (ECCS) PIPING

4.9.1 DESIGN BASIS

The capability of the emergency core cooling system (ECCS) piping that is attached to the primary coolant piping to withstand the effects of the design basis pipe breaks has been evaluated by analysis. The effect of each break is experienced by the ECCS piping through the motion of the ECCS nozzles on the discahrge leg piping. The motions of the nozzles have been computed by the reactor coolant system structural analysis described in Section 4.5. No credit has been taken for de-pressurization.

4.9.2 METHODS OF ANALYSIS

The ECCS piping has been analyzed by traditional dynamic elastic analysis and evaluated according to appropriate elastic stress limits for ASME Level B and Level D conditions. Where these limits are not satisfied, a detailed elastic plastic analysis to demonstrate functionability of the piping has been performed.

4.9.2.1 Dynamic Analysis

An elastic dynamic analysis of the ECCS piping was performed using lumped parameter models and the appropriate ECCS nozzle motion history. The physical definition of the piping has been represented in STRUDL (Ref. 3.2) to generate the appropriate condensed stiffness matrix of the structure. The condensed matrix and mass has been input to the DAGS (Ref. 3.4) program. The DAGS program determined the motion history of the ECCS pipe by performing a time history analysis.

4.9.2.2 Detailed Analysis

Where the stresses computed by the elastic dynamic analysis exceed the prescribed limits an elastic plastic finite element analysis was performed for each region where significant plasticity was expected. This analysis is similar to the instability analyses discussed in Paragraph 4.5.3. The analysis provides details of the deformation necessary to evaluate the functionability and ultimate load carrying capability of the plastic region. The elastic plastic analysis has been performed by the MARC (Ref. 3.10) computer program. The material properties for the piping material used in the analysis was determined from the extensive collection of piping data available.

4.9 EMERGENCY CORE COOLING SYSTEM (ECCS) PIPING

4.9.1 DESIGN BASIS

The capability of the emergency core cooling system (ECCS) piping that is attached to the primary coolant piping to withstand the effects of the design basis pipe breaks has been evaluated by analysis. The effect of each break is experienced by the ECCS piping through the motion of the ECCS nozzles on the discahrge leg piping. The motions of the nozzles have been computed by the reactor coolant system structural analysis described in Section 4.5. No credit has been taken for de-pressurization.

4.9.2 METHODS OF ANALYSIS

The ECCS piping has been analyzed by traditional dynamic elastic analysis and evaluated according to appropriate elastic stress limits for ASME Level B and Level D conditions. Where these limits are not satisfied, a detailed elastic plastic analysis to demonstrate functionability of the piping has been performed.

4.9.2.1 Dynamic Analysis

An elastic dynamic analysis of the ECCS piping was performed using lumped parameter models and the appropriate ECCS nozzle motion history. The physical definition of the piping has been represented in STRUDL (Ref. 3.2) to generate the appropriate condensed stiffness matrix of the structure. The condensed matrix and mass has been input to the DAGS (Ref. 3.4) program. The DAGS program determined the motion history of the ECCS pipe by performing a time history analysis.

4.9.2.2 Detailed Analysis

Where the stresses computed by the elastic dynamic analysis exceed the prescribed limits an elastic plastic finite element analysis was performed for each region where significant plasticity was expected. This analysis is similar to the instability analyses discussed in Paragraph 4.5.3. The analysis provides details of the deformation necessary to evaluate the functionability and ultimate load carrying capability of the plastic region. The elastic plastic analysis has been performed by the MARC (Ref. 3.10) computer program. The material properties for the piping material used in the analysis was determined from the extensive collection of piping data available.

4.9.3 RESULTS OF ANALYSIS

The results of elastic and elastic plastic dynamic analyses are the displacements, moments, and stresses at the critical sections of the ECCS piping as a function of time during the LOCA event. ECCS piping support reactions are also computed in these analyses. All analyses have been performed on specific plant ECCS piping and support systems. Analyses have been performed for the design basis pipe breaks considered in Section 4.5. A summary of maximum piping moments vs. allowable limits is presented in Figure 4.9.1. Specific plant results are discussed in Section 4.9.4.

4.9.4 EVALUATION OF ECCS PIPING

4.9.4.1 Acceptance Criteria

The integrity and functionability of the ECCS piping must be demonstrated. Integrity and functionability are assured if the Level B (upset condition) limits of the ASME Boiler and Pressure Vessel Code Section III, Division 1, are not exceeded. Where the Level B limits are exceeded, then Level D or faulted limits are used to demonstrate that integrity is maintained. Functionability is assured by demonstrating that the deformations of the piping are acceptable.

4.9.4.2 Evaluation

The elastic dynamic stress results have been compared to the Level B and Level D stress limits of the ASME Code.

In the event that the stress limits are not satisfied, the elastic plastic analysis of Paragraph 4.9.2.2 has been performed.

The integrity of the piping has been evaluated by comparing the computed load to 70% of the instability load. The functionability has been evaluated by comparing the pipe section deformation to the deformation required for significant flow restriction.

4.9.4.2.1 Calvert Cliffs

The Calvert Cliffs ECCS piping has been evaluated for the generic plant motion. The maximum moment in the ECCS piping due to the hypothetical pipe break is 2,800,000 in-lbs at an elbow, and 3,090,000 in-lbs in a straight section of pipe. These moments satisfy the ASME Code Level D elastic limits. At these moment levels, the plastic strain is less than 1%. Functionability is not impaired at these strain levels. Analysis of the safety injection nozzle indicates

4.9.4.2.1 Calvert Cliffs (Continued)

that ASME Code Level B elastic limits are satisfied. A worst case elbow moment vs. time plot is presented in Fig. 4.92.

4.9.4.2.2 Millstone

The input motion to the ECCS piping is identical to the generic plant motion. The maximum moments in the piping due to the hypothetical pipe break exceeds the ASME Code Level D elastic limits. An elastic-plastic analysis per paragraph 4.9.2.2 has, therefore, been performed. The maximum moment in the piping is 3,300,000 in-lbs at an elbow, and 5,800,000 in-lbs in a straight section of pipe. These moments satisfy the ASME Code Level D criteria of 70% of the collapse load. A plot of maximum elbow moment vs. time is presented in Fig. 4.9.3. The ultimate moment carrying capability of the elbow is presented in Fig. 4.9.6. At these moment levels, the plastic strain is less than 2%. Functionability is not impaired at these strain levels. Analysis of the Safety Injection Nozzle indicates that ASME Code Level B elastic limits are satisfied.

4.9.4.2.3 Palisades

A plant specific analysis of the Palisades ECCS piping has been performed. The maximum moments in the piping due to the hypothetical pipe break exceeds the ASME Code Level D elastic limits. An elastic-plastic analysis per paragraph 4.9.2.2 has, therefore, been performed. The maximum moment in the piping is 2,880,000 in-lbs at an elbow, and 4,160,000 in-lbs in a straight section of pipe. These moments satisfy the ASME Code Level D criteria of 70% of the collapse load. A plot of maximum elbow moment vs. time is presented in Fig. 4.9.4. The ultimate moment carrying capability of the elbow is presented in Fig. 4.9.6. At these moment levels, the plastic strain is less than 2%. Functionability is not impaired at these strain levels. Analysis of the Safety Injection Nozzle indicates that ASME Code Level B elastic limits are satisfied.

4.9.4.2.4 Fort Calhoun

A plant specific analysis of the Fort Calhoun ECCS piping has been performed. The maximum moments in the piping due to the hypothetical pipe break is 2,160,000 in-lbs at an elbow and in a straight section of pipe. These moments satisfy the ASME Code Level D elastic limits. At these moment levels, the plastic strain is less than 1%. Functionability is not impaired at these strain levels. Analysis of the safety injection nozzle indicates that ASME Code Level B elastic limits

4.9.4.2.4 Fort Calhoun (Continued)

are satisfied. A plot of maximum elbow moment vs. time is presented in Fig. 4.9.5. A comparison of the motions on the ECCS piping due to hot and cold leg guillotines was performed. The motions resulting from the cold leg guillotine govern the response of the ECCS piping.

ECCS PIPING EVALUATION

SUMMARY OF MAXIMUM MOMENTS

(UNITS 10^6 IN-LBS)

PLANT	HYPOTHETICAL PIPE BREAK	MAXIMUM MOMENT ELBOW	ALLOWABLE MOMENT ELBOW	MAXIMUM MOMENT STRAIGHT PIPE	ALLOWABLE MOMENT STRAIGHT PIPE	ANALYTICAL METHOD
CALVERT CLIFFS	HOT LEG	2.65	2.93	3.09	4.73	ELASTIC
	COLD LEG	2.80	2.93	2.82	4.73	ELASTIC
MILLSTONE	HOT LEG	3.3	3.85	5.8	7.0	PLASTIC
	COLD LEG	2.24	2.93	4.53	4.73	ELASTIC
PALISADES	HOT LEG	1.73	2.93	3.55	4.73	ELASTIC
	COLD LEG	2.88	3.85	4.16	7.0	PLASTIC
FORT CALHOUN	COLD LEG	2.16	2.54	2.16	5.39	ELASTIC

FIGURE 4.9.1

CALVERT CLIFFS ECCS LINE 12B RSS MOMENT

(NOTE: RSS MOMENTS PLOTTED IN ABSOLUTE VALUES)

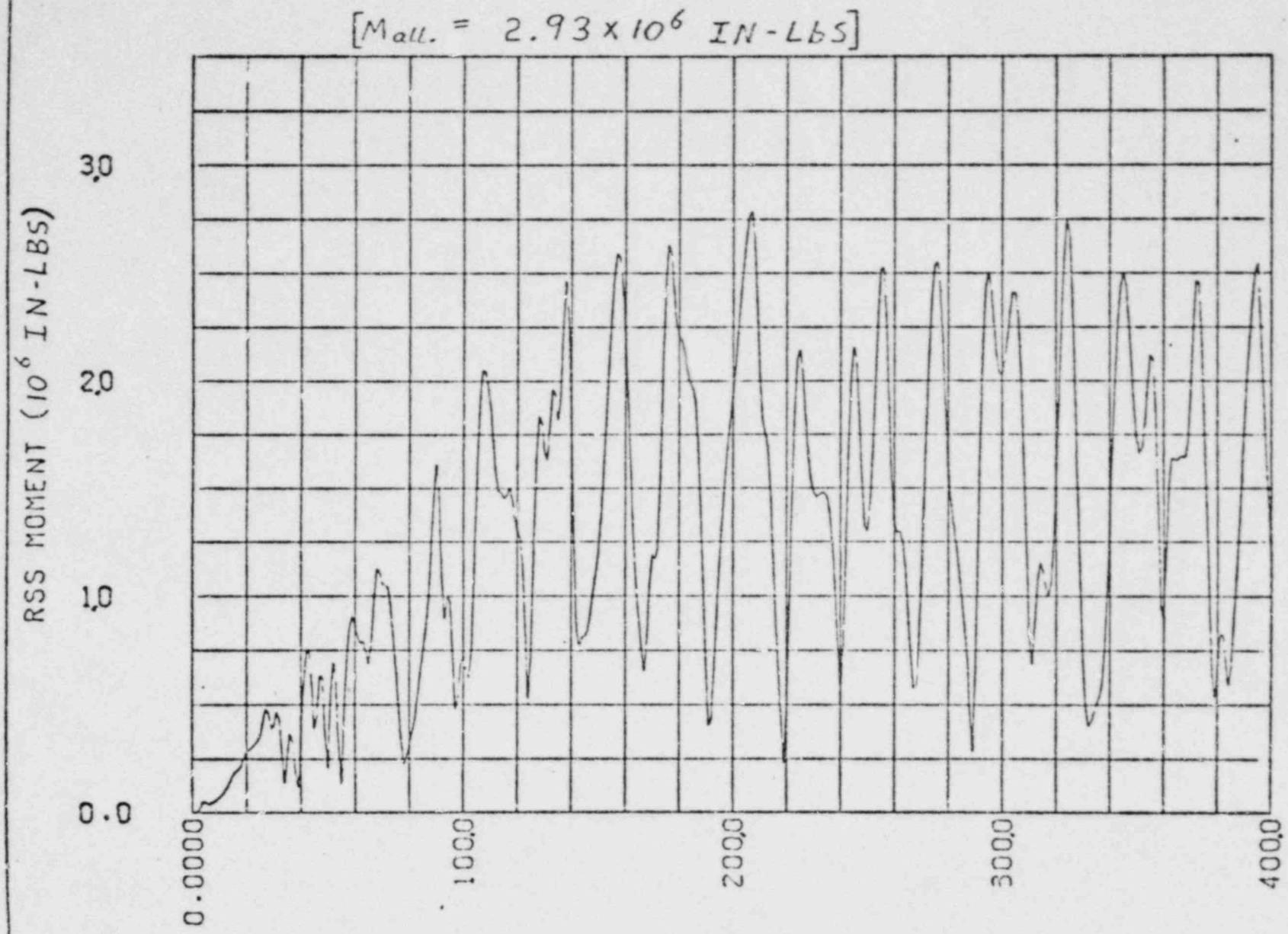

FIGURE 4.9.2

4.9-6

MILLSTONE
MOMENT - ELBOW

VERSUS
TIME

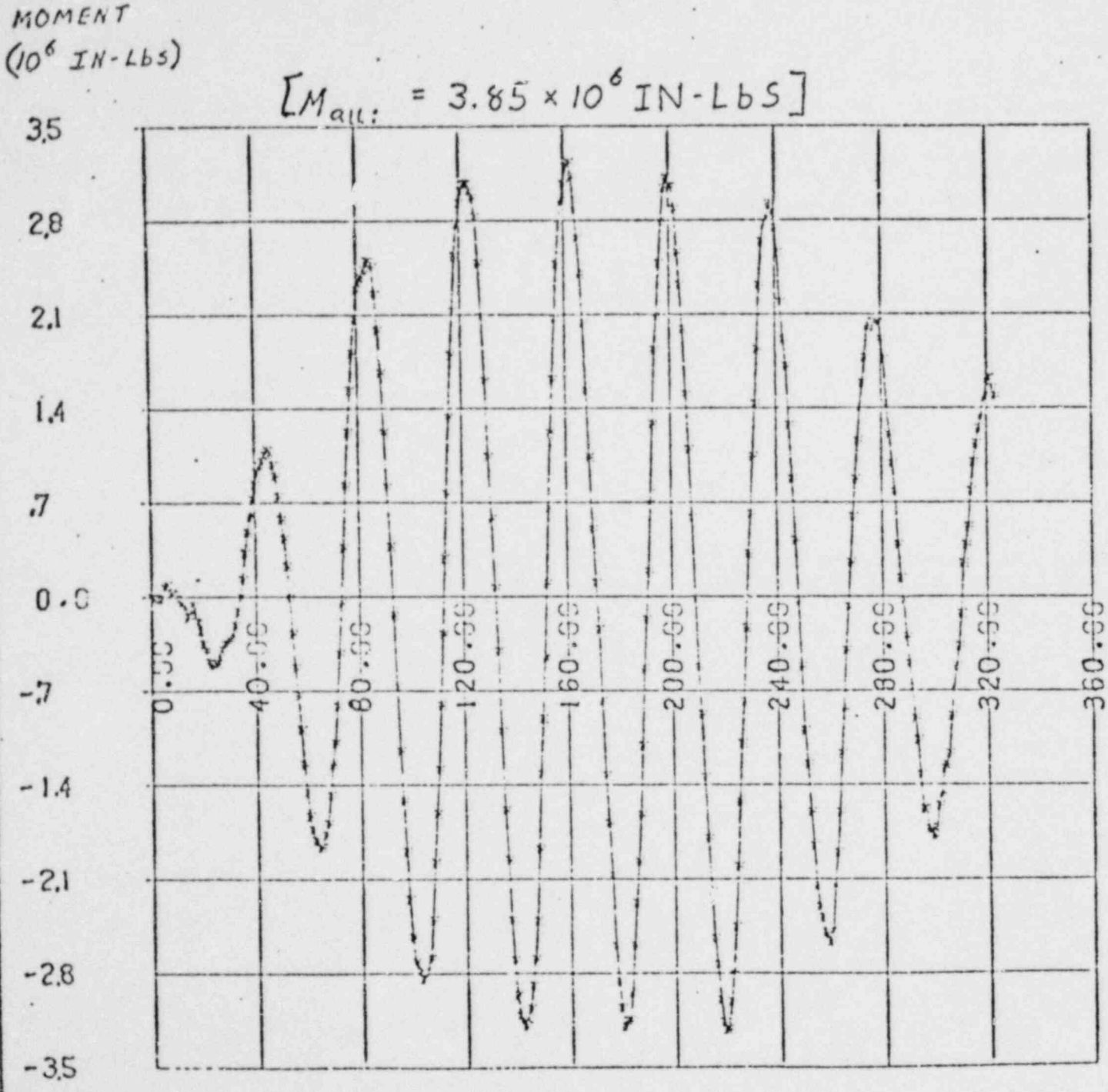

FIGURE 4.9.3

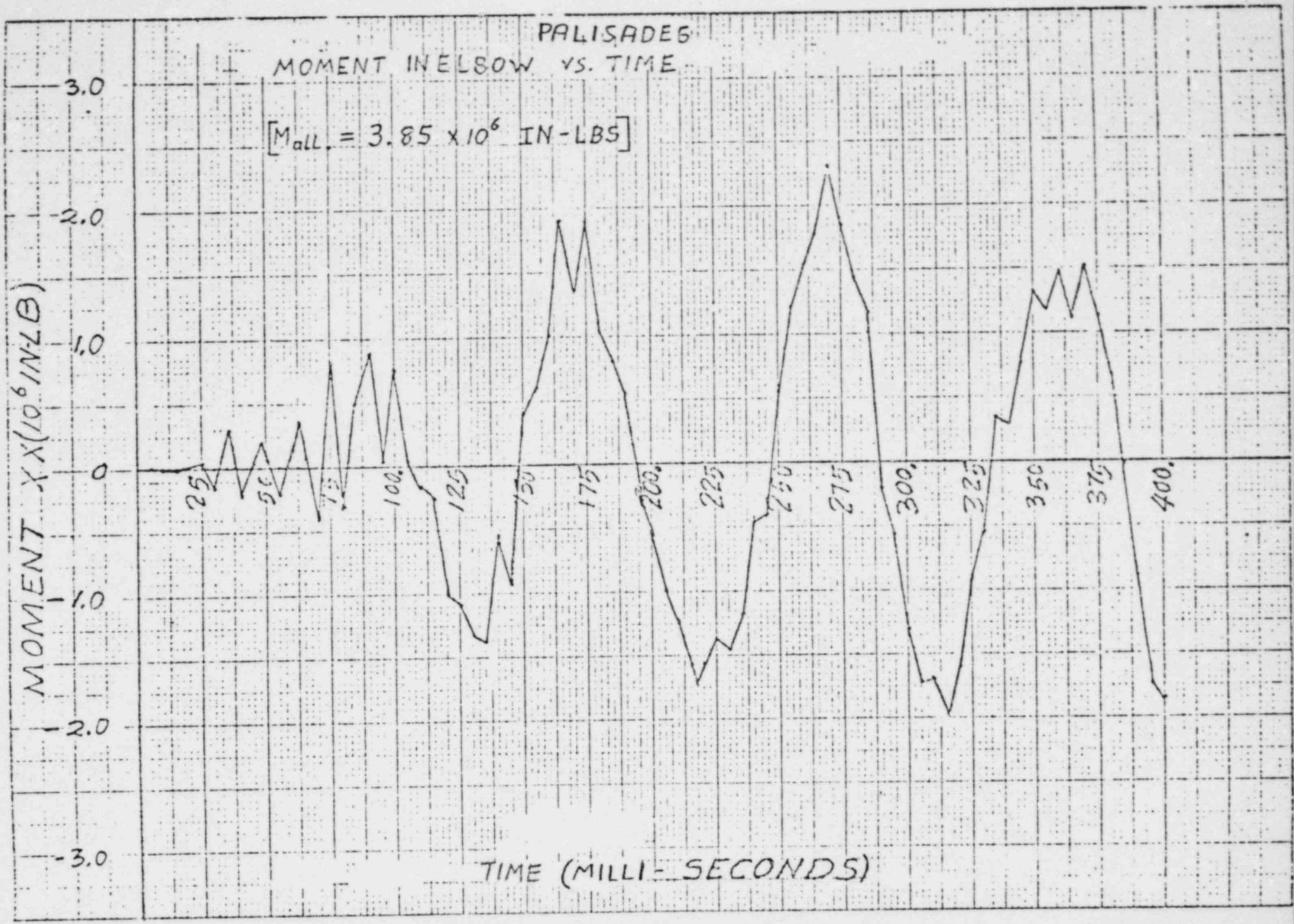
PALISADES
⊥ MOMENT IN ELBOW VS. TIME
[$M_{all.} = 3.85 \times 10^6$ IN-LBS]
MOMENT - X X(10^6 IN-LB)
3.0
2.0
1.0
0
-1.0
-2.0
-3.0
25.
50.
75.
100.
125.
150.
175.
200.
225.
250.
275.
300.
325.
350.
375.
400.
TIME (MILLI-SECONDS)

FIGURE 4.4-8

FORT CALHOUN ECCS LINE RSS MOMENT

(NOTE: RSS MOMENTS PLOTTED IN ABSOLUTE VALUES)

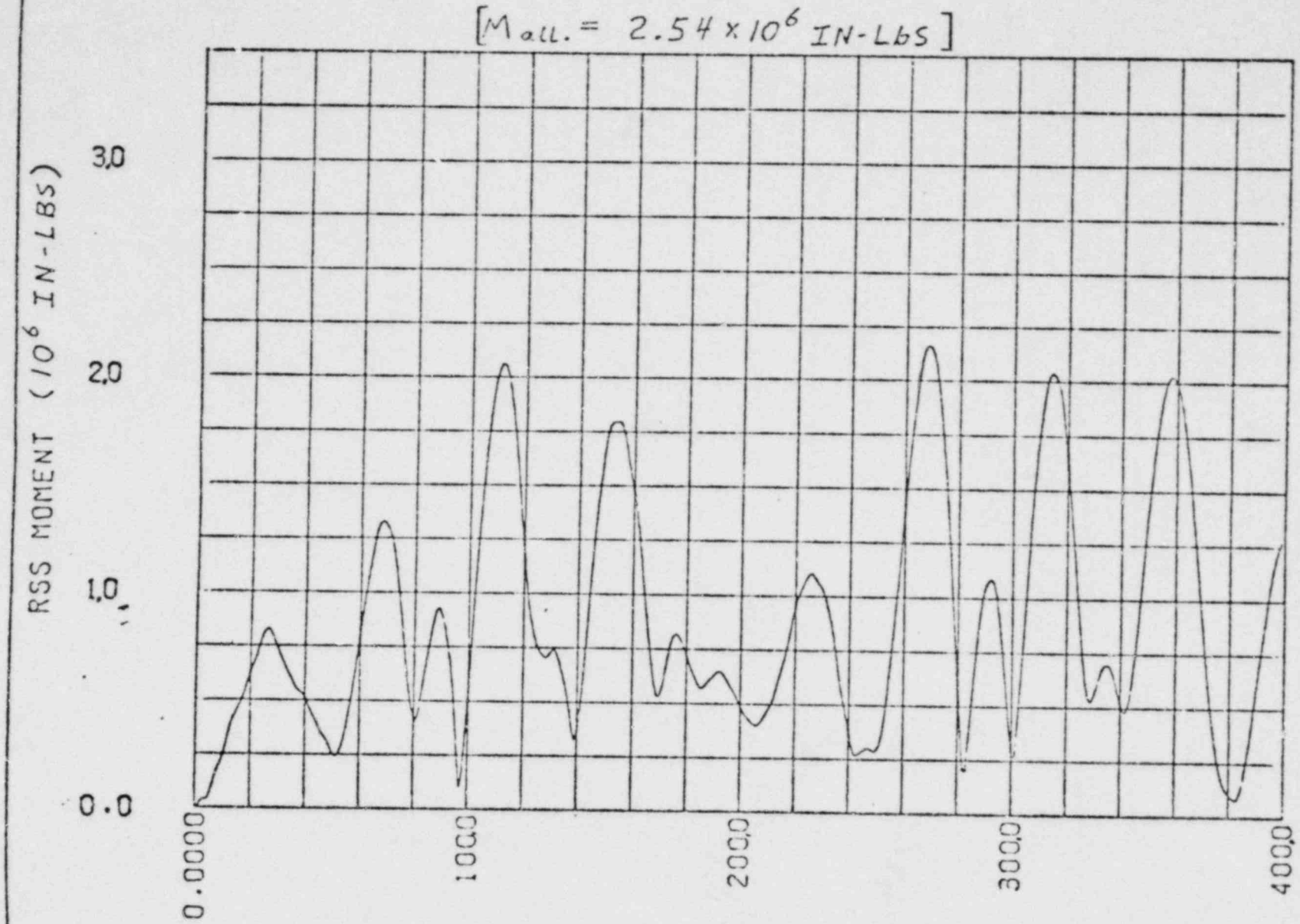

FIGURE 4.9.5

TOTAL MOMENT AT ELBOW

VERSUS

DISPLACEMENT

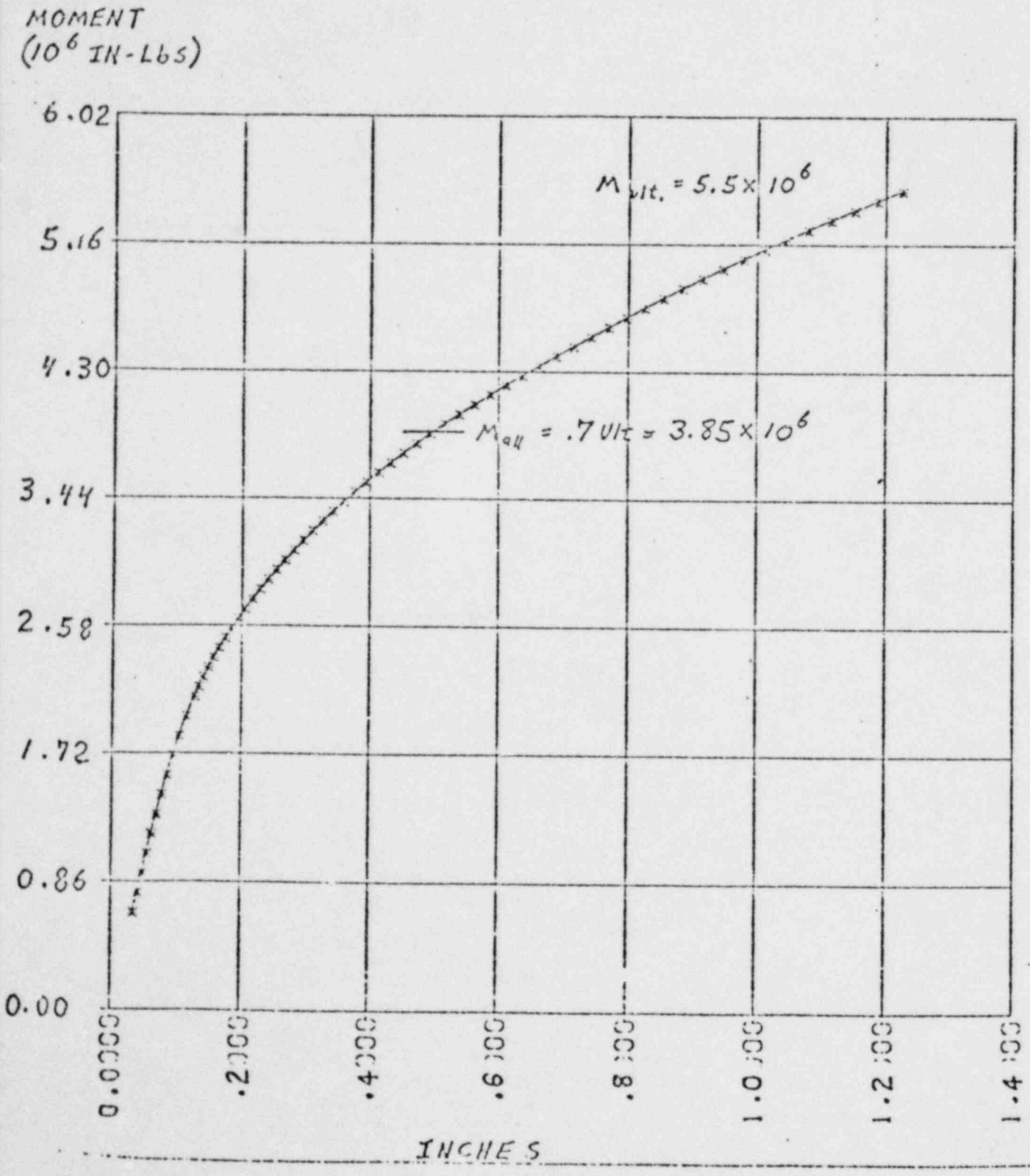

FIGURE 4.9.6

4.9 EMERGENCY CORE COOLING SYSTEM (ECCS) PIPING

4.9.1 DESIGN BASIS

The capability of the emergency core cooling system (ECCS) piping that is attached to the primary coolant piping to withstand the effects of the design basis pipe breaks has been evaluated by analysis. The effect of each break is experienced by the ECCS piping through the motion of the ECCS nozzles on the discahrge leg piping. The motions of the nozzles have been computed by the reactor coolant system structural analysis described in Section 4.5. No credit has been taken for de-pressurization.

4.9.2 METHODS OF ANALYSIS

The ECCS piping has been analyzed by traditional dynamic elastic analysis and evaluated according to appropriate elastic stress limits for ASME Level B and Level D conditions. Where these limits are not satisfied, a detailed elastic plastic analysis to demonstrate functionability of the piping has been performed.

4.9.2.1 Dynamic Analysis

An elastic dynamic analysis of the ECCS piping was performed using lumped parameter models and the appropriate ECCS nozzle motion history. The physical definition of the piping has been represented in STRUDL (Ref. 3.2) to generate the appropriate condensed stiffness matrix of the structure. The condensed matrix and mass has been input to the DAGS (Ref. 3.4) program. The DAGS program determined the motion history of the ECCS pipe by performing a time history analysis.

4.9.2.2 Detailed Analysis

Where the stresses computed by the elastic dynamic analysis exceed the prescribed limits an elastic plastic finite element analysis was performed for each region where significant plasticity was expected. This analysis is similar to the instability analyses discussed in Paragraph 4.5.3. The analysis provides details of the deformation necessary to evaluate the functionability and ultimate load carrying capability of the plastic region. The elastic plastic analysis has been performed by the MARC (Ref. 3.10) computer program. The material properties for the piping material used in the analysis was determined from the extensive collection of piping data available.

4.9.3 RESULTS OF ANALYSIS

The results of elastic and elastic plastic dynamic analyses are the displacements, moments, and stresses at the critical sections of the ECCS piping as a function of time during the LOCA event. ECCS piping support reactions are also computed in these analyses. All analyses have been performed on specific plant ECCS piping and support systems. Analyses have been performed for the design basis pipe breaks considered in Section 4.5. A summary of maximum piping moments vs. allowable limits is presented in Figure 4.9.1. Specific plant results are discussed in Section 4.9.4.

4.9.4 EVALUATION OF ECCS PIPING

4.9.4.1 Acceptance Criteria

The integrity and functionability of the ECCS piping must be demonstrated. Integrity and functionability are assured if the Level B (upset condition) limits of the ASME Boiler and Pressure Vessel Code Section III, Division 1, are not exceeded. Where the Level B limits are exceeded, then Level D or faulted limits are used to demonstrate that integrity is maintained. Functionability is assured by demonstrating that the deformations of the piping are acceptable.

4.9.4.2 Evaluation

The elastic dynamic stress results have been compared to the Level B and Level D stress limits of the ASME Code.

In the event that the stress limits are not satisfied, the elastic plastic analysis of Paragraph 4.9.2.2 has been performed.

The integrity of the piping has been evaluated by comparing the computed load to 70% of the instability load. The functionability has been evaluated by comparing the pipe section deformation to the deformation required for significant flow restriction.

4.9.4.2.1 Calvert Cliffs

The Calvert Cliffs ECCS piping has been evaluated for the generic plant motion. The maximum moment in the ECCS piping due to the hypothetical pipe break is 2,800,000 in-lbs at an elbow, and 3,090,000 in-lbs in a straight section of pipe. These moments satisfy the ASME Code Level D elastic limits. At these moment levels, the plastic strain is less than 1%. Functionability is not impaired at these strain levels. Analysis of the safety injection nozzle indicates

4.9.4.2.1 Calvert Cliffs (Continued)

that ASME Code Level B elastic limits are satisfied. A worst case elbow moment vs. time plot is presented in Fig. 4.92.

4.9.4.2.2 Millstone

The input motion to the ECCS piping is identical to the generic plant motion. The maximum moments in the piping due to the hypothetical pipe break exceeds the ASME Code Level D elastic limits. An elastic-plastic analysis per paragraph 4.9.2.2 has, therefore, been performed. The maximum moment in the piping is 3,300,000 in-lbs at an elbow, and 5,800,000 in-lbs in a straight section of pipe. These moments satisfy the ASME Code Level D criteria of 70% of the collapse load. A plot of maximum elbow moment vs. time is presented in Fig. 4.9.3. The ultimate moment carrying capability of the elbow is presented in Fig. 4.9.6. At these moment levels, the plastic strain is less than 2%. Functionability is not impaired at these strain levels. Analysis of the Safety Injection Nozzle indicates that ASME Code Level B elastic limits are satisfied.

4.9.4.2.3 Palisades

A plant specific analysis of the Palisades ECCS piping has been performed. The maximum moments in the piping due to the hypothetical pipe break exceeds the ASME Code Level D elastic limits. An elastic-plastic analysis per paragraph 4.9.2.2 has, therefore, been performed. The maximum moment in the piping is 2,880,000 in-lbs at an elbow, and 4,160,000 in-lbs in a straight section of pipe. These moments satisfy the ASME Code Level D criteria of 70% of the collapse load. A plot of maximum elbow moment vs. time is presented in Fig. 4.9.4. The ultimate moment carrying capability of the elbow is presented in Fig. 4.9.3. At these moment levels, the plastic strain is less than 2%. Functionability is not impaired at these strain levels. Analysis of the Safety Injection Nozzle indicates that ASME Code Level B elastic limits are satisfied.

4.9.4.2.4 Fort Calhoun

A plant specific analysis of the Fort Calhoun ECCS piping has been performed. The maximum moments in the piping due to the hypothetical pipe break is 2,160,000 in-lbs at an elbow and in a straight section of pipe. These moments satisfy the ASME Code Level D elastic limits. At these moment levels, the plastic strain is less than 1%. Functionability is not impaired at these strain levels. Analysis of the safety injection nozzle indicates that ASME Code Level B elastic limits

4.9.4.2.4 Fort Calhoun (Continued)

are satisfied. A plot of maximum elbow moment vs. time is presented in Fig. 4.9.5. A comparison of the motions on the ECCS piping due to hot and cold leg guillotines was performed. The motions resulting from the cold leg guillotine govern the response of the ECCS piping.

ECCS PIPING EVALUATION

SUMMARY OF MAXIMUM MOMENTS

(UNITS 10^6 IN-LBS)

PLANT	HYPOTHETICAL PIPE BREAK	MAXIMUM MOMENT ELBOW	ALLOWABLE MOMENT ELBOW	MAXIMUM MOMENT STRAIGHT PIPE	ALLOWABLE MOMENT STRAIGHT PIPE	ANALYTICAL METHOD
CALVERT CLIFFS	HOT LEG	2.65	2.93	3.09	4.73	ELASTIC
	COLD LEG	2.80	2.93	2.82	4.73	ELASTIC
MILLSTONE	HOT LEG	3.3	3.85	5.8	7.0	PLASTIC
	COLD LEG	2.24	2.93	4.53	4.73	ELASTIC
PALISADES	HOT LEG	1.73	2.93	3.55	4.73	ELASTIC
	COLD LEG	2.88	3.85	4.16	7.0	PLASTIC
FORT CALHOUN	COLD LEG	2.16	2.54	2.16	5.39	ELASTIC

FIGURE 4.9.1

CALVERT CLIFFS ECCS LINE 12B RSS MOMENT

(NOTE: RSS MOMENTS PLOTTED IN ABSOLUTE VALUES)

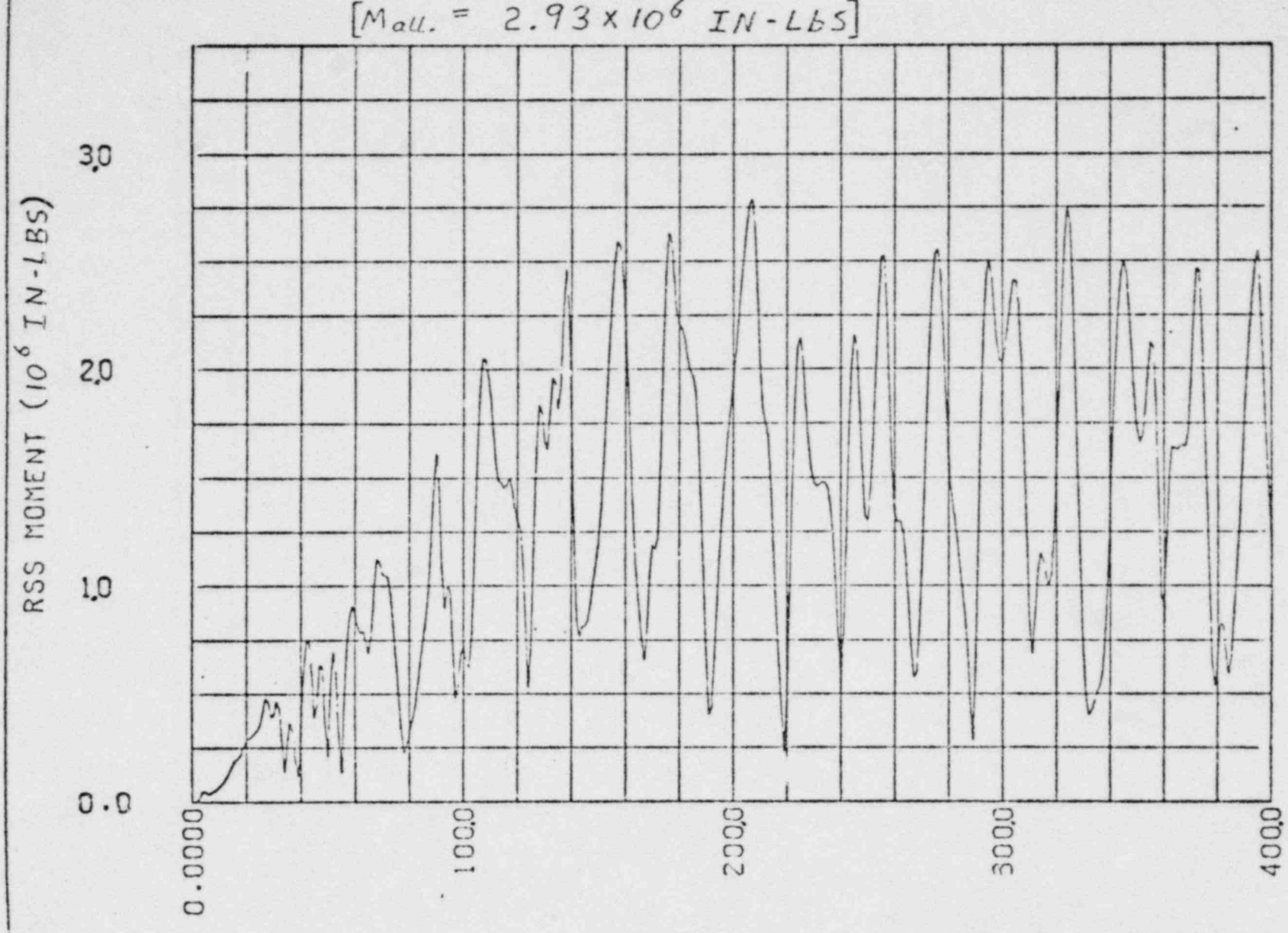

FIGURE 4.9.2

MILLSTONE
MOMENT - ELBOW

VERSUS
TIME

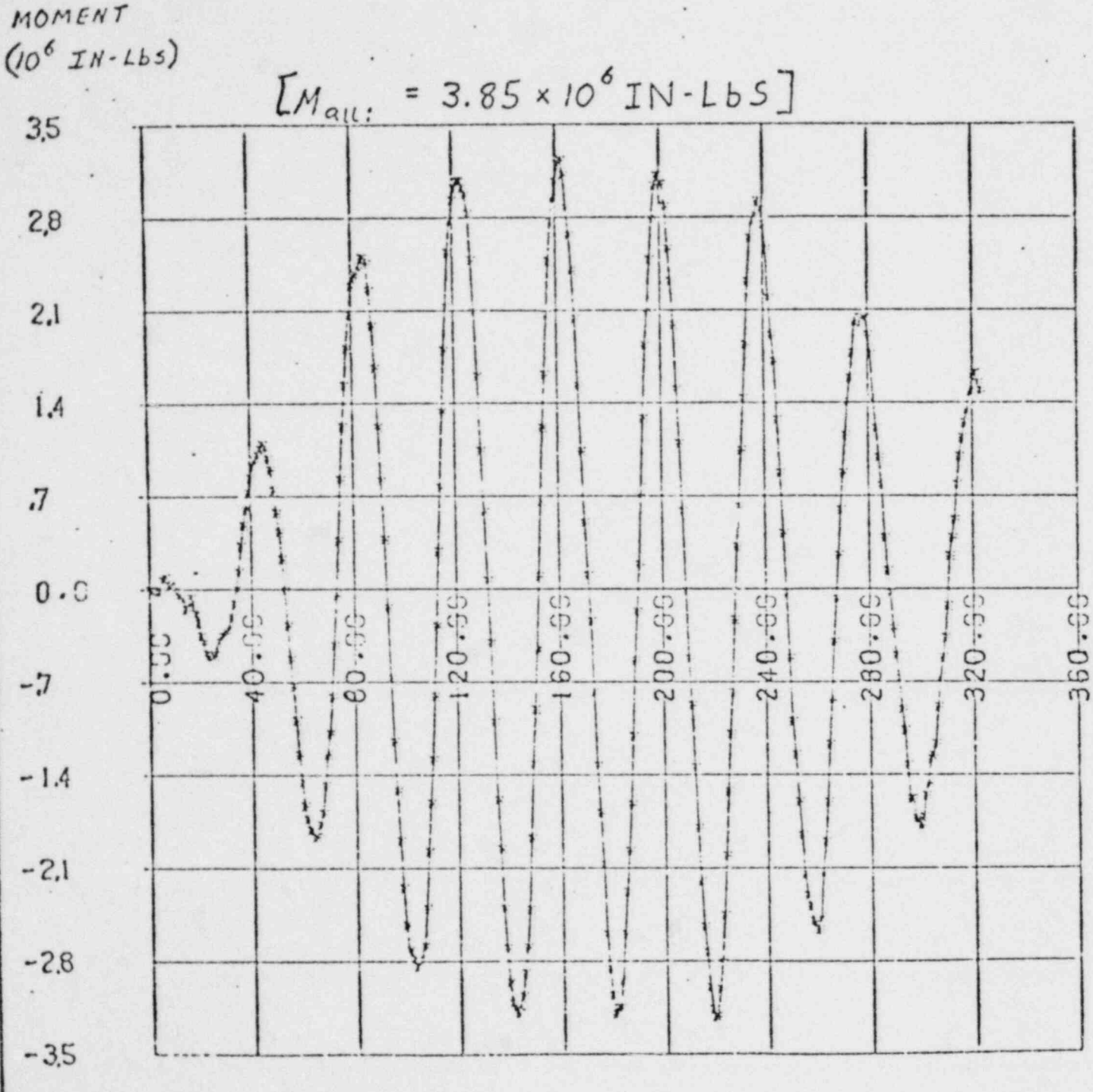

FIGURE 4.9.3

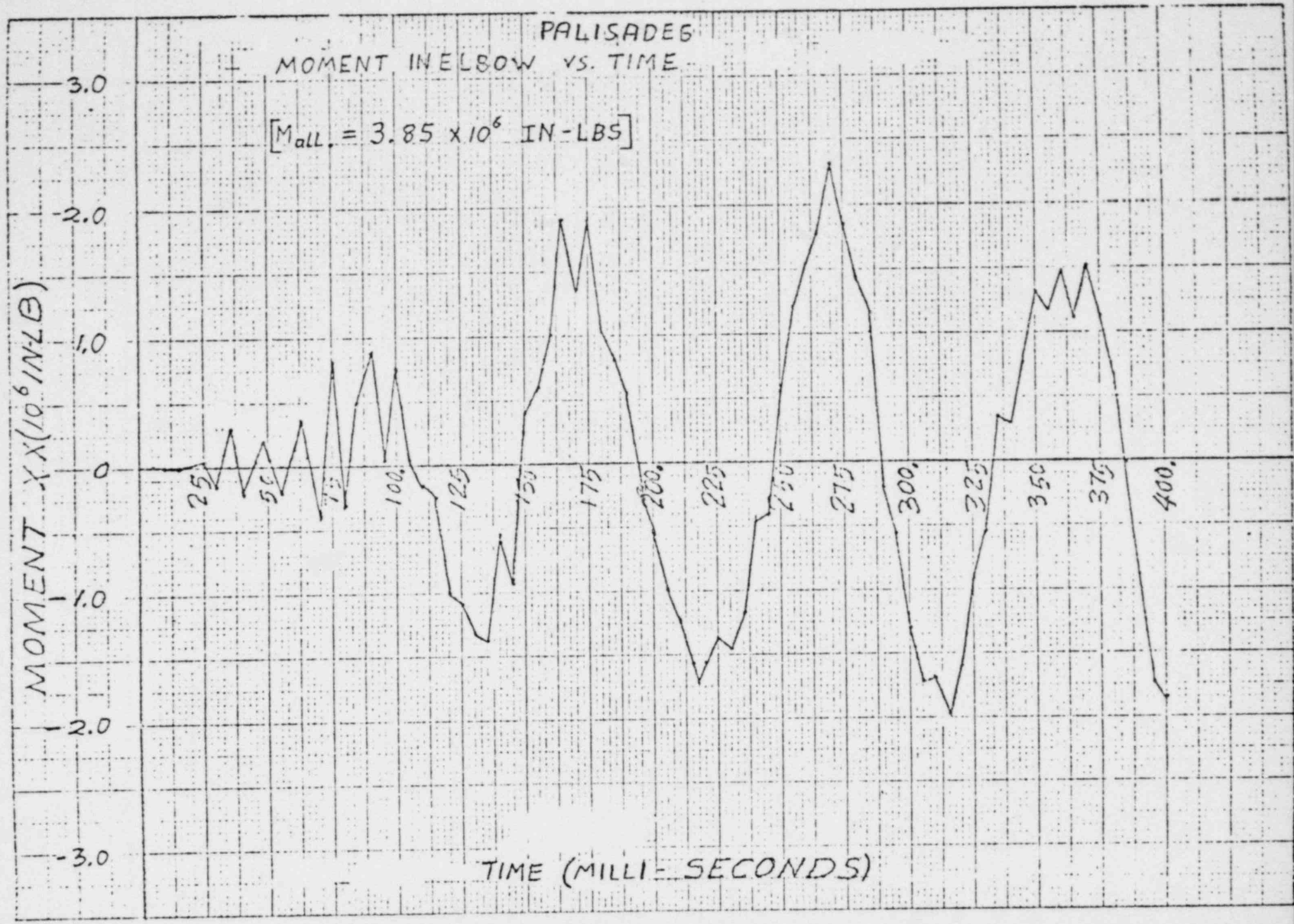
PALISADES
MOMENT IN ELBOW VS. TIME
[$M_{all.} = 3.85 \times 10^6$ IN-LBS]
MOMENT - X X(10^6 IN-LB)
3.0
2.0
1.0
0
-1.0
-2.0
-3.0
25
50
75
100.
125
150
175
200.
225
250
275
300.
325
350
375
400.
TIME (MILLI-SECONDS)

FIGURE 4.4-8

FORT CALHOUN ECCS LINE RSS MOMENT

(NOTE: RSS MOMENTS PLOTTED IN ABSOLUTE VALUES)

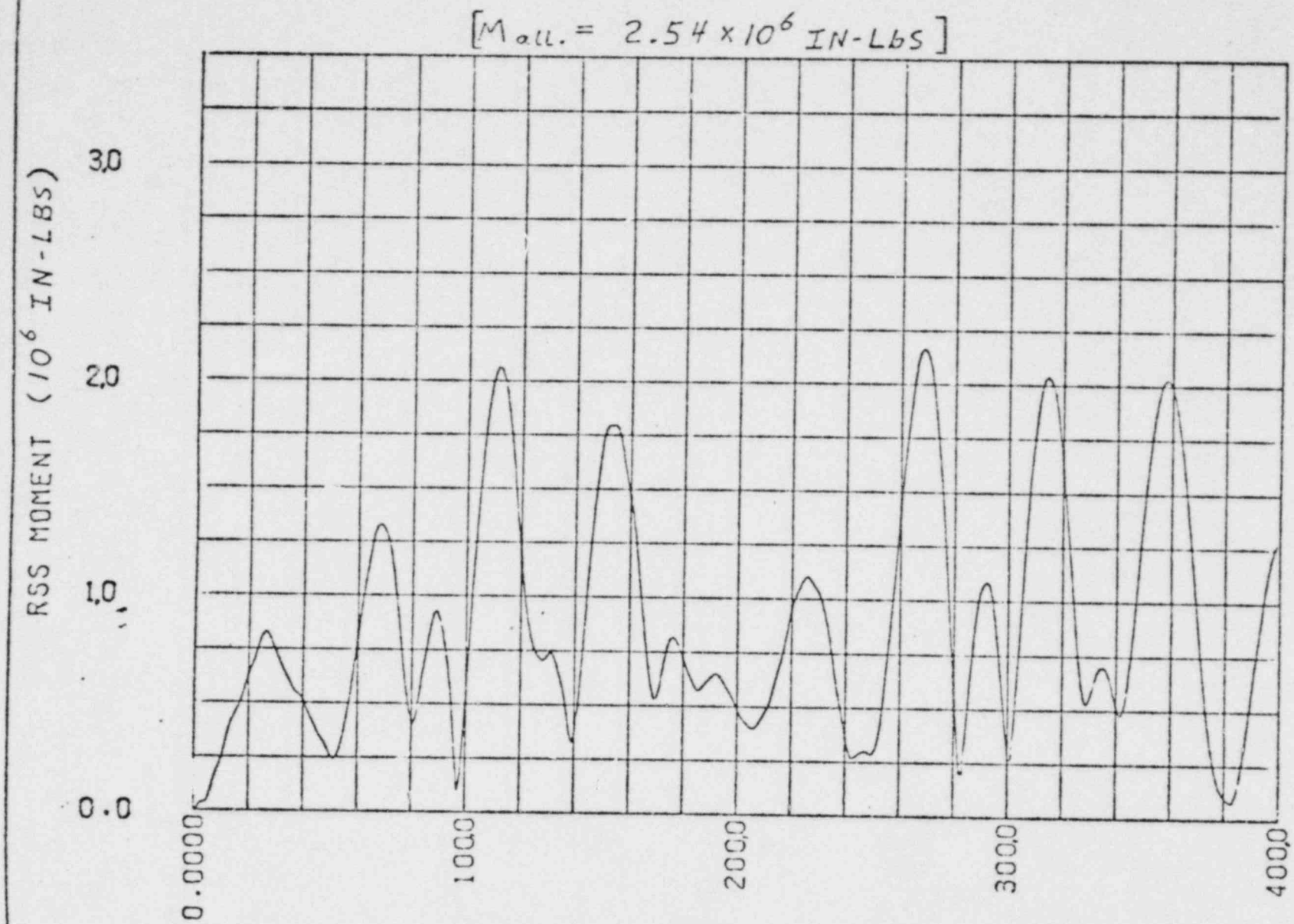

FIGURE 4.9.5

TOTAL MOMENT AT ELBOW

VERSUS

DISPLACEMENT

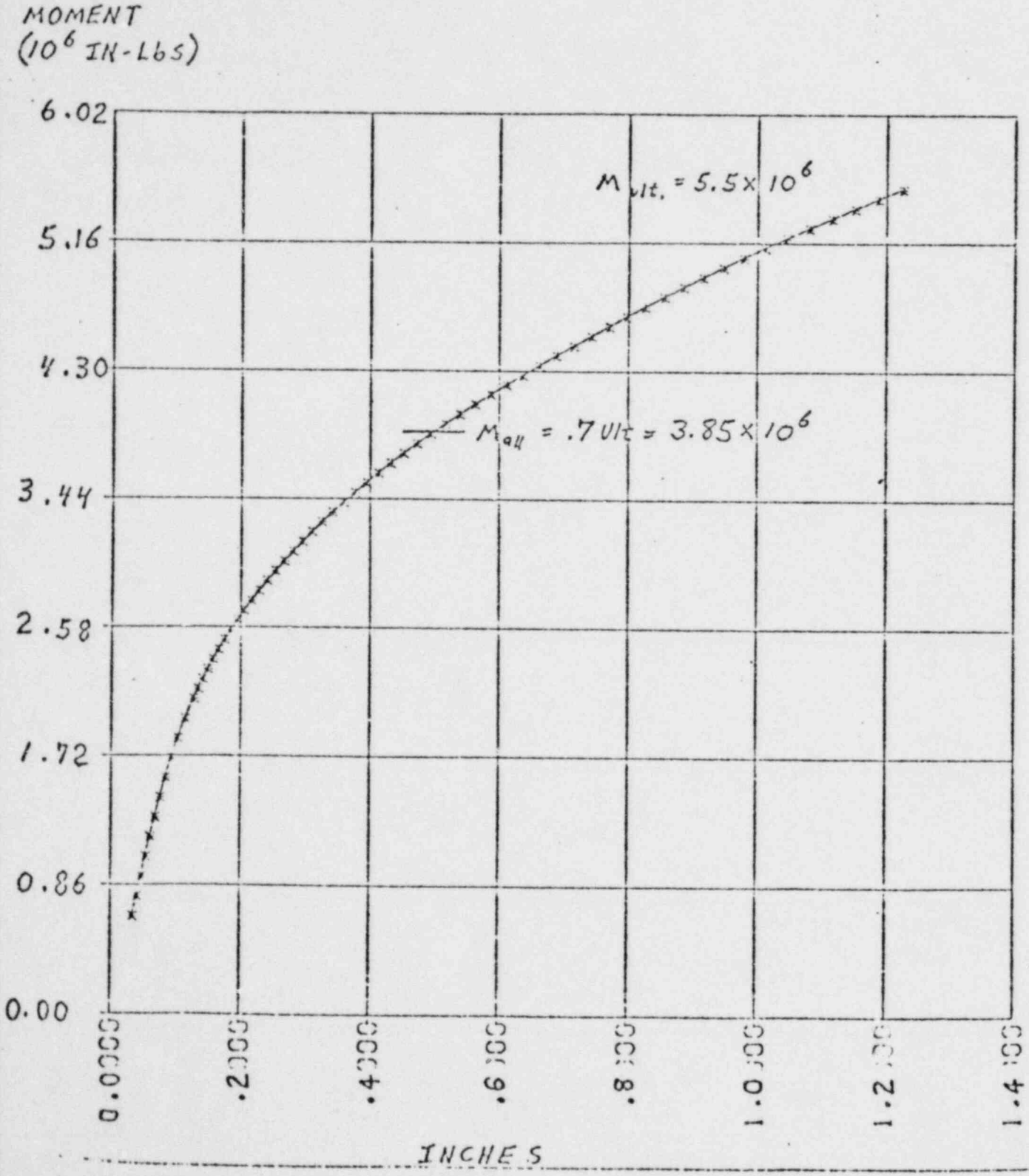

FIGURE 4.9.6

4.10 PRIMARY SHIELD WALL

4.10.1 Calvert Cliffs 1 & 2, Millstone 2

The following summarizes the analysis of the Calvert Cliffs/ Millstone reactor shield wall when subjected to a hypothetical guillotine break in its number one hot leg and its number one-A cold leg. The analysis incorporates transient pressure, operating temperature and break loads as static loads applied to the structure. The vertical and horizontal pipe break loads were assumed to act on the concrete supports, while the pressure and temperature gradients were assumed to act on and within the reactor cavity walls.

The structure under analysis consists of three major components (See Figures 4.3.14 through 4.3.21). The shield wall, which runs from the base to elevation 69'-0" is in the shape of a rectangle. The reactor cavity wall, which is in the shape of an octagon, extends from the base to elevation 44'-0". Lastly, the steam generators' pedestals are at floor elevation 31'-0". Also included are two slabs that are tied to the reactor cavity and the shield wall.

The static loads applied at the supports for the reactor vessel were taken from the study of the generic operating plant's reactor vessel supports (See Section 4.5.7). They are summarized in Table 4.10.1. The loads used represent the maximum values occurring during the time history for each of the breaks, the worst case was chosen, at each support. The horizontal loads are projected directly onto the primary shield wall ignoring the protruding segment of the wall with which the support is tied. The vertical loads are applied directly at the base of the supports.

The values used for the pressure distributions were taken from the study of pressure loads on the reactor cavity wall of Calvert Cliffs. The study's results gave the pressure transient for each element of the modeled reactor cavity. The peak values for each element were used and applied as a continuous static pressure. These values ranged from a maximum of 200 psi to a minimum of 50 psi. Pressures acting outside the reactor cavity were constant and throughout, and thus assumed not to have any effect (See Section 4.3.3.5).

The effects of temperature were accounted for by considering an operating temperature of 105^{o} throughout except inside the cavity wall where 125^{o} operating temperature was used. The as-built concrete temperature was assumed at 75^{o}.

The gravity load on the structure was calculated directly by the NASTRAN Program using an acceleration of 385.4 in/sec^2 and the section properties of each element. The material properties of the structure were assumed throughout. 5000 psi and 60 ksi were used for the concrete and steel respectively.

The NASTRAN Program was used to analyze the structure under the applied static loads. The structure was modeled using plate elements. The model was assumed fixed at the base. Output consisted of displacements at all the nodal points, forces at fixed nodes, and element forces (See Figure 4.10.1).

Findings of the Analysis

The structure was checked using the critical results from the computer output against the various interaction diagrams of the concrete sections. No problems were seen with any of the critical sections under axial compression or tension and bending. Also, there were no elements showing failure because of acting shear forces. It can be concluded that the structure will not have any problems in coping with any of the forces that might occur from the proposed pipe break loads. Figure 4.10.2 exemplifies the interaction diagrams and shows where the element load conditions lie.

4.10.2 Palisades

The evaluation of the primary shield wall for Palisades is still in progress. Based on a preliminary assessment of the structure, the shield wall is adequate to withstand the combined effects of component support loads and pressure differentials across the wall.

4.10.3 Fort Calhoun

A comparison of the calculated reactor vessel support loads and the loads employed in the original design of the primary shield wall shows that the original design loads have been exceeded. An evaluation of the capability of the primary shield wall for Fort Calhoun would require state of the art analytical methods. We believe that such an analysis is unwarranted and instead propose to show, by fracture mechanics techniques, that the postulated pipe break is incredible and that the primary shield wall is capable of withstanding the largest credible pipe break predicted by those techniques. The plan for fracture mechanics evaluation is presented in Appendix D. In addition, a feasibility study of adding pipe whipping restraints to the Fort Calhoun pump discharge piping to reduce break size has been performed and is presented in Appendix C.

Table 4.10.1

Generic Plant
(Calvert Cliffs 1 & 2, Millstone 2)
Reactor Vessel Support Loads

CASE / SUPPORT LOCATION	GUILLOTINE AT RV INLET NOZZLE 1A		GUILLOTINE AT RV OUTLET NOZZLE #1	
	HORIZ. SPPT. LOAD (KIPS)	VERT. SPPT. LOAD (KIPS)	HORIZ. SPPT. LOAD (KIPS)	VERT. SPPT. LOAD (KIPS)
HOT LEG #2	7897.	4612.	0.	3281.
COLD LEG 1A	2192.	4164.	2998.	1557.
COLD LEG 1B	6452.	4642.	3005.	1584.

FIGURE 4.10.1

CALVERT CLIFFS 1 & 2, MILLSTONE 2

MATHMATICAL MODEL

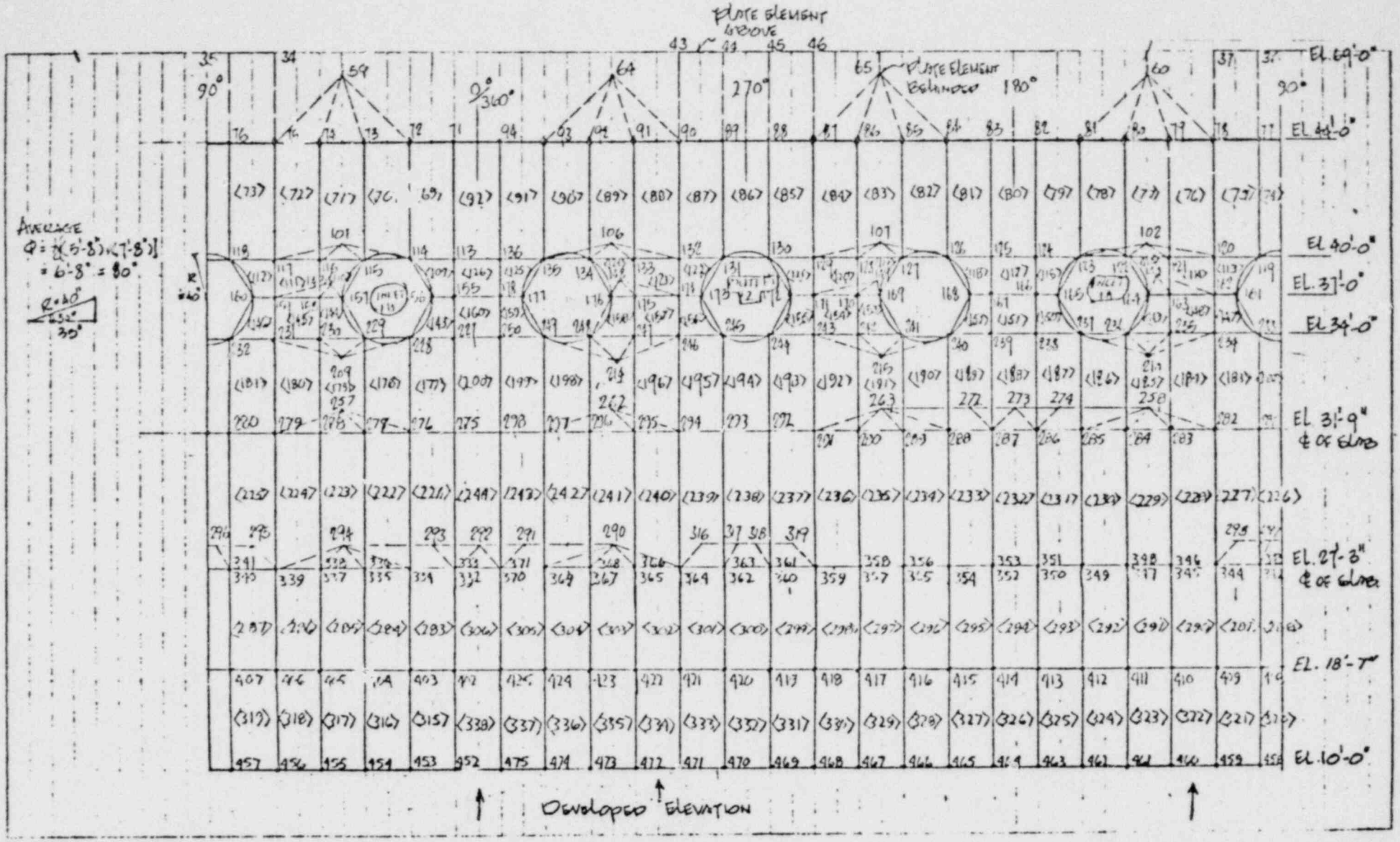

Figure 4.10.2

CALVERT CLIFFS/MILLSTONE
PRIMARY SHIELD WALL ANALYSIS-INTERACTION DIAGRAMS

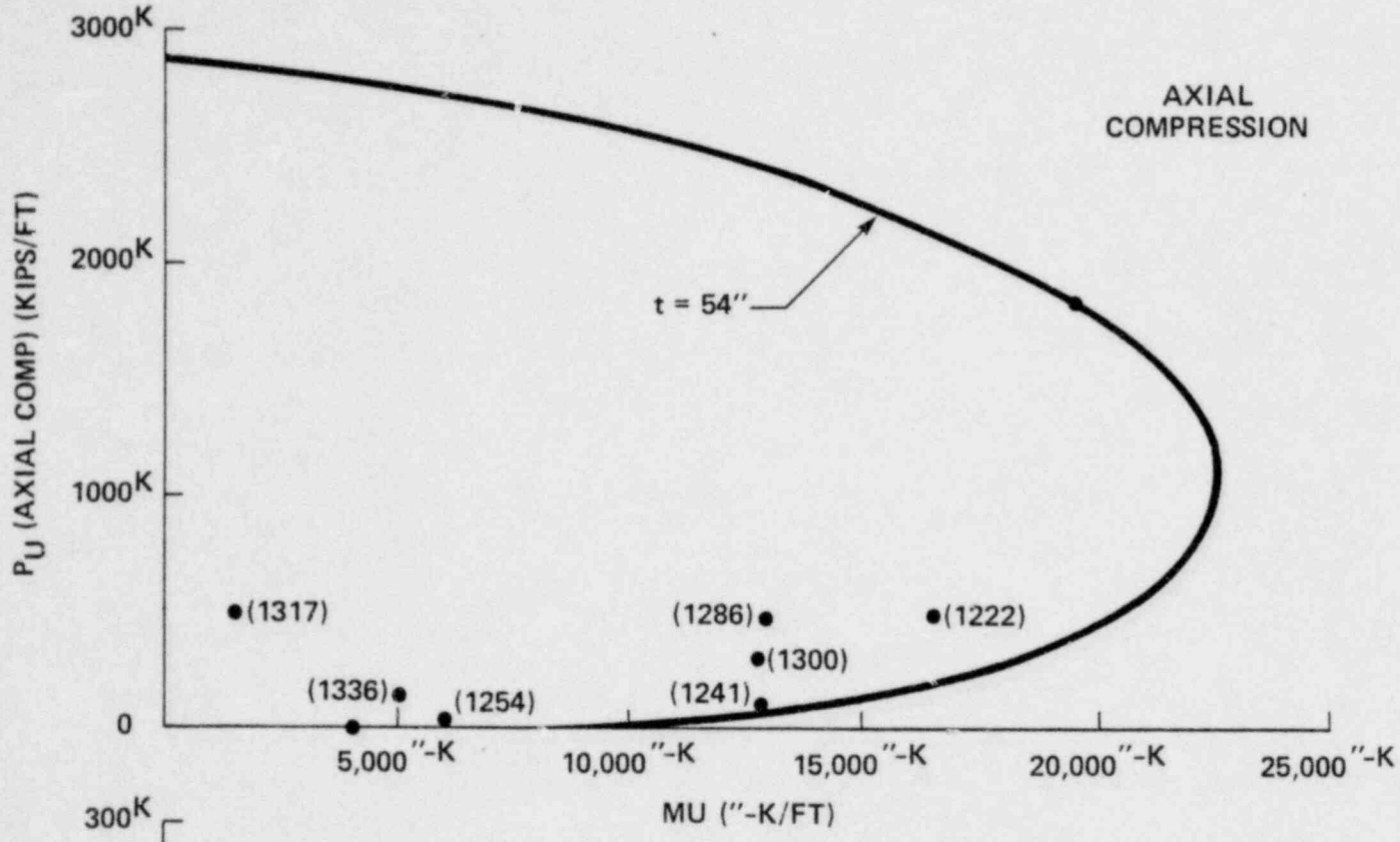

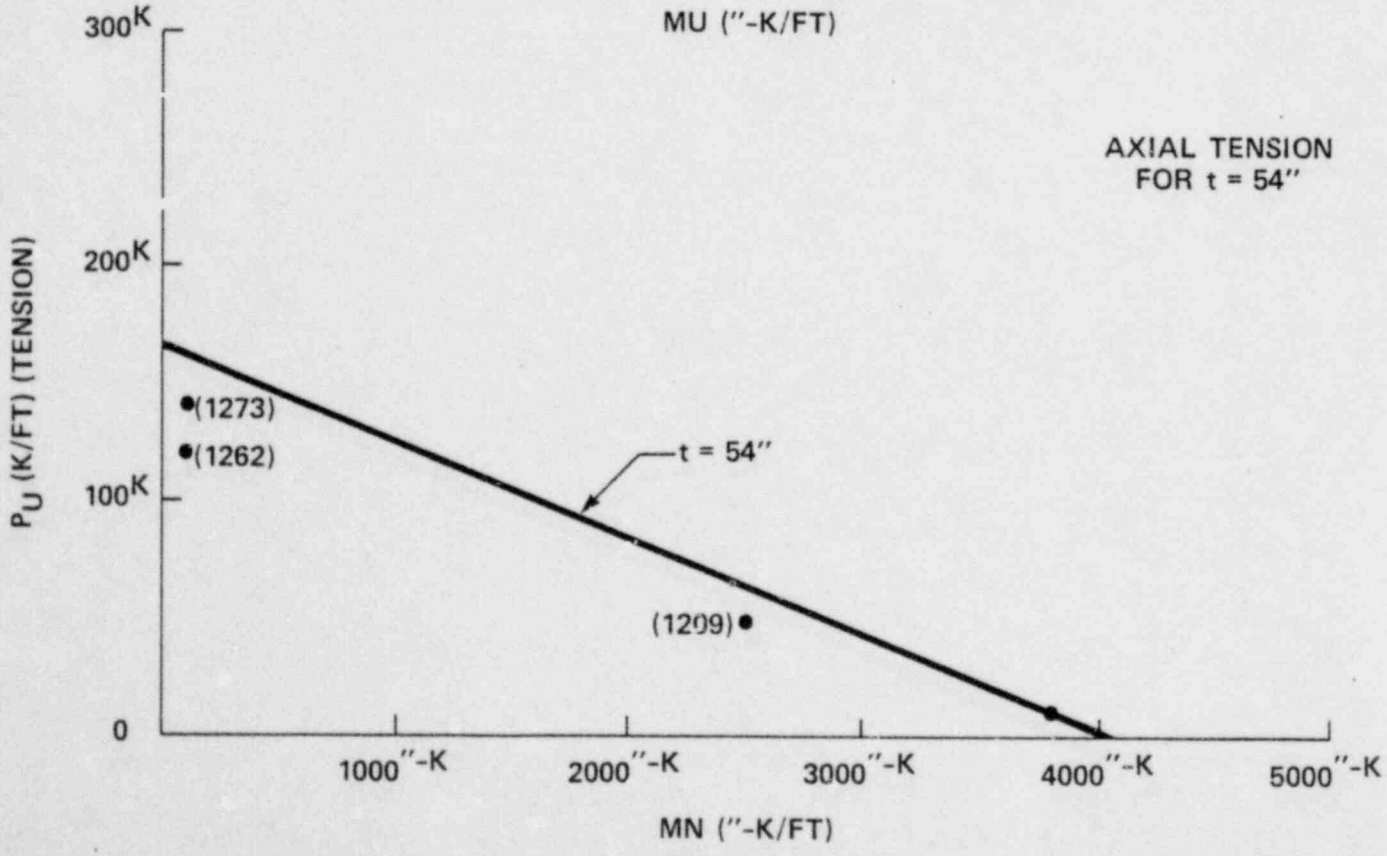

Figure 4.10.2 (Cont'd)

CALVERT CLIFFS/MILLSTONE
PRIMARY SHIELD WALL ANALYSIS-INTERACTION DIAGRAMS